# LIBRARY Michigan State University

PLACE IN RETURN BOX to remove this checkout from your record.

TO AVOID FINES return on or before date due.

MAY BE RECALLED with earlier due date if requested.

DATE DUE	DATE DUE	DATE DUE

11/00 c:/CIRC/DateDue.p85-p.14

# TRANSIENT ANALYSIS OF PLANE WAVE SCATTERING IN A LAYERED MEDIUM

By

Jungwook Suk

# A DISSERTATION

Submitted to
Michigan State University
in partial fulfillment of the requirements
for the degree of

# DOCTOR OF PHILOSOPHY

Department of Electrical and Computer Engineering

2000

12-1:

III-Ş

f.c

<del>5</del>-12

Ŧ

#### **ABSTRACT**

# TRANSIENT ANALYSIS OF PLANE WAVE SCATTERING IN A LAYERED MEDIUM

Bv

#### Jungwook Suk

The transient scattering of plane electromagnetic waves from a dispersive layered medium has been a difficult problem to solve, even though its frequency domain behavior is well known. In this study, analytical transient solutions for the electromagnetic waves scattered from a multi-layered medium excited at oblique incidence by a uniform plane wave are derived for both TE and TM polarizations. It is assumed that each layer has infinite width in space but finite thickness, and isotropic, homogeneous and frequency independent electrical parameters.

First, the time-domain reflection coefficient for a single interface in the medium is derived using the inverse Fourier transform of the frequency domain formulation. Then, the overall transient scattered field is found for a layered medium by combining the individual transient reflection coefficients using a series expansion and convolution integrals. The derived expressions are verified by comparison with data measured from laboratory experiments.

The results obtained in this study may be used as a basis for material parameter estimation by transient probing.

Copyright by Jungwook Suk 2000 To my Father and Mother

There are in d

#### ACKNOWLEDGMENTS

There are many people who deserve my acknowledgement for this work. First of all, my greatest thanks should be to my advisor Dr. Edward J. Rothwell, who has motivated, trained and encouraged me as well as given invaluable knowledge and advice, to overcome obstacles from the beginning of my degree program to the end of this thesis. I has been so fortunate to study under his guidance. My special thanks is to Dr. Dennis P. Nyquist for his excellent teaching and precious helps for this work during past years. I also wish to express my thanks to Dr. Kun-Mu Chen and Dr. Byron Drachman, who have provided useful knowledge, and participated in my guidance committee.

I appreciate the helps provided by Jeong Seok Lee, Chi-Wei Wu, Ung Sik Kim and Chris Colemann in experiments, and the friendship we have shared during my study. From the other measurement works with Dr. Ahmet Kizlay, I could obtain valuable experiences, and his help was important in writing this thesis. I have been happy to study with the other colleagues in Electromagnetics Lab of Michigan State University.

Finally, I would like to say my deep thanks to my parents and sister. Their constant love and care have always encouraged me through my life.

UST OF FIGURE

CHAPTER 1  $\underline{\operatorname{Lipdiction}}$  .

CHAPTER 2

Irreria ial Reties

 $2.1 \cdot Introd \gamma$ 

22 Frequen

2.2.1 I 222

223 (

2.24 I

23 Derivati 2.3.1

2.3.2

 $24 \cdot Numeri$ 

2.4.1 V 2.4.2

25 Appr xi 2.5.1

2.5.2

CHAPTER 3 Inerfacial Reflec

3.1 Introdu

32 Freque 3.2.1

3.2.2 3.2.3

3.3 Deriva:

3.4 Names 3.4.1

3.4.2

## TABLE OF CONTENTS

LIST C	F FIGU	JRES	viii
CHAP7. Introdu			1
CHAPT Interfac		ection Coefficients for TE-Polarization	5
2.1	Introd	uction	5
2.2	Freque 2.2.1 2.2.2 2.2.3 2.2.4	Pency Domain Formulation of Interfacial Reflection Coefficient  Derivation  Branch-cuts  Classification of frequency domain coefficients  Reduction of the interfacial reflection coefficients	5 12 15 17
2.3	Deriva 2.3.1 2.3.2	tion of Transient Interfacial Reflection Coefficients	21 21 36
2.4	Numer 2.4.1 2.4.2	Verification of theoretical expressions	41 41 48
2.5	Appro 2.5.1 2.5.2	ximation of Interfacial Reflection Coefficients	51 56 62
CHAPT Interfac		ection Coefficients for TM-Polarization	69
3.1	Introd	uction	69
3.2	Freque 3.2.1 3.2.2 3.2.3	Pency Domain Formulation of Interfacial Reflection Coefficient .  Derivation	69 69 76 79
3.3	Deriva	tion of Transient Interfacial Reflection Coefficients	84
3.4	Numer 3.4.1 3.4.2	Verification of theoretical expressions	90 90 92

44 Numeric

# CHAPTER 5

Experiments . . .

5.1 Introducti

...

52 Experime:

53 Calibrati

54 Measurem

5.4.1 Th

5.4.2 Fix

5.4.3 Lor

CHAPTER 6
Concinsions

APPENDIX A

Operations of Con-

APPENDIX B Inverse Fourier Tra

POSTATE Source Co

EIBLIOGRAPHY

CHAPT Scatteri	TER 4 ng from A Multi-Layered Medium	101
4.1	Introduction	101
4.2	Formulation of Transient Overall Reflection Coefficient	101
4.3	Transient Propagation	105
4.4	Numerical Examples of Overall Reflection	107
СНАРТ		100
Experin	nents	120
5.1	Introduction	120
5.2	Experimental Set Up	120
5.3	Calibration	125
5.4	Measurements	126
	5.4.1 Three lossless layer measurements	126
	5.4.2 Five lossless layer measurements	129
	5.4.3 Lossy layered medium measurements	148
CHAPT Conclus	`ER 6 ions	162
APPEN	DIV A	
		165
APPEN	DIX B	
Inverse	Fourier Transform Pairs	167
APPEN	DIX C	
Progran	a Source Codes in FORTRAN 77	170
BIBLIOGRAPHY		

Figure 1.1 Till a

Figure 2.1 T

Figure 2.2 T

Figure 2.3 T

Figure 2.4 T

Figure 2.5

Figure 2.5

Figure 2.6

Figure 2.7

Figure 2.7

Figure 2.8

Figure 2.5

Figure 2.5

## LIST OF FIGURES

Figure 1.1	The geometry for analysis of transient plane wave scattering from a multi-layered medium	4
Figure 2.1	The incident, reflected and transmitted TE-polarized plane wave at an interface	6
Figure 2.2	The brach cut setting. (a) Evaluation of $\sqrt{z(\omega_1)}$ and (b) allowed region of branch cuts	14
Figure 2.3	The time relationship of wavefronts	37
Figure 2.4	The consideration of the existence of a precursor	39
Figure 2.5	(a) Numerical comparison of the derived transient reduced interfacial reflection coefficient with that from the IFFT (TE polarization): $\mu_n = \mu_0$ , $\epsilon_n = \epsilon_0$ , $\sigma_n = 0[\mho/m]$ , $\mu_{n+1} = \mu_0$ , $\epsilon_{n+1} = 72\epsilon_0$ , $\sigma_{n+1} = 4[\mho/m]$ , $\theta_{i1} = 30^\circ$ , $P_2 = 0.64 \times 10^{10}$	43
Figure 2.5	(b) Numerical comparison of the derived transient reduced interfacial reflection coefficient with that from the IFFT (TE polarization): $\mu_n = \mu_0$ , $\epsilon_n = 2.59\epsilon_0$ , $\sigma_n = 9.73 \times 10^{-3} [\mho/m]$ , $\mu_{n+1} = \mu_0$ , $\epsilon_{n+1} = 1.70\epsilon_0$ , $\sigma_{n+1} = 5.60 \times 10^{-2} [\mho/m]$ , $\theta_{i1} = 30^\circ$ , $P_2 = -0.59 \times 10^{10}$	44
Figure 2.6	An example of double exponential input waveform	45
Figure 2.7	(a) Numerical comparison of the transient reflected electric field waveform for the input waveform shown in Figure 2.6 with the IFFT (TE polarization): $\mu_n = \mu_0$ , $\epsilon_n = \epsilon_0$ , $\sigma_n = 0[\mho/m]$ , $\mu_{n+1} = \mu_0$ , $\epsilon_{n+1} = 72\epsilon_0$ , $\sigma_{n+1} = 4[\mho/m]$ , $\theta_{i1} = 30^\circ$ , $P_2 = 0.64 \times 10^{10}$	46
Figure 2.7	(b) Numerical comparison of the transient reflected electric field waveform for the input waveform shown in Figure 2.6 with the IFFT (TE polarization): $\mu_n = \mu_0$ , $\epsilon_n = 2.59\epsilon_0$ , $\sigma_n = 9.73 \times 10^{-3} [\mho/m]$ , $\mu_{n+1} = \mu_0$ , $\epsilon_{n+1} = 1.70\epsilon_0$ , $\sigma_{n+1} = 5.60 \times 10^{-2} [\mho/m]$ , $\theta_{i1} = 30^{\circ}$ , $P_2 = -0.59 \times 10^{10}$	47
Figure 2.8	(a) The transient reflected electrical field waveform for a unit step excitation: $\mu_n = \mu_0$ , $\epsilon_n = \epsilon_0$ , $\sigma_n = 0$ , $\mu_{n+1} = \mu_0$ , $\epsilon_{n+1} = 9\epsilon_0$ , $\sigma_{n+1} = 1.00 \times 10^{-3} [\mho/m]$ , $\theta_i = 0^{\circ}$	49
Figure 2.8	(b) The transient transmitted electrical field waveform for a unit step excitation: $\mu_n = \mu_0$ , $\epsilon_n = \epsilon_0$ , $\sigma_n = 0$ , $\mu_{n+1} = \mu_0$ , $\epsilon_{n+1} = 9\epsilon_0$ , $\sigma_{n+1} = 1.00 \times 10^{-3} [\mho/m]$ , $\theta_i = 30^{\circ}$	50
Figure 2.9	Time domain reduced interfacial reflection coefficients for various values of permittivity (TE polarization): $\mu_n = \mu_{n+1} = \mu_0$ , $\epsilon_n = 2.59\epsilon_0$ , $\sigma_n = 9.73 \times 10^{-3}$ , $\sigma_{n+1} = 5.60 \times 10^{-2} [\mho/m]$ , $\theta_{i1} = 30^{\circ}$ .	52

Figure 2.11 Time  $\operatorname{Val}^{1} \operatorname{P}$ 2.50.

> Figure 2.12 Time value 2.7%

10 - 0

Figure 2.13 Trans lariza:

 $P_2 =$ 

Figure 2.14 Trans tion

C. : Figure 3.1 The :

at an Figure 3.2 Numa.

Itiles

 $\mu_{\tau} = \frac{1}{10}$ 

Figure 3.3 Number field the I

 $\mu_{\tau,-1}$ Figure 3.4 (a) T

 $\theta_i = 0$ 

Figure 3.4 (b) T

 $exp_{0}; \\ \theta_{i} = .$ 

Figure 3.5 Times  $V_{\mathbf{d}_{i-1}^{(i)},i}$ 

 $\sigma_{\rm r_i} =$ 

Egge 3.6 Time  $V_{\mathbf{G}_{\mathbf{a}}^{-1}(\underline{1})}$ 

 $\mu_{\gamma} =$ 

Figure 2.10	Time domain reduced interfacial reflection coefficients for various values of permeability (TE polarization): $\mu_n = 1.5\mu_0$ , $\epsilon_n = 2.59\epsilon_0$ , $\sigma_n = 9.73 \times 10^{-3}$ , $\epsilon_{n+1} = 1.70\epsilon_0$ , $\sigma_{n+1} = 5.60 \times 10^{-2} [\mho/m]$ , $\theta_{i1} = 30^{\circ}$	53
Figure 2.11	Time domain reduced interfacial reflection coefficients for various values of conductivity (TE polarization): $\mu_n = \mu_{n+1} = \mu_0$ , $\epsilon_n = 2.59\epsilon_0$ , $\epsilon_{n+1} = 1.70\epsilon_0$ , $\sigma_{n+1} = 5.60 \times 10^{-2} [\mho/m]$ , $\theta_{i1} = 30^\circ$	54
Figure 2.12	Time domain reduced interfacial reflection coefficients for various values of incident angle (TE polarization): $\mu_n = 1.5\mu_0$ , $\epsilon_n = 2.59\epsilon_0$ , $\sigma_n = 9.73 \times 10^{-3}$ , $\mu_{n+1} = \mu_0$ , $\epsilon_{n+1} = 1.70\epsilon_0$ , $\sigma_{n+1} = 5.60 \times 10^{-2} [\mho/m]$	55
Figure 2.13	Transient interfacial reflection coefficient for $P_2 < 0$ (TE polarization): $\mu_n = \mu_0$ , $\epsilon_n = 2.59\epsilon_0$ , $\sigma_n = 9.73 \times 10^{-3} [\mho/m]$ , $\mu_{n+1} = \mu_0$ , $\epsilon_{n+1} = 1.7\epsilon_0$ , $\sigma_{n+1} = 5.60 \times 10^{-2} [\mho/m]$ , $\theta_{i1} = 30^\circ$ , $P_2 = -0.59 \times 10^{10}$ , and $a = 0.37$	63
Figure 2.14	Transient interfacial reflection coefficient for $P_2 > 0$ (TE polarization): $\mu_n = \mu_0$ , $\epsilon_n = \epsilon_0$ , $\sigma_n = 0[\mho/m]$ , $\mu_{n+1} = \mu_0$ , $\epsilon_{n+1} = 72\epsilon_0$ , $\sigma_{n+1} = 4[\mho/m]$ , $\theta_{i1} = 30^\circ$ , $P_2 = 0.64 \times 10^{10}$ and $a = 0.65$	68
Figure 3.1	The incident, reflected and transmitted TM-polarized plane wave at an interface.	70
Figure 3.2	Numerical comparison of the derived transient reduced interfacial reflection coefficient with that from the IFFT (TM polarization): $\mu_n = \mu_0$ , $\epsilon_n = \epsilon_0$ , $\sigma_n = 0[\mho/m]$ , $\mu_{n+1} = \mu_0$ , $\epsilon_{n+1} = 72\epsilon_0$ , $\sigma_{n+1} = 4[\mho/m]$ , $\theta_{i1} = 30^\circ$	91
Figure 3.3	Numerical comparison of the derived transient reflected electric field waveform for the input waveform shown in Figure 2.6 with the IFFT (TM polarization): $\mu_n = \mu_0$ , $\epsilon_n = \epsilon_0$ , $\sigma_n = 0[\mho/m]$ , $\mu_{n+1} = \mu_0$ , $\epsilon_{n+1} = 72\epsilon_0$ , $\sigma_{n+1} = 4[\mho/m]$ , $\theta_{i1} = 30^\circ$	93
Figure 3.4	(a) The transient reflected magnetic field waveform for a double exponential excitation : $\epsilon = 10\epsilon_0$ , $\mu = \mu_0$ , $\sigma = 2 \times 10^{-2} [\mho/m]$ , $\theta_i = 45^{\circ}$	94
Figure 3.4	(b) The transient transmitted magnetic field waveform for a double exponential excitation : $\epsilon = 10\epsilon_0$ , $\mu = \mu_0$ , $\sigma = 2 \times 10^{-2} [\mho/m]$ , $\theta_i = 45^{\circ}$	95
Figure 3.5	Time domain reduced interfacial reflection coefficients for various values of permittivity (TM polarization): $\epsilon_n = \epsilon_0$ , $\mu_n = \mu_{n+1} = \mu_0$ , $\sigma_n = 0$ , $\sigma_{n+1} = 4[\mho/m]$ , $\theta_{i1} = 30^{\circ}$	97
Figure 3.6	Time domain reduced interfacial reflection coefficients for various values of permeability (TM polarization): $\epsilon_n = \epsilon_0$ , $\epsilon_{n+1} = 72\epsilon_0$ , $\mu_n = \mu_0$ , $\sigma_n = 0$ , $\sigma_{n+1} = 4[\mho/m]$ , $\theta_{i1} = 30^\circ$ .	98

Figure 3.7 Tim. valu μ, =

Figure 3.8 Time  $Va_{\bullet}^{(1)})$ μ, =

Figure 4.1 The

Figure 4.2 Num.  $\mathbf{w}(t)$  $l_n =$ 

Figure 4.3 A. de

Figure 4.4 Numer layer.

 $\mu_{c}$  .

Egge 4.5 Number layeres

 $\mu_0, \epsilon_1$ Figure 4.6 Mustip

Matie:  $\mu_3 =$ 

 $C_4 = 1$ 

Figure 4.7 Mintip

 $\begin{array}{l}
\vdots \quad \mu_2 \\
\epsilon_3 = \\
\sigma_4 = \epsilon
\end{array}$ 

Figure 4.8 Marily  $\vdots \mu_{\bullet}$   $\mathfrak{S} =$ 

 $\sigma_{i} = 0$ 

Figure 4.9 Index 5 laye

0.1 ::.

Pare 4.10 Time  ${}_{i}TE_{i}$ 

 $\mu_{\beta} = 2.5 G_{\alpha_{\beta}}$ 

Egge 5.1 Experi

Figure 3.7	Time domain reduced interfacial reflection coefficients for various values of conductivity (TM polarization): $\epsilon_n = \epsilon_0$ , $\epsilon_{n+1} = 72\epsilon_0$ , $\mu_n = \mu_{n+1} = \mu_0$ , $\sigma_n = 0[\mathfrak{V}/m]$ , $\theta_{i1} = 30^{\circ}$	99
Figure 3.8	Time domain reduced interfacial reflection coefficients for various values of incident angle (TM polarization): $\epsilon_n = \epsilon_0$ , $\epsilon_{n+1} = 72\epsilon_0$ , $\mu_n = \mu_{n+1} = \mu_0$ , $\sigma_n = 0$ , $\sigma_{n+1} = 4[\mho/m]$	100
Figure 4.1	The $n^{th}$ layer of a multi-layered environment	102
Figure 4.2	Numerical comparison of the derived transient propagation term with that from the IFFT: $\mu_n = \mu_0$ , $\epsilon_n = 72\epsilon_0$ , $\sigma_n = 4[\mathfrak{O}/m]$ , $l_n = 0.01[m]$ , $\theta_{i1} = 30^{\circ}$	108
Figure 4.3	A double exponential input waveform	111
Figure 4.4	Numerical comparison of the derived overall reflection from a 3 layered medium with that from the IFFT (TE polarization): $\mu_2 = \mu_0$ , $\epsilon_2 = 2.59\epsilon_0$ , $\sigma_2 = 0[\mho/m]$ , $l_2 = 0.1[m]$ , $\theta_{i1} = 30^\circ$	112
Figure 4.5	Numerical comparison of the derived overall reflection from a 3 layered medium with that from the IFFT (TM polarization): $\mu_2 = \mu_0$ , $\epsilon_2 = 2.59\epsilon_0$ , $\sigma_2 = 0[\mho/m]$ , $l_2 = 0.1[m]$ , $\theta_{i1} = 30^\circ$	113
Figure 4.6	Mutiple reflection from a lossless 5 layered medium (TE polarization): $\mu_2 = \mu_0$ , $\epsilon_2 = 2.59\epsilon_0$ , $\sigma_2 = 0[\mho/m]$ , $l_2 = 0.1[m]$ , $\mu_3 = \mu_0$ , $\epsilon_3 = \epsilon_0$ , $\sigma_3 = 0[\mho/m]$ , $l_3 = 0.1[m]$ , $\mu_4 = \mu_0$ , $\epsilon_4 = 2.59\epsilon_0$ , $\sigma_4 = 0[\mho/m]$ , $l_4 = 0.1[m]$ , $\theta_{i1} = 30^\circ$	114
Figure 4.7	Mutiple reflection from a lossy 5 layered medium (TE polarization) : $\mu_2 = \mu_0$ , $\epsilon_2 = 2.59\epsilon_0$ , $\sigma_2 = 0[\mho/m]$ , $l_2 = 0.1[m]$ , $\mu_3 = \mu_0$ , $\epsilon_3 = 55\epsilon_0$ , $\sigma_3 = 16.7[\mho/m]$ , $l_3 = 0.1[m]$ , $\mu_4 = \mu_0$ , $\epsilon_4 = 2.59\epsilon_0$ , $\sigma_4 = 0[\mho/m]$ , $l_4 = 0.1[m]$ , $\theta_{i1} = 30^\circ$	115
Figure 4.8	Mutiple reflection from a lossy 5 layered medium (TM polarization) : $\mu_2 = \mu_0$ , $\epsilon_2 = 2.59\epsilon_0$ , $\sigma_2 = 0[\mho/m]$ , $l_2 = 0.1[m]$ , $\mu_3 = \mu_0$ , $\epsilon_3 = 55\epsilon_0$ , $\sigma_3 = 16.7[\mho/m]$ , $l_3 = 0.1[m]$ , $\mu_4 = \mu_0$ , $\epsilon_4 = 2.59\epsilon_0$ , $\sigma_4 = 0[\mho/m]$ , $l_4 = 0.1[m]$ , $\theta_{i1} = 30^\circ$	116
Figure 4.9	Indentification of indivisual reflection in overall scattering from a 5 layered medium (TE polarization): $\mu_2 = \mu_0$ , $\epsilon_2 = 2.59\epsilon_0$ , $\sigma_2 = 0[\mho/m]$ , $l_2 = 0.1[\mathrm{m}]$ , $\mu_3 = \mu_0$ , $\epsilon_3 = 55\epsilon_0$ , $\sigma_3 = 16.7[\mho/m]$ , $l_3 = 0.1[\mathrm{m}]$ , $\mu_4 = \mu_0$ , $\epsilon_4 = 2.59\epsilon_0$ , $\sigma_4 = 0[\mho/m]$ , $l_4 = 0.1[\mathrm{m}]$ , $\theta_{i1} = 30^\circ$ .	118
Figure 4.10	Time domain overall reflection for various values of incident angle (TE polarization): $\mu_2 = \mu_0$ , $\epsilon_2 = 2.59\epsilon_0$ , $\sigma_2 = 0[\mho/m]$ , $l_2 = 0.1[m]$ , $\mu_3 = \mu_0$ , $\epsilon_3 = 55\epsilon_0$ , $\sigma_3 = 16.7[\mho/m]$ , $l_3 = 0.1[m]$ , $\mu_4 = \mu_0$ , $\epsilon_4 = 2.59\epsilon_0$ , $\sigma_4 = 0[\mho/m]$ , $l_4 = 0.1[m]$	119
Figure 5.1	Experimental set up	122

Figure 5.2 (a lb work

Figure 5.2 (b) S form.

Figure 5.3 Test

Egge 5.4 - a T  $\theta_{\rm to} = 1$ 

fişue 5.4 - (b. 1 p-1y-

Figure 5.5 (a. 7)

6: - 7 Figure 5.5 h F:

plate

Figure 5.6 (a. S)

Figure 5.6  $\pm i = S_1$ 

Figure 5.7 (a. Ca

Figure 5.7 (b) C

Spect:

Specia

Regres. 8 a T:

al.:].

Figure 5.8 (b. T:  $a_{i,\, j})_{i}$ 

Figure 5.9 (a Tr  $a_{\Pi_{\overline{S}}^{-1}_{p}}$ 

Figure 5.9 (b) T:  $\mathtt{d}!_{i, \overline{\mathbb{S}}^{1}_{+}}.$ 

Figure 5.10 (a) Tr  $\operatorname{al}[q]_{t}$ 

figue 5.10 (b). Tr

ang]<sub>f</sub>.

Figure 5.11 (a) Tr dence

हेड्ड 5.11 के T:

detre. Figure 5.12 (a) T:

 $\mathrm{d}\omega_{L^{p_{1}}}$ 

Figure 5.2	(a) Impulse shaped waveform transmitted from pulse forming network	123
Figure 5.2	(b) Spectrum of impulse shaped waveform transmitted from pulse forming network	124
Figure 5.3	Test measurement of background noise level for the arch range	128
Figure 5.4	(a) Time domain raw measurement data of a polystyrene plate with $\theta_{i1}=6^\circ$ (TE polarization)	130
Figure 5.4	(b) Frequency domain spectrum of raw measurement data of a polystyrene plate with $\theta_{i1}=6^{\circ}$ (TE polarization)	131
Figure 5.5	(a) Time domain raw measurement data of a PEC plate with $\theta_{i1} = 6^{\circ}$ (TE polarization)	132
Figure 5.5	(b) Frequency domain spectrum of raw measurement data of a PEC plate with $\theta_{i1} = 6^{\circ}$ (TE polarization)	133
Figure 5.6	(a) Spectrum of intermediate system function	134
Figure 5.6	(b) Spectrum of intermediate system function after truncation	135
Figure 5.7	(a) Calibrated trasient scattering from a polystyrene layer without spectrum truncation (TE polarization)	136
Figure 5.7	(b) Calibrated trasient scattering from a polystyrene layer with spectrum truncation (TE polarization)	137
Figure 5.8	(a) Transient scattered field from a plexiglass layer with incidence angle 6° (TE polarization)	138
Figure 5.8	(b) Transient scattered field from a plexiglass layer with incidence angle 6° (TM polarization)	139
Figure 5.9	(a) Transient scattered field from a plexiglass layer with incidence angle 15° (TE polarization)	140
Figure 5.9	(b) Transient scattered field from a plexiglass layer with incidence angle 15° (TM polarization)	141
Figure 5.10	(a) Transient scattered field from a plexiglass layer with incidence angle 30° (TE polarization)	142
Figure 5.10	(b) Transient scattered field from a plexiglass layer with incidence angle 30° (TM polarization)	143
Figure 5.11	(a) Transient scattered field from a plexiglass container with incidence angle 6° (TE polarization)	144
Figure 5.11	(b) Transient scattered field from a plexiglass container with incidence angle 6° (TM polarization)	145
Figure 5.12	(a) Transient scattered field from a plexiglass container with incidence angle 15° (TE polarization)	146

Figure 5.12 (b details

figure 5.13 a - 1 deti -

Figure 5.13 (b. 1) detac

Figure 5.14 (a) C plex...

lariza Egue 5.14 ab Ca

plexit TE p

Figure 5.15 - 6 .

Figure 5.16 Trial ered

Figure 5.17 a 7 included

Figure 5.17 (b)

Figure 5.18 - a inci

Figure 5.18 % inc.

Figure 5.19 a

ine

हिन्द्र 5.19 - हे in

Figure 5.12	(b) Transient scattered field from a plexiglass container with incidence angle 15° (TM polarization)	147
Figure 5.13	(a) Transient scattered field from a plexiglass container with incidence angle 30° (TE polarization)	149
Figure 5.13	(b) Transient scattered field from a plexiglass container with incidence angle 30° (TM polarization)	150
Figure 5.14	(a) Comparison of trasient reflection from a mechanically adhered plexiglass plates with that for a single material ( $\theta_{i1} = 6^{\circ}$ , TE polarization)	151
Figure 5.14	(b) Comparison of trasient reflection from a mechanically adhered plexiglass plates with that for an air gap inserted model ( $\theta_{i1} = 6^{\circ}$ , TE polarization)	152
Figure 5.15	$-\epsilon"/\epsilon_0$ curve for water at 20°C given by the Debye model	153
Figure 5.16	Trial measurements for trasient scattered field from a 5 lossy layered medium with incidence angle 6° (TE polarization)	155
Figure 5.17	(a) Transient scattered field from a 5 lossy layered medium with incidence angle 6° (TE polarization)	156
Figure 5.17	(b) Transient scattered field from a 5 lossy layered medium with incidence angle 6° (TM polarization)	157
Figure 5.18	(a) Transient scattered field from a 5 lossy layered medium with incidence angle 15° (TE polarization)	158
Figure 5.18	(b) Transient scattered field from a 5 lossy layered medium with incidence angle 15° (TM polarization)	159
Figure 5.19	(a) Transient scattered field from a 5 lossy layered medium with incidence angle 30° (TE polarization)	160
Figure 5.19	(b) Transient scattered field from a 5 lossy layered medium with incidence angle 30° (TM polarization)	161

The topic of this dationiagnetic v zaferni platar war lis assumed that Stopical materi unductivity. A.s. The first layer is a puarizations of th magnetic TM po Although this each layer in the r Millem has a wi ispection, geoph amining that t Talina, or on re brain solution with anount and Employee the ex to available. Ti Glation directly

Station form

demagnetic wave

ided to solve this

#### CHAPTER 1

#### INTRODUCTION

The topic of this study is to find an analytical solution for the transient scattering of electromagnetic waves from a multi-layered medium, excited at oblique incidence by a uniform plane wave. The geometry for the structure of concern is shown in Figure 1.1. It is assumed that each layer of the multi-layered medium consists of a homogeneous, isotropical material, and has frequency independent permeability, permittivity and conductivity. Also, each layer is assumed to have infinite width, but finite thickness. The first layer is assumed to be lossless. Transient solutions are obtained for both polarizations of the incident plane wave, i.e. transverse electic (TE) and transverse magnetic (TM) polarization.

Although this research is motivated by a desire to estimate the parameters of each layer in the medium by using its time domain scattered field, the solution to this problem has a wide area of practical applications, such as industrial non-destructive inspection, geophysical probing and subsurface communication. Therefore, it is not surprising that there have been many studies on transient scattering from a lossy medium, or on related topics in the field of electromagnetics. While the frequency domain solution to this problem in terms of Fresnel's reflection coefficient is already well known, and can be found in many text books and papers, to the best of our knowledge the exact analytical transient solution for an arbitrary input waveform is not available. This is partly because of the difficulty in solving the time domain wave equation directly.

Stratton formulated the inverse Laplace transform pair for propagation of electromagnetic wave in a dispersive medium [1], and since then many researchers have tried to solve the scattering problem by formulating the solution in the frequency do-

tasform pair.

approach is tal n a multi-layer

deprous soluri.

Werall Ital. sie:

tits are veriti

In the following

interface in a l The inverse F

obtain the tra

main and then finding the exact analytical inverse transform. Many of these studies use certain types of approximations; e.g., the diffusion approximation obtained by neglecting the displacement current term in Maxwell's equations [2], or restrictions on the incident angle and material parameters [3]. Other researchers have formulated the problem directly in the time domain, and have employed numerical techniques to solve it [4], [5]. Various contour integral techniques in the Laplace domain had been developed and closed form transient solutions for both polarizations had been obtained for a double exponential and unit step input waveform excitation using incomplete Lipschitz-Hankel integrals (ILHI's) in [6], [7]. Though these solutions are restricted to specific input waveforms and are valid for a single interface, they may have been the first closed form transient solutions to the problem. Therefore, the results derived in this study are verified by those previous works.

In this thesis, the problem is formulated in the frequency domain first, in the same manner as the previous studies. The constant offset value in the derived frequency domain reflection coefficient is then identified and subtracted from the original expression and its inverse Fourier transform is determined. Next, the reduced form of the original reflection coefficient is manipulated so as to use known inverse Fourier transform pairs. This method was developed for a single interface in [8]. This same approach is taken, but extended to treat the more general case of a single interface in a multi-layered medium. Proper branch cuts are derived and applied for this more rigorous solution. The results for a single interface reflection are used to derive the overall transient reflection from a multi-layered medium. Finally, the derived solutions are verified by laboratory experiments.

In the following chapter, the frequency domain reflection coefficients for a single interface in a multi-layered medium are formulated and classified for TE polarization. The inverse Fourier transform of each classified reflection coefficient is performed to obtain the transient reflection coefficient. The various aspects of the transient forms,

including causality problems, are discussed, and approximate forms, which might be useful in practical applications, are derived. The same procedures are taken to obtain the transient reflection coefficients for TM polarization in Chapter 3. The transient reflection coefficients for multi-layered medium are derived in Chapter 4 using series expansion in the frequency domain and applying the convolution theorem. The descriptions for procedures and results of experiments performed to verify the derived formulas are provided in Chapter 5.

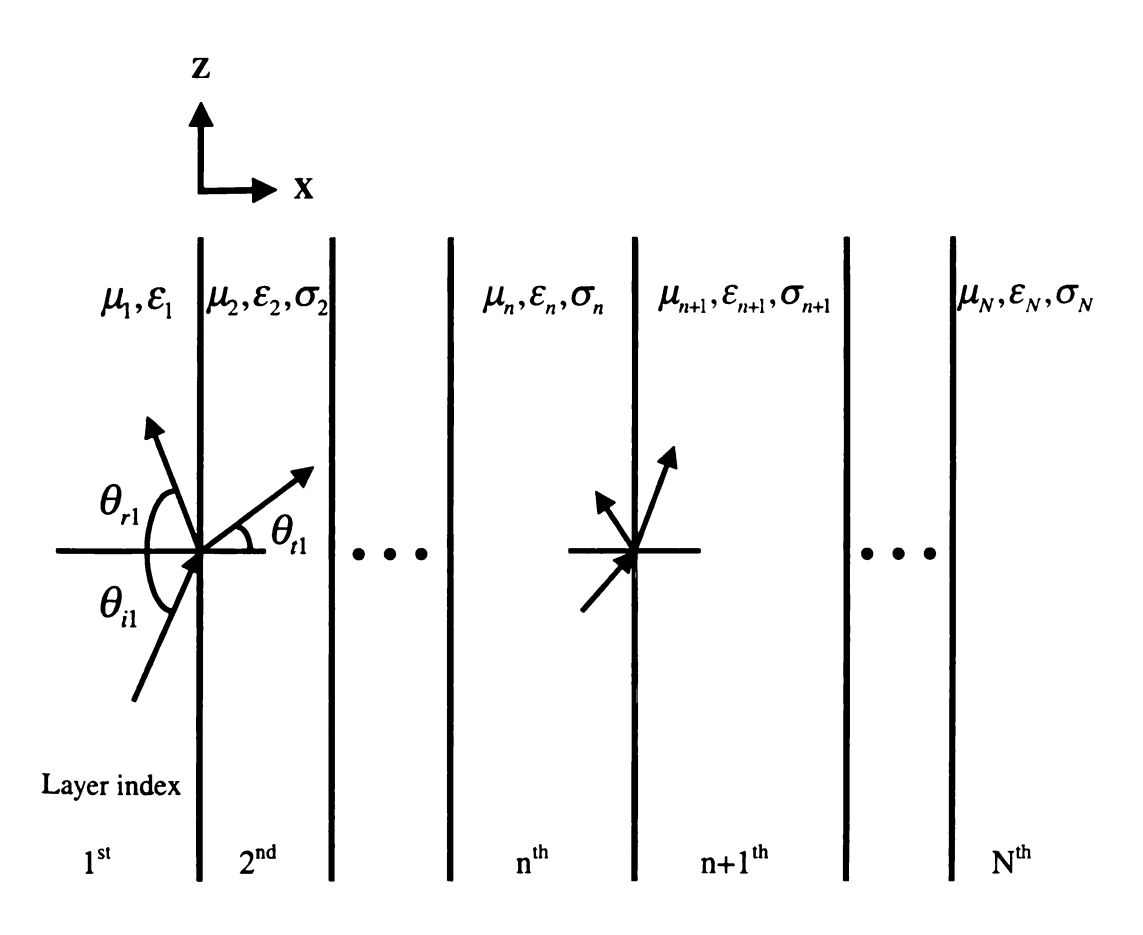


Figure 1.1. The geometry for analysis of transient plane wave scattering from a multi-layered medium.

The interfacial res

hariely extended

tansent scatterin

nividial inversa

ions of transien

hand before older

unisem in effe

deficient will

Im is obtained

Sme algebraic p

Miestion (coeffic

# 2.2 Frequen

2.2.1 Deriva

Consider an is

Figure 2.1. wh

THE PARTY

Em region 1

### CHAPTER 2

# INTERFACIAL REFLECTION COEFFICIENTS FOR TE-POLARIZATION

### 2.1 Introduction

The interfacial reflection coefficient is defined as the ratio of reflected wave amplitude to incident wave amplitude at an interface between two layers, each of which has infinitely extended depth as shown in Figure 2.1. Because, in this study, the overall transient scattering from a multi-layered medium is derived from a combination of the individual interfacial coefficients for the layers (as discussed in chapter 4), the closed forms of transient interfacial reflection coefficients for TE-polarized plane waves are found before obtaining the total transient scattered field from the medium. To find the transient interfacial reflection coefficient, the frequency domain interfacial reflection coefficient, which is known as Fresnel's coefficient, is found first. Then the transient form is obtained using the inverse Fourier transform from a transform table after some algebraic manipulation. Finally, approximate forms of the transient interfacial reflection coefficients are derived.

## 2.2 Frequency Domain Formulation of Interfacial Reflection Coefficient

### 2.2.1 Derivation

Consider an interface between two homogeneous, isotropic materials as shown in Figure 2.1, where region n has time-independent constitutive parameters  $(\mu_n, \epsilon_n, \sigma_n)$  while region (n+1) has  $(\mu_{n+1}, \epsilon_{n+1}, \sigma_{n+1})$ . A plane wave is assumed to be incident from region 1 onto interface N between the two regions. From Maxwell's equations,

$$\nabla \times \bar{E}(x, z, \omega) = -j\omega \mu_n \bar{H}(x, z, \omega)$$
 (2.1)

Figure 2.1.

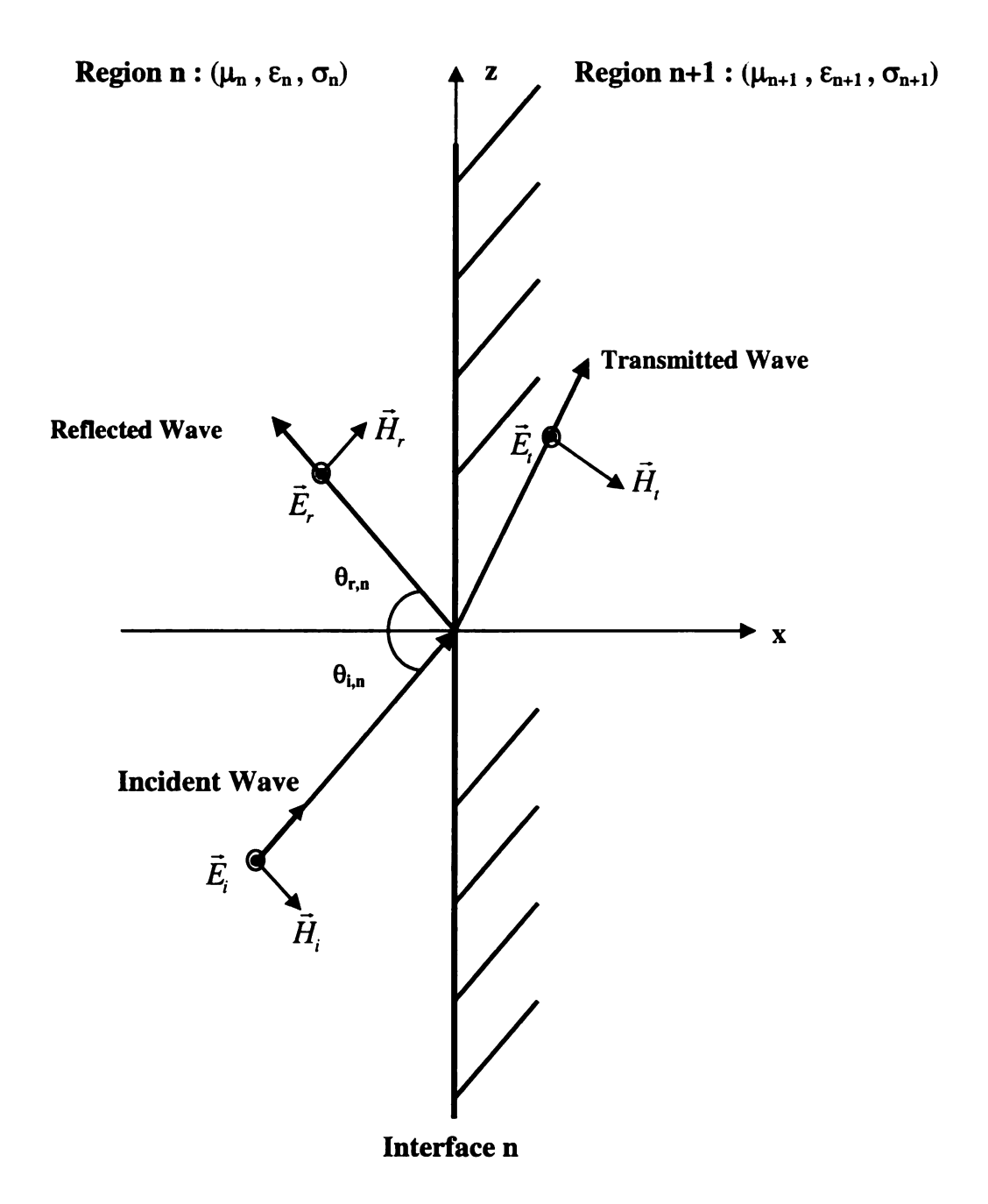


Figure 2.1. The incident, reflected and transmitted TE-polarized plane wave at an interface.

The solution for

there the comp.

Only if region in

The speak of

Mr 184 - L. . . . .

$$\nabla \times \bar{H}(x, z, \omega) = (\sigma_n + j\omega\epsilon_n)\bar{E}(x, z, \omega)$$
 (2.2)

and the vetor Helmholtz equation for the electric field of region n is

$$\nabla^2 \bar{E}(x, z, \omega) - \gamma_n^2 \bar{E}(x, z, \omega) = 0 \tag{2.3}$$

where the propagation constant for the n-th layer is given by

$$\gamma_n^2 = j\omega\mu_n(\sigma_n + j\omega\epsilon_n) = -\omega^2\mu_n\epsilon_n + j\omega\mu_n\sigma_n. \tag{2.4}$$

For TE polarization  $\bar{E} = \hat{y}E_y$  and (2.3) can be rewritten as

$$\left(\frac{\partial^2}{\partial x^2} + \frac{\partial^2}{\partial z^2}\right) E_y(x, z, \omega) - \gamma_n^2 E_y(x, z, \omega) = 0.$$
 (2.5)

The solution for the electric field is

$$\bar{E}(x,z,\omega) = \hat{y}E_o(\omega)e^{\gamma_{nx}x + \gamma_{nz}z}$$
(2.6)

where the components of the propagation constants are defined by

$$\gamma_n^2 = \gamma_{nx}^2 + \gamma_{nx}^2. \tag{2.7}$$

Only if region n is the first region of a multi-layered material and this region is lossless will we speak of an angle of incidence and an angle of reflection. Otherwise, we will only use  $\gamma_{nx}^i, \gamma_{nz}^i, \gamma_{nx}^r$  and  $\gamma_{nz}^r$ . For the incident wave,

$$\gamma_{nx} = \gamma_{nx}^i = \gamma_n \cos \theta_{in} \tag{2.8}$$

$$\gamma_{nz} = \gamma_{nz}^i = \gamma_n \sin \theta_{in}, \tag{2.9}$$

and while for \*

Here  $\theta_{i,h}$  is the  $\phi_{i}$ 

21. The market

Й г. :

Esimmary, the

Ē. z. :

 $ilde{H}_{i}(x_{i})$ 

Ē. ..

Ĥ. J.

In region in

and, while for the reflected wave

$$\gamma_{nx} = \gamma_{nx}^r = -\gamma_n \cos \theta_{rn} \tag{2.10}$$

$$\gamma_{nz} = \gamma_{nz}^r = \gamma_n \sin \theta_{rn}. \tag{2.11}$$

Here  $\theta_{i,n}$  is the angle of incidence and  $\theta_{r,n}$  is the angle of reflection, as shown in Figure 2.1. The magnetic field in region n is obtained by

$$\bar{H}(x,z,\omega) = -\frac{1}{j\omega\mu_{n}}\nabla \times \bar{E}(x,z,\omega)$$

$$= -\frac{1}{j\omega\mu_{n}} \left\{ -\hat{x}\frac{\partial E_{y}}{\partial z} + \hat{z}\frac{\partial E_{y}}{\partial x} \right\}$$

$$= -\frac{E_{o}(\omega)}{j\omega\mu_{n}} \left\{ -\hat{x}\gamma_{nz}e^{\gamma_{nx}x+\gamma_{nz}z} + \hat{z}\gamma_{nx}e^{\gamma_{nx}x+\gamma_{nz}z} \right\}$$

$$= \hat{x}\frac{\gamma_{nz}}{j\omega\mu_{n}}E_{o}(\omega)e^{\gamma_{nx}x+\gamma_{nz}z} - \hat{z}\frac{\gamma_{nx}}{j\omega\mu_{n}}E_{o}(\omega)e^{\gamma_{nx}x+\gamma_{nz}z}. \quad (2.12)$$

In summary, the fields in region n can be expressed as

$$\bar{E}_{i}(x,z,\omega) = \hat{y}E_{io}(\omega)e^{\gamma_{nx}^{i}x+\gamma_{nz}^{i}z}$$

$$\bar{H}_{i}(x,z,\omega) = \hat{x}\frac{\gamma_{nz}^{i}}{j\omega\mu_{n}}E_{io}(\omega)e^{\gamma_{nx}^{i}x+\gamma_{nz}^{i}z} - \hat{z}\frac{\gamma_{nx}^{i}}{j\omega\mu_{n}}E_{io}(\omega)e^{\gamma_{nx}^{i}x+\gamma_{nz}^{i}z} \qquad (2.13)$$

$$\bar{E}_{r}(x,z,\omega) = \hat{y}E_{ro}(\omega)e^{\gamma_{nx}^{r}x+\gamma_{nz}^{r}z}$$

$$\bar{H}_{r}(x,z,\omega) = \hat{x}\frac{\gamma_{nz}^{r}}{j\omega\mu_{n}}E_{io}(\omega)e^{\gamma_{nx}^{r}x+\gamma_{nz}^{r}z} - \hat{z}\frac{\gamma_{nx}^{r}}{j\omega\mu_{n}}E_{io}(\omega)e^{\gamma_{nx}^{r}x+\gamma_{nz}^{r}z}.$$
(2.14)

In region (n+1), (2.3) is

$$\nabla^2 \bar{E}(x, z, \omega) - \gamma_{n+1}^2 \bar{E}(x, z, \omega) = 0 \tag{2.15}$$

where the propagation constant is

$$\gamma_{n+1}^2 = j\omega\mu_{n+1}(\sigma_{n+1} + j\omega\epsilon_{n+1}) = -\omega^2\mu_{n+1}\epsilon_{n+1} + j\omega\mu_{n+1}\sigma_{n+1}. \tag{2.16}$$

Then, the vector Helmhotz equation for the electric field in region (n+1) (i.e., the transmitted electric field) is given by

$$\left(\frac{\partial^2}{\partial x^2} + \frac{\partial^2}{\partial z^2}\right) E_y(x, z, \omega) - \gamma_{n+1}^2 E_y(x, z, \omega) = 0.$$
 (2.17)

This has the solution

$$\bar{E}_t(x, z, \omega) = \hat{y} E_{to}(\omega) e^{\gamma_{n+1,z} x + \gamma_{n+1,z} z}$$
(2.18)

where the components of propagation constants are defined by

$$\gamma_{n+1}^2 = \gamma_{n+1,x}^2 + \gamma_{n+1,z}^2. \tag{2.19}$$

When both regions n and (n+1) are lossless, we may define a transmission angle  $\theta_t$  such that

$$\gamma_{n+1,x} = \gamma_{n+1} \cos \theta_t \tag{2.20}$$

$$\gamma_{n+1,z} = \gamma_{n+1} \sin \theta_t. \tag{2.21}$$

The transmitted magnetic field is given by

$$\bar{H}_{t}(x,z,\omega) = -\frac{1}{j\omega\mu_{n+1}} \nabla \times \bar{E}_{t}(x,z,\omega) 
= -\frac{1}{j\omega\mu_{n+1}} \left\{ -\hat{x}\frac{\partial E_{y}}{\partial z} + \hat{z}\frac{\partial E_{y}}{\partial x} \right\} 
= -\frac{E_{to}(\omega)}{j\omega\mu_{n+1}} \left\{ -\hat{x}\gamma_{n+1,z}e^{\gamma_{n+1,z}x+\gamma_{n+1,z}z} + \hat{z}\gamma_{n+1,x}e^{\gamma_{n+1,x}x+\gamma_{n+1,z}z} \right\}$$

It summary, the

: (1.2.2) :

 $\hat{H}_{1}(z,z,\omega) = 0$ 

To obtain the two boundary co-continuity of the for all z.

Ü.,

Then, to satisfy

The be sailed, of

$$= \hat{x} \frac{\gamma_{n+1,z}}{j\omega\mu_{n+1}} E_{to}(\omega) e^{\gamma_{n+1,x}x+\gamma_{n+1,z}z} - \hat{z} \frac{\gamma_{n+1,x}}{j\omega\mu_{n+1}} E_{to}(\omega) e^{\gamma_{n+1,x}x+\gamma_{n+1,z}z}.$$
(2.22)

In summary, the fields in region (n+1) can be expressed as

$$\bar{E}_{t}(x,z,\omega) = \hat{y}E_{to}(\omega)e^{\gamma_{n+1,x}x+\gamma_{n+1,z}z}$$

$$\bar{H}_{t}(x,z,\omega) = \hat{x}\frac{\gamma_{n+1,z}}{j\omega\mu_{n+1}}E_{to}(\omega)e^{\gamma_{n+1,x}x+\gamma_{n+1,z}z} - \hat{z}\frac{\gamma_{n+1,x}}{j\omega\mu_{n+1}}E_{to}(\omega)e^{\gamma_{n+1,x}x+\gamma_{n+1,z}z}.$$
(2.23)

To obtain the ratio of the reflected and transmitted electric field amplitudes, two boundary conditions are applied. The first one is the boundary condition for continuity of the tangential components of the electric field at the interface. That is, for all z,

$$\bar{E}_i(x=0^-) + \bar{E}_r(x=0^-) = \bar{E}_t(x=0^+)$$

or,

$$E_{io}(\omega)e^{\gamma_{nz}^{i}z} + E_{ro}(\omega)e^{\gamma_{nz}^{r}z} = E_{to}(\omega)e^{\gamma_{n+1,z}z}. \tag{2.24}$$

Then, to satisfy the above boundary condition, the equations

$$\gamma_{nz}^i = \gamma_{nz}^r = \gamma_{n+1,z} \tag{2.25}$$

$$E_{io}(\omega) + E_{ro}(\omega) = E_{to}(\omega) \tag{2.26}$$

must be satisfied. For lossless materials, (2.25) becomes

$$\gamma_n \sin \theta_i = \gamma_n \sin \theta_r = \gamma_{n+1} \sin \theta_t \tag{2.27}$$

and thus

$$\theta_i = \theta_r \tag{2.28}$$

$$\frac{\gamma_n}{\gamma_{n+1}} = \frac{\sin \theta_t}{\sin \theta_i} \tag{2.29}$$

which are the well-known Snell's law of reflection and refraction. From (2.7), (2.25) and considering the direction of propagation,

$$\gamma_{nx}^i = -\gamma_{nx}^r = \gamma_{nx}. \tag{2.30}$$

The second boundary condition requires the continuity of tangential magnetic field on the interface. That is, for all z,

$$\bar{H}_{iz}(x=0^-) + \bar{H}_{rz}(x=0^-) = \bar{H}_{tz}(x=0^+)$$

or,

$$-\frac{\gamma_{nx}^{i}}{j\omega\mu_{n}}E_{io}(\omega)e^{\gamma_{nz}^{i}z} - \frac{\gamma_{nx}^{r}}{j\omega\mu_{n}}E_{ro}(\omega)e^{\gamma_{nz}^{r}z} = -\frac{\gamma_{n+1,x}}{j\omega\mu_{n+1}}E_{to}(\omega)e^{\gamma_{n+1,z}z}. \quad (2.31)$$

Using (2.30), this equation simplifies to

$$\frac{\gamma_{nx}}{\mu_n} E_{io}(\omega) - \frac{\gamma_{nx}}{\mu_n} E_{ro}(\omega) = \frac{\gamma_{n+1,x}}{\mu_{n+1}} E_{to}(\omega). \tag{2.32}$$

Now, multiplying (2.26) by  $\frac{\gamma_{n+1,x}}{\mu_{n+1}}$  and subtracting (2.32) yields

$$\left(\frac{\gamma_{n+1,x}}{\mu_{n+1}} - \frac{\gamma_{n,x}}{\mu_n}\right) E_{io}(\omega) + \left(\frac{\gamma_{n+1,x}}{\mu_{n+1}} + \frac{\gamma_{n,x}}{\mu_n}\right) E_{ro}(\omega) = 0.$$
 (2.33)

Therefore, the frequency domain interfacial reflection coefficient for TE-polarized

RTE is the sa

2.2.2 Branch

Because 2.34 i

outs for square the interface is t

bilis actions can

It is assumed t

There  $\theta_i$ ; is if

the propagatio

plane waves is

$$R^{TE}(\omega) = \frac{E_{ro}(\omega)}{E_{io}(\omega)} = \left(\frac{\gamma_{nx}}{\mu_n} - \frac{\gamma_{n+1,x}}{\mu_{n+1}}\right) / \left(\frac{\gamma_{nx}}{\mu_n} + \frac{\gamma_{n+1,x}}{\mu_{n+1}}\right)$$
$$= \frac{\mu_{n+1}\gamma_{nx}(\omega) - \mu_n\gamma_{n+1,x}(\omega)}{\mu_{n+1}\gamma_{nx}(\omega) + \mu_n\gamma_{n+1,x}(\omega)}. \tag{2.34}$$

This is a generalized form of the Fresnel's reflection coefficient for TE-polarized incident and reflect waves at an interface in a layered structure. Note that the form of  $R^{TE}(\omega)$  is the same as that given in [1].

#### 2.2.2 Branch-cuts

Because (2.34) includes square root functions of complex argument, proper branchcuts (or, square root rules) must be set. To do this properly, it must be assumed that the interface is the n'th interface in a multi-layered material. Since Snell's law (2.25) holds across each interface, we must have

$$\gamma_{n+1,z} = \gamma_{nz} = \dots = \gamma_{1z}. \tag{2.35}$$

It is assumed that region 1 is lossless and thus

$$\gamma_{1z} = \omega^2 \mu_1 \epsilon_1 \sin \theta_{i1} \tag{2.36}$$

where  $\theta_{i1}$  is the incident angle of the plane wave in region 1. The x-components of the propagation constants are

$$\gamma_{nx}(\omega) = \sqrt{\gamma_n^2 - \gamma_{nz}^2}$$

$$\gamma_{n+1,x}(\omega) = \sqrt{\gamma_{n+1}^2 - \gamma_{n+1,z}^2}.$$
(2.37)

of the frequency

eraliate a squa

onsierently th

operations of a

Using (2.35), this becomes

$$\gamma_{nx}(\omega) = \sqrt{\gamma_n^2 - \gamma_{1z}^2}$$

$$= \sqrt{(-\omega^2 \mu_n \epsilon_n + j\omega \mu_n \sigma_n) - (-\omega^2 \mu_1 \epsilon_1 \sin^2 \theta_{i1})}$$

$$= \sqrt{-\omega^2 (\mu_n \epsilon_n - \mu_1 \epsilon_1 \sin^2 \theta_{i1}) + j\omega \mu_n \sigma_n}$$

$$\gamma_{n+1,x}(\omega) = \sqrt{\gamma_{n+1,z}^2 - \gamma_{1z}^2}$$

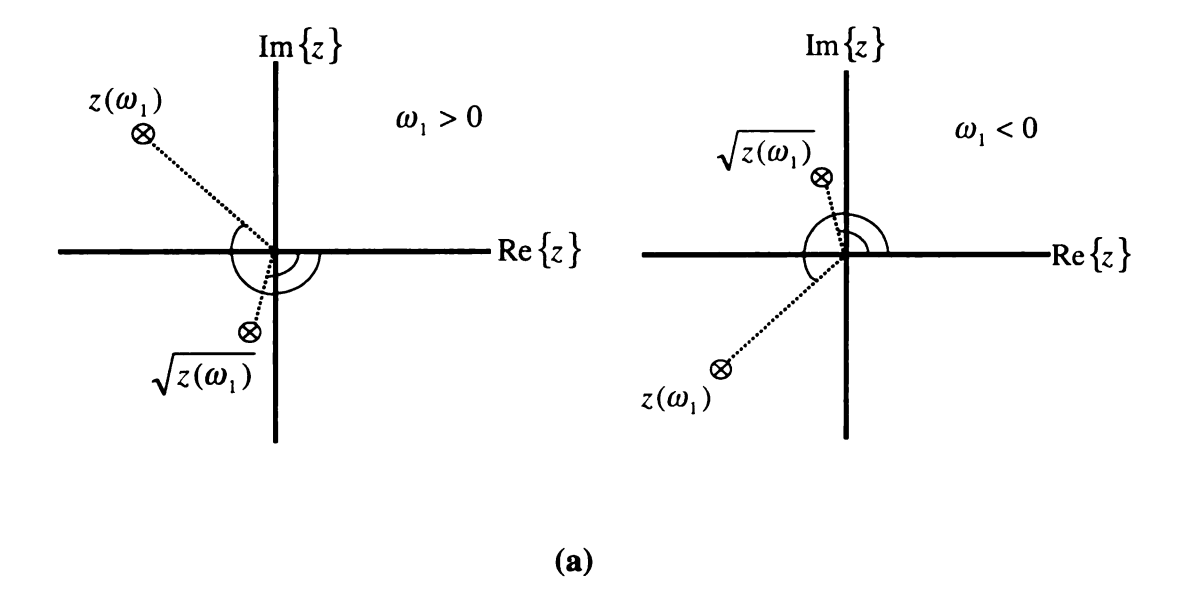
$$= \sqrt{-\omega^2 (\mu_{n+1} \epsilon_{n+1} - \mu_1 \epsilon_1 \sin^2 \theta_{i1}) + j\omega \mu_{n+1} \sigma_{n+1}}.$$
 (2.38)

The condition that region 1 must be lossless confines the locations of the resulting propagation constants on the complex plane, and contributes to the definition of the branch cuts. The condition for setting branch cuts is the radiation conditon, which says that, by the energy conservation law [9], an isolated wave cannot increase during its propagation. To satisfy this condition, the real part of each component of the propagation constant must not be positive for both positive and negative frequency. The z-component always satisfies this condition since  $Re\{\gamma_{nz}\} = Re\{\gamma_{n-1,z}\} = \dots = Re\{\gamma_{1z}\} = 0$ . However, two different branch cuts must be applied to  $\gamma_{n,x}$ , since the imaginary part inside of the square root has two different signs according to the sign of the frequency variable  $\omega$ , as shown in Figure 2.2 (a). The resulting branch cuts to evaluate a square root of complex value  $\sqrt{z(\omega=\omega_1)}$  are given by

$$\omega_1 > 0 : \frac{1}{2} arg[z(\omega_1)] < \theta_B < arg[z(\omega_1)]$$

$$\omega_1 < 0 : arg[z(\omega_1)] < \theta_B < \frac{1}{2} arg[z(\omega_1)] + \pi$$
(2.39)

where  $\theta_B$  and  $arg[z(\omega_1)]$  indicate the argument angles of a branch cut line and  $z(\omega_1)$  respectively, and  $0 \le arg[z(\omega_1)] < 2\pi$ . The branch cuts of (2.39) should be applied consistently through the entire derivation procedure, and Appendix A shows the operations of square root functions used in this study, which are obtained by applying



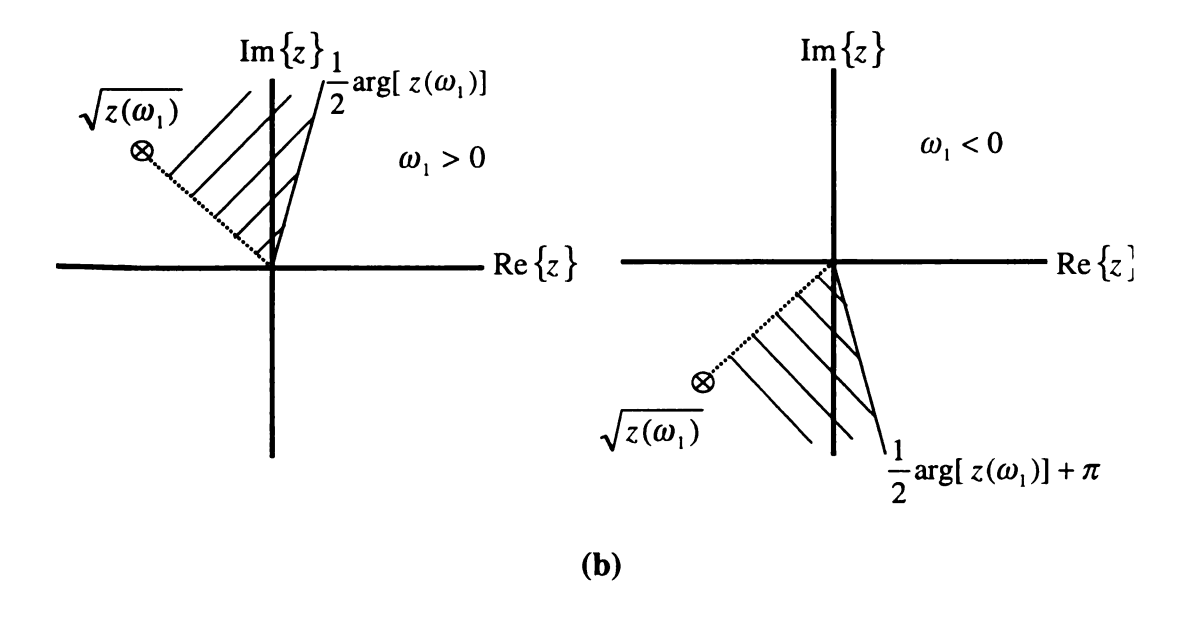


**Figure 2.2.** The brach cut setting. (a) Evaluation of  $\sqrt{z(\omega_1)}$  and (b) allowed region of branch cuts.

Note that  $\tilde{B}_n$  is appropriate by an

and  $\tilde{B}_{n+1}$  . All p

Denoting . :

ad (2.34) may

Now, the freque

forms according

layer parameter.

and in the deriva

the branch cuts.

#### 2.2.3 Classification of frequency domain coefficients

The Fresnel's coefficient given by (2.34) can be classified according to the signs of some constant values included within it. Therefore, layer constants may be defined as

$$\tilde{D}_n = (\mu_n \epsilon_n - \mu_1 \epsilon_1 \sin^2 \theta_{i1}) / \mu_n^2 \tag{2.40}$$

$$\tilde{B}_n = \sigma_n/\mu_n. \tag{2.41}$$

Note that  $\tilde{B}_n$  is always positive. In order to compute the square root functions, the appropriate branch cuts must be applied. This depends on the signs of  $\tilde{D}_n$ ,  $\tilde{B}_n$ ,  $\tilde{D}_{n+1}$  and  $\tilde{B}_{n+1}$ . All possibilities are considered next.

Denoting  $s = j\omega$  the terms in (2.34) become

$$\frac{\gamma_{nx}}{\mu_n} = \sqrt{s(\tilde{D}_n s + \tilde{B}_n)}$$

$$\frac{\gamma_{n+1,x}}{\mu_{n+1}} = \sqrt{s(\tilde{D}_{n+1} s + \tilde{B}_{n+1})}$$

and (2.34) may be rewritten as

$$R^{TE}(s) = \frac{\sqrt{s(\tilde{D}_n s + \tilde{B}_n)} - \sqrt{s(\tilde{D}_{n+1} s + \tilde{B}_{n+1})}}{\sqrt{s(\tilde{D}_n s + \tilde{B}_n)} + \sqrt{s(\tilde{D}_{n+1} s + \tilde{B}_{n+1})}}.$$
 (2.42)

Now, the frequency domain reflection coefficient can be classified to four different forms according to which branch cut is needed. This depends on the signs of the layer parameters  $\tilde{D}_n$  and  $\tilde{D}_{n+1}$ . The algebraic manipulations with the branch cuts used in the derivation processes are given by (A.1) and (A.2).

(i)  $\hat{D}_{n-1} > 0$  at

 $R^{\cdot}$ 

Simplifying giv-

 $2\|\tilde{D}_{n+1}<0\text{ at.}$ 

 $R^{IE}(s)$ 

Simplifying gives

 $\tilde{\sigma} \tilde{D}_{n-1} > 0$  and

 $R^{TE}$ ,

Simplifying gives

(1)  $\tilde{D}_{n+1} > 0$  and  $\tilde{D}_n > 0$ 

$$R^{TE}(s) = \frac{-\sqrt{\tilde{D}_n}\sqrt{s}\sqrt{s + \frac{\tilde{B}_n}{\tilde{D}_n}} + \sqrt{\tilde{D}_{n+1}}\sqrt{s}\sqrt{s + \frac{\tilde{B}_{n+1}}{\tilde{D}_{n+1}}}}{-\sqrt{\tilde{D}_n}\sqrt{s}\sqrt{s + \frac{\tilde{B}_n}{\tilde{D}_n}} - \sqrt{\tilde{D}_{n+1}}\sqrt{s}\sqrt{s + \frac{\tilde{B}_{n+1}}{\tilde{D}_{n+1}}}}.$$

Simplifying gives

$$R^{TE}(s) = \frac{\sqrt{s + \frac{\tilde{B}_n}{\tilde{D}_n}} - \sqrt{\frac{\tilde{D}_{n+1}}{\tilde{D}_n}} \sqrt{s + \frac{\tilde{B}_{n+1}}{\tilde{D}_{n+1}}}}{\sqrt{s + \frac{\tilde{B}_n}{\tilde{D}_n}} + \sqrt{\frac{\tilde{D}_{n+1}}{\tilde{D}_n}} \sqrt{s + \frac{\tilde{B}_{n+1}}{\tilde{D}_{n+1}}}}.$$
(2.43)

(2)  $\tilde{D}_{n+1} < 0$  and  $\tilde{D}_n < 0$ 

$$R^{TE}(s) = \frac{\pm j\sqrt{|\tilde{D}_{n}|}\sqrt{s}\sqrt{s - \frac{\tilde{B}_{n}}{|\tilde{D}_{n}|}} \mp j\sqrt{|\tilde{D}_{n+1}|}\sqrt{s}\sqrt{s - \frac{\tilde{B}_{n+1}}{|\tilde{D}_{n+1}|}}}{\pm j\sqrt{|\tilde{D}_{n}|}\sqrt{s}\sqrt{s - \frac{\tilde{B}_{n}}{|\tilde{D}_{n}|}} \pm j\sqrt{|\tilde{D}_{n+1}|}\sqrt{s}\sqrt{s - \frac{\tilde{B}_{n+1}}{|\tilde{D}_{n+1}|}}}.$$

Simplifying gives

$$R^{TE}(s) = \frac{\sqrt{s - \frac{\tilde{B}_n}{|\tilde{D}_n|}} - \sqrt{\frac{|\tilde{D}_{n+1}|}{|\tilde{D}_n|}} \sqrt{s - \frac{\tilde{B}_{n+1}}{|\tilde{D}_{n+1}|}}}{\sqrt{s - \frac{\tilde{B}_n}{|\tilde{D}_n|}} + \sqrt{\frac{|\tilde{D}_{n+1}|}{|\tilde{D}_n|}} \sqrt{s - \frac{\tilde{B}_{n+1}}{|\tilde{D}_{n+1}|}}}.$$
(2.44)

(3)  $\tilde{D}_{n+1} > 0$  and  $\tilde{D}_n < 0$ 

$$R^{TE}(s) = \frac{\pm j\sqrt{|\tilde{D}_{n}|}\sqrt{s}\sqrt{s - \frac{\tilde{B}_{n}}{|\tilde{D}_{n}|}} + \sqrt{|\tilde{D}_{n+1}|}\sqrt{s}\sqrt{s + \frac{\tilde{B}_{n+1}}{|\tilde{D}_{n+1}|}}}{\pm j\sqrt{|\tilde{D}_{n}|}\sqrt{s}\sqrt{s - \frac{\tilde{B}_{n}}{|\tilde{D}_{n}|}} - \sqrt{|\tilde{D}_{n+1}|}\sqrt{s}\sqrt{s + \frac{\tilde{B}_{n+1}}{|\tilde{D}_{n+1}|}}}.$$

Simplifying gives

$$R^{TE}(s) = \frac{\sqrt{s - \frac{\tilde{B}_n}{|\tilde{D}_n|}} \mp j\sqrt{\frac{|\tilde{D}_{n+1}|}{|\tilde{D}_n|}}\sqrt{s + \frac{\tilde{B}_{n+1}}{|\tilde{D}_{n+1}|}}}{\sqrt{s - \frac{\tilde{B}_n}{|\tilde{D}_n|}} \pm j\sqrt{\frac{|\tilde{D}_{n+1}|}{|\tilde{D}_n|}}\sqrt{s + \frac{\tilde{B}_{n+1}}{|\tilde{D}_{n+1}|}}}.$$
(2.45)

## 2.2.4 Reducti

Otherwing 243.

requercy domain

cefficient by the

be integrable i.

taisform, the co-

To make the

 $\bar{L}$ 

B

and take the limit

(4)  $\tilde{D}_{n+1} < 0 \text{ and } \tilde{D}_n > 0$ 

$$R^{TE}(s) = \frac{-\sqrt{|\tilde{D}_n|}\sqrt{s}\sqrt{s + \frac{\tilde{B}_n}{|\tilde{D}_n|}} \mp j\sqrt{|\tilde{D}_{n+1}|}\sqrt{s}\sqrt{s - \frac{\tilde{B}_{n+1}}{|\tilde{D}_{n+1}|}}}{-\sqrt{|\tilde{D}_n|}\sqrt{s}\sqrt{s + \frac{\tilde{B}_n}{|\tilde{D}_n|}} \pm j\sqrt{|\tilde{D}_{n+1}|}\sqrt{s}\sqrt{s - \frac{\tilde{B}_{n+1}}{|\tilde{D}_{n+1}|}}}.$$
(2.46)

Simplifying gives

$$R^{TE}(s) = \frac{\sqrt{s + \frac{\tilde{B}_n}{|\tilde{D}_n|}} \pm j\sqrt{\frac{|\tilde{D}_{n+1}|}{|\tilde{D}_n|}}\sqrt{s - \frac{\tilde{B}_{n+1}}{|\tilde{D}_{n+1}|}}}{\sqrt{s + \frac{\tilde{B}_n}{|\tilde{D}_n|}} \mp j\sqrt{\frac{|\tilde{D}_{n+1}|}{|\tilde{D}_n|}}\sqrt{s - \frac{\tilde{B}_{n+1}}{|\tilde{D}_{n+1}|}}}.$$
(2.47)

In each of these expressions the upper sign corresponds to  $\omega > 0$  and lower sign does to  $\omega < 0$ . Note again that the branch cuts defined in section 2.2.2 have been used through the whole manipulation steps for the square root functions.

#### 2.2.4 Reduction of the interfacial reflection coefficients

Observing (2.43)-(2.47), it is realized that there is a constant offset value inside of each frequency domain expression. Since we are supposed to find the transient reflection coefficient by the inverse Fourier transform, and the frequency domain function must be integrable (i.e.  $\int_{-\infty}^{\infty} |R^{TE}(\omega)|^2 d\omega \leq \infty$ ) for the existence of the inverse Frourier transform, the constant offset value should be extracted first.

To make the (2.43)-(2.47) more readable, let

$$D_{n} = \sqrt{\frac{|\tilde{D}_{n+1}|}{|\tilde{D}_{n}|}} = \sqrt{\frac{\mu_{n}^{2}}{\mu_{n+1}^{2}} \frac{|\mu_{n+1}\epsilon_{n+1} - \mu_{1}\epsilon_{1}\sin^{2}\theta_{i1}|}{|\mu_{n}\epsilon_{n} - \mu_{1}\epsilon_{1}\sin^{2}\theta_{i1}|}}$$

$$B_{n} = \frac{\tilde{B}_{n}}{|\tilde{D}_{n}|} = \frac{\mu_{n}\sigma_{n}}{|\mu_{n}\epsilon_{n} - \mu_{1}\epsilon_{1}\sin^{2}\theta_{i1}|}.$$
(2.48)

and take the limit values at infinite frequency. Then,

(1)  $\tilde{D}_{n+1} > 0$  and  $\tilde{D}_n > 0$ 

$$R^{TE}(s) = \frac{\sqrt{s + B_n} - \sqrt{D_n}\sqrt{s + B_{n+1}}}{\sqrt{s + B_n} + \sqrt{D_n}\sqrt{s + B_{n+1}}},$$
(2.49)

$$\lim_{\omega \to \infty} R^{TE}(s) = \frac{1 - \sqrt{D_n}}{1 + \sqrt{D_n}}.$$
(2.50)

(2)  $\tilde{D}_{n+1} < 0$  and  $\tilde{D}_n < 0$ 

$$R^{TE}(s) = \frac{\sqrt{s - B_n} - \sqrt{D_n}\sqrt{s - B_{n+1}}}{\sqrt{s - B_n} + \sqrt{D_n}\sqrt{s - B_{n+1}}},$$
(2.51)

$$\lim_{\omega \to \infty} R^{TE}(s) = \frac{1 - \sqrt{D_n}}{1 + \sqrt{D_n}}.$$
(2.52)

(3)  $\tilde{D}_{n+1} > 0$  and  $\tilde{D}_n < 0$ 

$$R^{TE}(s) = \frac{\sqrt{s - B_n} \mp j\sqrt{D_n}\sqrt{s + B_{n+1}}}{\sqrt{s - B_n} \pm j\sqrt{D_n}\sqrt{s + B_{n+1}}},$$
(2.53)

$$\lim_{\omega \to \infty} R^{TE}(s) = \frac{1 \mp j\sqrt{D_n}}{1 \pm j\sqrt{D_n}}.$$
 (2.54)

(4)  $\tilde{D}_{n+1} < 0$  and  $\tilde{D}_n > 0$ 

$$R^{TE}(s) = \frac{\sqrt{s + B_n} \pm j\sqrt{D_n}\sqrt{s - B_{n+1}}}{\sqrt{s + B_n} \mp j\sqrt{D_n}\sqrt{s - B_{n+1}}},$$
(2.55)

$$\lim_{\omega \to \infty} R^{TE}(s) = \frac{1 \pm j\sqrt{D_n}}{1 \mp j\sqrt{D_n}}.$$
 (2.56)

In these expressions the upper sign corresponds to  $\omega > 0$  and lower sign does to  $\omega < 0$ . Next, the obtained constant values have to be subtracted from the original  $R^{TE}(s)$ . Let's define  $\tilde{R}^{TE}(s) = R^{TE}(s) - R^{TE}(s) = \pm j\infty$ , then

(1)  $\tilde{D}_{n+1} > 0$  and  $\tilde{D}_n > 0$ 

$$\tilde{R}^{TE}(s) = \frac{\sqrt{s + B_n} - \sqrt{D_n}\sqrt{s + B_{n+1}}}{\sqrt{s + B_n} + \sqrt{D_n}\sqrt{s + B_{n+1}}} - \frac{1 - \sqrt{D_n}}{1 + \sqrt{D_n}}$$

$$= \frac{2\sqrt{D_n}}{1 + \sqrt{D_n}} \frac{\sqrt{s + B_n} - \sqrt{s + B_{n+1}}}{\sqrt{s + B_n} + \sqrt{D_n}\sqrt{s + B_{n+1}}}$$
(2.57)

Eliminating the square roots in the denominator of (2.57), gives

$$\tilde{R}^{TE}(s) = \frac{2\sqrt{D_n}}{1+\sqrt{D_n}} \frac{\{\sqrt{s+B_n} - \sqrt{s+B_{n+1}}\}\{\sqrt{s+B_n} - \sqrt{D_n}\sqrt{s+B_{n+1}}\}}{(s+B_n) - D_n(s+B_{n+1})} \\
= \frac{2\sqrt{D_n}}{(1-D_n)(1+\sqrt{D_n})} \times \frac{(1+\sqrt{D_n})(s+B_n) - (1+\sqrt{D_n})\sqrt{s+B_n}\sqrt{s+B_{n+1}} - \sqrt{D_n}(B_n-B_{n+1})}{s+\left(\frac{B_n-D_nB_{n+1}}{1-D_n}\right)}.$$
(2.58)

The  $s + B_n$  term can be factored out of the first and second term in the numerator of (2.58), giving

$$\tilde{R}^{TE}(s) = \frac{2\sqrt{D_n}}{1 - D_n} \frac{(s + B_n) \left\{ 1 - \frac{\sqrt{s + B_n} \sqrt{s + B_{n+1}}}{(s + B_n)} \right\}}{s + \left( \frac{B_n - D_n B_{n+1}}{1 - D_n} \right)} \\
- \frac{2D_n (B_n - B_{n+1})}{(1 - D_n)(1 + \sqrt{D_n})} \frac{1}{s + \left( \frac{B_n - D_n B_{n+1}}{1 - D_n} \right)} \\
= \frac{2B_n \sqrt{D_n}}{1 - D_n} \frac{1}{s + \left( \frac{B_n - D_n B_{n+1}}{1 - D_n} \right)} \left\{ 1 - \sqrt{\frac{s + B_{n+1}}{s + B_n}} \right\} \\
+ \frac{2\sqrt{D_n}}{1 - D_n} \frac{s}{s + \left( \frac{B_n - D_n B_{n+1}}{1 - D_n} \right)} \left\{ 1 - \sqrt{\frac{s + B_{n+1}}{s + B_n}} \right\} \\
- \frac{2D_n (B_n - B_{n+1})}{(1 - D_n)(1 + \sqrt{D_n})} \frac{1}{s + \left( \frac{B_n - D_n B_{n+1}}{1 - D_n} \right)} \tag{2.59}$$

where (A.3) is

of (2.59). For

procedure mus

 $\hat{y}$  and  $\hat{D}_n < 0$  .

 $\tilde{\mathcal{D}}_{n+1} < 0$  a

 $\hat{R}^{\mathbb{N}}$ 

 $\Im |\tilde{D}_{n+1}>0.$ 

Ř

 $\downarrow \hat{D}_{n-1} < 0$ 

 $\hat{R}^{TL}$ 

where (A.3) is used. Known inverse Fourier transform pairs are available for all terms of (2.59). For the other cases, the quite similar steps are taken, except that the procedure must be done separately for  $\omega > 0$  and  $\omega < 0$  in the cases of  $\tilde{D}_{n+1} > 0$  and  $\tilde{D}_n < 0$ , and  $\tilde{D}_{n+1} < 0$  and  $\tilde{D}_n > 0$ . These are

(2)  $\tilde{D}_{n+1} < 0$  and  $\tilde{D}_n < 0$ 

$$\tilde{R}^{TE}(s) = \frac{\sqrt{s - B_n} - \sqrt{D_n}\sqrt{s - B_{n+1}}}{\sqrt{s - B_n} + \sqrt{D_n}\sqrt{s - B_{n+1}}} - \frac{1 - \sqrt{D_n}}{1 + \sqrt{D_n}}$$

$$= -\frac{2B_n\sqrt{D_n}}{1 - D_n} \frac{1}{s + \left(\frac{B_n - D_n B_{n+1}}{1 - D_n}\right)} \left\{1 - \sqrt{\frac{s - B_{n+1}}{s - B_n}}\right\}$$

$$+ \frac{2\sqrt{D_n}}{1 - D_n} \frac{s}{s + \left(\frac{B_n - D_n B_{n+1}}{1 - D_n}\right)} \left\{1 - \sqrt{\frac{s - B_{n+1}}{s - B_n}}\right\}$$

$$- \frac{2D_n(B_{n+1} - B_n)}{(1 - D_n)(1 + \sqrt{D})} \frac{1}{s + \left(\frac{B_n - D_n B_{n+1}}{1 - D_n}\right)}.$$
(2.60)

(3)  $\tilde{D}_{n+1} > 0$  and  $\tilde{D}_n < 0$ 

$$\tilde{R}^{TE}(s) = \frac{\sqrt{s - B_n} \mp j\sqrt{D_n}\sqrt{s + B_{n+1}}}{\sqrt{s - B_n} \pm j\sqrt{D_n}\sqrt{s + B_{n+1}}} - \frac{1 \mp j\sqrt{D_n}}{1 \pm j\sqrt{D_n}}$$

$$= \mp \frac{2jB_n\sqrt{D_n}}{1 + D_n} \frac{1}{s - \left(\frac{B_n - D_nB_{n+1}}{1 + D_n}\right)} \left\{1 - \sqrt{\frac{s + B_{n+1}}{s - B_n}}\right\}$$

$$\mp \frac{2j\sqrt{D_n}}{1 + D_n} \frac{s}{s - \left(\frac{B_n - D_nB_{n+1}}{1 + D_n}\right)} \left\{1 - \sqrt{\frac{s + B_{n+1}}{s - B_n}}\right\}$$

$$- \frac{2D_n(B_{n+1} + B_n)}{(1 + D_n)(1 \mp j\sqrt{D_n})} \frac{1}{s - \left(\frac{B_n - D_nB_{n+1}}{1 + D_n}\right)}.$$
(2.61)

(4)  $\tilde{D}_{n+1} < 0 \text{ and } \tilde{D}_n > 0$ 

$$\tilde{R}^{TE}(s) = \frac{\sqrt{s+B_n} \pm j\sqrt{D_n}\sqrt{s-B_{n+1}}}{\sqrt{s+B_n} \mp j\sqrt{D_n}\sqrt{s-B_{n+1}}} - \frac{1 \pm j\sqrt{D_n}}{1 \mp j\sqrt{D_n}}$$

$$= \mp \frac{2jB_n\sqrt{D_n}}{1+D_n} \frac{1}{s + \left(\frac{B_n - D_n B_{n+1}}{1+D_n}\right)} \left\{1 + \sqrt{\frac{s-B_{n+1}}{s+B_n}}\right\}$$

discussed later

इंग्ला क तेन्।

· i D, ... >

$$\mp \frac{2j\sqrt{D_n}}{1+D_n} \frac{s}{s+\left(\frac{B_n-D_nB_{n+1}}{1+D_n}\right)} \left\{ 1+\sqrt{\frac{s-B_{n+1}}{s+B_n}} \right\} \\
+ \frac{2D_n(B_{n+1}+B_n)}{(1+D_n)(1\mp j\sqrt{D_n})} \frac{1}{s+\left(\frac{B_n-D_nB_{n+1}}{1+D_n}\right)}, \tag{2.62}$$

and (A.4),(A.5), and (A.6) are used respectively. In these expressions the upper sign corresponds to  $\omega > 0$  and lower sign does to  $\omega < 0$ .

 $R^{TE}(s=\pm j\infty)$  is the reflection coefficient obtained at infinitely high frequency, and is equivalent to the coefficient when the medium has no conductivity. Therefore, it depends on the diplacement current term only in the Maxwell's equation of (2.2), and may be called an aymptotic reflection coefficient, since the value of  $R^{TE}(s)$  approaches this (or these) value(s). In contrast,  $\tilde{R}^{TE}(s)$  exists only when at least one of the two media has some conductivity. Let's call it a reduced interfacial reflection coefficient. The physical meaning of the two reflection coefficients in transient analysis will be discussed later.

#### 2.3 Derivation of Transient Interfacial Reflection Coefficients

#### 2.3.1 The transient forms

The transient forms of the frequency domain interfacial reflection coefficients are given by the inverse Fourier transform. Because the asymptotic reflection coefficients  $R^{TE}(s=\pm j\infty)$  are constants in the frequency domain, their transforms are simply given as delta-functions multiplied by the constants. Let's denote it by  $R_{\infty}^{TE}(t)$ . Then, (1)  $\tilde{D}_{n+1} > 0$  and  $\tilde{D}_n > 0$ 

$$R_{\infty}^{TE}(t) = F^{-1} \left\{ \lim_{\omega \to \infty} R^{TE}(s) \right\}$$
$$= \frac{1 - \sqrt{D_n}}{1 + \sqrt{D_n}} \delta(t)$$
(2.63)

he in the play

(2)  $\tilde{D}_{n+1} < 0$  and  $\tilde{D}_n < 0$ 

$$R_{\infty}^{TE}(t) = F^{-1} \left\{ \lim_{\omega \to \infty} R^{TE}(s) \right\}$$
$$= \frac{1 - \sqrt{D_n}}{1 + \sqrt{D_n}} \delta(t)$$
(2.64)

where  $F^{-1}$  denotes the inverse Fourier transform.

(3) 
$$\tilde{D}_{n+1} > 0$$
 and  $\tilde{D}_n < 0$ 

As shown by (2.54), there are two different asymptotic values in this case according to the sign of  $\omega$ . Therefore, letting  $G = \frac{1 - j\sqrt{D_n}}{1 + j\sqrt{D_n}}$  then (2.54) can be rewritten as

$$\lim_{\omega \to \infty} R^{TE}(\omega) = GU(\omega) + G^*U(-\omega)$$
 (2.65)

where  $G^*$  denotes complex conjugate value of G, and  $U(\omega)$  is a frequency domain unit step function defined by  $U(\omega) = 1$  for  $\omega > 0$  and  $U(\omega) = 0$  for  $\omega < 0$ . From the transform table given in (B.2),

$$R_{\infty}^{TE}(t) = F^{-1} \{GU(\omega) + G^*U(-\omega)\}$$

$$= \frac{1}{2} (G + G^*) \delta(t) + \frac{j}{2\pi} \frac{1}{t} * (G - G^*) \delta(t)$$

$$= \frac{1 - D_n}{1 + D_n} \delta(t) + \frac{2\sqrt{D_n}}{\pi (1 + D_n)} \left\{ \frac{1}{t} * \delta(t) \right\}$$
(2.66)

where a(t) \* b(t) is the convolution of a(t) and b(t). The convolution of a function with a delta function gives the function itself. Thus,

$$R_{\infty}^{TE}(t) = \frac{1 - D_n}{1 + D_n} \delta(t) + \frac{2\sqrt{D_n}}{\pi (1 + D_n)t}.$$
 (2.67)

Notice that the transient reflection coefficient is a real valued function as it should be in the physical world.

A)  $\hat{D}_{n-1} < 0$ The transient with case (3)

The inverse be found directions:

Then for  $1. \dot{D}_{t-1} > 0.a$ 

239) is rewrit

This form has

and the inverse

(4)  $\tilde{D}_{n+1} < 0 \text{ and } \tilde{D}_n > 0$ 

The transient form for this case is easily obtained by applying the same procedure with case (3). Thus,

$$R_{\infty}^{TE}(t) = \frac{1+D_n}{1-D_n}\delta(t) - \frac{2\sqrt{D_n}}{\pi(1+D_n)t}.$$
 (2.68)

The inverse Fourier transforms of the reduced interfacial reflection coefficient can be found directly from the transform table given in Appendix B. Let's define the following constants

$$P_1 = (B_{n+1} + B_n)/2 (2.69)$$

$$P_2 = (B_n - D_n B_{n+1})/(1 - D_n) (2.70)$$

$$\beta = (B_{n+1} - B_n)/2. (2.71)$$

Then for

(1) 
$$\tilde{D}_{n+1} > 0$$
 and  $\tilde{D}_n > 0$ 

(2.59) is rewritten as

$$\tilde{R}^{TE}(s) = \frac{2B_n\sqrt{D_n}}{1-D_n} \frac{1}{s+P_2} \left\{ 1 - \sqrt{\frac{s+B_{n+1}}{s+B_n}} \right\} + \frac{2\sqrt{D_n}}{1-D_n} \frac{s}{s+P_2} \left\{ 1 - \sqrt{\frac{s+B_{n+1}}{s+B_n}} \right\} - \frac{2D_n(B_n - B_{n+1})}{(1-D_n)(1+\sqrt{D_n})} \frac{1}{s+P_2}.$$
(2.72)

This form has two different inverse Fourier transforms according to the sign of  $P_2$ , and the inverse Fourier transform for each term can be found in (B.3)-(B.4). Thus,

when  $P_2 > 0$ .

$$\hat{R}^{\tilde{t}\tilde{E}}(t) = \begin{bmatrix} 2t \\ 1 \end{bmatrix}$$

where 
$$I_n \in \mathbb{R}$$

property of the

$$\hat{R}^{TE}(t) = 0$$

### =

# It is neces.

when  $P_2 > 0$ ,

$$\tilde{R}^{TE}(t) = \left[ \frac{2B_n \sqrt{D_n}}{1 - D_n} e^{-P_2 t} u(t) + \frac{2\sqrt{D_n}}{1 - D_n} e^{-P_2 t} \left\{ \delta(t) - P_2 u(t) \right\} \right] * \\
\left[ -\beta e^{-P_1 t} \left\{ I_1(\beta t) + I_0(\beta t) \right\} u(t) \right] - \frac{2D_n (B_n - B_{n+1})}{(1 - D_n)(1 + \sqrt{D_n})} e^{-P_2 t} u(t) \\
= \frac{2\sqrt{D_n}}{1 - D_n} e^{-P_2 t} \delta(t) * (-\beta) e^{-P_1 t} \left\{ I_1(\beta t) + I_0(\beta t) \right\} u(t) \\
+ \left\{ \frac{2B_n \sqrt{D_n}}{1 - D_n} - \frac{2\sqrt{D_n}}{1 - D_n} P_2 \right\} e^{-P_2 t} u(t) * (-\beta) e^{-P_1 t} \left\{ I_1(\beta t) + I_0(\beta t) \right\} u(t) \\
- \frac{2D_n (B_n - B_{n+1})}{(1 - D_n)(1 + \sqrt{D_n})} e^{-P_2 t} u(t) \tag{2.73}$$

where  $I_n(t)$  is the first kind modified Bessel function of order n. Using the convolution property of the delta function, (2.73) becomes

$$\tilde{R}^{TE}(t) = \frac{(B_n - B_{n+1})\sqrt{D_n}}{1 - D_n} e^{-P_1 t} \left\{ I_1(\beta t) + I_0(\beta t) \right\} u(t) 
+ \frac{2D_n \sqrt{D_n} (B_{n+1} - B_n)}{(1 - D_n)^2} \frac{(B_n - B_{n+1})}{2} e^{-P_2 t} u(t) * 
e^{-P_1 t} \left\{ I_1(\beta t) + I_0(\beta t) \right\} u(t) - \frac{2D_n (B_n - B_{n+1})}{(1 - D_n)(1 + \sqrt{D_n})} e^{-P_2 t} u(t) 
= \frac{(B_n - B_{n+1})\sqrt{D_n}}{1 - D_n} e^{-P_1 t} \left\{ I_1(\beta t) + I_0(\beta t) \right\} u(t) 
- \frac{(B_n - B_{n+1})^2 D_n \sqrt{D_n}}{(1 - D_n)^2} e^{-P_2 t} u(t) \int_0^t e^{-(P_1 - P_2)x} \left\{ I_1(\beta x) + I_0(\beta x) \right\} dx 
+ \frac{2D_n (B_{n+1} - B_n)}{(1 - D_n)(1 + \sqrt{D_n})} e^{-P_2 t} u(t).$$
(2.74)

It is necessary to check whether the integral term from time domain convolution  $e^{-P_2 t} u(t) \int_0^t e^{-(P_1 - P_2)x} \{I_1(\beta x) + I_0(\beta x)\} dx$  exists as  $t \to \infty$ . Let

$$I(t) = \int_0^t e^{-P_2 t} e^{-(P_1 - P_2)x} \left\{ I_1(\beta x) + I_0(\beta x) \right\} dx.$$

When t is large, the integrand varies as  $e^{-(P_1-P_2+\beta)x}e^{-P_2t}=e^{-P_2(t-x)}e^{-(\beta+P_1)x}$  for  $x\approx t$ , since  $I_v(x)\approx \frac{e^x}{\sqrt{2\pi x}}$  for large x. When  $P_2>0$ , since t-x>0 and  $\beta+P_1>0$ ,

when  $P_2 > 0$ .

$$\tilde{R}^{TE}(t) = \begin{bmatrix} \frac{2B}{1-t} \\ \frac{1}{1-t} \end{bmatrix}$$

$$= \frac{2\sqrt{t}}{1-t}$$

$$= \frac{2\sqrt{t}}{1-t}$$

where  $I_n(t)$  is the t

property of the de

$$\hat{R}^{TE}(t) = \frac{-B}{-B}$$

It is necessar,  $e^{-P_{2l}}u^{i}t$ ,  $\int_{t}^{t}e^{-P_{2l}}$ 

When t is large.

 $t \approx t$ , since  $L_{i,T}$ 

when  $P_2 > 0$ ,

$$\tilde{R}^{TE}(t) = \left[ \frac{2B_{n}\sqrt{D_{n}}}{1 - D_{n}} e^{-P_{2}t} u(t) + \frac{2\sqrt{D_{n}}}{1 - D_{n}} e^{-P_{2}t} \left\{ \delta(t) - P_{2}u(t) \right\} \right] * \\
\left[ -\beta e^{-P_{1}t} \left\{ I_{1}(\beta t) + I_{0}(\beta t) \right\} u(t) \right] - \frac{2D_{n}(B_{n} - B_{n+1})}{(1 - D_{n})(1 + \sqrt{D_{n}})} e^{-P_{2}t} u(t) \right] \\
= \frac{2\sqrt{D_{n}}}{1 - D_{n}} e^{-P_{2}t} \delta(t) * (-\beta) e^{-P_{1}t} \left\{ I_{1}(\beta t) + I_{0}(\beta t) \right\} u(t) \\
+ \left\{ \frac{2B_{n}\sqrt{D_{n}}}{1 - D_{n}} - \frac{2\sqrt{D_{n}}}{1 - D_{n}} P_{2} \right\} e^{-P_{2}t} u(t) * (-\beta) e^{-P_{1}t} \left\{ I_{1}(\beta t) + I_{0}(\beta t) \right\} u(t) \\
- \frac{2D_{n}(B_{n} - B_{n+1})}{(1 - D_{n})(1 + \sqrt{D_{n}})} e^{-P_{2}t} u(t) \tag{2.73}$$

where  $I_n(t)$  is the first kind modified Bessel function of order n. Using the convolution property of the delta function, (2.73) becomes

$$\tilde{R}^{TE}(t) = \frac{(B_n - B_{n+1})\sqrt{D_n}}{1 - D_n} e^{-P_1 t} \left\{ I_1(\beta t) + I_0(\beta t) \right\} u(t) 
+ \frac{2D_n \sqrt{D_n} (B_{n+1} - B_n)}{(1 - D_n)^2} \frac{(B_n - B_{n+1})}{2} e^{-P_2 t} u(t) * 
e^{-P_1 t} \left\{ I_1(\beta t) + I_0(\beta t) \right\} u(t) - \frac{2D_n (B_n - B_{n+1})}{(1 - D_n)(1 + \sqrt{D_n})} e^{-P_2 t} u(t) 
= \frac{(B_n - B_{n+1})\sqrt{D_n}}{1 - D_n} e^{-P_1 t} \left\{ I_1(\beta t) + I_0(\beta t) \right\} u(t) 
- \frac{(B_n - B_{n+1})^2 D_n \sqrt{D_n}}{(1 - D_n)^2} e^{-P_2 t} u(t) \int_0^t e^{-(P_1 - P_2)x} \left\{ I_1(\beta x) + I_0(\beta x) \right\} dx 
+ \frac{2D_n (B_{n+1} - B_n)}{(1 - D_n)(1 + \sqrt{D_n})} e^{-P_2 t} u(t).$$
(2.74)

It is necessary to check whether the integral term from time domain convolution  $e^{-P_2t}u(t)\int_0^t e^{-(P_1-P_2)x} \{I_1(\beta x) + I_0(\beta x)\} dx$  exists as  $t \to \infty$ . Let

$$I(t) = \int_0^t e^{-P_2 t} e^{-(P_1 - P_2)x} \left\{ I_1(\beta x) + I_0(\beta x) \right\} dx.$$

When t is large, the integrand varies as  $e^{-(P_1-P_2+\beta)x}e^{-P_2t}=e^{-P_2(t-x)}e^{-(\beta+P_1)x}$  for  $x\approx t$ , since  $I_v(x)\approx \frac{e^x}{\sqrt{2\pi x}}$  for large x. When  $P_2>0$ , since t-x>0 and  $\beta+P_1>0$ ,

the integrand doca

When  $P_2 < 0$ .

 $\hat{R}^{\text{IE}}(t) = \begin{bmatrix} -2 \\ -2 \end{bmatrix}$ 

.

= 'D.

= 1

This expression

However, in is

expression, a

! < 0.

Ř<sup>TE</sup>IT

Let a = P

Re(3) >

the integrand decays exponentially, and thus the integral converges between  $x=0\sim t$ . When  $P_2<0$ , the inverse Fourier transform of (2.72) is

$$\tilde{R}^{TE}(t) = \left[ -\frac{2B_n \sqrt{D_n}}{1 - D_n} e^{-P_2 t} u(-t) + \frac{2\sqrt{D_n}}{1 - D_n} e^{-P_2 t} \left\{ \delta(t) + P_2 u(t) \right\} \right] * \\
\left[ -\beta e^{-P_1 t} \left\{ I_1(\beta t) + I_0(\beta t) \right\} u(t) \right] + \frac{2D_n (B_n - B_{n+1})}{(1 - D_n)(1 + \sqrt{D_n})} e^{-P_2 t} u(-t) \right] \\
= \frac{(B_n - B_{n+1}) \sqrt{D_n}}{1 - D_n} e^{-P_1 t} \left\{ I_1(\beta t) + I_0(\beta t) \right\} u(t) \\
\left\{ -\frac{2B_n \sqrt{D_n}}{1 - D_n} + \frac{2\sqrt{D_n}}{1 - D_n} P_2 \right\} (-\beta) e^{-P_2 t} u(-t) * e^{-P_1 t} \left\{ I_1(\beta t) + I_0(\beta t) \right\} u(t) \right. \\
+ \frac{2D_n (B_n - B_{n+1})}{(1 - D_n)(1 + \sqrt{D_n})} e^{-P_2 t} u(-t) \\
= \frac{(B_n - B_{n+1}) \sqrt{D_n}}{1 - D_n} e^{-P_1 t} \left\{ I_1(\beta t) + I_0(\beta t) \right\} u(t) \\
+ \frac{(B_n - B_{n+1})^2 D_n \sqrt{D_n}}{(1 - D_n)^2} e^{-P_2 t} \int_{max(t,0)}^{\infty} e^{-(P_1 - P_2)x} \left\{ I_1(\beta x) + I_0(\beta x) \right\} dx \\
+ \frac{2D_n (B_n - B_{n+1})}{(1 - D_n)(1 + \sqrt{D_n})} e^{-P_2 t} u(-t). \tag{2.75}$$

This expression apparently includes non-causal terms in its second and third terms. However, it is shown that these non-causal terms can be removed by reforming the expression, and there are only causal terms remaining in the result. That is, when t < 0,

$$\tilde{\mathbf{R}}^{TE}(t) = \frac{(B_n - B_{n+1})^2 D_n \sqrt{D_n}}{(1 - D_n)^2} e^{-P_2 t} \int_0^\infty e^{-(P_1 - P_2)x} \left\{ I_1(\beta x) + I_0(\beta x) \right\} dx + \frac{2D_n (B_n - B_{n+1})}{(1 - D_n)(1 + \sqrt{D_n})} e^{-P_2 t} u(-t)$$
(2.76)

Let  $\alpha = (P_1 - P_2) = \frac{(1 + D_n)(B_{n+1} - B_n)}{2(1 - D_n)}$  and check the requirements that  $Re\{\alpha\} - |Re\{\beta\}| > 0$  to use 6.611.4 of [10] given by

$$\int_0^\infty e^{-\alpha x} I_v(\beta x) dx = \frac{\beta^{-v} \left[\alpha - \sqrt{\alpha^2 - \beta^2}\right]^v}{\sqrt{\alpha^2 - \beta^2}}.$$
 (2.77)

For  $B_{n+1} > B_n$ .

 $Re\{a\} = Re\{a\}$ 

For  $B_{n+1} < B_n$ .

 $Re\{\alpha\} = Re\{$ 

Therefore, to its

Now. comsider t

 $B_{n-1}$  and thus

and thus  $D_r >$ 

ध्यव

\$17ES

Ř<sup>T</sup>E<sub>III</sub> =

For  $B_{n+1} > B_n$ ,

$$Re\{\alpha\} - |Re\{\beta\}| = \frac{(1+D_n)(B_{n+1} - B_n)}{2(1-D_n)} - \frac{(B_{n+1} - B_n)}{2} = \frac{D_n(B_{n+1} - B_n)}{1-D_n}.$$
(2.78)

For  $B_{n+1} < B_n$ ,

$$Re\{\alpha\} - |Re\{\beta\}| = \frac{(1+D_n)(B_{n+1} - B_n)}{2(1-D_n)} + \frac{(B_{n+1} - B_n)}{2} = \frac{(B_{n+1} - B_n)}{1-D_n}. \quad (2.79)$$

Therefore, to use 6.611.4 of [10]  $\begin{cases} B_{n+1} > B_n & \Leftrightarrow 0 < D_n < 1 \\ B_{n+1} < B_n & \Leftrightarrow D_n > 1 \end{cases}$  must be satisfied.

Now, consider the case  $P_2 = \frac{B_n - D_n B_{n+1}}{1 - D_n} < 0$ . Then  $1 - D_n > 0 \Leftrightarrow B_n < D_n B_{n+1} < B_{n+1}$  and thus  $0 < D_n < 1 \Leftrightarrow B_{n+1} > B_n$ . Also,  $1 - D_n < 0 \Leftrightarrow B_n > D_n B_{n+1} > B_{n+1}$  and thus  $D_n > 1 \Leftrightarrow B_n > B_{n+1}$ . Using,

$$\int_0^\infty e^{-\alpha x} I_1(\beta x) dx = \frac{1}{\beta} \left\{ \frac{\alpha}{\sqrt{\alpha^2 - \beta^2}} - 1 \right\} = \frac{(\alpha/\beta)}{\sqrt{\alpha^2 - \beta^2}} - \frac{1}{\beta}, \tag{2.80}$$

$$\sqrt{\alpha^2 - \beta^2} = \left\{ \frac{(1 + D_n)^2 (B_{n+1} - B_n)^2}{4(1 - D_n)^2} - \frac{(B_{n+1} - B_n)^2}{4} \right\}^{\frac{1}{2}}$$
$$= \frac{(B_{n+1} - B_n)\sqrt{D_n}}{1 - D_n}$$

and

$$\int_0^\infty e^{-\alpha x} I_0(\beta x) dx = \frac{1}{\sqrt{\alpha^2 - \beta^2}}$$
 (2.81)

gives

$$\tilde{R}^{TE}(t) = \frac{(B_n - B_{n+1})^2 D_n \sqrt{D_n}}{(1 - D_n)^2} e^{-P_2 t} \left\{ \frac{(\alpha/\beta)}{\sqrt{\alpha^2 - \beta^2}} - \frac{1}{\beta} + \frac{1}{\sqrt{\alpha^2 - \beta^2}} \right\}$$

Therefore, (2.7

 $\tilde{R}^{TE}(t) =$ 

where  $\int_{0}^{\infty}$  that (2.53)

$$+\frac{2D_{n}(B_{n}-B_{n+1})}{(1-D_{n})(1+\sqrt{D_{n}})}e^{-P_{2}t}u(-t)$$

$$= e^{-P_{2}t}\left[\left\{\frac{1-D_{n}}{(B_{n+1}-B_{n})\sqrt{D_{n}}}\left(\frac{(1+D_{n})(B_{n+1}-B_{n})}{2(1-D_{n})}\frac{2}{(B_{n+1}-B_{n})}+1\right)\right.$$

$$-\frac{2}{(B_{n+1}-B_{n})}\right\} \times \frac{(B_{n}-B_{n+1})^{2}D_{n}\sqrt{D_{n}}}{(1-D_{n})^{2}} + \frac{2D_{n}(B_{n}-B_{n+1})}{(1-D_{n})(1+\sqrt{D_{n}})}\right]$$

$$= e^{-P_{2}t}\left[\frac{2D_{n}(B_{n+1}-B_{n})(1-\sqrt{D_{n}})}{(1-D_{n})(1-\sqrt{D_{n}})} + \frac{2D_{n}(B_{n}-B_{n+1})}{(1-D_{n})(1+\sqrt{D_{n}})}\right] = 0.$$
(2.82)

Therefore, (2.75) consists of pure causal terms, and can be rewritten as, when t > 0

$$\tilde{R}^{TE}(t) = \frac{(B_n - B_{n+1})\sqrt{D_n}}{1 - D_n} e^{-P_1 t} \left\{ I_1(\beta t) + I_0(\beta t) \right\} u(t) 
+ \frac{(B_n - B_{n+1})^2 D_n \sqrt{D_n}}{(1 - D_n)^2} e^{-P_2 t} u(t) \int_t^{\infty} e^{-(P_1 - P_2)x} \left\{ I_1(\beta x) + I_0(\beta x) \right\} dx 
= \frac{(B_n - B_{n+1})\sqrt{D_n}}{1 - D_n} e^{-P_1 t} \left\{ I_1(\beta t) + I_0(\beta t) \right\} u(t) 
+ \frac{(B_n - B_{n+1})^2 D_n \sqrt{D_n}}{(1 - D_n)^2} e^{-P_2 t} u(t) \int_0^{\infty} e^{-(P_1 - P_2)x} \left\{ I_1(\beta x) + I_0(\beta x) \right\} dx 
- \frac{(B_n - B_{n+1})^2 D_n \sqrt{D_n}}{(1 - D_n)^2} e^{-P_2 t} u(t) \int_0^t e^{-(P_1 - P_2)x} \left\{ I_1(\beta x) + I_0(\beta x) \right\} dx 
= \frac{(B_n - B_{n+1})\sqrt{D_n}}{1 - D_n} e^{-P_1 t} \left\{ I_1(\beta t) + I_0(\beta t) \right\} u(t) 
- \frac{(B_n - B_{n+1})^2 D_n \sqrt{D_n}}{(1 - D_n)^2} e^{-P_2 t} u(t) \int_0^t e^{-(P_1 - P_2)x} \left\{ I_1(\beta x) + I_0(\beta x) \right\} dx 
+ \frac{2D_n (B_{n+1} - B_n)}{(1 - D_n)(1 + \sqrt{D_n})} e^{-P_2 t} u(t) \tag{2.83}$$

where  $\int_0^\infty e^{-(P_1-P_2)x} \{I_1(\beta x) + I_0(\beta x)\} dx = \frac{2(1-D_n)}{(B_{n+1}-B_n)\sqrt{D_n}}$  was used. Notice that (2.83) is exactly same with (2.74).

(2)  $\tilde{\boldsymbol{D}}_{n+1} < 0$  and  $\tilde{D}_n < 0$ 

$$\tilde{R}^{TE}(s) = -\frac{2B_n\sqrt{D_n}}{1 - D_n} \frac{1}{s - P_2} \left\{ 1 - \sqrt{\frac{s - B_{n+1}}{s - B_n}} \right\}$$

When  $P_1 > 0$ .

 $\dot{R}^{TE}(t) = \int_{t}^{t}$ 

=

and when P

 $\tilde{R}^{TE}(t)$ 

$$+\frac{2\sqrt{D_n}}{1-D_n}\frac{s}{s-P_2}\left\{1-\sqrt{\frac{s-B_{n+1}}{s-B_n}}\right\} + \frac{2D_n(B_n-B_{n+1})}{(1-D_n)(1+\sqrt{D_n})}\frac{1}{s-P_2}.$$
 (2.84)

When  $P_2 > 0$ , (2.84) has the inverse Fourier transform (see B.7 as

$$\tilde{R}^{TE}(t) = \left[ \frac{2B_n \sqrt{D_n}}{1 - D_n} e^{P_2 t} u(-t) + \frac{2\sqrt{D_n}}{1 - D_n} e^{P_2 t} \left\{ \delta(t) - P_2 u(-t) \right\} \right] *$$

$$\left[ \beta e^{P_1 t} \left\{ I_1(\beta t) - I_0(\beta t) \right\} u(-t) \right] - \frac{2D_n(B_n - B_{n+1})}{(1 - D_n)(1 + \sqrt{D_n})} e^{P_2 t} u(-t)$$

$$= \frac{2B_n \sqrt{D_n}}{1 - D_n} \beta e^{P_1 t} \left\{ I_1(\beta t) - I_0(\beta t) \right\} u(-t)$$

$$+ \beta \left\{ \frac{2B_n \sqrt{D_n}}{1 - D_n} - P_2 \frac{2\sqrt{D_n}}{1 - D_n} \right\} e^{P_2 t} u(-t) * e^{P_1 t} \left\{ I_1(\beta t) - I_0(\beta t) \right\} u(-t)$$

$$- \frac{2D_n(B_n - B_{n+1})}{(1 - D_n)(1 + \sqrt{D_n})} e^{P_2 t} u(-t)$$

$$= \frac{(B_{n+1} - B_n)\sqrt{D_n}}{1 - D_n} e^{P_1 t} \left\{ I_1(\beta t) - I_0(\beta t) \right\} u(-t)$$

$$+ \frac{(B_{n+1} - B_n)^2 D_n \sqrt{D_n}}{(1 - D_n)^2} e^{P_2 t} u(-t) \int_t^0 e^{(P_1 - P_2)x} \left\{ I_1(\beta x) - I_0(\beta x) \right\} dx$$

$$+ \frac{2D_n(B_{n+1} - B_n)}{(1 - D_n)(1 + \sqrt{D_n})} e^{P_2 t} u(-t)$$

$$(2.85)$$

and, when  $P_2 < 0$ ,

$$\tilde{R}^{TE}(t) = \left[ -\frac{2B_n\sqrt{D_n}}{1 - D_n} e^{P_2 t} u(t) + \frac{2\sqrt{D_n}}{1 - D_n} e^{P_2 t} \left\{ \delta(t) + P_2 u(t) \right\} \right] *$$

$$\left[ \beta e^{P_1 t} \left\{ I_1(\beta t) - I_0(\beta t) \right\} u(-t) \right] - \frac{2D_n(B_{n+1} - B_n)}{(1 - D_n)(1 + \sqrt{D_n})} e^{P_2 t} u(t)$$

$$= \frac{(B_{n+1} - B_n)\sqrt{D_n}}{1 - D_n} e^{P_1 t} \left\{ I_1(\beta t) - I_0(\beta t) \right\} u(-t)$$

$$\left\{ -\frac{2B_n\sqrt{D_n}}{1 - D_n} + \frac{2\sqrt{D_n}}{1 - D_n} P_2 \right\} \beta e^{P_2 t} u(t) * e^{P_1 t} \left\{ I_1(\beta t) - I_0(\beta t) \right\} u(-t)$$

$$-\frac{2D_n(B_{n+1} - B_n)}{(1 - D_n)(1 + \sqrt{D_n})} e^{P_2 t} u(t)$$

$$= \frac{(B_{n+1} - B_n)\sqrt{D_n}}{1 - D_n} e^{P_1 t} \left\{ I_1(\beta t) - I_0(\beta t) \right\} u(-t)$$

Then, since t >

 $\tilde{R}^{TE}(t) =$ 

Consedite 114,17.

 $\tilde{R}^{TE}(t) =$ 

$$-\frac{(B_{n+1}-B_n)^2 D_n \sqrt{D_n}}{(1-D_n)^2} e^{P_2 t} \int_{-\infty}^{\min(t,0)} e^{(P_1-P_2)x} \left\{ I_1(\beta x) - I_0(\beta x) \right\} dx$$

$$-\frac{2D_n (B_{n+1}-B_n)}{(1-D_n)(1+\sqrt{D_n})} e^{P_2 t} u(t). \tag{2.86}$$

In contrast to the  $\tilde{D}_{n+1} > 0$ , and  $\tilde{D}_n > 0$  case, (2.86) has apparent causal terms, and these terms can be converted to pure non-causal terms. When t > 0, (2.86) becomes

$$\tilde{R}^{TE}(t) = -\frac{(B_{n+1} - B_n)^2 D_n \sqrt{D_n}}{(1 - D_n)^2} e^{P_2 t} \int_{-\infty}^0 e^{(P_1 - P_2)x} \left\{ I_1(\beta x) - I_0(\beta x) \right\} dx + \frac{2D_n (B_n - B_{n+1})}{(1 - D_n)(1 + \sqrt{D_n})} e^{P_2 t} u(t).$$
(2.87)

Letting x = -z, the integral term is rewritten as

$$\int_{-\infty}^{0} e^{(P_1 - P_2)x} \left\{ I_1(\beta x) - I_0(\beta x) \right\} dz = \int_{\infty}^{0} e^{-(P_1 - P_2)z} \left\{ I_1(-\beta z) - I_0(-\beta z) \right\} dz$$

$$= -\int_{\infty}^{0} e^{-(P_1 - P_2)z} \left\{ -I_1(\beta z) - I_0(\beta z) \right\} dz$$

$$= -\int_{0}^{\infty} e^{-(P_1 - P_2)z} \left\{ I_1(\beta z) + I_0(\beta z) \right\} dz.$$
(2.88)

Then, since t > 0

$$\tilde{R}^{TE}(t) = e^{P_2 t} \left[ \frac{(B_{n+1} - B_n)^2 D_n \sqrt{D_n}}{(1 - D_n)^2} \int_0^\infty e^{-(P_1 - P_2)x} \left\{ I_1(\beta x) + I_0(\beta x) \right\} dx + \frac{2D_n(B_n - B_{n+1})}{(1 - D_n)(1 + \sqrt{D_n})} \right]$$

$$= 0 \qquad (2.89)$$

Consequently, when t < 0, (2.86) becomes

$$\tilde{R}^{TE}(t) = \frac{(B_{n+1} - B_n)\sqrt{D_n}}{1 - D_n} e^{P_1 t} \left\{ I_1(\beta t) - I_0(\beta t) \right\} u(-t)$$

às

Three

I we let g:

$$-\frac{(B_{n+1} - B_n)^2 D_n \sqrt{D_n}}{(1 - D_n)^2} e^{P_2 t} u(-t) \int_{-\infty}^t e^{(P_1 - P_2)x} \left\{ I_1(\beta x) - I_0(\beta x) \right\} dx$$

$$= \frac{(B_{n+1-B_n}) \sqrt{D_n}}{1 - D_n} e^{P_1 t} \left\{ I_1(\beta t) - I_0(\beta t) \right\} u(-t)$$

$$-\frac{(B_{n+1} - B_n)^2 D_n \sqrt{D_n}}{(1 - D_n)^2} e^{P_2 t} u(-t) \int_{-\infty}^0 e^{(P_1 - P_2)x} \left\{ I_1(\beta x) - I_0(\beta x) \right\} dx$$

$$+\frac{(B_{n+1} - B_n)^2 D_n \sqrt{D_n}}{(1 - D_n)^2} e^{P_2 t} u(-t) \int_t^0 e^{(P_1 - P_2)x} \left\{ I_1(\beta x) - I_0(\beta x) \right\} dx$$

$$= \frac{(B_{n+1} - B_n) \sqrt{D_n}}{1 - D_n} e^{P_1 t} \left\{ I_1(\beta t) - I_0(\beta t) \right\} u(-t)$$

$$+\frac{(B_{n+1} - B_n)^2 D_n \sqrt{D_n}}{(1 - D_n)^2} e^{P_2 t} u(-t) \int_t^0 e^{(P_1 - P_2)x} \left\{ I_1(\beta x) - I_0(\beta x) \right\} dx$$

$$+\frac{2D_n (B_{n+1} - B_n)}{(1 - D_n)(1 + \sqrt{D_n})} e^{P_2 t} u(-t)$$

$$(2.90)$$

which includes non-causal terms only.

(3) 
$$\tilde{D}_{n+1} > 0$$
 and  $\tilde{D}_n < 0$ 

Using the frequency domain unit step function  $U(s) = U(j\omega)$ , (2.61) can be expressed as

$$\tilde{R}^{TE}(s) = G(s)U(s) + G^*(-s)U(-s)$$
(2.91)

where

$$G(s) = -\frac{2jB_{n}\sqrt{D_{n}}}{1+D_{n}} \frac{1}{s-P_{2}} \left\{ 1 - \sqrt{\frac{s+B_{n+1}}{s-B_{n}}} \right\}$$

$$+ \frac{2j\sqrt{D_{n}}}{1+D_{n}} \frac{s}{s-P_{2}} \left\{ 1 - \sqrt{\frac{s+B_{n+1}}{s-B_{n}}} \right\}$$

$$- \frac{2D_{n}(B_{n}+B_{n+1})}{(1+D_{n})(1+j\sqrt{D_{n}})} \frac{1}{s-P_{2}}.$$

$$(2.92)$$

If we let  $g(t) = F^{-1}\{G(s)\}$ , then, from (B.2),

$$\tilde{R}^{TE}(t) = \frac{1}{2} \{g(t) + g^*(t)\} + \frac{j}{2\pi t} * \{g(t) - g^*(t)\}$$

$$= Re\{g(t)\} - \frac{1}{\pi t} * Im\{g(t)\}.$$
(2.93)

When P

g. •

Wirle

fitt

fran (

ând.

I

Filip

When  $P_2 > 0$ ,

$$g(t) = \frac{2jB_n\sqrt{D_n}}{1+D_n}e^{P_2t}u(-t)*f_3(t) + \frac{2j\sqrt{D_n}}{1+D_n}\{\delta(t) - P_2u(-t)\}e^{P_2t}*f_3(t) - \frac{2D_n(B_n + B_{n+1})}{(1+D_n)(1-j\sqrt{D_n})}e^{P_2t}u(-t)$$
(2.94)

where

$$f_{3}(t) = F^{-1} \left\{ 1 - \sqrt{\frac{s + B_{n+1}}{s - B_{n}}} \right\}$$

$$= \frac{B_{n}}{2} e^{\frac{B_{n}}{2}t} \left\{ I_{1}(\frac{B_{n}}{2}t) + I_{0}(\frac{B_{n}}{2}t) \right\} u(-t)$$

$$- \frac{B_{n+1}}{2} e^{-\frac{B_{n+1}}{2}t} \left\{ I_{1}(\frac{B_{n+1}}{2}t) + I_{0}(\frac{B_{n+1}}{2}t) \right\} u(t)$$

$$+ \frac{B_{n+1}B_{n}}{4} e^{\frac{B_{n}}{2}t} \int_{max(t,0)}^{\infty} e^{-\frac{(B_{n+1}+B_{n})}{2}x} \left\{ I_{1}\left[\frac{B_{n}}{2}(t-x)\right] + I_{0}\left[\frac{B_{n}}{2}(t-x)\right] \right\}$$

$$\times \left\{ I_{1}(\frac{B_{n+1}}{2}x) + I_{0}(\frac{B_{n+1}}{2}x) \right\} dx$$

$$(2.95)$$

from (B.10). Now,

$$Re\{g(t)\} = \frac{2D_n(B_n + B_{n+1})}{(1 + D_n)^2} e^{P_2 t} u(-t)$$
(2.96)

and,

$$Im\{g(t)\} = \frac{2B_{n}\sqrt{D_{n}}}{1+D_{n}}e^{P_{2}t}u(-t)*f_{3}(t) + \frac{2\sqrt{D_{n}}}{1+D_{n}}\{\delta(t) - P_{2}u(-t)\}e^{P_{2}t}*f_{3}(t) - \frac{2D_{n}\sqrt{D_{n}}(B_{n} + B_{n+1})}{(1+D_{n})^{2}}e^{P_{2}t}u(-t).$$
(2.97)

Finally, for  $P_2 > 0$ , the transient interfacial reflection coefficient is

$$\tilde{R}^{TE}(t) = Re\{g(t)\} - \frac{1}{\pi t} * Im\{g(t)\}$$

$$= \frac{2D_n(B_n + B_{n+1})}{(1 + D_n)^2} e^{P_2 t} u(-t) - \frac{2\sqrt{D_n}}{1 + D_n} f_3(t) * \frac{1}{\pi t}$$

$$-\frac{2D_{n}\sqrt{D_{n}}(B_{n}+B_{n+1})}{(1+D_{n})^{2}}e^{P_{2}t}u(-t)*f_{3}(t)*\frac{1}{\pi t}$$

$$+\frac{2D_{n}\sqrt{D_{n}}(B_{n}+B_{n+1})}{(1+D_{n})^{2}}e^{P_{2}t}u(-t)*\frac{1}{\pi t}.$$
(2.98)

Alternatively,

$$\tilde{R}^{TE}(t) = \frac{2D_n\sqrt{D_n}(B_n + B_{n+1})}{(1+D_n)^2} \left[ \frac{1}{\sqrt{D_n}} e^{P_2 t} u(-t) + \{1 - f_3(t)\} * \frac{1}{\pi t} * e^{P_2 t} u(-t) \right] - \frac{2\sqrt{D_n}}{1+D_n} * \frac{1}{\pi t} * f_3(t).$$
(2.99)

Similarly, for  $P_2 < 0$ ,

$$Re\{g(t)\} = -\frac{2D_n(B_n + B_{n+1})}{(1 + D_n)^2} e^{P_2 t} u(t)$$
 (2.100)

and,

$$Im\{g(t)\} = -\frac{2B_n\sqrt{D_n}}{1+D_n}e^{P_2t}u(t) * f_3(t) + \frac{2\sqrt{D_n}}{1+D_n}\{\delta(t) + P_2u(t)\} * f_3(t) + \frac{2D_n\sqrt{D_n}(B_n + B_{n+1})}{(1+D_n)^2}e^{P_2t}u(t).$$
(2.101)

Therefore, the resulting transient interfacial reflection coefficient for  $P_2 < 0$  is given by

$$\tilde{R}^{TE}(t) = Re\{g(t)\} - \frac{1}{\pi t} * Im\{g(t)\} 
= -\frac{2D_n(B_n + B_{n+1})}{(1 + D_n)^2} e^{P_2 t} u(t) - \frac{2\sqrt{D_n}}{1 + D_n} f_3(t) * \frac{1}{\pi t} 
+ \frac{2D_n\sqrt{D_n}(B_n + B_{n+1})}{(1 + D_n)^2} e^{P_2 t} u(t) * f_3(t) * \frac{1}{\pi t} 
- \frac{2D_n\sqrt{D_n}(B_n + B_{n+1})}{(1 + D_n)^2} e^{P_2 t} u(t) * \frac{1}{\pi t}.$$
(2.102)

Alternati

 $\tilde{R}^{TE}_{\gamma}t$ 

4 D<sub>n</sub>. Using fi

71.-16

lt we

#<u>.</u>

Alternatively,

$$\tilde{R}^{TE}(t) = -\frac{2D_n\sqrt{D_n}(B_n + B_{n+1})}{(1+D_n)^2} \left[ \frac{1}{\sqrt{D_n}} e^{P_2 t} u(t) + \{1 - f_3(t)\} * \frac{1}{\pi t} * e^{P_2 t} u(t) \right] - \frac{2\sqrt{D_n}}{1+D_n} * \frac{1}{\pi t} * f_3(t).$$
(2.103)

(4)  $\tilde{D}_{n+1} < 0 \text{ and } \tilde{D}_n > 0$ 

Using frequency domain unit step function  $U(\omega)$ , (2.62) can be expressed as

$$\tilde{R}^{TE}(s) = G(s)U(s) + G^*(-s)U(-s)$$
(2.104)

where

$$G(s) = -\frac{2jB_{n}\sqrt{D_{n}}}{1+D_{n}} \frac{1}{s+P_{2}} \left\{ 1 + \sqrt{\frac{s-B_{n+1}}{s+B_{n}}} \right\}$$

$$-\frac{2j\sqrt{D_{n}}}{1+D_{n}} \frac{s}{s+P_{2}} \left\{ 1 + \sqrt{\frac{s-B_{n+1}}{s+B_{n}}} \right\}$$

$$+\frac{2D_{n}(B_{n}+B_{n+1})}{(1+D_{n})(1-j\sqrt{D_{n}})} \frac{1}{s+P_{2}}.$$

$$(2.105)$$

If we let  $g(t) = F^{-1}\{G(s)\}$ , then, from (B.2),

$$\tilde{R}^{TE}(t) = \frac{1}{2} \{g(t) + g^*(t)\} + \frac{j}{2\pi t} * \{g(t) - g^*(t)\}$$

$$= Re\{g(t)\} - \frac{1}{\pi t} * Im\{g(t)\}.$$
(2.106)

When  $P_2 > 0$ ,

$$g(t) = -\frac{2jB_n\sqrt{D_n}}{1+D_n}e^{-P_2t}u(t) * f_4(t) - \frac{2j\sqrt{D_n}}{1+D_n} \{\delta(t) - P_2u(t)\}e^{-P_2t} * f_4(t) + \frac{2D_n(B_n + B_{n+1})}{(1+D_n)(1-j\sqrt{D_n})}e^{-P_2t}u(t)$$
(2.107)

where

$$f_{4}(t) = F^{-1} \left\{ 1 + \sqrt{\frac{s - B_{n+1}}{s + B_{n}}} \right\}$$

$$= \frac{B_{n+1}}{2} e^{\frac{B_{n+1}}{2}t} \left\{ I_{1}(\frac{B_{n+1}}{2}t) - I_{0}(\frac{B_{n+1}}{2}t) \right\} u(-t)$$

$$- \frac{B_{n}}{2} e^{-\frac{B_{n}}{2}t} \left\{ I_{1}(\frac{B_{n}}{2}t) - I_{0}(\frac{B_{n}}{2}t) \right\} u(t) + \frac{(B_{n+1}B_{n})}{4} e^{\frac{B_{n+1}}{2}t} \times$$

$$\int_{max(t,0)}^{\infty} e^{-\frac{(B_{n+1}+B_{n})}{2}x} \left\{ I_{1} \left[ \frac{B_{n+1}}{2}(t-x) \right] - I_{0} \left[ \frac{B_{n+1}}{2}(t-x) \right] \right\}$$

$$\times \left\{ I_{1}(\frac{B_{n}}{2}x) - I_{0}(\frac{B_{n}}{2}x) \right\} dx \tag{2.108}$$

from (B.11). Now,

$$Re\{g(t)\} = \frac{2D_n(B_n + B_{n+1})}{(1 + D_n)^2} e^{-P_2 t} u(t)$$
 (2.109)

and,

$$Im\{g(t)\} = -\frac{2B_n\sqrt{D_n}}{1+D_n}e^{-P_2t}u(t) * f_4(t) - \frac{2\sqrt{D_n}}{1+D_n}\{\delta(t) - P_2u(t)\}e^{-P_2t} * f_4(t) + \frac{2D_n\sqrt{D_n}(B_n + B_{n+1})}{(1+D_n)^2}e^{-P_2t}u(t).$$
(2.110)

Thus, for  $P_2 > 0$ , the transient interfacial reflection coefficient is

$$\tilde{R}^{TE}(t) = Re\{g(t)\} - \frac{1}{\pi t} * Im\{g(t)\}$$

$$= \frac{2D_n(B_n + B_{n+1})}{(1 + D_n)^2} e^{-P_2 t} u(t) + \frac{2\sqrt{D_n}}{1 + D_n} f_4(t) * \frac{1}{\pi t}$$

$$+ \frac{2D_n\sqrt{D_n}(B_n + B_{n+1})}{(1 + D_n)^2} e^{-P_2 t} u(t) * f_4(t) * \frac{1}{\pi t}$$

$$- \frac{2D_n\sqrt{D_n}(B_n + B_{n+1})}{(1 + D_n)^2} e^{-P_2 t} u(t) * \frac{1}{\pi t}.$$
(2.111)

Alternatively,

$$\tilde{R}^{TE}(t) = \frac{2D_n\sqrt{D_n}(B_n + B_{n+1})}{(1+D_n)^2} \left[ \frac{1}{\sqrt{D_n}} e^{-P_2 t} u(t) + \{f_4(t) - 1\} * \frac{1}{\pi t} * e^{-P_2 t} u(t) \right] + \frac{2\sqrt{D_n}}{1+D_n} * \frac{1}{\pi t} * f_4(t).$$
(2.112)

Similarly, for  $P_2 < 0$ ,

$$Re\{g(t)\} = -\frac{2D_n(B_n + B_{n+1})}{(1 + D_n)^2} e^{-P_2 t} u(-t)$$
(2.113)

and,

$$Im\{g(t)\} = \frac{2B_n\sqrt{D_n}}{1+D_n}e^{-P_2t}u(-t) * f_4(t) - \frac{2\sqrt{D_n}}{1+D_n}\{\delta(t) + P_2u(-t)\} * f_4(t) - \frac{2D_n\sqrt{D_n}(B_n + B_{n+1})}{(1+D_n)^2}e^{-P_2t}u(-t).$$
(2.114)

Therefore, the resulting transient interfacial reflection coefficient for  $P_2 < 0$  is given by

$$\tilde{R}^{TE}(t) = Re\{g(t)\} - \frac{1}{\pi t} * Im\{g(t)\} 
= -\frac{2D_n(B_n + B_{n+1})}{(1 + D_n)^2} e^{-P_2 t} u(-t) + \frac{2\sqrt{D_n}}{1 + D_n} f_4(t) * \frac{1}{\pi t} 
- \frac{2D_n\sqrt{D_n}(B_n + B_{n+1})}{(1 + D_n)^2} e^{-P_2 t} u(-t) * f_4(t) * \frac{1}{\pi t} 
+ \frac{2D_n\sqrt{D_n}(B_n + B_{n+1})}{(1 + D_n)^2} e^{-P_2 t} u(-t) * \frac{1}{\pi t}.$$
(2.115)

Alternatively,

$$\tilde{R}^{TE}(t) = -\frac{2D_n\sqrt{D_n}(B_n + B_{n+1})}{(1+D_n)^2} \left[ -\frac{1}{\sqrt{D_n}} e^{-P_2 t} u(-t) + \left[ 1 - f_4(t) \right] * \frac{1}{\pi t} * e^{-P_2 t} u(-t) \right] + \frac{2\sqrt{D_n}}{1+D_n} * \frac{1}{\pi t} * f_4(t). \quad (2.116)$$

it shet

Callyai

<u> 1</u>05-0

Fg','h

**#**275

NÇN 1

A go

dele

رز ه (

]

ú. a

1055

 $G_{08}^1$ 

**\$**()

Ü

II.

V.

:}

<u>.</u>

.

### 2.3.2 Causality

In the transient forms for the cases of (2), (3) and (4), there are non-causal terms involving u(-t) or  $\frac{1}{t}$ . These are unexpected results, because the convolution of any causal (thus, physically realizable) input waveform with these terms will produce non-causal transient reflected waveform components that appears to disobey Einstein's causality, which says that nothing can travel faster than the speed of light. Also, it should be noted that this is 'pure' non-causality which is different from the non-causality caused by the diffusion approximation referred in [11]. The existence of the non-causal terms depends on the sign of  $\tilde{D}_{n+1}$  and  $\tilde{D}_n$ . That is, the non-causality happens when the sign of either one of the two parameters is negative. When the sign is negative, the real part of  $\gamma_x$  is always negative by the branch cut; therefore the wave propagates in an evanescent mode, regardless of the existence of conductivity. A good example of this case is total internal reflection at the interface of lossless dielectric material layers.

The conventional geometrical ray optics approach can not explain this non-causality. Consider the geometry shown in Figure 2.3, where total internal reflection of an impulse incident plane wave is assumed to occur at the interface between two lossless dielectric layers. The reflected wave packet from the point Q1 arrives at the observation plane at t=0, at the same moment as the reflection of the incident wave from Q2, because their propagation velocities are the same in this same region, and the lengths of travel along paths P1 and P2 are identical. Consider a surface wave in region 2, which starts at Q1 and propagates along the z-axis with propagation velocity equal to or less then  $v_{2z} = \frac{\omega}{\gamma_{2z}} = \frac{\omega}{\gamma_{1z}} = \frac{\omega}{\gamma_1 \sin \theta_{i1}}$ . Then, the travel time of the surface wave is  $t_d \geq \frac{d}{v_{2z}} = \frac{d\gamma_1 \sin \theta_{i1}}{\omega} = \frac{P2}{\sin \theta_{i1}} \frac{\omega}{\gamma_1 \sin \theta_{i1}} = \frac{P2}{(\omega/\gamma_1)}$ . Therefore, the surface wave arrives at Q2 at the same or later moment at which the incident wave impinges on this point.

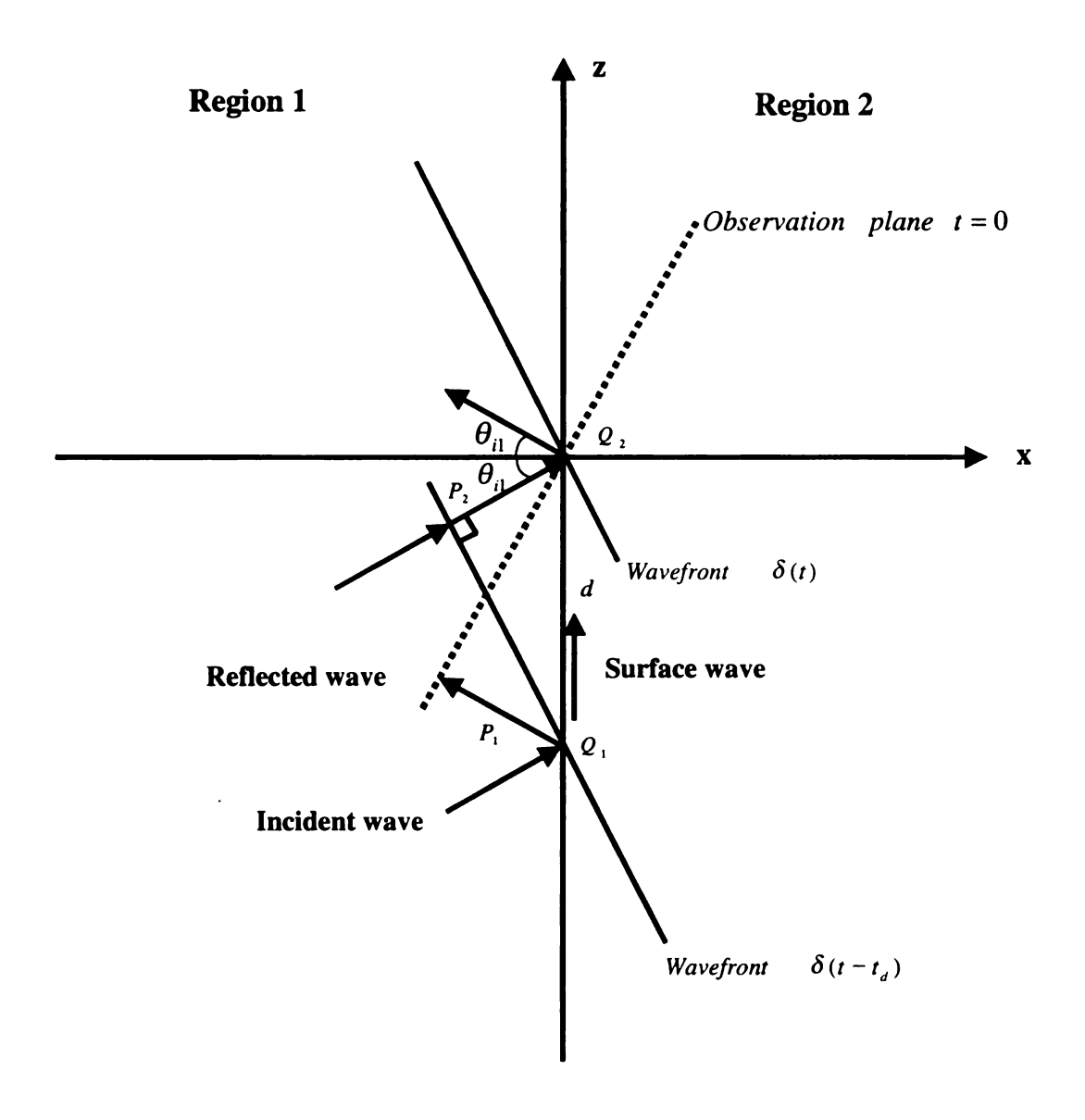


Figure 2.3. The time relationship of wavefronts.

åLd

ihe

là:

of t

(215)

The

aid:

Sum

ود بن

]

this the e

ir II

if a Herr

ilê ç

iett.

Next, consider the possible existence of a precursor effect. Any wave front of the spherical wave excited at Q1 that arrives at a point on the observation plane faster than the wave reflected from Q2 might be a precursor and thus a source of the non-causality. From Figure 2.4, consider path 1 with  $l_1 = \sqrt{h^2 + l_3^2} = \sqrt{(d+x)^2 + \left(\frac{x}{\tan\theta_{i1}}\right)^2}$  and path 2 with  $l_2 + l_3 = d\sin\theta_{i1} + \frac{x}{\sin\theta_{i1}}$ . To be a precursor, path 1 must be less than path 2. However

$$l_1^2 - (l_2 + l_3)^2 = \left\{ (d+x)^2 + \left(\frac{x}{\tan\theta_{i1}}\right)^2 \right\} - \left(d\sin\theta_{i1} + \frac{x}{\tan\theta_{i1}}\right)^2$$

$$= d^2 + x^2 + x^2 \left(\frac{1}{\tan^2\theta_{i1}} - \frac{1}{\sin^2\theta_{i1}}\right) - d^2\sin^2\theta_{i1}$$

$$= d^2\cos^2\theta_{i1} > 0$$
 (2.117)

and thus, there is no precursor.

In this study, a reasonable explanation of the non-causality has not been found. The non-causality might originate from the impractical assumption of infinite layer width because the incident plane wave interacts with the interface an infinite amount time ago, i.e. as far back as  $t = -\infty$ , although the relationship between this assumption and non-causality could not be found using ordinary ray optics approach as explained above.

There are several interesting ongoing research activities that might help explain this phenonmenon. In physics, there have been some trials to measure or compute the exact tunneling time of a particle through a potential barrier, which is important in modern microelectronic tunneling devices [12], [13]. It turns out that the tunneling of a particle (or a wavepacket) is quite similar to the transmission of an evanescent electromagnetic wave, e.g. the propagation of a wave having a frequency less than the cut-off frequency in a waveguide [14]. Therefore, there were many experiments performed by using optical pulses (e.g. [15] and [16]), or microwave propagation in a

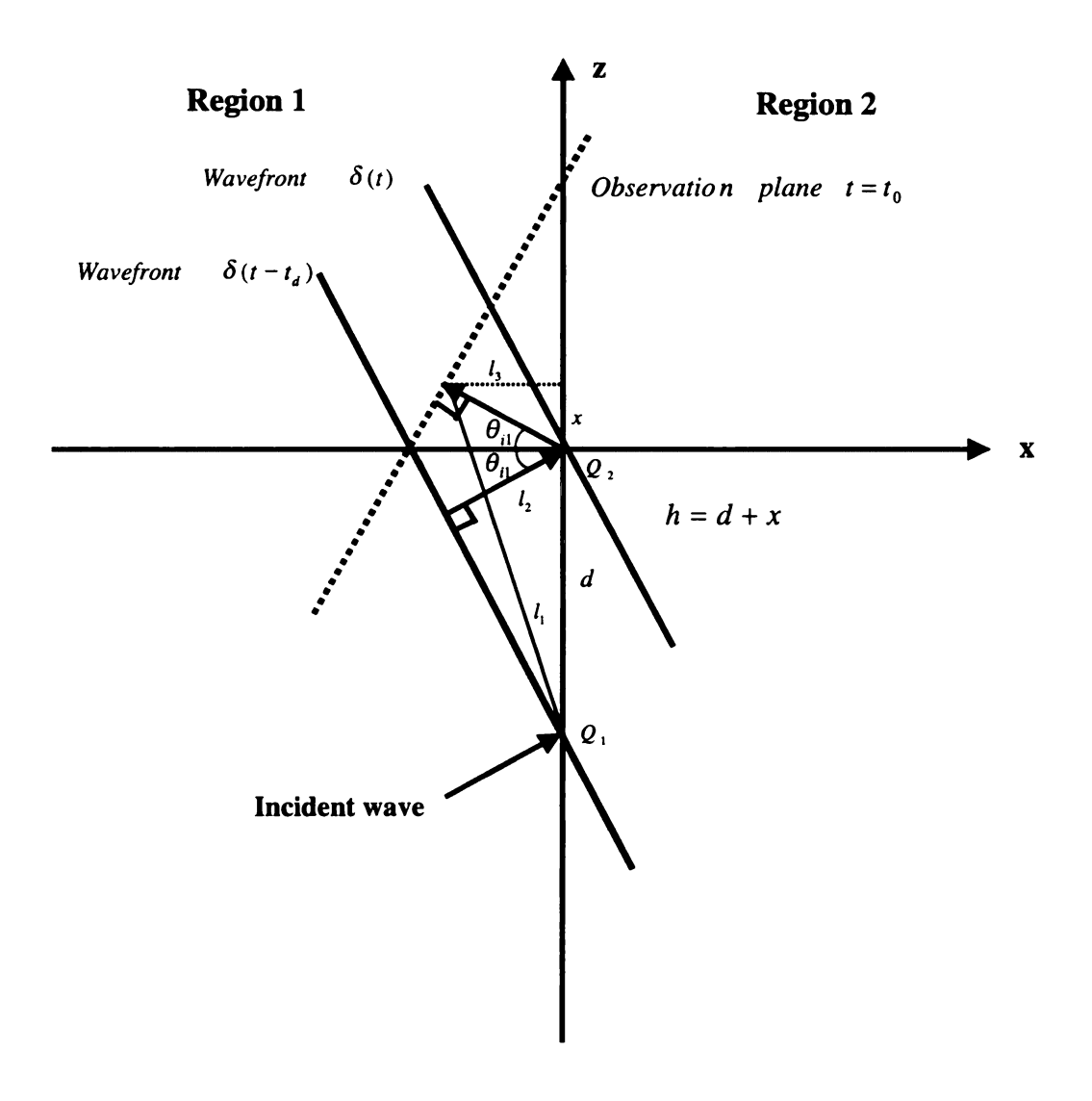


Figure 2.4. The consideration of the existence of a precursor.

waveguide (e.g. In these exp agation velociti an evanescent t minal propaga were to become therefore faster Einstein causa the past [18]. tempted to ex attenuation of is known abo question abou since it is sor It should nomenon" o impulse resi point is caus ties were mie shape of the experiment. and the no the fact the mode. Æ a re

eration, s

non-causal

waveguide (e.g. [17]).

In these experiments, it has been commonly observed that the pulse peak propagation velocities seem to be independent of the thickness of a potential barrier (or an evanescent region, equivalently), which consequently implies so-called "super luminal" propagation velocity of the wave modes. For example, if the width of region were to become infinite, then the speed of wave propagation would increase infinitely, therefore faster than the speed of light, which leads to apparent contradiction of the Einstein causality. Although this phenomenon had been theoretically predicted in the past [18], the exact theoretical explanation has yet been given. Many have attempted to explain this phenomenon as a reshaping of the pulse [15], [16]. That is, attenuation of the pulse in the barrier shifts the peak of the pulse forward. But little is known about why the barriers attenuate pulses unevenly [19]. Also, there is a question about the validity of 'peak' measurement methodology in dispersive media, since it is sometimes hard to define the pulse peak in that case.

It should be noted that there is some possiblity that the "super luminal phenomenon" of those experiments might be different from the non-causal tail in the impulse response waveform described in this study. In this study the pulse peak point is causal (located at the time origin of t=0), while the "super luminal" velocities were measured only using the location of the pulse peak, and did not consider the shape of the waveform since very short optical pulse waveforms were used in the past experiments. Neverthless, there might be a relationship between the observed results and the non-causality in the transient interfacial reflection coefficients, considering the fact that both happen in the same situation, i.e. only in evanescent propagation mode.

As a result, only the causal case will be considered in the remainder of this dissertation, simply because there is no reliable explanation for the non-causality. The non-causal case can be studied in separate research. Note that the non-causal case is

unlikely to occ parameter  $\tilde{D}_{\eta}$ 

The first layer because it has to sidering that sin

# 2.4 Numerica

condition of 2.1

# 2.4.1 Verifica

The previously compared to dis The most count Fast Fourier tra

mentioned earli

Since the as

in the time dor

interfacial refle

comparison of t forms obtained

respectively. T!

free-space and t

Figure 2.5 (b) as

h 21. Note tha

and  $|\sigma_{n-1}/\sigma_n|$  >

unlikely to occur in a practical situation. That is, to be a non-causal case, the layer parameter  $\tilde{D}_n = (\mu_n \epsilon_n - \mu_1 \epsilon_1 \sin^2 \theta_{i1})/\mu_n^2$  must be negative, and thus

$$\frac{\mu_n}{\mu_1} < \frac{\epsilon_1}{\epsilon_n} \sin^2 \theta_{i1}. \tag{2.118}$$

The first layer can be any lossless dielectric, but is typically free space in practice because it has to have infinite depth and width. Then,  $\epsilon_1 = \epsilon_0$  and  $\mu_1 = \mu_0$ . Considering that  $\sin^2 \theta_{i1} < 1$  and  $\epsilon_0 < \epsilon_n$  always, it can be recognized that satisfying the condition of (2.118) is improbable.

### 2.4 Numerical Examples

### 2.4.1 Verification of theoretical expressions

The previously derived transient forms for interfacial reflection coefficients may be compared to direct numerical computation to ensure that the transform are correct. The most common method to do this is simply to compute the numerical inverse Fast Fourier transforms (IFFT) from the frequency domain forms. For the reasons mentioned earlier, only the causal case  $(\tilde{D}_{n+1} > 0 \text{ and } \tilde{D}_n > 0)$  will be discussed.

Since the asymptotic interfacial reflection coefficients appear as delta functions in the time domain, and are thus difficult to express numerically, only the reduced interfacial reflection coefficients are compared. Figure 2.5 (a) and (b) shows the comparison of the derived transient interfacial reflection coefficients with the transient forms obtained by using a 3072 point IFFT, for the  $P_2 > 0$  and  $P_2 < 0$  cases, respectively. The material parameters for Figure 2.5 (a) are those for an interface of free-space and typical sea water at low frequency as described in [20], while those for Figure 2.5 (b) are for an interface of plexiglass and ethyl alcohol 10GHz, as described in [21]. Note that for the non-magnetic materials,  $P_2 < 0$  case happens when  $\epsilon_n > \epsilon_{n+1}$  and  $(\sigma_{n+1}/\sigma_n) > (\tilde{D}_{n+1}/\tilde{D}_n) > 1$ , or  $\epsilon_n < \epsilon_{n+1}$  and  $(\sigma_{n+1}/\sigma_n) < (\tilde{D}_{n+1}/\tilde{D}_n) < 1$ .

The transient :
identical, and the
for TE polarize
To verify the
coefficient, the

ar input wave

where X(t) of the t

nential pulse

where K. a the input wife Figure 2.7

input wave and  $P_2 < 0$ 

well match

As mer previous re

Wateform.

study. Fig.

The transient reflection coefficient curves from the two different methods are nearly identical, and thus correctness of the derived transient interfacial reflection coefficients for TE polarization have been verified.

To verify the combination of the asymptotic and the reduced transient reflection coefficient, the time domain convolution of the interfacial reflection coefficient with an input waveform is needed, i.e.

$$S(t) = X(t) * R^{TE}(t)$$

$$= X(t) * \left\{ R_{\infty}^{TE} \delta(t) + \tilde{R}^{TE}(t) \right\}$$

$$= R_{\infty}^{TE} X(t) + \tilde{R}^{TE}(t) * X(t)$$
(2.119)

where X(t) denotes the input waveform and S(t) is the resulting reflected waveform.

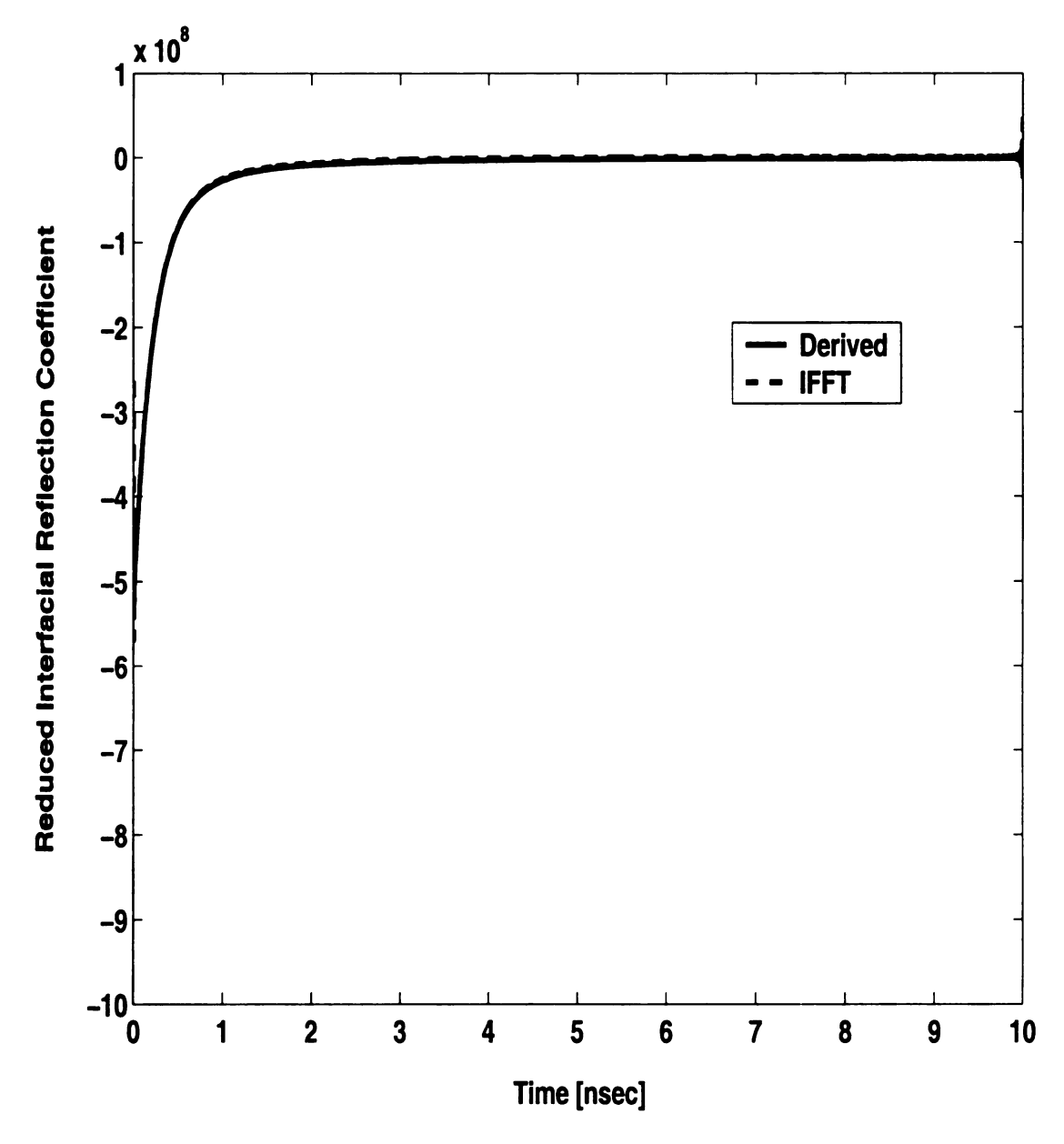
One of the most commonly used input waveforms for this purpose is a double exponential pulse waveform, given as

$$X(t) = K \left( e^{-at} - e^{-bt} \right) \tag{2.120}$$

where K, a and b are arbitrary positive constants. Figure 2.6 shows an example of the input waveform where K = 30.71,  $a = 2 \times 10^9$  and  $b = 4 \times 10^9$ . Figure 2.7 (a) and Figure 2.7 (b) shows the comparison of the time domain reflected waveforms with the input waveform shown in Figure 2.6 for the two different layer parameter sets  $(P_2 > 0)$  and  $P_2 < 0$ . Again, in both cases, the derived expressions and the IFFT results are well matched.

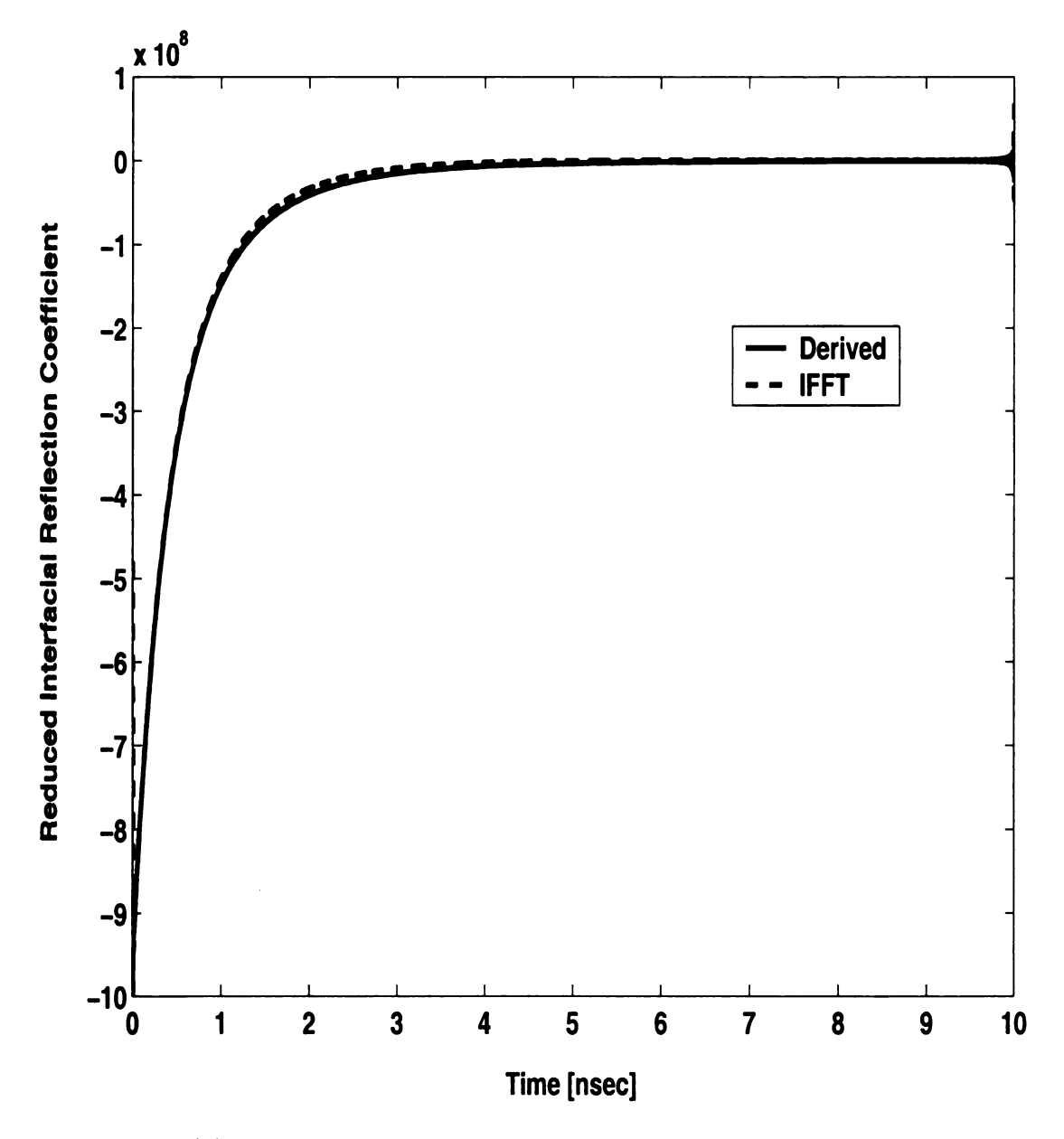
As mentioned in chapter 1, exact theoretical expressions are available from the previous research [11] for transient interfactial reflection due to a unit step input waveform. A comparison with those results also helps to verify the work in this study. Figure 2.8 (a) and Figure 2.8 (b) shows that the re-produced results of the

Figure 2.5. As  $replace{1}{repla$ 



**Figure 2.5.** (a) Numerical comparison of the derived transient reduced interfacial reflection coefficient with that from the IFFT (TE polarization):  $\mu_n = \mu_0$ ,  $\epsilon_n = \epsilon_0$ ,  $\sigma_n = 0[\mho/m]$ ,  $\mu_{n+1} = \mu_0$ ,  $\epsilon_{n+1} = 72\epsilon_0$ ,  $\sigma_{n+1} = 4[\mho/m]$ ,  $\theta_{i1} = 30^\circ$ ,  $P_2 = 0.64 \times 10^{10}$ .

-9



**Figure 2.5.** (b) Numerical comparison of the derived transient reduced interfacial reflection coefficient with that from the IFFT (TE polarization):  $\mu_n = \mu_0$ ,  $\epsilon_n = 2.59\epsilon_0$ ,  $\sigma_n = 9.73 \times 10^{-3} [\mho/m]$ ,  $\mu_{n+1} = \mu_0$ ,  $\epsilon_{n+1} = 1.70\epsilon_0$ ,  $\sigma_{n+1} = 5.60 \times 10^{-2} [\mho/m]$ ,  $\theta_{i1} = 30^\circ$ ,  $P_2 = -0.59 \times 10^{10}$ .

 $F_{igure}$ 

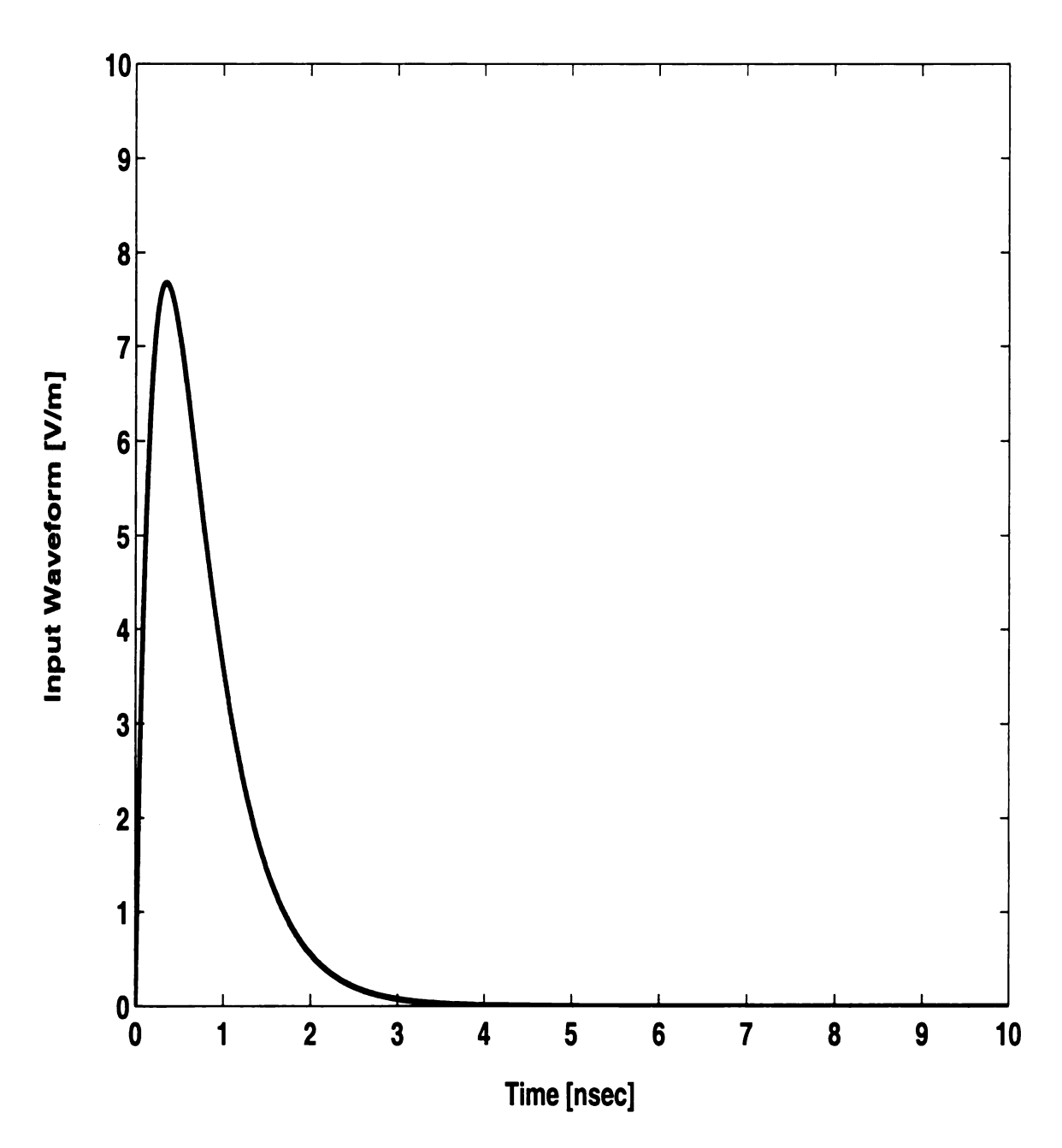
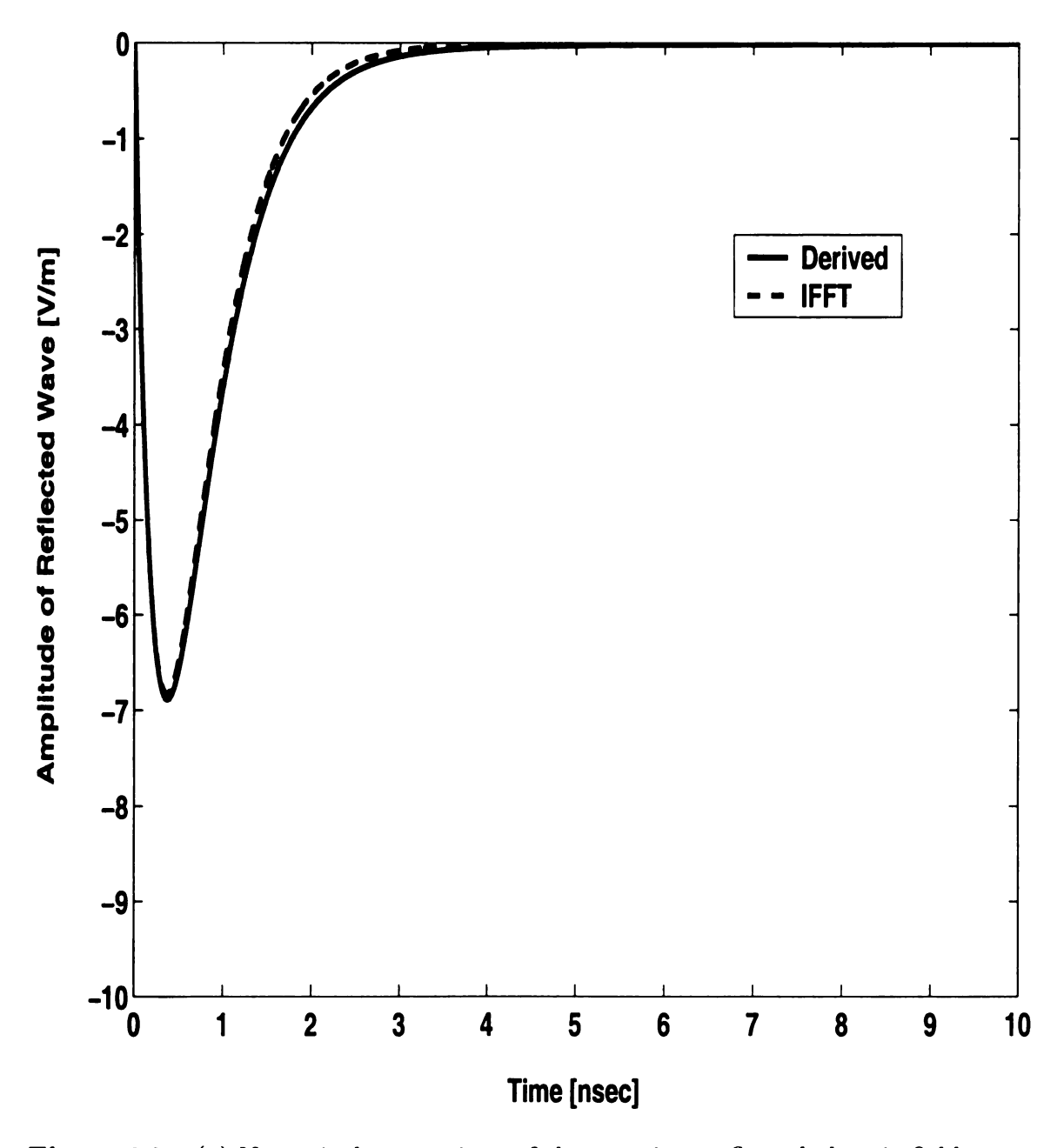


Figure 2.6. An example of double exponential input waveform.

Figure 2.7. Figure 1.7. Figure 2.7. Figure 2.7. Figure 2.7. Figure 2.7. Figure 3.7. Figur



**Figure 2.7.** (a) Numerical comparison of the transient reflected electric field waveform for the input waveform shown in Figure 2.6 with the IFFT (TE polarization):  $\mu_n = \mu_0$ ,  $\epsilon_n = \epsilon_0$ ,  $\sigma_n = 0[\mho/m]$ ,  $\mu_{n+1} = \mu_0$ ,  $\epsilon_{n+1} = 72\epsilon_0$ ,  $\sigma_{n+1} = 4[\mho/m]$ ,  $\theta_{i1} = 30^\circ$ ,  $P_2 = 0.64 \times 10^{10}$ .

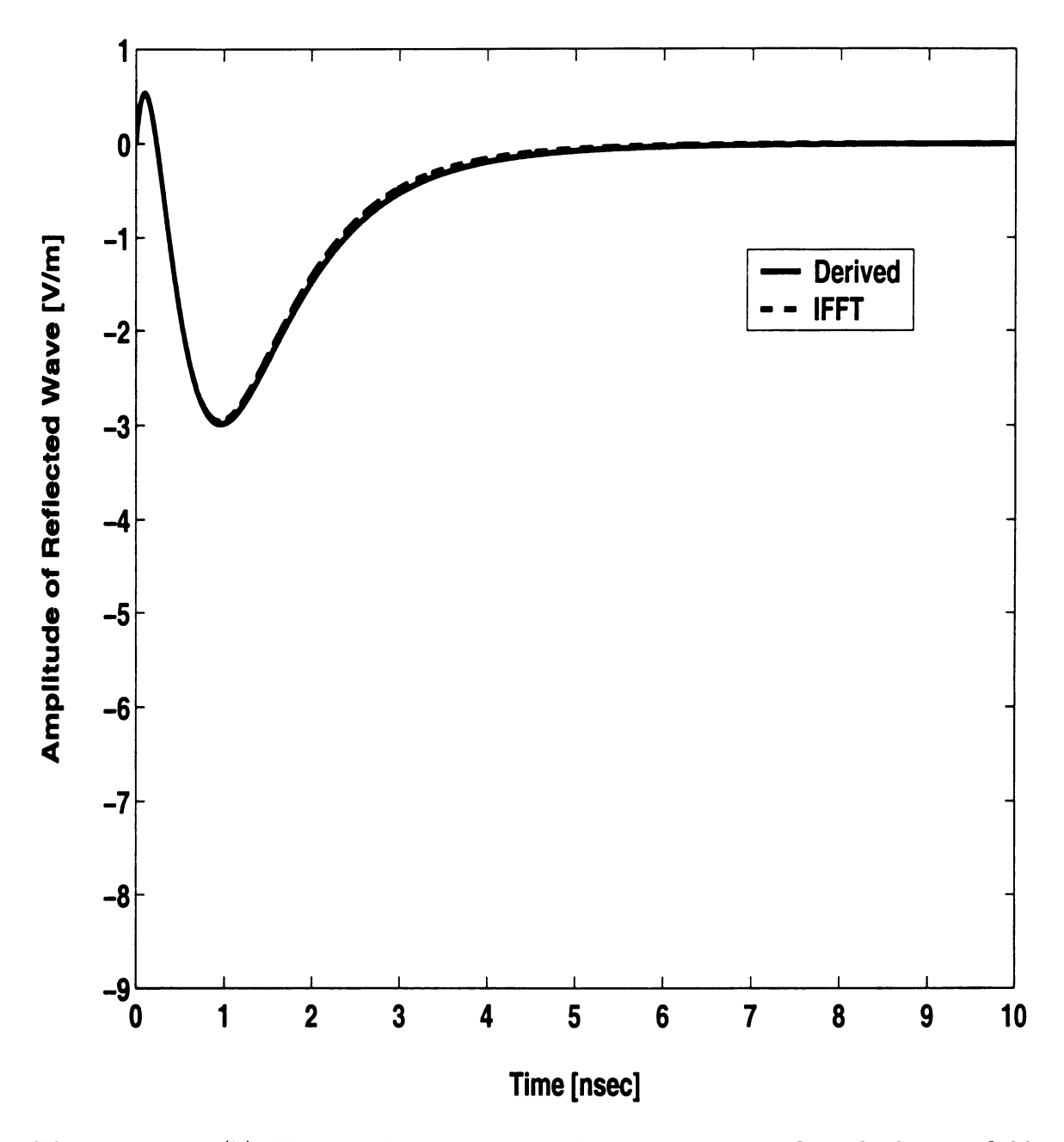


Figure 2.7. (b) Numerical comparison of the transient reflected electric field waveform for the input waveform shown in Figure 2.6 with the IFFT (TE polarization):  $\mu_n = \mu_0$ ,  $\epsilon_n = 2.59\epsilon_0$ ,  $\sigma_n = 9.73 \times 10^{-3} [\mho/m]$ ,  $\mu_{n+1} = \mu_0$ ,  $\epsilon_{n+1} = 1.70\epsilon_0$ ,  $\sigma_{n+1} = 5.60 \times 10^{-2} [\mho/m]$ ,  $\theta_{i1} = 30^\circ$ ,  $P_2 = -0.59 \times 10^{10}$ .

electric interfac same a: drawn v

It ca

waveform
coefficient
is due to
2.4.2
It is intervarious I
angle. C
Figure 2
the first
effects of
the Perm
The curv

greater if

Pording

gie blobol bloboutiol

where the

electric fields to a unit step input waveform excitation obtained by using the transient interfacial reflection coefficient and transmission coefficient of this study, are exactly same as those found in Figure 4.5 and Figure 4.4 in [11]. Note that these plots are drawn with the nomalized time axis given by

$$at = \frac{\sigma_{n+1}t}{2\epsilon_{n+1}\left(1 - \frac{\mu_1\epsilon_1\sin\theta_{i1}^2}{\mu_{n+1}\epsilon_{n+1}}\right)}.$$

It can be easily realized that the early time portion of the scattered electrical field waveform is dominated by the high frequency component of the interfacial reflection coefficient, i.e. the asymptotic interfacial reflection coefficient. The late time portion is due to the lower frequency components of the interfacial reflection coefficient.

#### 2.4.2 The transient responses for various parameter sets

It is interesting to study the dependence of the transient reflection coefficient on the various parameter values, i.e. permittivity, permeability, conductivity and aspect angle. Comparisons of the reduced reflection coefficients are shown in Figure 2.9 - Figure 2.12 which are plotted using semilog scales for easier identification. Note that the first two curves in each plot, except Figure 2.12, are for  $P_2 < 0$  cases, so that the effects of parameter change can be observed for both cases of  $P_2 > 0$  and  $P_2 < 0$ .

#### (1) Permittivity

The curves in Figure 2.9 are plotted for  $\epsilon_{r,n+1} = 1.7$ , 2.5, 10 and 72. The corresponding values of  $R_{\infty}^{TE}$  are 0.12, 0.0098, -0.34 and -0.69, respectively. Note that the phase reversal of the asymptotic reflection coefficient happens when  $\epsilon_{n+1}$  becomes greater than  $\epsilon_n$ . It can be seen that the slopes of different  $\tilde{R}^{TE}(t)$  curves are inversely proportional to the increasing permittivity values, while the asymptotic reflections are proportional to the increasing permittivity values except the case  $\epsilon_{r,n+1} = 2.5$ , where the material constants of the two layers approach each other, and therefore

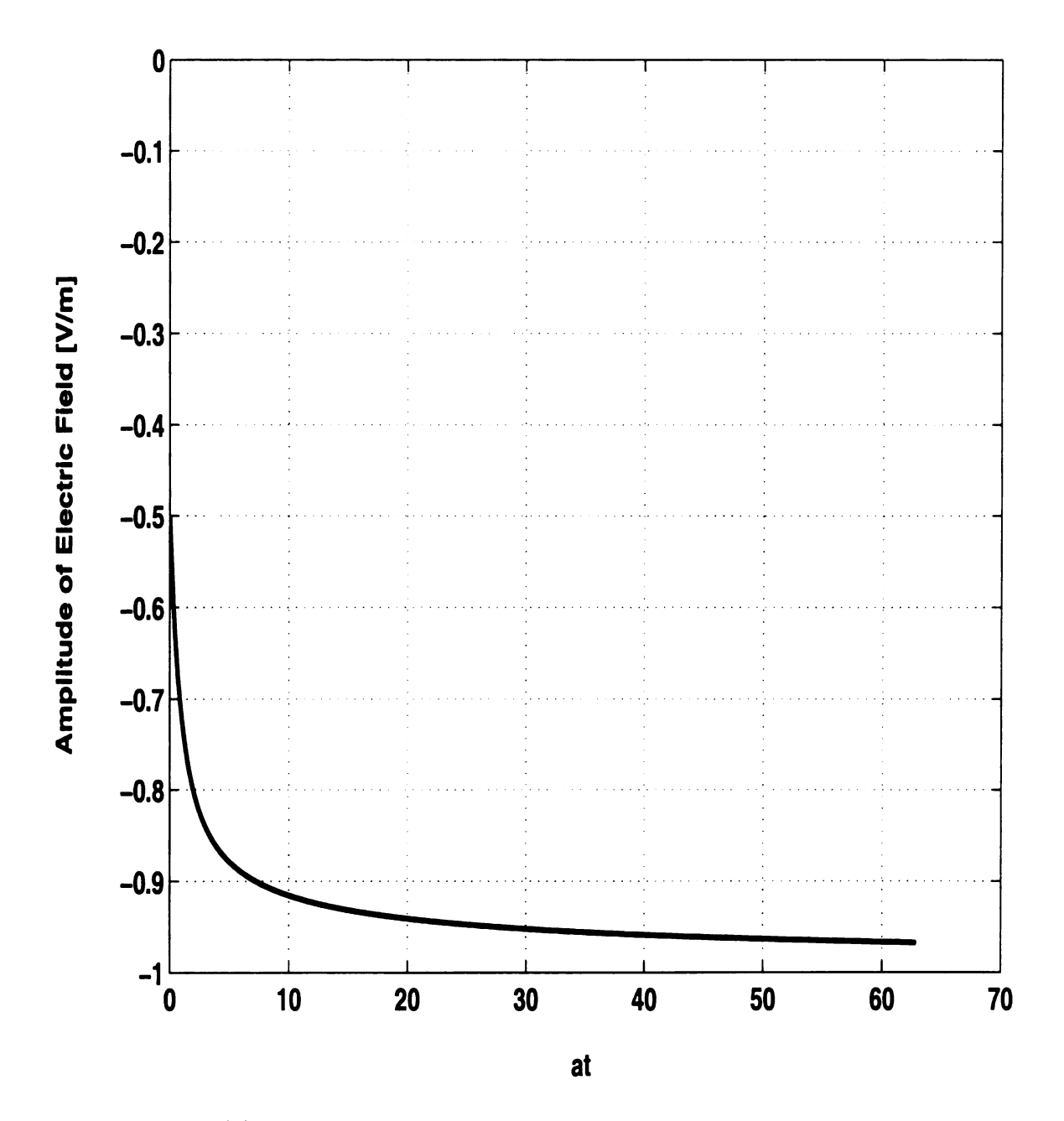


**Figure 2.8.** (a) The transient reflected electrical field waveform for a unit step excitation:  $\mu_n = \mu_0$ ,  $\epsilon_n = \epsilon_0$ ,  $\sigma_n = 0$ ,  $\mu_{n+1} = \mu_0$ ,  $\epsilon_{n+1} = 9\epsilon_0$ ,  $\sigma_{n+1} = 1.00 \times 10^{-3} [\mho/m]$ ,  $\theta_i = 0^{\circ}$ .

Figure 2.8. (
excitation:  $\mu_n$   $\theta_1 = 30^{\circ}$ .

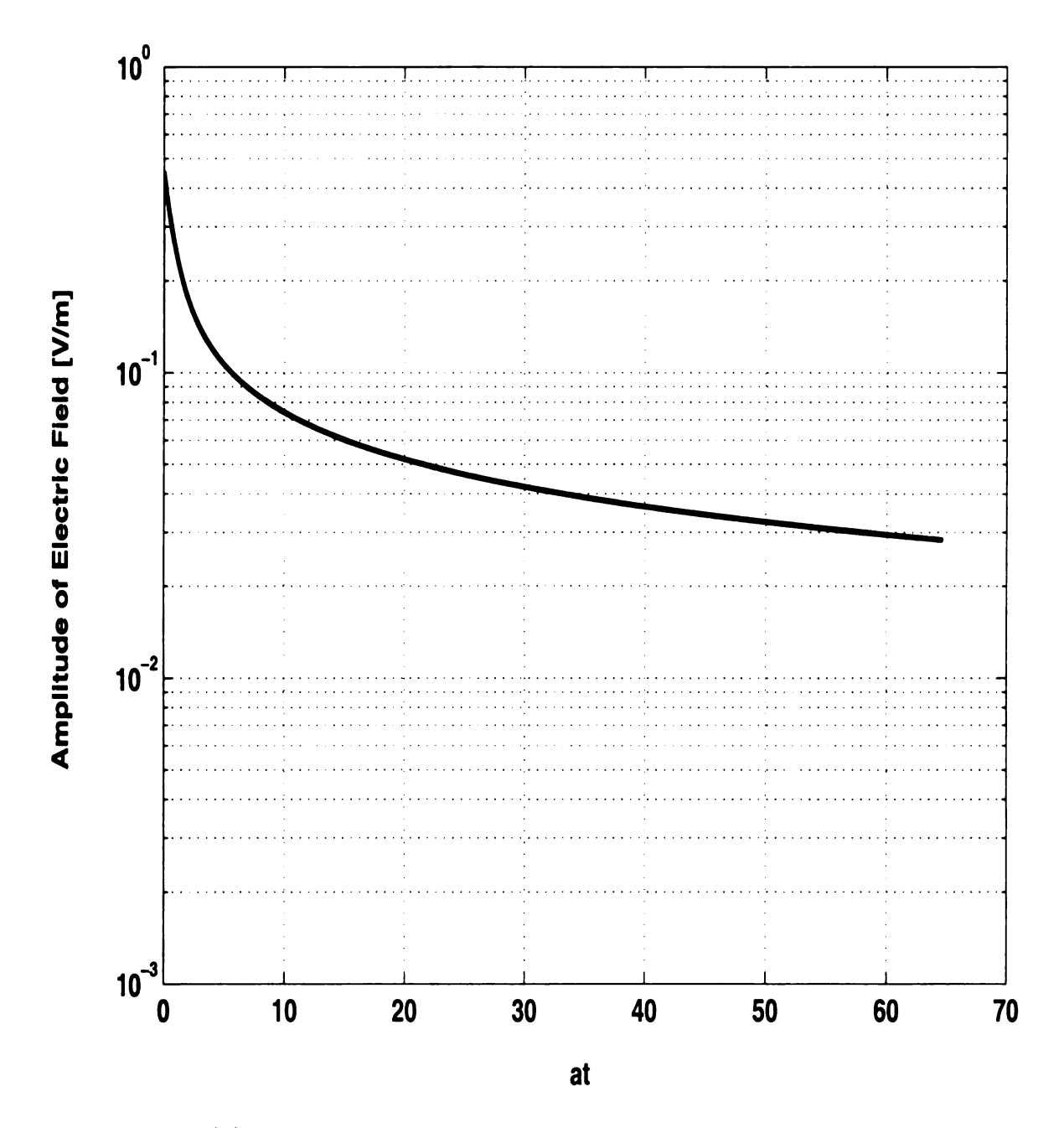


**Figure 2.8.** (b) The transient transmitted electrical field waveform for a unit step excitation:  $\mu_n = \mu_0$ ,  $\epsilon_n = \epsilon_0$ ,  $\sigma_n = 0$ ,  $\mu_{n+1} = \mu_0$ ,  $\epsilon_{n+1} = 9\epsilon_0$ ,  $\sigma_{n+1} = 1.00 \times 10^{-3} [\mho/m]$ ,  $\theta_i = 30^\circ$ .

the overall re increases who (2: Permeal.. The curves in ing values of A are seen to beasymptotic re: fore, the amount (3) Conductiv Because an inc. sient response I component is in where  $\sigma_n = 0.03$ (4) Aspect and The curves show corresponding va slope of the red: component incre

## 2.5 Approxim

dependent on it.

It may be useful

dection coefficient
tation of repeated
scattering as disc

computation time

finding the approx

the overall reflection itself is weak. This means that the overall transient reflection increases when the permittivity contrast of both layers is sharper.

#### (2) Permeability

The curves in Figure 2.10 are plotted for  $\mu_{r,n+1} = 1$ , 5, 10 and 75. The corresponding values of  $R_{\infty}^{TE}$  are 0.027, 0.38, 0.51 and 0.79 respectively. The slopes of  $\tilde{R}^{TE}(t)$  are seen to be inversely proportional to the increasing permeability values, while the asymptotic reflections are proportional to the increasing permeability values. Therefore, the amount of overall reflection increases with the increasing permeability.

#### (3) Conductivity

Because an increase in conductivity causes attenuation in wave propagation, the transient response  $\tilde{R}^{TE}(t)$  suffers a more rapid decrease with time, while the asymptotic component is independent of the change. This can be seen explicitly in Figure 2.11 where  $\sigma_n = 0.01, 0.03, 4$  and 10, respectively.

### (4) Aspect angle

The curves shown in Figure 2.12 are plotted for  $\theta_{i1} = 0^{\circ}$ , 30°, 45° and 75°, while the corresponding values of  $R_{\infty}^{TE}$  are 0.11, 0.12, 0.14 and 0.19 respectively. Therefore, the slope of the reduced reflection coefficient as well as the amplitude of the asymptotic component increases with increasing aspect angle, and the reflection becomes more dependent on its early time portion comming from the aymptotic reflection term.

## 2.5 Approximation of Interfacial Reflection Coefficients

It may be useful to obtain approximate forms of the previously derived transient reflection coefficients, as long as accuracy is maintained. Because the numerical computation of repeated time domain convolution integrals (needed for obtaining multi-layer scattering as discussed in chapter 4) requires a significant amount of time, the total computation time could be burdensome in real time applications. Also, the process of finding the approximate forms gives some insight into the roles of previously defined

Figure 2.9. The of permittivity  $\sigma_{k-1} = 5.60 \times 10^{-2}$ 

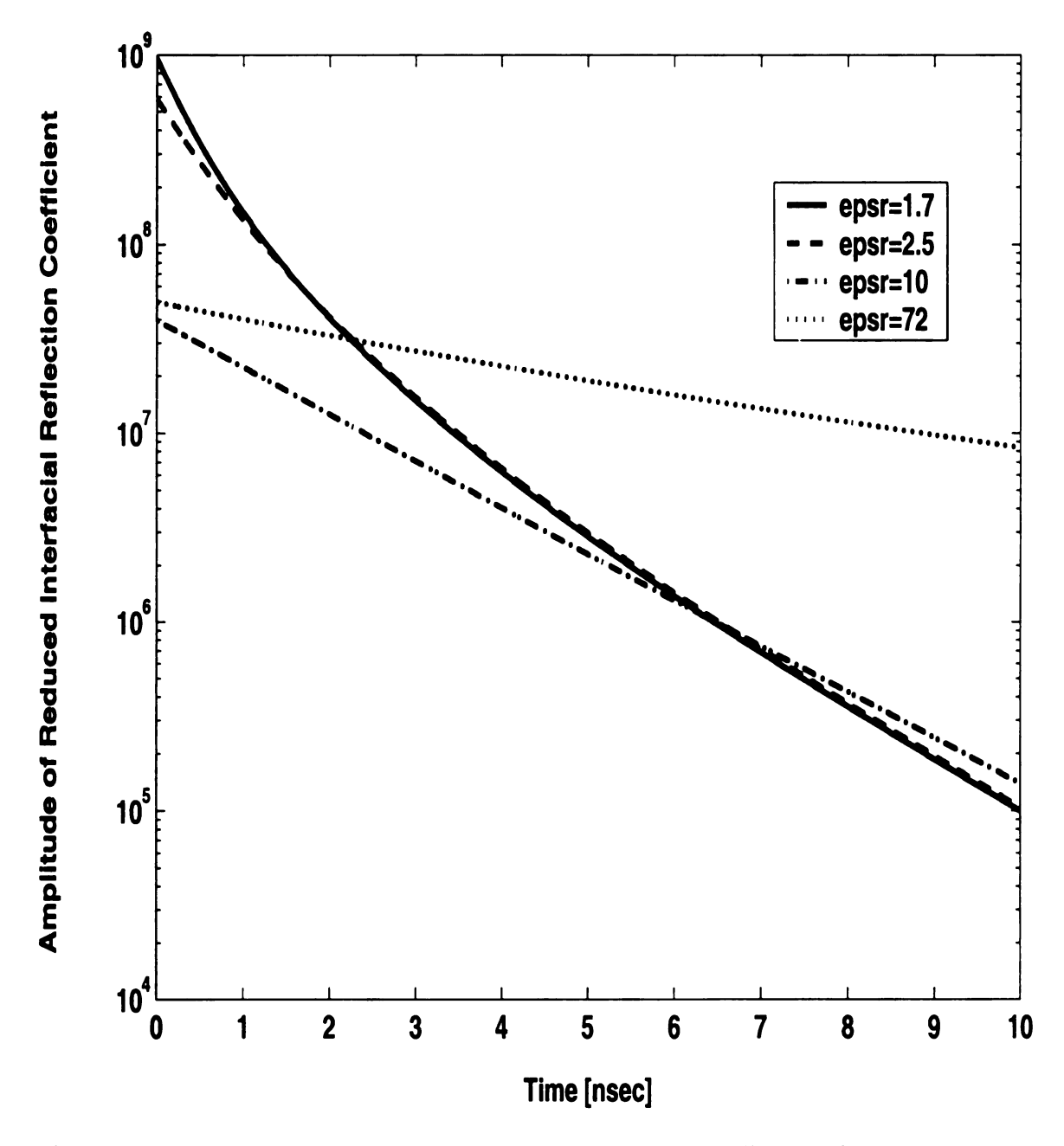


**Figure 2.9.** Time domain reduced interfacial reflection coefficients for various values of permittivity (TE polarization):  $\mu_n = \mu_{n+1} = \mu_0$ ,  $\epsilon_n = 2.59\epsilon_0$ ,  $\sigma_n = 9.73 \times 10^{-3}$ ,  $\sigma_{n+1} = 5.60 \times 10^{-2} [\mho/m]$ ,  $\theta_{i1} = 30^\circ$ .

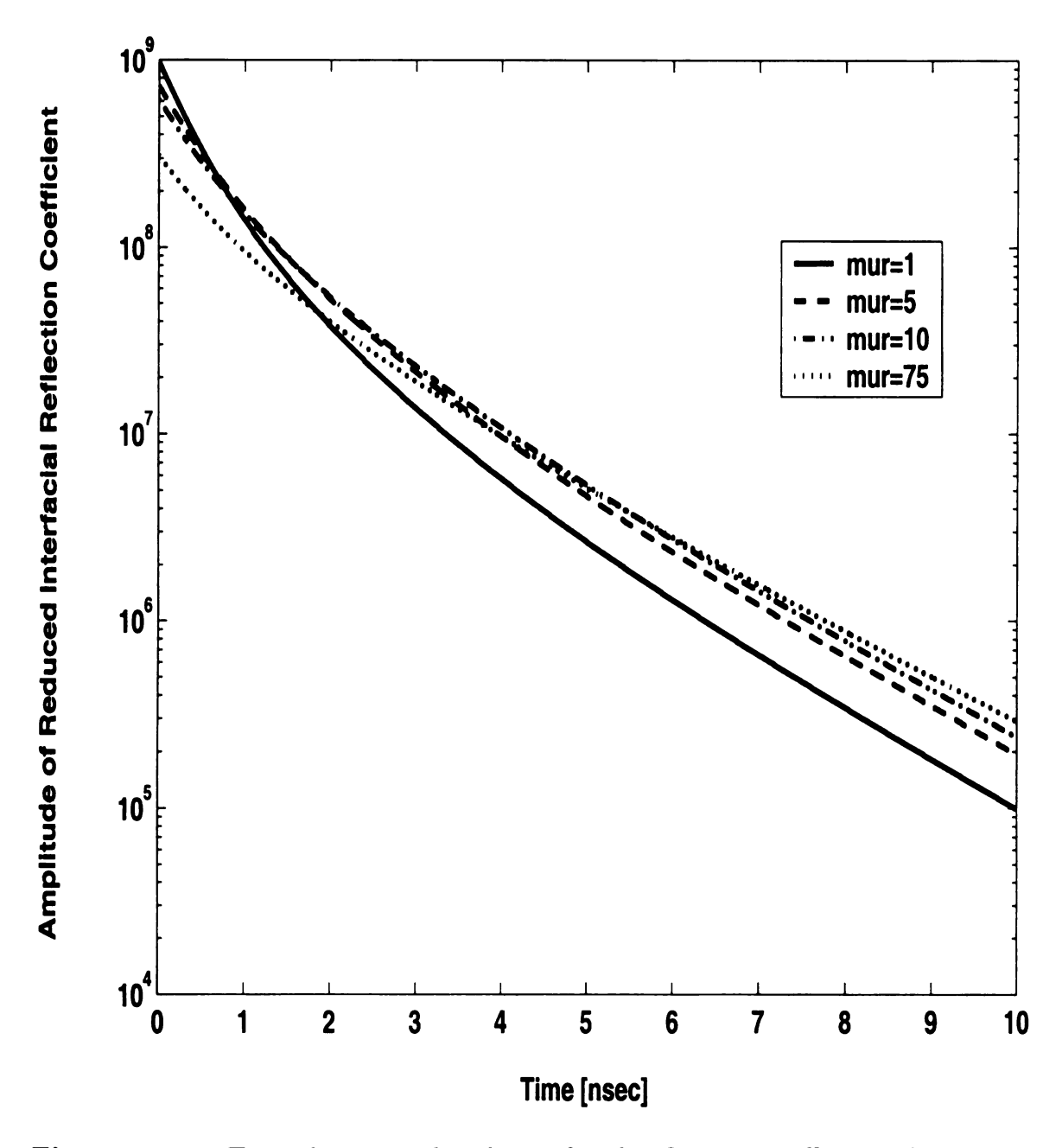


**Figure 2.10.** Time domain reduced interfacial reflection coefficients for various values of permeability (TE polarization):  $\mu_n = 1.5\mu_0$ ,  $\epsilon_n = 2.59\epsilon_0$ ,  $\sigma_n = 9.73 \times 10^{-3}$ ,  $\epsilon_{n+1} = 1.70\epsilon_0$ ,  $\sigma_{n+1} = 5.60 \times 10^{-2} [\mho/m]$ ,  $\theta_{i1} = 30^\circ$ .

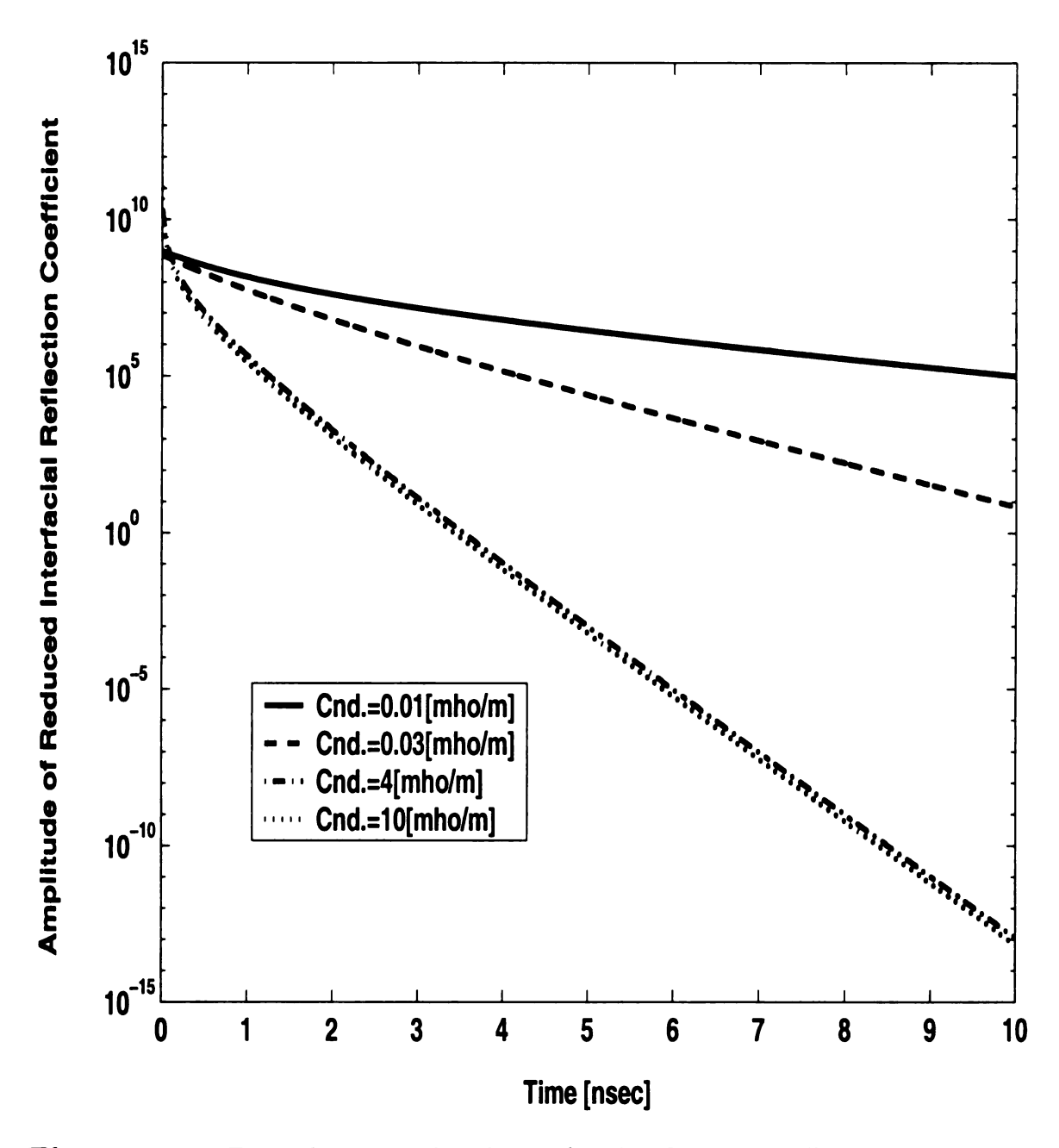


**Figure 2.11.** Time domain reduced interfacial reflection coefficients for various values of conductivity (TE polarization):  $\mu_n = \mu_{n+1} = \mu_0$ ,  $\epsilon_n = 2.59\epsilon_0$ ,  $\epsilon_{n+1} = 1.70\epsilon_0$ ,  $\sigma_{n+1} = 5.60 \times 10^{-2} [\mho/m]$ ,  $\theta_{i1} = 30^\circ$ .

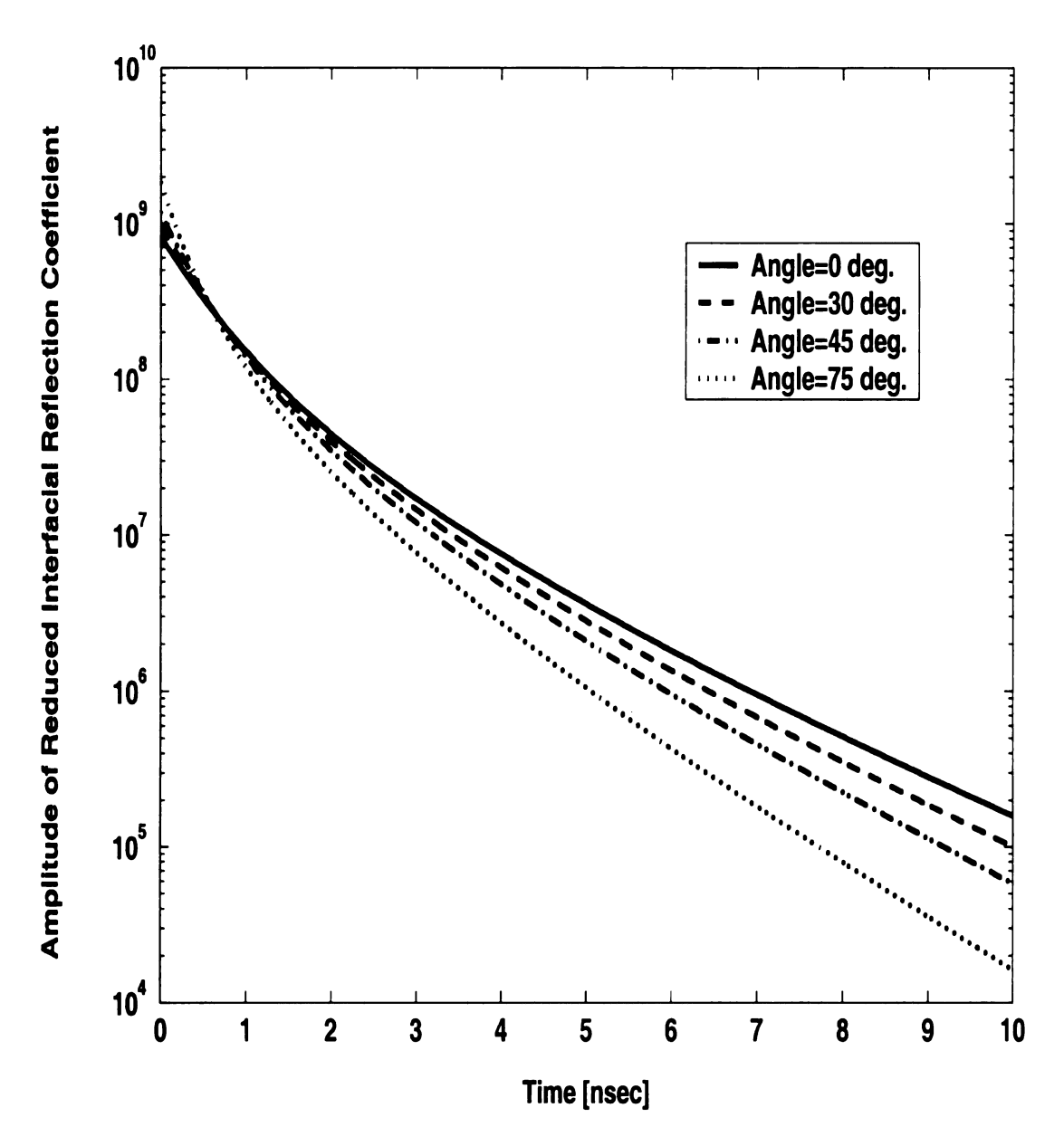


**Figure 2.12.** Time domain reduced interfacial reflection coefficients for various values of incident angle (TE polarization):  $\mu_n = 1.5\mu_0$ ,  $\epsilon_n = 2.59\epsilon_0$ ,  $\sigma_n = 9.73 \times 10^{-3}$ ,  $\mu_{n+1} = \mu_0$ ,  $\epsilon_{n+1} = 1.70\epsilon_0$ ,  $\sigma_{n+1} = 5.60 \times 10^{-2} [\mho/m]$ .

constants in the transient interfacial reflection coefficient expressions. In this section, therefore, the approximate forms for the transient interfacial reflection coefficients  $(\tilde{D}_{n+1} > 0 \text{ and } \tilde{D}_n > 0 \text{ case})$  are derived, and the accuracy of the approximation method is discussed.

There are two different approximate forms since the  $\tilde{D}_{n+1} > 0$  and  $\tilde{D}_n > 0$  case has two different transient reflection coefficients according to the sign of the constant  $P_2$ . For each transient reflection coefficient, The approximations for large values of the time variable t and small values of the time variable t are derived. Then they are combined by using a pair of weighting functions to produce a smooth curve. For convenience, the simpler reflection coefficient (for  $P_2 < 0$ ) will be discussed first.

## **2.5.1** Case $I : P_2 < 0$

#### (1) Large t approximation

For simpler notation, let's define the constants

$$C_{1} = \frac{(B_{n} - B_{n+1})\sqrt{D_{n}}}{(1 - D_{n})}$$

$$C_{2} = \frac{(B_{n} - B_{n+1})^{2}D_{n}\sqrt{D_{n}}}{(1 - D_{n})^{2}}$$

$$C_{3} = \frac{2D_{n}(B_{n+1} - B_{n})}{(1 - D_{n})(1 + \sqrt{D_{n}})}$$
(2.121)

and a function

$$Q(t) = e^{-P_1 t} \left\{ I_1(\beta t) + I_0(\beta t) \right\}, \tag{2.122}$$

then (2.83) is rewritten as

$$\tilde{R}^{TE}(t) = C_1 Q(t) u(t) + C_2 u(t) \int_t^\infty e^{-P_2(t-x)} Q(x) dx.$$
 (2.123)

Using the change of variables  $u = P_2(t - x)$ , then  $x = -\frac{u}{P_2} + t$ , and  $dx = -\frac{du}{P_2}$ . Therefore  $x = \infty$  leads to  $u = \infty$ , x = t leads to u = 0 and (2.123) becomes

$$\tilde{R}^{TE}(t) = C_1 Q(t) u(t) - C_2 \frac{1}{P_2} u(t) \int_0^\infty e^{-u} Q(-\frac{u}{P_2} + t) du$$

$$= C_1 Q(t) u(t) - \frac{C_2}{P_2} u(t) \int_0^\infty e^{-u} \left\{ Q(t - \frac{u}{P_2}) - Q(t) \right\} du$$

$$+ \frac{C_2}{P_2} Q(t) u(t) \int_0^\infty e^{-u} du \qquad (2.124)$$

In (2.124),

$$\int_{0}^{\infty} e^{-u} \left\{ Q(t - \frac{u}{P_{2}}) - Q(t) \right\} du = \int_{0}^{\infty} e^{-u} \frac{\left\{ Q(t - \frac{u}{P_{2}}) - Q(t) \right\}}{(-\frac{u}{P_{2}})} (-\frac{u}{P_{2}}) du$$

$$\approx -\frac{1}{P_{2}} Q'(t) \int_{0}^{\infty} u e^{-u} du. \tag{2.125}$$

This approximation is possible since for large  $P_2$ , most of the contribution to the integration occurs when u is small due to  $e^{-u}$  term. Also,  $\int_0^\infty u e^{-u} du = 1$ . Finally, for large t,

$$\tilde{R}^{TE}(t) \approx \frac{(B_{n} - B_{n+1})B_{n}\sqrt{D_{n}}}{(B_{n} - D_{n}B_{n+1})}Q(t) + \frac{(B_{n} - B_{n+1})^{2}D_{n}\sqrt{D_{n}}}{(B_{n} - D_{n}B_{n+1})^{2}}Q'(t)$$

$$= \frac{(B_{n} - B_{n+1})B_{n}\sqrt{D_{n}}}{(B_{n} - D_{n}B_{n+1})}e^{-P_{1}t}\left\{I_{1}(\beta t) + I_{0}(\beta t)\right\}u(t) - \frac{(B_{n} - B_{n+1})^{2}D_{n}\sqrt{D_{n}}}{(B_{n} - D_{n}B_{n+1})^{2}}e^{-P_{1}t}\left\{(B_{n} + \frac{1}{t})I_{1}(\beta t) + B_{n}I_{0}(\beta t)\right\}u(t).$$
(2.126)

## (2) Small t approximation

Recall that (2.83) originates from (2.75), then

$$\tilde{R}^{TE}(t) = C_1 e^{-P_1 t} \left\{ I_1(\beta t) + I_0(\beta t) \right\} u(t) - C_3 e^{-P_2 t} u(-t)$$

$$-C_2 e^{-P_2 t} u(-t) * e^{-P_1 t} \left\{ I_1(\beta t) + I_0(\beta t) \right\} u(t)$$
(2.127)

For  $|P_2| \gg |P_1|$ , the  $e^{-P_2t}u(-t)$  term behaves like a  $\delta$ -function by its peaking property. Therefore,

$$\tilde{R}^{TE}(t) \approx C_1 e^{-P_1 t} \left\{ I_1(\beta t) + I_0(\beta t) \right\} u(t) - C_2 e^{-P_1 t} \left\{ I_1(\beta t) + I_0(\beta t) \right\} u(t) + 0$$

$$\approx (C_1 - C_2) e^{-P_1 t} \left\{ 0 + 1 \right\} u(t) = A e^{-P_1 t} u(t)$$
(2.128)

for small t, where A is a constant which will be determined later.

For 
$$|P_2| \approx |P_1|$$
,  $-P_2 \approx P_1$  and

$$\tilde{R}^{TE}(t) = C_1 e^{-P_1 t} \left\{ I_1(\beta t) + I_0(\beta t) \right\} u(t)$$

$$-C_2 e^{+P_1 t} u(-t) * e^{-P_1 t} \left\{ I_1(\beta t) + I_0(\beta t) \right\} u(t) + C_3 e^{P_1 t} u(-t)$$

$$\approx C_1 e^{-P_1 t} \left\{ 0 + 1 \right\} u(t) - C_2 e^{P_1 t} u(-t) * e^{-P_1 t} \left\{ 0 + 1 \right\} u(t) + C_3 e^{P_1 t} u(-t)$$

$$\approx C_1 e^{-P_1 t} u(t) - \frac{C_2}{2P_1} e^{P_1 t} + C_3 e^{P_1 t} u(-t)$$

for small t. However, it has already been shown that the exact form does not have any non-causal term. Therefore,

$$\tilde{R}^{TE}(t) \approx C_1 e^{-P_1 t} u(t) - \frac{C_2}{2P_1} e^{P_1 t} u(t) \approx A e^{-P_1 t} u(t)$$
 (2.129)

For  $|P_2| \ll |P_1|$ , the  $e^{-P_1t}u(t)$  term has the role of the  $\delta$ -function, and

$$\tilde{R}^{TE}(t) \approx C_1 e^{-P_1 t} u(t) + C_2 e^{-P_2 t} u(-t) + C_3 e^{-P_2 t} u(-t)$$

$$\approx A C_3 e^{-P_1 t} u(t) \tag{2.130}$$

where the second and third terms must be discarded to maintain causality. In a conclusion, the small t approximation for the  $P_2 < 0$  case is given by

$$\tilde{R}^{TE}(t) \approx Ae^{-P_1 t} u(t). \tag{2.131}$$

Ţ<sub>0</sub>

#### (3) Combined approximation

From the large and small t approximations derived above, a direct combination is

$$\tilde{R}_{approx}^{TE}(t) = \frac{(B_{n} - B_{n+1})B_{n}\sqrt{D_{n}}}{(B_{n} - D_{n}B_{n+1})}e^{-P_{1}t}\left\{I_{1}(\beta t) + I_{0}(\beta t)\right\}u(t) - \frac{(B_{n} - B_{n+1})^{2}D_{n}\sqrt{D_{n}}}{(B_{n} - D_{n}B_{n+1})^{2}}e^{-P_{1}t}\left\{(B_{n} + \frac{1}{t})I_{1}(\beta t) + B_{n}I_{0}(\beta t)\right\}u(t) + Ae^{-P_{1}t}u(t). \tag{2.132}$$

The most intuitive way to determine the constant A is using the function value of the reduced reflection coefficient at t=0, i.e. by letting  $\tilde{R}_{approx}^{TE}(t)\Big|_{t=0} = \tilde{R}_{exact}^{TE}(t)\Big|_{t=0}$  and

$$\tilde{R}_{approx}^{TE}(t)\Big|_{t=0} = \frac{(B_n - B_{n+1})B_n\sqrt{D_n}}{(B_n - D_nB_{n+1})} \left\{ 0 + 1 \right\} - \frac{(B_n - B_{n+1})^2 D_n\sqrt{D_n}}{(B_n - D_nB_{n+1})^2} \left\{ (0 + \frac{\beta}{2}) + B_n \right\} + A$$

$$= A + \frac{(B_n - B_{n+1})B_n\sqrt{D_n}}{(B_n - D_nB_{n+1})}$$

$$- \frac{(B_n - B_{n+1})^2 D_n\sqrt{D_n}}{(B_n - D_nB_{n+1})^2} \frac{(B_{n+1} + 3B_n)}{4}$$
(2.133)

$$\tilde{R}_{exact}^{TE}(t)\Big|_{t=0} = \frac{(B_n - B_{n+1})\sqrt{D_n}}{(1 - D_n)} - \frac{(B_n - B_{n+1})^2 D_n \sqrt{D_n}}{(1 - D_n)^2} \times 0 
+ \frac{2D_n(B_{n+1} - B_n)}{(1 - D_n)(1 + \sqrt{D_n})} 
= \frac{(B_n - B_{n+1})\sqrt{D_n}}{(1 + \sqrt{D_n})^2}.$$
(2.134)

To evaluate A, equate (2.133) and (2.134) to give

$$\frac{(B_n - B_{n+1})\sqrt{D_n}}{(1 + \sqrt{D_n})^2} = \frac{(B_n - B_{n+1})B_n\sqrt{D_n}}{(B_n - D_nB_{n+1})}$$

$$-\frac{(B_n - B_{n+1})^2 D_n \sqrt{D_n}}{(B_n - D_n B_{n+1})^2} \frac{(B_{n+1} + 3B_n)}{4} + A.$$

So,

$$A = \frac{(B_n - B_{n+1})\sqrt{D_n}}{(1 + \sqrt{D_n})^2} - \frac{(B_n - B_{n+1})B_n\sqrt{D_n}}{(B_n - D_nB_{n+1})} + \frac{(B_n - B_{n+1})^2D_n\sqrt{D_n}}{(B_n - D_nB_{n+1})^2} \frac{(B_{n+1} + 3B_n)}{4}$$
(2.135)

Therefore, for  $P_2 < 0$ , an approximate form is given by

$$\tilde{R}^{TE}(t) \approx \frac{(B_n - B_{n+1})B_n\sqrt{D_n}}{(B_n - D_nB_{n+1})}e^{-P_1t}\left\{I_1(\beta t) + I_0(\beta t)\right\}u(t) - \frac{(B_n - B_{n+1})^2D_n\sqrt{D_n}}{(B_n - D_nB_{n+1})^2}e^{-P_1t}\left\{(B_n + \frac{1}{t})I_1(\beta t) + B_nI_0(\beta t)\right\}u(t) + \left\{\frac{(B_n - B_{n+1})\sqrt{D_n}}{(1 + \sqrt{D_n})^2} - \frac{(B_n - B_{n+1})B_n\sqrt{D_n}}{(B_n - D_nB_{n+1})} + \frac{(B_n - B_{n+1})^2D_n\sqrt{D_n}}{(B_n - D_nB_{n+1})^2}\frac{(B_{n+1} + 3B_n)}{4}\right\}e^{-P_1t}u(t) \tag{2.136}$$

Let's consider the accuracy of the approximate form (2.136). Actually the large t approximation is exact except for the term in (2.125), which is valid when  $t\gg u/|P_2|$  (or  $|P_2|t\gg u$ ) is satisfied. Note that the constant power  $P_1$  is not involved with the large t approximation. For the small approximation, of course, the  $\delta$ -function approximation of exponential term contributes to the error, especially when the ratio  $|P_1|/|P_2|$  is not sufficiently big or small. However, the selection of the constant A using  $\tilde{R}_{approx}^{TE}(t)\Big|_{t=0} = \tilde{R}_{large\ t\ approx}^{TE}(t)\Big|_{t=0} + \tilde{R}_{small\ t\ approx}^{TE}(t)\Big|_{t=0} = \tilde{R}_{exact}^{TE}(t)\Big|_{t=0}$  is the main source, because the function values from the large t approximation, which should be excluded in the small t interval (including t=0), is imposed on the early time period. Therefore, the constant A should be given by  $\tilde{R}_{exact}^{TE}(t)\Big|_{t=0} = \tilde{R}_{small\ t\ approx}^{TE}(t)\Big|_{t=0} = \frac{(B_n - B_{n+1})\sqrt{D_n}}{(1+\sqrt{D_n})^2}$  only. However, this choice of A has trouble

as well, since it will introduce a discontinuity at the junction of the small t and large t approximations. Therefore, in this study, a pair of weighting functions are introduced to avoid the discontinuity. From observing the derivation process the approximate transient reflection coefficient, it can be realized that the constant  $P_2$  behaves like a 'switch' which turns 'on' and 'off' the validity of the large t approximation, as a power factor of an exponential function. Also, note that  $P_2$  does not appear in the small t approximation. In addition to these, the product  $P_2t$  provides a normalized time axis. As a result of these observations, a pair of weighting functions is selected to combine the large and small t approximation functions as

$$W_L(t) = (1 - e^{-a|P_2|t})$$

$$W_S(t) = e^{-a|P_2|t}$$
(2.137)

In this definition,  $W_L(t)$  is a weighting function for the large t approximation, while  $W_S(t)$  is for the small t approximation. The constant transition factor a determines the transition time from small t approximation to large t approximation. That is, the bigger value of a means an earlier transition from the small t to the large t approximation. Although the choice of a has some flexibility, in this study, the selection method is as follows. First, set the value of reflection coefficient at the 'transition' time as the exact transition reflection coefficient which is given by, for example,  $0.5 \ \tilde{R}_{exact}^{TE}(t) \Big|_{t=0}$ . Next find the time corresponding to the function value, say,  $t_{trans}$ . Then a is obtained by letting  $e^{-a|P_2|t_{trans}} = 0.5$ .

In summary, the complete approximation for  $P_2 < 0$  is given by

$$\tilde{R}^{TE}(t) \approx W_L(t) \left[ \frac{(B_n - B_{n+1})B_n\sqrt{D_n}}{(B_n - D_n B_{n+1})} e^{-P_1 t} \left\{ I_1(\beta t) + I_0(\beta t) \right\} u(t) - \frac{(B_n - B_{n+1})^2 D_n\sqrt{D_n}}{(B_n - D_n B_{n+1})^2} e^{-P_1 t} \left\{ (B_n + \frac{1}{t})I_1(\beta t) + B_n I_0(\beta t) \right\} u(t) \right]$$

$$+W_{S}(t)\frac{(B_{n}-B_{n+1})\sqrt{D_{n}}}{(1+\sqrt{D_{n}})^{2}}e^{-P_{1}t}u(t)$$

$$=W_{S}(t)\frac{2\beta\sqrt{D_{n}}}{(1+\sqrt{D_{n}})^{2}}e^{-P_{1}t}u(t)$$

$$-W_{L}(t)\frac{\beta^{2}\sqrt{D_{n}}}{P_{2}(1-D)}\left[\frac{B_{n}}{\beta}e^{-P_{1}t}\left\{I_{1}(\beta t)+I_{0}(\beta t)\right\}\right]$$

$$+\frac{4D}{P_{2}(1-D)}e^{-P_{1}t}\left\{(B_{n}+\frac{1}{t})I_{1}(\beta t)+B_{n}I_{0}(\beta t)\right\}\right]u(t). \tag{2.138}$$

A example of the transient reduced interfacial reflection coefficient for this case is plotted along the normalized time axis of  $a|P_2|t$  in Figure 2.13. It can be observed that the largest error occurs in the transition region as expected. Small t approximation shows relatively poorer performance than large t approximation, since it relies on one exponential term only. Also, it is observed that the large t approximation is well matched with the exact reflection coefficient curve in large t interval.

## **2.5.2** Case II : $P_2 > 0$

## (1) Large t approximation

Using previous definitions for the constants and the function Q(t), (2.74) is rewritten as

$$\tilde{R}^{TE}(t) = C_1 Q(t) u(t) - C_2 u(t) \int_0^t e^{-P_2(t-x)} Q(x) dx + C_3 e^{-P_2 t} u(t). \quad (2.139)$$

Let  $u = P_2(x - t)$ , then  $x = \frac{u}{P_2} + t$  and  $dx = \frac{du}{P_2}$ . Also, x = t for u = 0 and x = 0 for  $u = -P_2t$ . Thus (2.139) becomes

$$\tilde{R}^{TE}(t) = C_1 Q(t) u(t) - C_2 u(t) \int_{-P_2 t}^{0} e^{u} Q(x) dx + C_3 e^{-P_2 t} u(t) 
= C_1 Q(t) u(t) - \frac{C_2}{P_2} u(t) \int_{-P_2 t}^{0} e^{u} Q(t + \frac{u}{P_2}) du + C_3 e^{-P_2 t} u(t) 
= C_1 Q(t) u(t) - \frac{C_2}{P_2} u(t) \int_{-P_2 t}^{0} e^{u} \left\{ Q(t + \frac{u}{P_2}) - Q(t) \right\} du$$

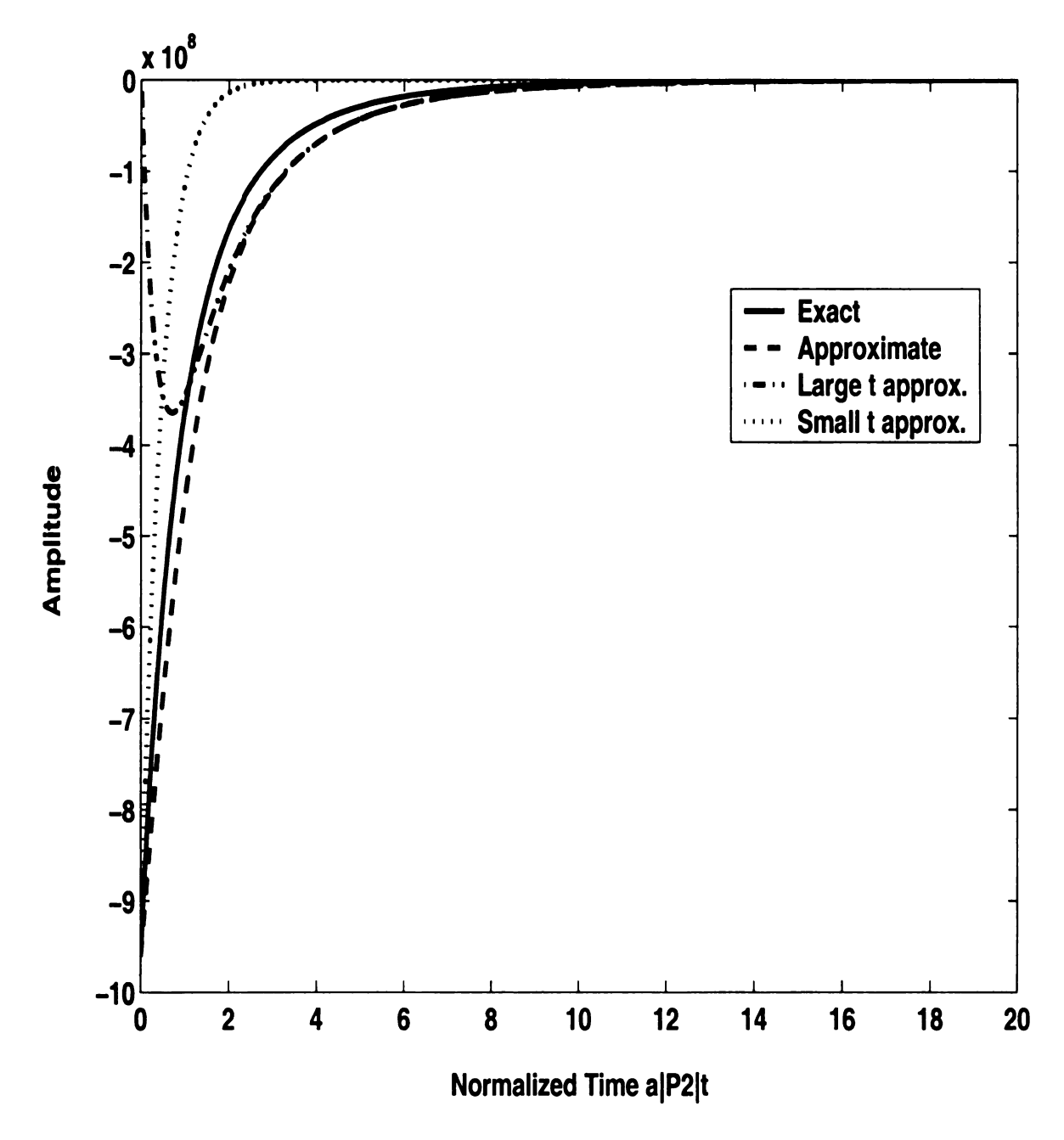


**Figure 2.13.** Transient interfacial reflection coefficient for  $P_2 < 0$  (TE polarization):  $\mu_n = \mu_0$ ,  $\epsilon_n = 2.59\epsilon_0$ ,  $\sigma_n = 9.73 \times 10^{-3} [\mho/m]$ ,  $\mu_{n+1} = \mu_0$ ,  $\epsilon_{n+1} = 1.7\epsilon_0$ ,  $\sigma_{n+1} = 5.60 \times 10^{-2} [\mho/m]$ ,  $\theta_{i1} = 30^{\circ}$ ,  $P_2 = -0.59 \times 10^{10}$ , and a = 0.37.

$$-\frac{C_2}{P_2}u(t)\int_{-P_2t}^0 e^u Q(t)du + C_3 e^{-P_2t}u(t), \qquad (2.140)$$

and the approximate form is

$$\tilde{R}^{TE}(t) \approx C_1 Q(t) u(t) - \frac{C_2}{P_2} (1 - e^{-P_2 t}) Q(t) u(t)$$

$$- \frac{C_2}{P_2^2} u(t) \int_{-P_2 t}^{0} e^{u} Q'(t) du + C_3 e^{-P_2 t} u(t)$$
(2.141)

for large t. This can be rewritten as

$$\begin{split} \tilde{R}_{approx}^{TE}(t) &= (C_1 - \frac{C_2}{P_2})Q(t)u(t) + \frac{C_2}{P_2}e^{-P_2t}Q(t)u(t) \\ &- \frac{C_2}{P_2^2}Q'(t)u(t) \int_{-P_2t}^{0} e^{u}du + C_3e^{-P_2t}u(t) \\ &= (C_1 - \frac{C_2}{P_2})Q(t)u(t) + \frac{C_2}{P_2}e^{-P_2t}Q(t)u(t) + C_3e^{-P_2t}u(t) \\ &+ \frac{C_2}{P_2^2}Q'(t)u(t) \left\{1 - (P_2t + 1)e^{P_2t}\right\} \end{split}$$

where

$$Q'(t) = -P_1 e^{-P_1 t} \left\{ I_1(\beta t) + I_0(\beta t) \right\} + \beta e^{-P_1 t} \left\{ I_1(\beta t) - \frac{1}{\beta t} I_1(\beta t) + I_0(\beta t) \right\}$$

$$= -e^{-P_1 t} \left\{ (B_n + \frac{1}{t}) I_1(\beta t) + B_n I_0(\beta t) \right\}. \tag{2.142}$$

Therefore, the large t approximation of transient interfacial reflection coefficient for  $P_2 > 0$  is

$$\tilde{R}^{TE}(t) \approx \left\{ \frac{(B_n - B_{n+1})B_n\sqrt{D_n}}{(B_n - D_nB_{n+1})} + \frac{(B_n - B_{n+1})^2D_n\sqrt{D_n}}{(1 - D_n)(B_n - D_nB_{n+1})}e^{-P_2t} \right\} \times e^{-P_1t} \left\{ I_1(\frac{(B_{n+1} - B_n)}{2}t) + I_0(\frac{(B_{n+1} - B_n)}{2}t) \right\} u(t) - \frac{(B_n - B_{n+1})^2D_n\sqrt{D_n}}{(B_n - D_nB_{n+1})^2} \left\{ 1 - (P_2t + 1)e^{P_2t} \right\} e^{-P_1t} \times e^{-P_1t}$$

$$\left\{ (B_n + \frac{1}{t})I_1(\frac{(B_{n+1} - B_n)}{2}t) + B_n I_0(\frac{(B_{n+1} - B_n)}{2}t) \right\} u(t) 
+ \frac{2D_n(B_{n+1} - B_n)}{(1 - D_n)(1 + \sqrt{D_n})} e^{-P_2 t} u(t).$$
(2.143)

#### (2) Small t approximation

It has been shown that (2.74) can be weritten in exactly the same form as (2.83), and therefore also as (2.75), as long as 6.611.4 in [10] is applicable. Let's consider the required condition for this conversion. As mentioned earlier, to use 6.611.4 in [10],  $B_{n+1} > B_n$  and  $0 < D_n < 1$ , or  $B_{n+1} < B_n$  and  $D_n > 1$  must be satisfied. But, the given assumption for this case  $P_2 = (B_n - D_n B_{n+1})(1 - D_n) > 0$  does not produce any relation for  $B_n$  and  $B_{n+1}$  that makes 6.611.4 applicable, since it is equivalent to either one of  $1 > D_n$  and  $B_n > D_n B_{n+1}$ , or  $1 < D_n$  and  $B_n < D_n B_{n+1}$ . On the other hand, considering

$$P_{1} - P_{2} = \frac{(B_{n+1} + B_{n})}{2} - \left(\frac{B_{n} - D_{n}B_{n+1}}{1 - D_{n}}\right)$$

$$= \frac{(1 + D_{n})(B_{n+1} - B_{n})}{2(1 - D_{n})},$$
(2.144)

if  $P_1 > P_2$  then 6.611.4 is applicable. Then,

$$\tilde{R}^{TE}(t) = C_1 e^{-P_1 t} \left\{ I_1(\beta t) + I_0(\beta t) \right\} u(t)$$

$$+ C_2 e^{-P_2 t} u(-t) * e^{-P_1 t} \left\{ I_1(\beta t) + I_0(\beta t) \right\} u(t)$$

$$- C_3 e^{-P_2 t} u(-t).$$
(2.145)

If the ratio  $P_1/P_2$  is sufficiently large, then the  $e^{-P_1t}$  term, by its peaking property, provides a good approximation of a  $\delta$ -function. Thus

$$\tilde{R}^{TE}(t) \approx C_1 e^{-P_1 t} \{ I_1(\beta t) + I_0(\beta t) \} u(t)$$

$$+C_{2}e^{-P_{2}t}u(t) * \delta(t) - C_{3}e^{-P_{2}t}u(-t)$$

$$\approx C_{1}e^{-P_{1}t}u(t) + C_{2}e^{-P_{2}t}u(-t) - C_{3}e^{-P_{2}t}u(-t)$$
(2.146)

Previously, it has been proved that  $\tilde{R}^{TE}(t)$  is purely causal for  $\tilde{D}_{n+1} > 0$  and  $\tilde{D}_n > 0$ , and thus the non-causal components may be neglected. Consequently  $\tilde{R}^{TE}(t) \approx Ae^{-P_1t}u(t)$  for small t, where A is a constant which will be determined later.

When  $P_1 < P_2$ , 6.611.4 is not applicable. Since  $P_2 > P_1$ ,  $e^{-P_2 t} \approx \delta(t)$  and (2.74) is approximated as

$$\tilde{R}^{TE}(t) = C_1 e^{-P_1 t} \left\{ I_1(\beta t) + I_0(\beta t) \right\} u(t)$$

$$-C_2 e^{-P_2 t} u(t) * e^{-P_1 t} \left\{ I_1(\beta t) + I_0(\beta t) \right\} u(t)$$

$$+C_3 e^{-P_2 t} u(-t)$$

$$\approx C_1 e^{-P_1 t} \left\{ 0 + 1 \right\} u(t) - C_2 \delta(t) * e^{-P_1 t} \left\{ 0 + 1 \right\} u(t) + C_3 \cdot 0$$

$$\approx A e^{-P_1 t} u(t)$$
(2.147)

where A is a constant. Consequently, the small t approximation for  $P_2 > 0$  includes the  $Ae^{-P_1t}u(t)$  term only, and the constant A is obtained by letting  $\tilde{R}^{TE}_{exact}(t)\Big|_{t=0} = \tilde{R}^{TE}_{small\ t\ approx}(t)\Big|_{t=0}$ , and

$$A = \frac{2D_n(B_{n+1} - B_n)}{(1 - D_n)(1 + \sqrt{D_n})}. (2.148)$$

As a result, in a way similar to the  $P_2 < 0$  case, the approximation of a transient interfacial reflection coefficient for  $P_2 > 0$  may be constructed from the combination of the large and small t approximations using the same pair of weighting functions

$$\tilde{R}^{TE}(t) \approx W_L(t) \times \left\{ \frac{(B_n - B_{n+1})B_n\sqrt{D_n}}{(B_n - D_nB_{n+1})} + \frac{(B_n - B_{n+1})^2D_n\sqrt{D_n}}{(1 - D_n)(B_n - D_nB_{n+1})} e^{-P_2t} \right\} \times e^{-P_1t} \left\{ I_1(\frac{(B_{n+1} - B_n)}{2}t) + I_0(\frac{(B_{n+1} - B_n)}{2}t) \right\} u(t)$$

$$-\frac{(B_{n}-B_{n+1})^{2}D_{n}\sqrt{D_{n}}}{(B_{n}-D_{n}B_{n+1})^{2}}\left\{1-(P_{2}t+1)e^{P_{2}t}\right\}e^{-P_{1}t}\times$$

$$\left\{(B_{n}+\frac{1}{t})I_{1}\left(\frac{(B_{n+1}-B_{n})}{2}t\right)+B_{n}I_{0}\left(\frac{(B_{n+1}-B_{n})}{2}t\right)u(t)\right\}$$

$$+\frac{2D_{n}(B_{n+1}-B_{n})}{(1-D_{n})(1+\sqrt{D_{n}})}e^{-P_{t}}u(t)+W_{S}(t)\frac{2D_{n}(B_{n+1}-B_{n})}{(1-D_{n})(1+\sqrt{D_{n}})}e^{P_{1}t}u(t)$$

$$(2.149)$$

where  $W_L(t)$  and  $W_S(t)$  are given in (2.137). An example of the approximation for  $P_2 > 0$  is shown in Figure 2.14. In comparison with that shown in Figure 2.13, the combined approximation shows relatively better result in this example. The individual errors from each approximation are cancelled out each other in transition region, and thus the combined approximate function provides a good match with the exact reflection coefficient curve.

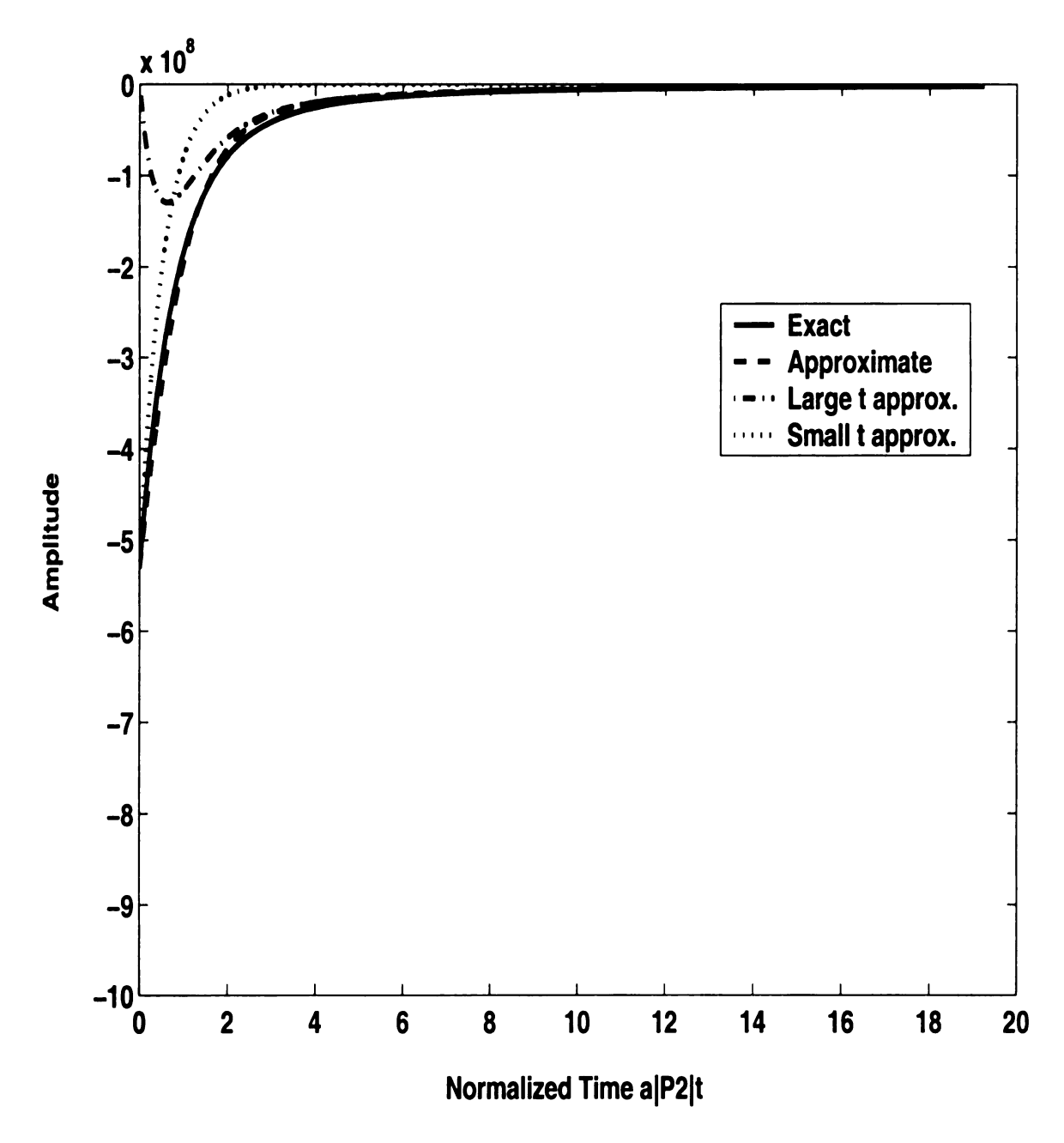


**Figure 2.14.** Transient interfacial reflection coefficient for  $P_2 > 0$  (TE polarization) :  $\mu_n = \mu_0$ ,  $\epsilon_n = \epsilon_0$ ,  $\sigma_n = 0[\mho/m]$ ,  $\mu_{n+1} = \mu_0$ ,  $\epsilon_{n+1} = 72\epsilon_0$ ,  $\sigma_{n+1} = 4[\mho/m]$ ,  $\theta_{i1} = 30^\circ$ ,  $P_2 = 0.64 \times 10^{10}$  and a = 0.65.

#### CHAPTER 3

# INTERFACIAL REFLECTION COEFFICIENTS FOR TM-POLARIZATION

#### 3.1 Introduction

In this chapter, the transient interfacial reflection coefficient for a transverse magnetic (TM) polarized incident plane wave is derived. For a TM polarized uniform plane wave, the direction of the magnetic field, rather than that of electric field as for TE polarization, is parallel to the interface. By a similar approach to that for TE polarization, the frequency domain formula is derived first, and its inverse Fourier transform is obtained after reducing and classifying the frequency domain reflection coefficients using algebraic manipulation with the previously defined branch cuts. The resulting reflection coefficients for the ratio of incident and reflected electric field are similar to those for TE polarization but more complicated as expected. The theoretically derived transient forms are verified by numreical comparisons with the IFFT of the frequency domain expressions. Finally, the dependence on various parameter sets is discussed.

#### 3.2 Frequency Domain Formulation of Interfacial Reflection Coefficient

#### 3.2.1 Derivation

The geometry for the frequency domain formulation is shown in Figure 3.1. From Maxwell's equations,

$$\nabla \times \bar{E}(x, z, \omega) = -j\omega \mu_n \bar{H}(x, z, \omega) \tag{3.1}$$

$$\nabla \times \bar{H}(x, z, \omega) = (\sigma_n + j\omega \epsilon_n) \bar{E}(x, z, \omega)$$
 (3.2)

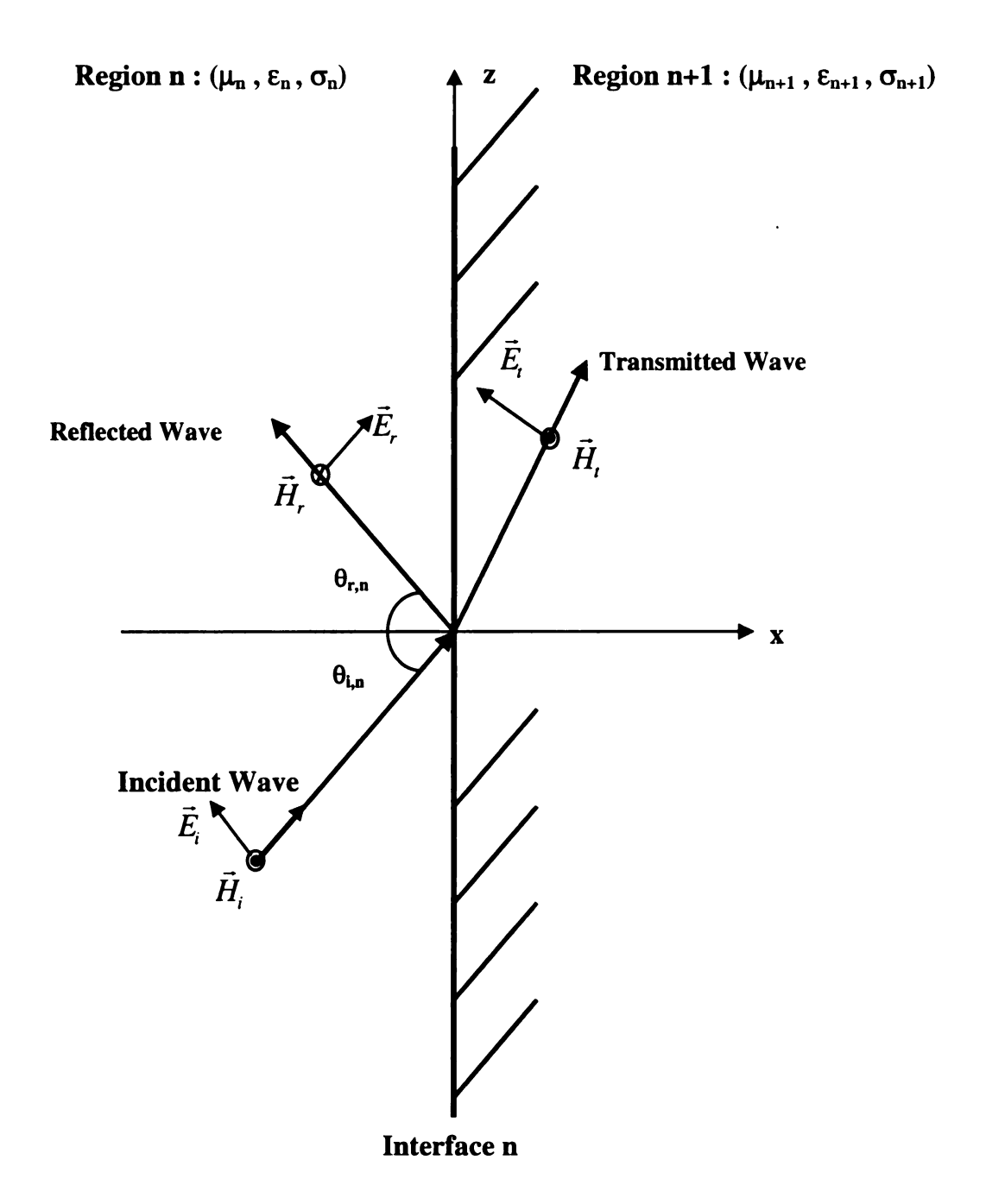


**Figure 3.1.** The incident, reflected and transmitted TM-polarized plane wave at an interface.

and  $\mathcal{K}_{\Gamma}^{p}$ F and the vetor Helmholtz equation for the magnetic field of region n is

$$\nabla^2 \bar{H}(x, z, \omega) - \gamma_n^2 \bar{H}(x, z, \omega) = 0$$
(3.3)

where the propagation constant for the n-th layer is given by

$$\gamma_n^2 = j\omega\mu_n(\sigma_n + j\omega\epsilon_n)$$

$$= -\omega^2\mu_n\epsilon_n + j\omega\mu_n\sigma_n. \tag{3.4}$$

For TM polarization  $\bar{H} = \hat{y}H_y$  and (3.3) can be rewritten as

$$\left(\frac{\partial^2}{\partial x^2} + \frac{\partial^2}{\partial z^2}\right) H_y(x, z, \omega) - \gamma_n^2 H_y(x, z, \omega) = 0.$$
 (3.5)

The solution for the magnetic field is

$$\bar{H}(x,z,\omega) = \hat{y}H_o(\omega)e^{\gamma_{nx}x + \gamma_{nz}z}$$
(3.6)

where the components of the propagation constants are defined by

$$\gamma_n^2 = \gamma_{nx}^2 + \gamma_{nz}^2. \tag{3.7}$$

Only if region n is the first region of a multi-layered material and this region is lossless will we speak of an angle of incidence and an angle of reflection. Otherwise, we will use  $\gamma_{nx}^i, \gamma_{nz}^i, \gamma_{nx}^r$  and  $\gamma_{nz}^r$ . For the incident wave,

$$\gamma_{nx} = \gamma_{nx}^i = \gamma_n \cos \theta_{in} \tag{3.8}$$

$$\gamma_{nz} = \gamma_{nz}^{i} = \gamma_n \sin \theta_{in}, \tag{3.9}$$

while for the reflected wave

$$\gamma_{nx} = \gamma_{nx}^r = -\gamma_n \cos \theta_{rn} \tag{3.10}$$

$$\gamma_{nz} = \gamma_{nz}^r = \gamma_n \sin \theta_{rn}. \tag{3.11}$$

Here  $\theta_{i,n}$  is the angle of incidence and  $\theta_{r,n}$  is the angle of reflection, as shown in Figure 3.1. The electric field in region n is obtained by

$$\bar{E}(x,z,\omega) = \frac{1}{\sigma_n + j\omega\mu_n} \nabla \times \bar{H}(x,z,\omega) 
= \frac{j\omega\mu_n}{\gamma_n^2} \left\{ -\hat{x}\frac{\partial H_y}{\partial z} + \hat{z}\frac{\partial H_y}{\partial x} \right\} 
= \frac{j\omega\mu_n H_o(\omega)}{\gamma_n^2} \left\{ -\hat{x}\gamma_{nz}e^{\gamma_{nx}x + \gamma_{nz}z} + \hat{z}\gamma_{nx}e^{\gamma_{nx}x + \gamma_{nz}z} \right\} 
= -\hat{x}\frac{j\omega\mu_n\gamma_{nz}}{\gamma_n^2} H_o(\omega)e^{\gamma_{nx}x + \gamma_{nz}z} + \hat{z}\frac{j\omega\mu_n\gamma_{nx}}{\gamma_n^2} H_o(\omega)e^{\gamma_{nx}x + \gamma_{nz}z}. (3.12)$$

In summary, the fields in region n can be expressed as

$$\bar{H}_{i}(x,z,\omega) = \hat{y}H_{io}(\omega)e^{\gamma_{nx}^{i}x+\gamma_{nz}^{i}z}$$

$$\bar{E}_{i}(x,z,\omega) = -\hat{x}\frac{j\omega\mu_{n}\gamma_{nz}^{i}}{\gamma_{n}^{2}}H_{io}(\omega)e^{\gamma_{nx}^{i}x+\gamma_{nz}^{i}z}$$

$$+\hat{z}\frac{j\omega\mu_{n}\gamma_{nx}^{i}}{\gamma_{n}^{2}}H_{io}(\omega)e^{\gamma_{nx}^{i}x+\gamma_{nz}^{i}z}$$
(3.13)

$$\bar{H}_{r}(x,z,\omega) = -\hat{y}H_{ro}(\omega)e^{\gamma_{nx}^{r}x+\gamma_{nz}^{r}z}$$

$$\bar{E}_{r}(x,z,\omega) = \hat{x}\frac{\gamma_{nz}^{r}}{j\omega\mu_{n}}H_{io}(\omega)e^{\gamma_{nx}^{r}x+\gamma_{nz}^{r}z} - \hat{z}\frac{\gamma_{nx}^{r}}{j\omega\mu_{n}}H_{io}(\omega)$$
(3.14)

Notice that, unlike with TE polarization, the direction of the reflected magnetic field is reversed from that of the incident field while the electric field maintains the same direction at the interface.

In region (n+1), (3.3) is

$$\nabla^2 \bar{H}(x, z, \omega) - \gamma_{n+1}^2 \bar{H}(x, z, \omega) = 0$$
(3.15)

where the propagation constant is

$$\gamma_{n+1}^2 = j\omega\mu_{n+1}(\sigma_{n+1} + j\omega\epsilon_{n+1})$$

$$= -\omega^2\mu_{n+1}\epsilon_{n+1} + j\omega\mu_{n+1}\sigma_{n+1}.$$
(3.16)

Then, the vector Helmhotz equation for the magentic field in region n+1 (i.e., the transmitted magnetic field) is given by

$$\left(\frac{\partial^2}{\partial x^2} + \frac{\partial^2}{\partial z^2}\right) H_y(x, z, \omega) - \gamma_{n+1}^2 H_y(x, z, \omega) = 0.$$
 (3.17)

This has the solution

$$\bar{H}_t(x, z, \omega) = \hat{y} H_{to}(\omega) e^{\gamma_{n+1, z} x + \gamma_{n+1, z} z}$$
(3.18)

where the components of the propagation constants are defined by

$$\gamma_{n+1}^2 = \gamma_{n+1,x}^2 + \gamma_{n+1,z}^2. \tag{3.19}$$

When both regions n and n+1 are lossless, we may define a transmission angle  $\theta_t$  such that

$$\gamma_{n+1,x} = \gamma_{n+1} \cos \theta_t \tag{3.20}$$

$$\gamma_{n+1,z} = \gamma_{n+1} \sin \theta_t. \tag{3.21}$$

The transmitted magnetic field is given by

$$\bar{E}_{t}(x,z,\omega) = -\frac{j\omega\mu_{n+1}}{\gamma_{n+1}^{2}}\nabla\times\bar{H}_{t}(x,z,\omega)$$

$$= -\frac{j\omega\mu_{n+1}}{\gamma_{n+1}^{2}}\left\{-\hat{x}\frac{\partial H_{y}}{\partial z} + \hat{z}\frac{\partial H_{y}}{\partial x}\right\}$$

$$= \frac{j\omega\mu_{n+1}H_{to}(\omega)}{\gamma_{n+1}^{2}}\left\{-\hat{x}\gamma_{n+1,z}e^{\gamma_{n+1,x}x+\gamma_{n+1,z}z} + \hat{z}\gamma_{n+1,x}e^{\gamma_{n+1,x}x+\gamma_{n+1,z}z}\right\}$$

$$= -\hat{x}\frac{j\omega\mu_{n+1}}{\gamma_{n+1}^{2}}\gamma_{n+1,z}H_{to}(\omega)e^{\gamma_{n+1,x}x+\gamma_{n+1,z}z}$$

$$+\hat{z}\frac{j\omega\mu_{n+1}}{\gamma_{n+1}^{2}}\gamma_{n+1,x}H_{to}(\omega)e^{\gamma_{n+1,x}x+\gamma_{n+1,z}z}.$$
(3.22)

In summary, the fields in region (n+1) can be expressed as

$$\bar{H}_{t}(x,z,\omega) = \hat{y}H_{to}(\omega)e^{\gamma_{n+1,x}x+\gamma_{n+1,z}z}$$

$$\bar{E}_{t}(x,z,\omega) = -\hat{x}\frac{j\omega\mu_{n+1}}{\gamma_{n+1}^{2}}\gamma_{n+1,z}H_{to}(\omega)e^{\gamma_{n+1,x}x+\gamma_{n+1,z}z}$$

$$+\hat{z}\frac{j\omega\mu_{n+1}}{\gamma_{n+1}^{2}}\gamma_{n+1,x}H_{to}(\omega)e^{\gamma_{n+1,x}x+\gamma_{n+1,z}z}$$
(3.23)

To obtain the ratio of the reflected and transmitted electric field amplitudes, two boundary conditions are applied. The first one is the boundary condition for continuity of the tangential components of the magnetic field at the interface. That is, for all z,

$$\bar{H}_i(x=0^-) + \bar{H}_r(x=0^-) = \bar{H}_t(x=0^+)$$

or,

$$H_{io}(\omega)e^{\gamma_{nz}^i z} - H_{ro}(\omega)e^{\gamma_{nz}^r z} = H_{to}(\omega)e^{\gamma_{n+1,z}z}. \tag{3.24}$$

Then, to satisfy the above boundary condition, the equations

$$\gamma_{nz}^i = \gamma_{nz}^r = \gamma_{n+1,z} \tag{3.25}$$

$$H_{io}(\omega) - H_{ro}(\omega) = H_{to}(\omega) \tag{3.26}$$

must be satisfied. For lossless materials, (3.25) becomes

$$\gamma_n \sin \theta_i = \gamma_n \sin \theta_r = \gamma_{n+1} \sin \theta_t \tag{3.27}$$

and thus

$$\theta_i = \theta_r \tag{3.28}$$

$$\frac{\gamma_n}{\gamma_{n+1}} = \frac{\sin \theta_t}{\sin \theta_i} \tag{3.29}$$

which are Snell's law of reflection and refraction, consistent with the result derived in Chapter 2. From (3.7), (3.25) and considering the direction of propagation,

$$\gamma_{nx}^i = -\gamma_{nx}^r = \gamma_{nx}.\tag{3.30}$$

The second boundary condition requires the continuity of tangential electric field on the interface. That is, for all z,

$$\bar{E}_{iz}(x=0^-) + \bar{E}_{rz}(x=0^-) = \bar{E}_{tz}(x=0^+)$$

or,

$$\gamma_{nx}^{i} \frac{j\omega\mu_{n}}{\gamma_{n}^{2}} H_{io}(\omega) e^{\gamma_{nz}^{i}z} - \gamma_{nx}^{r} \frac{j\omega\mu_{n}}{\gamma_{n}^{2}} H_{ro}(\omega) e^{\gamma_{nz}^{r}z} = \gamma_{n+1,x} \frac{j\omega\mu_{n+1}}{\gamma_{n+1}^{2}} H_{to}(\omega) e^{\gamma_{n+1,z}z}.$$
(3.31)

Using (3.30), this equation simplifies to

$$\frac{\mu_n}{\gamma_n^2} \gamma_{nx} H_{io}(\omega) + \frac{\mu_n}{\gamma_n^2} \gamma_{nx} H_{ro}(\omega) = \frac{\mu_{n+1}}{\gamma_{n+1}^2} \gamma_{n+1,x} H_{to}(\omega). \tag{3.32}$$

Alternatively,

$$H_{io}(\omega) + H_{ro}(\omega) = \frac{\mu_{n+1} \gamma_{n+1, x} \gamma_n^2}{\mu_n \gamma_{nx} \gamma_{n+1}^2} H_{to}(\omega). \tag{3.33}$$

Now, multiplying (3.26) by  $\frac{\mu_{n+1}\gamma_{n+1,x}\gamma_n^2}{\mu_n\gamma_{nx}\gamma_{n+1}^2}$  and subtracting (3.33) yields

$$\left(\frac{\mu_{n+1}\gamma_{n+1,x}\gamma_n^2}{\mu_n\gamma_{nx}\gamma_{n+1}^2} - 1\right)H_{io}(\omega) - \left(\frac{\mu_{n+1}\gamma_{n+1,x}\gamma_n^2}{\mu_n\gamma_{nx}\gamma_{n+1}^2} + 1\right)H_{ro}(\omega) = 0$$
(3.34)

Therefore, the frequency domain interfacial reflection coefficient for TM-polarized plane waves is

$$R^{TM}(\omega) = \frac{H_{ro}(\omega)}{H_{io}(\omega)}$$

$$= \left(\frac{\mu_{n+1}\gamma_{n+1,x}\gamma_{n}^{2}}{\mu_{n}\gamma_{nx}\gamma_{n+1}^{2}} - 1\right) / \left(\frac{\mu_{n+1}\gamma_{n+1,x}\gamma_{n}^{2}}{\mu_{n}\gamma_{nx}\gamma_{n+1}^{2}} + 1\right)$$

$$= \frac{\mu_{n+1}\gamma_{n+1,x}(\omega)\gamma_{n}^{2}(\omega) - \mu_{n}\gamma_{n,x}(\omega)\gamma_{n+1}^{2}}{\mu_{n+1}\gamma_{n+1,x}(\omega)\gamma_{n}^{2}(\omega) + \mu_{n}\gamma_{n,x}(\omega)\gamma_{n+1}^{2}}$$
(3.35)

This is a generalized form of Fresnel's reflection coefficient for TM-polarized incident and reflected waves at an interface in a layered structure. Note that the form of  $R^{TM}(\omega)$  is the same as that given in [1].

# 3.2.2 Classification of frequency domain coefficients

The Fresnel's coefficient given by (3.35) can be classified according to the signs of some constant values included within it. Therefore, layer constants may be defined as

$$A_n = \sigma_n/\epsilon_n \tag{3.36}$$

$$\tilde{D}_n = (\mu_n \epsilon_n - \mu_1 \epsilon_1 \sin^2 \theta_{i1}) / \epsilon_n^2 \tag{3.37}$$

$$\tilde{B}_n = \mu_n \sigma_n / \epsilon_n^2. \tag{3.38}$$

Note that  $A_n$  and  $\tilde{B}_n$  are always positive, and the definitions of layer parameters are slightly different from those for TE polarization. To compute the square root functions, the same branch cuts described in the TE case are applied. This depends on the signs of  $A_n$ ,  $\tilde{D}_n$ ,  $\tilde{B}_n$ ,  $A_{n+1}$ ,  $\tilde{D}_{n+1}$  and  $\tilde{B}_{n+1}$ .

Denoting  $s=j\omega$  and using the defined layer constants, (3.35) may be rewritten as

$$R^{TM}(s) = \frac{(s+A_n)\sqrt{s(\tilde{D}_n s + \tilde{B}_n)} - (s+A_{n+1})\sqrt{s(\tilde{D}_{n+1} s + \tilde{B}_{n+1})}}{(s+A_n)\sqrt{s(\tilde{D}_n s + \tilde{B}_n)} + (s+A_{n+1})\sqrt{s(\tilde{D}_{n+1} s + \tilde{B}_{n+1})}}.$$
 (3.39)

Now, the frequency domain reflection coefficient can be classified to four different forms according to which branch cut is needed. This depends on the signs of the layer parameters  $\tilde{D}_n$  and  $\tilde{D}_{n+1}$ . The algebraic manipulations with the branch cuts used in the derivation processes are given by (A.1) and (A.2).

(1) 
$$\tilde{D}_{n+1} > 0$$
 and  $\tilde{D}_n > 0$ 

$$R^{TM}(s) = \frac{-(s+A_n)\sqrt{\tilde{D}_{n+1}}\sqrt{s}\sqrt{s} + \frac{\tilde{B}_{n+1}}{\tilde{D}_{n+1}} + (s+A_{n+1})\sqrt{\tilde{D}_n}\sqrt{s}\sqrt{s} + \frac{\tilde{B}_n}{\tilde{D}_n}}{-(s+A_n)\sqrt{\tilde{D}_{n+1}}\sqrt{s}\sqrt{s} + \frac{\tilde{B}_{n+1}}{\tilde{D}_{n+1}} - (s+A_{n+1})\sqrt{\tilde{D}_n}\sqrt{s}\sqrt{s} + \frac{\tilde{B}_n}{\tilde{D}_n}}$$

Simplifying gives

$$R^{TM}(s) = \frac{(s+A_n)\sqrt{s+\frac{\tilde{B}_{n+1}}{\tilde{D}_{n+1}}} - (s+A_{n+1})\sqrt{\frac{\tilde{D}_n}{\tilde{D}_{n+1}}}\sqrt{s+\frac{\tilde{B}_n}{\tilde{D}_n}}}{(s+A_n)\sqrt{s+\frac{\tilde{B}_{n+1}}{\tilde{D}_{n+1}}} + (s+A_{n+1})\sqrt{\frac{\tilde{D}_n}{\tilde{D}_{n+1}}}\sqrt{s+\frac{\tilde{B}_n}{\tilde{D}_n}}}.$$
 (3.40)

(2)  $\tilde{D}_{n+1} < 0$  and  $\tilde{D}_n < 0$ 

$$R^{TM}(s) = \frac{\pm j(s+A_n)\sqrt{|\tilde{D}_{n+1}|}\sqrt{s}\sqrt{s-\frac{\tilde{B}_{n+1}}{|\tilde{D}_{n+1}|}} \mp j(s+A_{n+1})\sqrt{|\tilde{D}_n|}\sqrt{s}\sqrt{s-\frac{\tilde{B}_n}{|\tilde{D}_n|}}}{\pm j(s+A_n)\sqrt{|\tilde{D}_{n+1}|}\sqrt{s}\sqrt{s-\frac{\tilde{B}_{n+1}}{|\tilde{D}_{n+1}|}} \pm j(s+A_{n+1})\sqrt{|\tilde{D}_n|}\sqrt{s}\sqrt{s-\frac{\tilde{B}_n}{|\tilde{D}_n|}}}.$$

Simplifying gives

$$R^{TM}(s) = \frac{(s+A_n)\sqrt{s-\frac{\tilde{B}_{n+1}}{|\tilde{D}_{n+1}|}} - (s+A_{n+1})\sqrt{\frac{|\tilde{D}_n|}{|\tilde{D}_{n+1}|}}\sqrt{s-\frac{\tilde{B}_n}{|\tilde{D}_n|}}}{(s+A_n)\sqrt{s-\frac{\tilde{B}_{n+1}}{|\tilde{D}_{n+1}|}} + (s+A_{n+1})\sqrt{\frac{|\tilde{D}_n|}{|\tilde{D}_{n+1}|}}\sqrt{s-\frac{\tilde{B}_n}{|\tilde{D}_n|}}}.$$
(3.41)

(3)  $\tilde{D}_{n+1} > 0$ , and  $\tilde{D}_n < 0$ 

$$R^{TM}(s) = \frac{-(s+A_n)\sqrt{|\tilde{D}_{n+1}|}\sqrt{s}\sqrt{s+\frac{\tilde{B}_{n+1}}{|\tilde{D}_{n+1}|}} \mp j(s+A_{n+1})\sqrt{|\tilde{D}_n|}\sqrt{s}\sqrt{s-\frac{\tilde{B}_n}{|\tilde{D}_n|}}}{-(s+A_n)\sqrt{|\tilde{D}_{n+1}|}\sqrt{s}\sqrt{s+\frac{\tilde{B}_{n+1}}{|\tilde{D}_{n+1}|}} \pm j(s+A_{n+1})\sqrt{|\tilde{D}_n|}\sqrt{s}\sqrt{s-\frac{\tilde{B}_n}{|\tilde{D}_n|}}}$$

Simplifying gives

$$R^{TM}(s) = \frac{(s+A_n)\sqrt{s+\frac{\hat{B}_{n+1}}{|\hat{D}_{n+1}|}} \pm j(s+A_{n+1})\sqrt{\frac{|\hat{D}_n|}{|\hat{D}_{n+1}|}}\sqrt{s-\frac{\hat{B}_n}{|\hat{D}_n|}}}{(s+A_n)\sqrt{s+\frac{\hat{B}_{n+1}}{|\hat{D}_{n+1}|}} \mp j(s+A_{n+1})\sqrt{\frac{|\hat{D}_n|}{|\hat{D}_{n+1}|}}\sqrt{s-\frac{\hat{B}_n}{|\hat{D}_n|}}}.$$
(3.42)

(4)  $\tilde{D}_{n+1} < 0$ , and  $\tilde{D}_n > 0$ 

$$R^{TM}(s) = \frac{\pm j(s+A_n)\sqrt{|\tilde{D}_{n+1}|}\sqrt{s}\sqrt{s-\frac{\tilde{B}_{n+1}}{|\tilde{D}_{n+1}|}} + (s+A_{n+1})\sqrt{|\tilde{D}_n|}\sqrt{s}\sqrt{s+\frac{\tilde{B}_n}{|\tilde{D}_n|}}}{\pm j(s+A_n)\sqrt{|\tilde{D}_{n+1}|}\sqrt{s}\sqrt{s-\frac{\tilde{B}_{n+1}}{|\tilde{D}_{n+1}|}} - (s+A_{n+1})\sqrt{|\tilde{D}_n|}\sqrt{s}\sqrt{s+\frac{\tilde{B}_n}{|\tilde{D}_n|}}}.$$

Simplifying gives

$$R^{TM}(s) = \frac{(s+A_n)\sqrt{s-\frac{\tilde{B}_{n+1}}{|\tilde{D}_{n+1}|}} \mp j(s+A_{n+1})\sqrt{\frac{|\tilde{D}_n|}{|\tilde{D}_{n+1}|}}\sqrt{s+\frac{\tilde{B}_n}{|\tilde{D}_n|}}}{(s+A_n)\sqrt{s-\frac{\tilde{B}_{n+1}}{|\tilde{D}_{n+1}|}} \pm j(s+A_{n+1})\sqrt{\frac{|\tilde{D}_n|}{|\tilde{D}_{n+1}|}}\sqrt{s+\frac{\tilde{B}_n}{|\tilde{D}_n|}}}.$$
(3.43)

In each of these expressions the upper sign corresponds to  $\omega > 0$  and the lower sign

to  $\omega < 0$ . Note again that the branch cuts defined in section 2.2.2 have been used throughout for the square root functions.

#### 3.2.3 Reduction of the interfacial reflection coefficients

Observing (3.40)-(3.43), it is realized that there is a constant offset value inside of each frequency domain expression, as there was with the TE polarization. Therefore, the constant offset value, the asymptotic reflection coefficient, should be extracted first.

To make the (3.40)-(3.43) more readable, let

$$D_{n} = \sqrt{\frac{|\tilde{D}_{n}|}{|\tilde{D}_{n+1}|}} = \sqrt{\frac{\epsilon_{n+1}^{2}}{\epsilon_{n}^{2}} \frac{|\mu_{n}\epsilon_{n} - \mu_{1}\epsilon_{1}\sin^{2}\theta_{i1}|}{|\mu_{n+1}\epsilon_{n+1} - \mu_{1}\epsilon_{1}\sin^{2}\theta_{i1}|}}$$

$$B_{n} = \frac{\tilde{B}_{n}}{|\tilde{D}_{n}|} = \frac{\mu_{n}\sigma_{n}}{|\mu_{n}\epsilon_{n} - \mu_{1}\epsilon_{1}\sin^{2}\theta_{i1}|}.$$
(3.44)

and take the limiting values at infinite frequency. Then,

(1)  $\tilde{D}_{n+1} > 0$  and  $\tilde{D}_n > 0$ 

$$R^{TM}(s) = \frac{(s+A_n)\sqrt{s+B_{n+1}} - \sqrt{D_n}(s+A_{n+1})\sqrt{s+B_n}}{(s+A_n)\sqrt{s+B_{n+1}} + \sqrt{D_n}(s+A_{n+1})\sqrt{s+B_n}},$$
(3.45)

$$\lim_{\omega \to \infty} R^{TM}(s) = \frac{1 - \sqrt{D_n}}{1 + \sqrt{D_n}}.$$
(3.46)

(2)  $\tilde{D}_{n+1} < 0 \text{ and } \tilde{D}_n < 0$ 

$$R^{TM}(s) = \frac{(s+A_n)\sqrt{s-B_{n+1}} - \sqrt{D_n}(s+A_{n+1})\sqrt{s-B_n}}{(s+A_n)\sqrt{s-B_{n+1}} + \sqrt{D_n}(s+A_{n+1})\sqrt{s-B_n}},$$
(3.47)

$$\lim_{\omega \to \infty} R^{TM}(s) = \frac{1 - \sqrt{D_n}}{1 + \sqrt{D_n}}.$$
(3.48)

(3)  $\tilde{D}_{n+1} > 0 \text{ and } \tilde{D}_n < 0$ 

$$R^{TM}(s) = \frac{(s+A_n)\sqrt{s+B_{n+1}} \pm j\sqrt{D_n}(s+A_{n+1})\sqrt{s-B_n}}{(s+A_n)\sqrt{s+B_{n+1}} \mp j\sqrt{D_n}(s+A_{n+1})\sqrt{s-B_n}},$$
(3.49)

$$\lim_{\omega \to \infty} R^{TM}(s) = \frac{1 \pm j\sqrt{D_n}}{1 \mp j\sqrt{D_n}}.$$
(3.50)

(4)  $\tilde{D}_{n+1} < 0 \text{ and } \tilde{D}_n > 0$ 

$$R^{TM}(s) = \frac{(s+A_n)\sqrt{s-B_{n+1}} \mp j\sqrt{D_n}(s+A_{n+1})\sqrt{s+B_n}}{(s+A_n)\sqrt{s-B_{n+1}} \pm j\sqrt{D_n}(s+A_{n+1})\sqrt{s+B_n}},$$
(3.51)

$$\lim_{\omega \to \infty} R^{TM}(s) = \frac{1 \mp j\sqrt{D_n}}{1 \pm j\sqrt{D_n}}.$$
(3.52)

In these expressions the upper sign corresponds to  $\omega > 0$  and lower sign to  $\omega < 0$ . Next, the obtained asymptotic reflection coefficient have to be subtracted from the original  $R^{TM}(s)$ . Let's denote the asymptotic reflection coefficient as  $R^{TM}_{\infty}$  and define  $\tilde{R}^{TM}(s) = R^{TM}(s) - R^{TM}_{\infty}$ , then

(1)  $\tilde{D}_{n+1} > 0$  and  $\tilde{D}_n > 0$ 

$$\tilde{R}^{TM}(s) = \frac{(s+A_n)\sqrt{s+B_{n+1}} - (s+A_{n+1})\sqrt{D_n}\sqrt{s+B_n}}{(s+A_n)\sqrt{s+B_{n+1}} + (s+A_{n+1})\sqrt{D_n}\sqrt{s+B_n}} - \frac{1-\sqrt{D_n}}{1+\sqrt{D_n}}$$

$$= \frac{2\sqrt{D_n}}{1+\sqrt{D_n}} \frac{(s+A_n)\sqrt{s+B_{n+1}} - (s+A_{n+1})\sqrt{s+B_n}}{(s+A_n)\sqrt{s+B_{n+1}} + (s+A_{n+1})\sqrt{D_n}\sqrt{s+B_n}} \tag{3.53}$$

Eliminating the square roots in the denominator of (3.53), gives

$$\tilde{R}^{TM}(s) = \frac{2\sqrt{D_n}}{1+\sqrt{D_n}} \frac{(s+A_n)\sqrt{s+B_{n+1}} - (s+A_{n+1})\sqrt{s+B_n}}{(s+A_n)^2(s+B_{n+1}) - D_n(s+A_{n+1})^2(s+B_n)} \times \{(s+A_n)\sqrt{s+B_{n+1}} - \sqrt{D_n}(s+A_{n+1})\sqrt{s+B_n}\}.$$
(3.54)

In the above equation, the numerator is given as

$$(s+A_n)^2(s+B_{n+1}) + \sqrt{D_n}A_{n+1}^2(s+B_n)$$

$$-(1+\sqrt{D_n})(s+A_n)(s+A_{n+1})\sqrt{s+B_n}\sqrt{s+B_{n+1}}$$
(3.55)

while the denominator can be arranged as

$$(1 - D_n)s^3 + \{2(A_n - 2D_nA_{n+1}) + (B_{n+1} - B_n)\}s^2$$

$$+\{A_n(A_n + B_{n+1}) - D_nA_{n+1}(A_{n+1} + B_n)\}s + (A_n^2B_{n+1} - D_nA_{n+1}^2B_n)(3.56)$$

Zeroes of the denominator exist, therefore (3.54) can be expanded using partial fractions and a standard inverse Fourier transform is available for each of those fraction terms. However, that would be quite complex. So, the special but simpler cases of (3.54), i.e. when either one of the both layers has no conductivity, and  $D_{n+1} > 0$  and  $D_n > 0$  will be discussed in this study.

Assume that  $\sigma_n = 0$ , then  $A_n = B_n = 0$  and (3.45) becomes

$$R^{TM}(s) = \frac{\sqrt{s}\sqrt{s + B_{n+1}} - \sqrt{D_n}(s + A_{n+1})}{\sqrt{s}\sqrt{s + B_{n+1}} + \sqrt{D_n}(s + A_{n+1})}.$$
 (3.57)

Now, the asymptotic value still remains the same and is subtracted from the reflection coefficient (3.57) to obtain the reduced form as

$$\tilde{R}^{TM}(s) = \frac{\sqrt{s + B_{n+1}} - \sqrt{D_n}(s + A_{n+1})}{\sqrt{s + B_{n+1}} + \sqrt{D_n}(s + A_{n+1})} - \frac{1 - \sqrt{D_n}}{1 + \sqrt{D_n}}$$

$$= \frac{2\sqrt{D_n}}{1 + \sqrt{D_n}} \frac{\sqrt{s}\sqrt{s + B_{n+1}} - (s + A_{n+1})}{\sqrt{s}\sqrt{s + B_{n+1}} + \sqrt{D_n}(s + A_{n+1})}.$$
(3.58)

Eliminating the square root terms in the denominator of (3.58), gives more convenient

form to use partial fraction expansion as

$$\tilde{R}^{TM}(s) = \frac{2\sqrt{D_n}}{1+\sqrt{D_n}} \frac{\{\sqrt{s}\sqrt{s+B_{n+1}} - (s+A_{n+1})\}\{\sqrt{s}\sqrt{s+B_{n+1}} - \sqrt{D_n}(s+A_{n+1})\}}{s(s+B_{n+1}) - D_n(s+A_{n+1})^2} 
= \frac{2\sqrt{D_n}}{(1+\sqrt{D_n})(1-D_n)} \frac{(B_{n+1} - A_{n+1} + A_{n+1}\sqrt{D_n})s + A_{n+1}^2\sqrt{D_n}}{s^2 - \frac{2D_nA_{n+1} - B_{n+1}}{1-D_n}s - \frac{D_nA_{n+1}^2}{1-D_n}} 
+ \frac{2\sqrt{D_n}}{1-D_n} \frac{s(s+A_{n+1})}{s^2 - \frac{2D_nA_{n+1} - B_{n+1}}{1-D_n}s - \frac{D_nA_{n+1}^2}{1-D_n}} \left\{1 - \sqrt{\frac{s+B_{n+1}}{s}}\right\}.$$
(3.59)

Known inverse Fourier transform pairs are available for all terms of (3.59). To make it more readable, denote the constants in the numerator as

$$E = B_{n+1} - A_{n+1} + A_{n+1} \sqrt{D_n}$$

$$F = A_{n+1}^2 \sqrt{D_n}$$
(3.60)

and the costants in the denominator

$$b = \frac{2D_n A_{n+1} - B_{n+1}}{1 - D_n}$$

$$c = \frac{D_n A_{n+1}^2}{D_n - 1}.$$
(3.61)

Also, the common denominator of (3.59) can be expressed as  $(s - P_1)(s - P_2)$  using the two roots of the equation  $s^2 - bs + c = 0$ . It is necessary to check the signs of the constants before finding  $P_1$  and  $P_2$ , because if they have certain restriction on the signs, then that will confine the location of the roots in the complex plane. Let's examine

$$b = \frac{\sigma_{n+1} \{ \epsilon_n (2\mu_n \epsilon_{n+1} - \mu_{n+1} \epsilon_n) - 2\epsilon_{n+1} \mu_1 \epsilon_1 \sin^2 \theta_{i1} \}}{\epsilon_{n+1} \epsilon_n (\mu_{n+1} \epsilon_n - \mu_n \epsilon_{n+1}) - (\epsilon_n^2 - \epsilon_{n+1}^2) \mu_1 \epsilon_1 \sin^2 \theta_{i1}}$$

$$c = \frac{D_n \mu_{n+1} \epsilon_{n+1} - \mu_1 \epsilon_1 \sin^2 \theta_{i1}}{\epsilon_{n+1} \epsilon_n (\mu_{n+1} \epsilon_n - \mu_n \epsilon_{n+1}) - (\epsilon_n^2 - \epsilon_{n+1}^2) \mu_1 \epsilon_1 \sin^2 \theta_{i1}} \frac{\epsilon_n^2 \sigma_{n+1}^2}{\epsilon_{n+1}^2}$$
(3.62)

Thus b and c do not have any restriction on their signs even for the special case of  $\mu_n = \mu_{n+1} = \mu_1$ , and  $P_1$  and  $P_2$  can be any type of number. Using the partial fraction expansion, the frequency domain reflection coefficient (3.59) is rewritten as

$$\tilde{R}^{TM}(s) = \frac{2\sqrt{D_n}}{(1+\sqrt{D_n})(1-D_n)} \frac{Es+F}{(s-P_1)(s-P_2)} + \frac{2\sqrt{D_n}}{1-D_n} \frac{s(s+A_{n+1})}{(s-P_1)(s-P_2)} 
= \frac{2\sqrt{D_n}}{(1+\sqrt{D_n})(1-D_n)} \left\{ \frac{K_1}{s-P_1} + \frac{K_2}{s-P_2} \right\} 
+ \frac{2\sqrt{D_n}}{1-D_n} \left\{ \frac{sK_3}{s-P_1} + \frac{sK_4}{s-P_2} \right\} \left\{ 1 - \sqrt{\frac{s+B_{n+1}}{s}} \right\}.$$
(3.63)

and the constant coefficients are defined by

$$K_{1} = \frac{Es + F}{s - P_{2}} \Big|_{s=P_{1}} = \frac{EP_{1} + F}{P_{1} - P_{2}}$$

$$K_{2} = \frac{Es + F}{s - P_{1}} \Big|_{s=P_{2}} = \frac{EP_{2} + F}{P_{2} - P_{1}}$$

$$K_{3} = \frac{s + A_{n+1}}{s - P_{2}} \Big|_{s=P_{1}} = \frac{P_{1} + A_{n+1}}{P_{1} - P_{2}}$$

$$K_{4} = \frac{s + A_{n+1}}{s - P_{1}} \Big|_{s=P_{2}} = \frac{P_{2} + A_{n+1}}{P_{2} - P_{1}}.$$

$$(3.64)$$

Notice that  $K_2 = K_1^*$  and  $K_4 = K_3^*$  where  $K^*$  indicates a complex conjugate of K. The roots  $P_1$  and  $P_2$  are obtained as

$$P_1 = (b + \sqrt{b^2 - 4c})$$

$$P_2 = (b - \sqrt{b^2 - 4c}).$$
(3.65)

It should be noticed that the roots are in the relation of a complex conjugate pair, i.e.  $P_2 = P_1^*$ . It has been already shown that b has no restriction on its sign. Consider

the sign of

$$b^{2} - 4c = \frac{(2D_{n}A_{n+1} - B_{n+1})^{2}}{(1 - D_{n})^{2}} - \frac{4A_{n+1}^{2}}{D_{n} - 1}$$

$$= \frac{4(D_{n}^{2} - D_{n} + 1)A_{n+1}^{2} + B_{n+1}(B_{n+1} - 4D_{n}A_{n+1})}{(1 - D_{n})^{2}}$$
(3.66)

where  $4(D_n^2 - D_n + 1)A_{n+1}^2 > 0$  always, and

$$B_{n+1}(B_{n+1} - 4D_n A_{n+1}) = \frac{\mu_{n+1} \sigma_{n+1}}{|\mu_{n+1} \epsilon_{n+1} - \mu_1 \epsilon_1 \sin^2 \theta_{i1}|} - \frac{4\sigma_{n+1}}{\epsilon_{n+1}} \frac{\epsilon_{n+1}^2}{\epsilon_n^2} \left| \frac{\mu_n \epsilon_n - \mu_1 \epsilon_1 \sin^2 \theta_{i1}}{\mu_{n+1} \epsilon_{n+1} - \mu_1 \epsilon_1 \sin^2 \theta_{i1}} \right| = \frac{\sigma_{n+1} \left\{ \mu_{n+1} \epsilon_n^2 - 4\epsilon_{n+1} |\mu_n \epsilon_n - \mu_1 \epsilon_1 \sin^2 \theta_{i1}| \right\}}{\epsilon_n |\mu_{n+1} \epsilon_{n+1} - \mu_1 \epsilon_1 \sin^2 \theta_{i1}|}.$$
(3.67)

The definition (3.67) can have any value, even for  $\mu_{n+1} = \mu_n = \mu_1$ . As a result,  $b^2 - 4c$  can have any sign, and therefore  $P_1$  and  $P_2$  can be any type of number.

Assume that  $\sigma_{n+1} = 0$ , then  $A_{n+1} = B_{n+1} = 0$  and (3.45) is simplified to

$$R^{TM}(s) = \frac{(s + A_n) - \sqrt{D_n}\sqrt{s}\sqrt{s + B_n}}{(s + A_n) + \sqrt{D_n}\sqrt{s}\sqrt{s + B_n}}.$$
 (3.68)

Observing this expression carefully, it can be recognized that by replacing  $A_n$ ,  $B_n$  and  $D_n$  with  $A_{n+1}$ ,  $B_{n+1}$  and  $1/D_n$  respectively,  $R^{TM}(s)$  for  $\sigma_{n+1} = 0$  is equivalent to  $-R^{TM}(s)$  for  $\sigma_n = 0$ . That is, the reflection coefficients for both cases are in 'dual' relationship. Therefore, it is expected that the transient reflection coefficients for both cases have the same relationship.

#### 3.3 Derivation of Transient Interfacial Reflection Coefficients

The transient forms of the frequency domain interfacial reflection coefficients are given by the inverse Fourier transform. Because the asymptotic reflection coefficients  $R_{\infty}^{TM}$ 

are constants in the frequency domain, their transforms are simply given as deltafunctions multiplied by the constants. Let's denote them by  $R_{\infty}^{TM}(t)$ . For  $\tilde{D}_{n+1} > 0$  and  $\tilde{D}_n > 0$ ,

$$R_{\infty}^{TM}(t) = F^{-1} \left\{ \lim_{\omega \to \infty} R^{TM}(s) \right\}$$
$$= \frac{1 - \sqrt{D_n}}{1 + \sqrt{D_n}} \delta(t). \tag{3.69}$$

and the resulting transient interfacial reflection coefficient is given by

$$R^{TM}(t) = F^{-1} \left\{ \lim_{\omega \to \infty} R^{TM}(s) \right\} + F^{-1} \left\{ \tilde{R}^{TM}(s) \right\}$$
$$= \frac{1 - \sqrt{D_n}}{1 + \sqrt{D_n}} \delta(t) + \tilde{R}^{TM}(t). \tag{3.70}$$

By the 'dual' relationship of  $\sigma_n = 0$  and  $\sigma_{n+1} = 0$  mentioned earlier, only the transient interfacial reflection coefficients for  $\sigma_n = 0$  will be derived. Then, what is needed to obtain the transient form for the dual  $\sigma_{n+1} = 0$  case is just taking negative sign of the obtained transient reflection coefficient for  $\sigma_n = 0$ . The transform pair for each term in (3.63) can be found in Appendix B.

Since  $P_1$  and  $P_2$  can be any number, real or complex, the transient reflection coefficient has five different forms depending on the roots of the frequency domain denominator. Let's denote

$$P_r = Re\{P_1\} = Re\{P_2\}$$
  
 $P_i = Im\{P_1\} = -Im\{P_2\}.$  (3.71)

From (3.64), the constants  $K_1$ ,  $K_2$ ,  $K_3$  and  $K_4$  are generally complex numbers as

well, and using their complex conjugate relationship, let

$$K_{1r} = Re\{K_1\} = Re\{K_2\}$$
  
 $K_{1i} = Im\{K_1\} = -Im\{K_2\}$ 
  
 $K_{3r} = Re\{K_3\} = Re\{K_4\}$ 
  
 $K_{3i} = Im\{K_3\} = -Im\{K_4\}$ 
(3.72)

and denote  $\beta = \frac{B_{n+1}}{2}$ .

(1) When  $P_1$  and  $P_2$  are complex numbers, and  $P_r < 0$ , the transform of (3.63) is given by

$$\tilde{R}^{TM}(t) = \frac{2\sqrt{D_n}}{(1 - D_n)(1 + \sqrt{D_n})} \left\{ K_1 e^{P_1 t} + K_2 e^{P_2 t} \right\} u(t) + \frac{2\sqrt{D_n}}{1 - D_n} \left[ K_3 e^{P_1 t} \left\{ \delta(t) + P_1 u(t) \right\} + K_4 e^{P_2 t} \left\{ \delta(t) + P_2 u(t) \right\} \right] * (-\beta) e^{-\beta t} \left\{ I_1(\beta t) + I_0(\beta t) \right\} u(t).$$
(3.73)

Here  $I_n(t)$  is the first kind modified Bessel function of order n. Each term in this expression can be simplified using (3.71) and (3.72) as

$$K_{1}e^{P_{1}t} + K_{2}e^{P_{2}t} = Re\{K_{1}\}e^{P_{r}+jP_{1}t} + jIm\{K_{1}\}e^{P_{r}+jP_{1}t} + Re\{K_{1}\}e^{P_{r}+jP_{1}t} - jIm\{K_{1}\}e^{P_{r}+jP_{1}t}$$

$$= K_{1r}e^{P_{r}t}(e^{jP_{1}t} + e^{-jP_{1}t}) + jK_{1i}e^{P_{r}t}(e^{jP_{1}t} - e^{-jP_{1}t})$$

$$= 2e^{P_{r}t}(K_{1r}\cos P_{1}t - K_{1i}\sin P_{1}t), \qquad (3.74)$$

$$K_3 e^{P_1 t} \delta(t) + K_4 e^{P_2 t} \delta(t) = K_3 \delta(t) + K_4 \delta(t) = 2K_{3r} \delta(t),$$
 (3.75)

and

$$K_{3}P_{1}e^{P_{1}t} + K_{4}P_{2}e^{P_{2}t} = (K_{3r} + jK_{3i})(P_{r} + jP_{i})e^{P_{r} + jP_{i}t} + (K_{3r} - jK_{3i})(P_{r} - jP_{i})e^{P_{r} - jP_{i}t}$$

$$= e^{P_{r}t} \left\{ K_{3r}P_{r}(e^{jP_{i}t} + e^{-jP_{i}t}) - K_{3i}P_{i}(e^{jP_{i}t} + e^{-jP_{i}t}) - jK_{3r}P_{i}(e^{jP_{i}t} - e^{-jP_{i}t}) + jK_{3i}P_{r}(e^{jP_{i}t} - e^{-jP_{i}t}) \right\}$$

$$= 2e^{P_{r}t} \left\{ (K_{3r}P_{r} - K_{3i}P_{i}) \cos P_{i}t - (K_{3r}P_{i} + K_{3i}P_{r}) \sin P_{i}t \right\}.$$

$$(3.76)$$

Finally, the transient interfacial reflection coefficient is

$$\begin{split} \hat{R}^{TM}(t) &= \frac{4\sqrt{D_n}}{(1-D_n)(1+\sqrt{D_n})} e^{P_r t} (K_{1r} \cos P_i t - K_{1i} \sin P_i t) u(t) + \frac{4\sqrt{D_n}}{1-D_n} [K_{3r} \delta(t) \\ &+ e^{P_r t} \left\{ (K_{3r} P_r - K_{3i} P_i) \cos P_i t - (K_{3r} P_i + K_{3i} P_r) \sin P_i t \right\} u(t) \right] * \\ &= \frac{4\sqrt{D_n}}{(1-D_n)(1+\sqrt{D_n})} e^{P_r t} (K_{1r} \cos P_i t - K_{1i} \sin P_i t) u(t) \\ &- \frac{4K_{3r} \beta \sqrt{D_n}}{1-D_n} e^{-\beta t} \left\{ I_1(\beta t) + I_0(\beta t) \right\} u(t) \\ &- \frac{4\beta \sqrt{D_n}}{1-D_n} (K_{3r} P_r - K_{3i} P_i) e^{P_r t} u(t) \times \\ &\int_0^t \cos P_i (t-x) e^{-(P_r + \beta)x} \left\{ I_1(\beta x) + I_0(\beta x) \right\} dx \\ &+ \frac{4\beta \sqrt{D_n}}{1-D_n} (K_{3r} P_r + K_{3i} P_i) e^{P_r t} u(t) \times \\ &\int_0^t \sin P_i (t-x) e^{-(P_r + \beta)x} \left\{ I_1(\beta x) + I_0(\beta x) \right\} dx \\ &= \frac{4\sqrt{D_n}}{(1-D_n)(1+\sqrt{D_n})} e^{P_r t} (K_{1r} \cos P_i t - K_{1i} \sin P_i t) u(t) \\ &- \frac{4K_{3r} \beta \sqrt{D_n}}{1-D_n} e^{-\beta t} \left\{ I_1(\beta t) + I_0(\beta t) \right\} u(t) - \frac{4\beta \sqrt{D_n}}{1-D_n} e^{P_r t} u(t) \times \end{split}$$

$$\int_{0}^{t} \left\{ (K_{3r}P_{r} - K_{3i}P_{i})\cos P_{i}(t-x) - (K_{3r}P_{r} + K_{3i}P_{i})\sin P_{i}(t-x) \right\} \times e^{-(P_{r}+\beta)x} \left\{ I_{1}(\beta x) + I_{0}(\beta x) \right\} dx.$$
(3.77)

(2) When  $P_1$  and  $P_2$  are complex numbers, and  $P_r > 0$ , the transform of (3.63) is given by

$$\begin{split} \tilde{R}^{TM}(t) &= -\frac{2\sqrt{D_n}}{(1-D_n)(1+\sqrt{D_n})} \left\{ K_1 e^{P_1 t} + K_2 e^{P_2 t} \right\} u(-t) + \\ &= \frac{2\sqrt{D_n}}{1-D_n} \left[ K_3 e^{P_1 t} \left\{ \delta(t) - P_1 u(-t) \right\} + K_4 e^{P_2 t} \left\{ \delta(t) - P_2 u(-t) \right\} \right] * \\ &= (-\beta) e^{-\beta t} \left\{ I_1(\beta t) + I_0(\beta t) \right\} u(t) \\ &= -\frac{4\sqrt{D_n}}{(1-D_n)(1+\sqrt{D_n})} e^{P_r t} (K_{1r} \cos P_i t + K_{1i} \sin P_i t) u(-t) + \frac{4\sqrt{D_n}}{1-D_n} \times \left[ K_{3r} \delta(t) + e^{P_r t} \left\{ (K_{3r} P_r - K_{3i} P_i) \cos P_i t - (K_{3r} P_i + K_{3i} P_r) \sin P_i t \right\} \times \\ &= u(-t) \right] * (-\beta) e^{-\beta t} \left\{ I_1(\beta t) + I_0(\beta t) \right\} u(t) \\ &= -\frac{4\sqrt{D_n}}{(1-D_n)(1+\sqrt{D_n})} e^{P_r t} (K_{1i} \sin P_i t - K_{1r} \cos P_i t) u(-t) \\ &- \frac{4\beta\sqrt{D_n}}{1-D_n} e^{-\beta t} \left\{ I_1(\beta t) + I_0(\beta t) \right\} u(t) \\ &- \frac{4\beta\sqrt{D_n}}{1-D_n} e^{P_r t} \int_{\max(t,0)}^{\infty} \left\{ (K_{3r} P_r - K_{3i} P_i) \cos P_i (t-x) - (K_{3r} P_r + K_{3i} P_i) \sin P_i (t-x) \right\} e^{-(P_r + \beta)x} \left\{ I_1(\beta x) + I_0(\beta x) \right\} dx. \quad (3.78) \end{split}$$

(3) When  $P_1$  and  $P_2$  are real numbers, and  $P_1 > P_2 > 0$ , the transform of (3.63) is given by

$$\tilde{R}^{TM}(t) = -\frac{2\sqrt{D_n}}{(1-D_n)(1+\sqrt{D_n})} \left\{ K_1 e^{P_1 t} + K_2 e^{P_2 t} \right\} u(-t) + \frac{2\sqrt{D_n}}{1-D_n} \left[ K_3 e^{P_1 t} \left\{ \delta(t) - P_1 u(-t) \right\} + K_4 e^{P_2 t} \left\{ \delta(t) - P_2 u(-t) \right\} \right]$$

$$*(-\beta)e^{-\beta t} \{I_{1}(\beta t) + I_{0}(\beta t)\} u(t)$$

$$= -\frac{2\sqrt{D_{n}}}{(1 - D_{n})(1 + \sqrt{D_{n}})} \{K_{1}e^{P_{1}t} + K_{2}e^{P_{2}t}\} u(-t)$$

$$-\frac{2\beta\sqrt{D_{n}}}{1 - D_{n}}(K_{3} + K_{4})e^{-\beta t} \{I_{1}(\beta t) + I_{0}(\beta t)\} u(t)$$

$$+\frac{2K_{3}P_{1}\beta\sqrt{D_{n}}}{1 - D_{n}}e^{P_{1}t} \int_{max(t,0)}^{\infty} e^{-(P_{1}+\beta)x} \{I_{1}(\beta x) + I_{0}(\beta x)\} dx$$

$$+\frac{2K_{4}P_{2}\beta\sqrt{D_{n}}}{1 - D_{n}}e^{P_{2}t} \int_{max(t,0)}^{\infty} e^{-(P_{2}+\beta)x} \{I_{1}(\beta x) + I_{0}(\beta x)\} dx. \quad (3.79)$$

(4) When  $P_1$  and  $P_2$  are real numbers, and  $P_1 > 0 > P_2$ , the transform of (3.63) is given by

$$\tilde{R}^{TM}(t) = \frac{2\sqrt{D_n}}{(1-D_n)(1+\sqrt{D_n})} \left\{ -K_1 e^{P_1 t} u(-t) + K_2 e^{P_2 t} u(t) \right\} + \frac{2\sqrt{D_n}}{1-D_n} \left[ K_3 e^{P_1 t} \left\{ \delta(t) - P_1 u(-t) \right\} + K_4 e^{P_2 t} \left\{ \delta(t) + P_2 u(t) \right\} \right] \\ *(-\beta) e^{-\beta t} \left\{ I_1(\beta t) + I_0(\beta t) \right\} u(t) = \frac{2\sqrt{D_n}}{(1-D_n)(1+\sqrt{D_n})} \left\{ -K_1 e^{P_1 t} u(-t) + K_2 e^{P_2 t} u(t) \right\} \\ -\frac{2\beta\sqrt{D_n}}{(1-D_n)} (K_3 + K_4) e^{-\beta t} \left\{ I_1(\beta t) + I_0(\beta t) \right\} u(t) \\ + \frac{2K_3 P_1 \beta \sqrt{D_n}}{1-D_n} e^{P_1 t} \int_{max(t,0)}^{\infty} e^{-(P_1 + \beta)x} \left\{ I_1(\beta x) + I_0(\beta x) \right\} dx \\ -\frac{2K_4 P_2 \beta \sqrt{D_n}}{1-D_n} e^{P_2 t} u(t) \int_0^t e^{-(P_2 + \beta)x} \left\{ I_1(\beta x) + I_0(\beta x) \right\} dx. \quad (3.80)$$

(5) When  $P_1$  and  $P_2$  are real numbers, and  $0 > P_1 > P_2$ , the transform of (3.63) is given by

$$\tilde{R}^{TM}(t) = \frac{2\sqrt{D_n}}{(1 - D_n)(1 + \sqrt{D_n})} \left\{ K_1 e^{P_1 t} + K_2 e^{P_2 t} \right\} u(t) +$$

$$\frac{2\sqrt{D_n}}{1-D_n} \left[ K_3 e^{P_1 t} \left\{ \delta(t) + P_1 u(t) \right\} + K_4 e^{P_2 t} \left\{ \delta(t) + P_2 u(t) \right\} \right] 
* (-\beta) e^{-\beta t} \left\{ I_1(\beta t) + I_0(\beta t) \right\} u(t) 
= \frac{2\sqrt{D_n}}{(1-D_n)(1+\sqrt{D_n})} \left\{ K_1 e^{P_1 t} + K_2 e^{P_2 t} \right\} u(t) 
- \frac{2\beta\sqrt{D_n}}{1-D_n} (K_3 + K_4) e^{-\beta t} \left\{ I_1(\beta t) + I_0(\beta t) \right\} u(t) 
- \frac{2K_3 P_1 \beta\sqrt{D_n}}{1-D_n} e^{P_1 t} u(t) \int_0^t e^{-(P_1 + \beta)x} \left\{ I_1(\beta x) + I_0(\beta x) \right\} dx 
- \frac{2K_4 P_2 \beta\sqrt{D_n}}{1-D_n} e^{P_2 t} u(t) \int_0^t e^{-(P_2 + \beta)x} \left\{ I_1(\beta x) + I_0(\beta x) \right\} dx. \quad (3.81)$$

Notice that, for TM polarization, there are non-causal terms even for the  $D_{n+1} > 0$  and  $D_n > 0$  case.

## 3.4 Numerical Examples

## 3.4.1 Verification of theoretical expressions

The previously derived transient forms of the interfacial reflection coefficients may be compared to direct numerical computation to ensure that the transforms are correct. Again, the numerical IFFT, is used for this purpose. For the reasons explained in the previous chapter, only the causal case will be discussed.

Since the asymptotic interfacial reflection coefficients appear as delta functions in the time domain, and are thus difficult to express numerically, only the reduced interfacial reflection coefficients are compared. Figure 3.2 shows the comparison of the derived transient interfacial reflection coefficient with the transient forms obtained by using a 3072 point IFFT for  $\sigma_n = 0$ . The material parameters for Figure 3.2 are those for free-space and typical sea water at low frequency as described in [20]. The transient reflection coefficient curves from the two different methods are nearly identical, and thus the derived transient interfacial reflection coefficient for TM polarization has been verified.

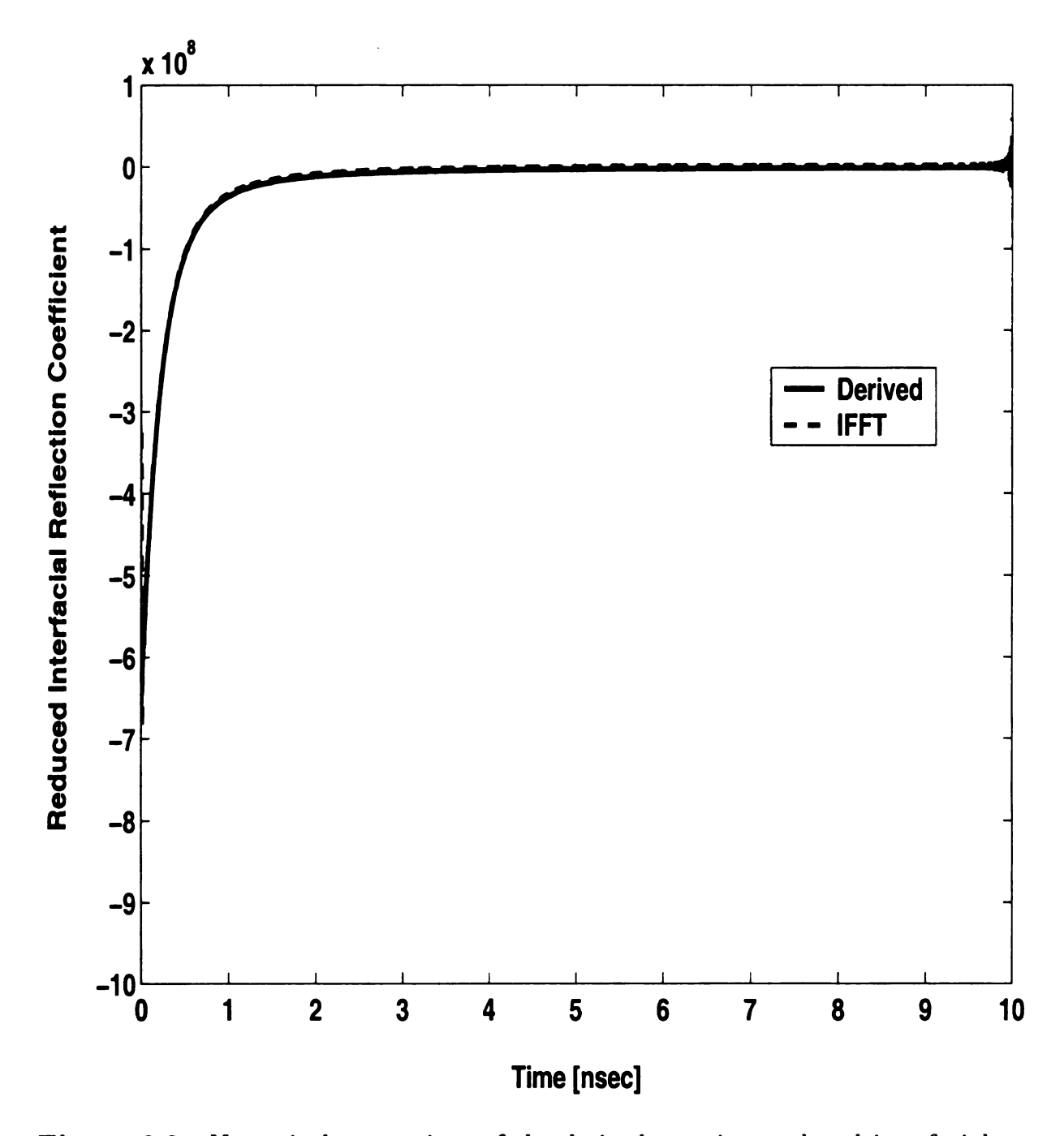


Figure 3.2. Numerical comparison of the derived transient reduced interfacial reflection coefficient with that from the IFFT (TM polarization):  $\mu_n = \mu_0$ ,  $\epsilon_n = \epsilon_0$ ,  $\sigma_n = 0[\mho/m]$ ,  $\mu_{n+1} = \mu_0$ ,  $\epsilon_{n+1} = 72\epsilon_0$ ,  $\sigma_{n+1} = 4[\mho/m]$ ,  $\theta_{i1} = 30^\circ$ .

To verify the combination of the asymptotic and the reduced transient reflection coefficient, the time domain convolution of the interfacial reflection coefficient with an input waveform is needed, i.e.

$$S(t) = X(t) * R^{TM}(t)$$

$$= X(t) * \left\{ R_{\infty}^{TM} \delta(t) + \tilde{R}^{TM}(t) \right\}$$

$$= R_{\infty}^{TM} X(t) + \tilde{R}^{TM}(t) * X(t). \tag{3.82}$$

Here X(t) denotes the input waveform and S(t) is the resulting reflected waveform. The same input waveform given in Figure 2.6 is used for TM polarization. Figure 3.3 shows the comparison of the time domain reflected waveforms with the input waveform shown in Figure 2.6 for  $\sigma_n = 0$ . Again, the derived expression and the IFFT results are well matched.

Exact theoretical expressions are available from the previous research [11] for TM polarized transient interfactial reflection due to a unit step input waveform. A comparison with those results also helps to verify the work in this study. Figure 3.4 (a) and (b) show that the re-produced results of the electric fields to a double exponential input waveform excitation as shown in Figure 4.1 in [11], obtained by using the transient interfacial reflection coefficient and transmission coefficient of this study, are exactly same as those found in Figure 5.3 and Figure 5.2 in [11].

#### 3.4.2 The transient responses for various parameter sets

It is interesting to study the dependence of the transient reflection coefficient on various parameter values, i.e. permittivity, permeability, conductivity and aspect angle. Comparisons of the reduced reflection coefficients are shown in Figure 3.5 - Figure 3.8, which are plotted using semilog scales for easier identification. Note that the curves in each plot are for the  $\sigma_n = 0$  case.

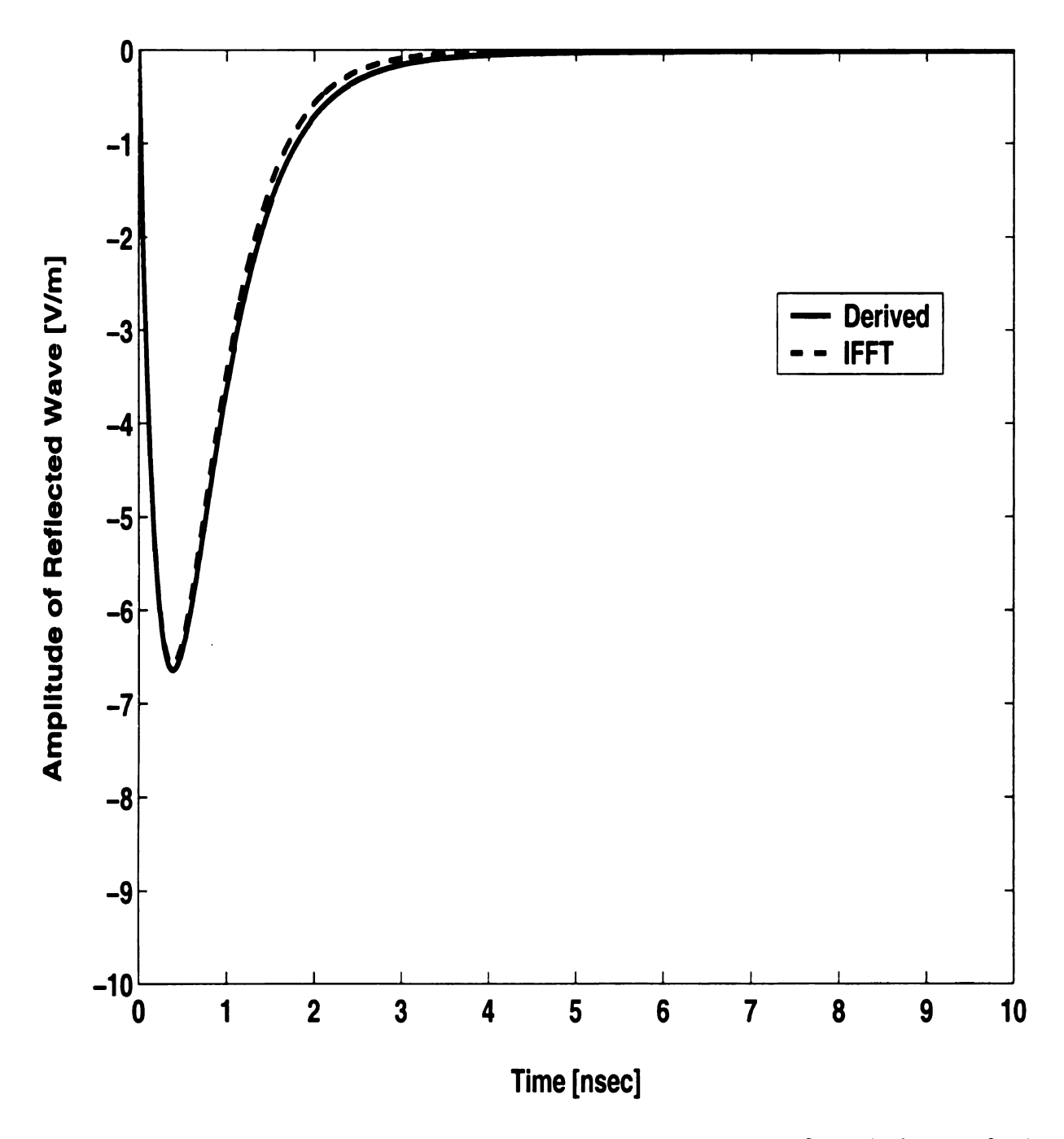


**Figure 3.3.** Numerical comparison of the derived transient reflected electric field waveform for the input waveform shown in Figure 2.6 with the IFFT (TM polarization):  $\mu_n = \mu_0$ ,  $\epsilon_n = \epsilon_0$ ,  $\sigma_n = 0[\mho/m]$ ,  $\mu_{n+1} = \mu_0$ ,  $\epsilon_{n+1} = 72\epsilon_0$ ,  $\sigma_{n+1} = 4[\mho/m]$ ,  $\theta_{i1} = 30^\circ$ .

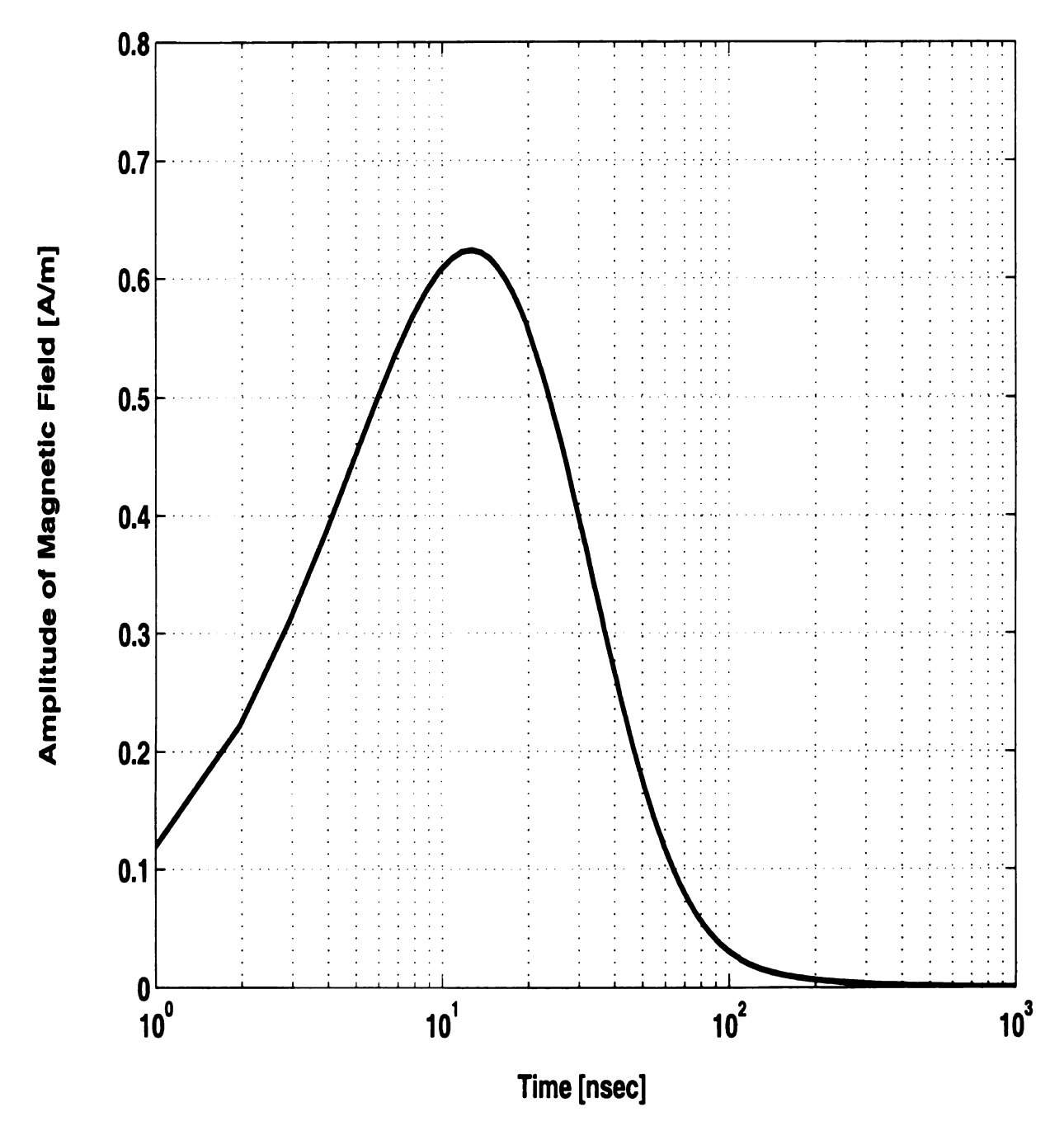


Figure 3.4. (a) The transient reflected magnetic field waveform for a double exponential excitation :  $\epsilon = 10\epsilon_0$ ,  $\mu = \mu_0$ ,  $\sigma = 2 \times 10^{-2} [\mho/m]$ ,  $\theta_i = 45^\circ$ .

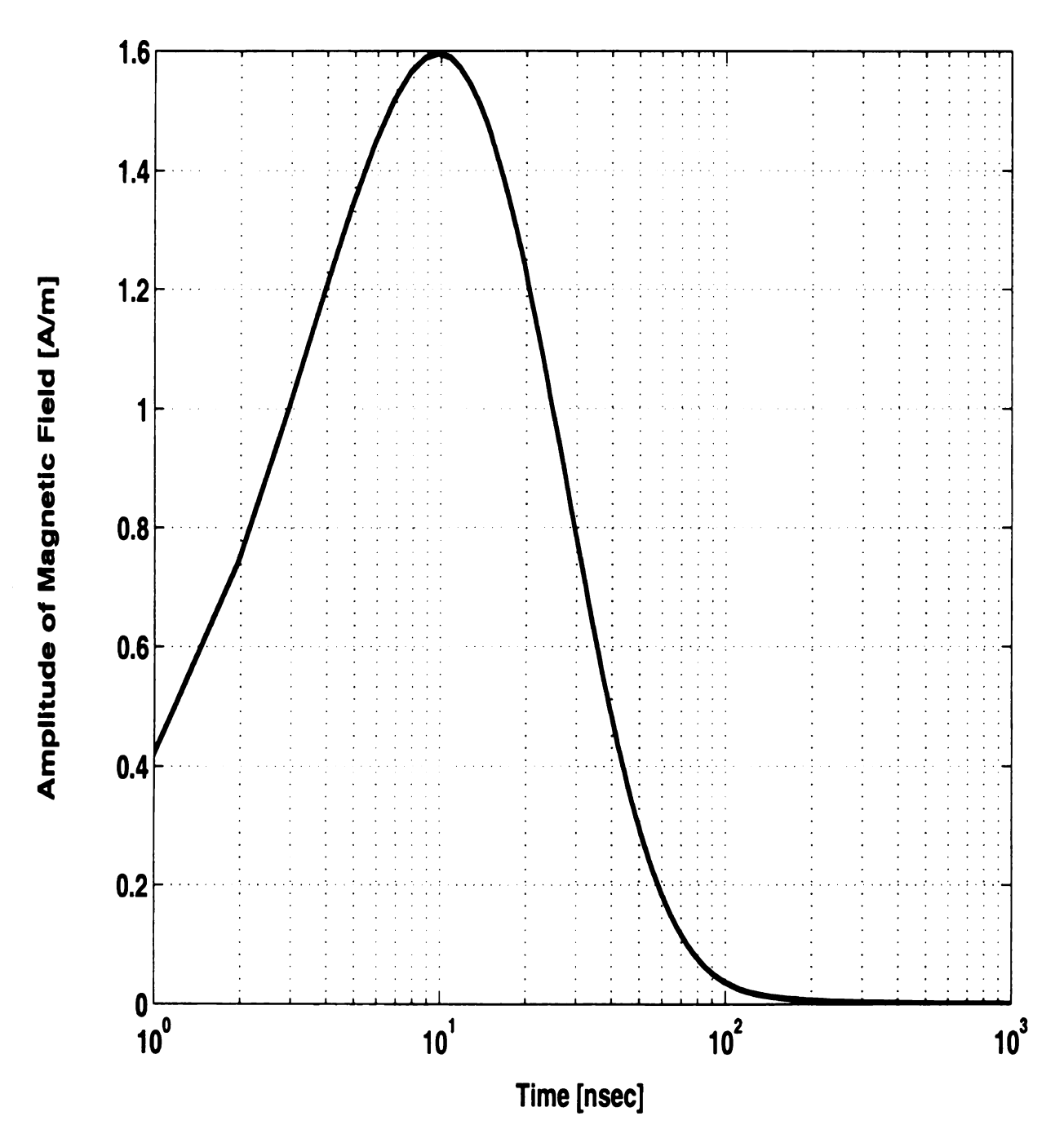


Figure 3.4. (b) The transient transmitted magnetic field waveform for a double exponential excitation:  $\epsilon = 10\epsilon_0$ ,  $\mu = \mu_0$ ,  $\sigma = 2 \times 10^{-2} [\mho/m]$ ,  $\theta_i = 45^\circ$ .

## (1) Permittivity

The curves in Figure 3.5 are plotted for  $\epsilon_{r,n+1}=1.7,\,2.5,\,10$  and 72. The corresponding values of  $R_{\infty}^{TM}$  are -0.10, -0.18, -0.47 and -0.76, respectively. It can be seen that the slopes of different  $\tilde{R}^{TM}(t)$  curves are proportional to the increasing permittivity values as well as increasing asymptotic reflection coefficient  $R_{\infty}^{TM}$ . This means that the transient reflection becomes more dependent on its early time portion coming from the asymptotic reflection term when the permittivity contrast of both layers is sharper.

## (2) Permeability

The curves in Figure 3.6 are plotted for  $\mu_{r,n+1} = 1$ , 5, 10 and 50. The corresponding values of  $R_{\infty}^{TM}$  are -0.76, -0.53, -0.40 and -0.019 respectively. The slopes of  $\tilde{R}^{TM}(t)$  are seen to be inversely proportional to increasing permeability values, and to increasing amplitude of the asymptotic reflection coefficient. This indicates that the transient reflection becomes more 'relaxed' with increasing values of permeability.

### (3) Conductivity

Because an increase in conductivity causes attenuation in wave propagation, the transient response  $\tilde{R}^{TM}(t)$  suffers a more rapid decrease with time as conductivity is increased, while the asymptotic component is independent of the change. This can be seen explicitly in Figure 3.7 where  $\sigma_n = 0.10$ , 1, 4 and 10, respectively.

#### (4) Aspect angle

The curves shown in Figure 3.8 are plotted for  $\theta_{i1} = 0^{\circ}$ ,  $30^{\circ}$ ,  $45^{\circ}$  and  $75^{\circ}$ , while the corresponding values of  $R_{\infty}^{TM}$  are -0.79, -0.76, -0.72 and -0.38 respectively. Therefore, the slope of the reduced reflection coefficient as well as the amplitude of the asymptotic component decreases with increasing aspect angle, and the transient reflection is less dependent on its early time portion.

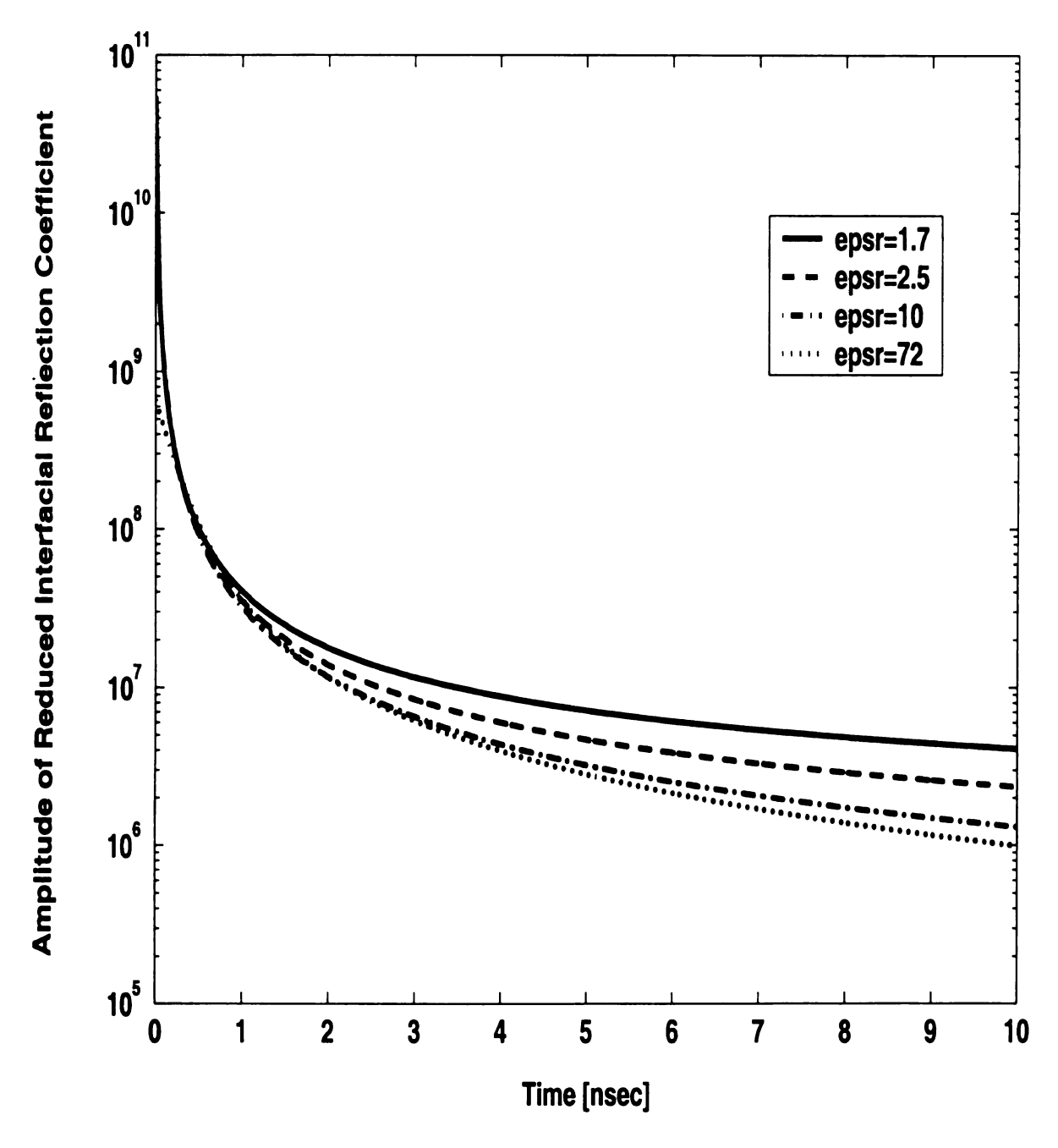
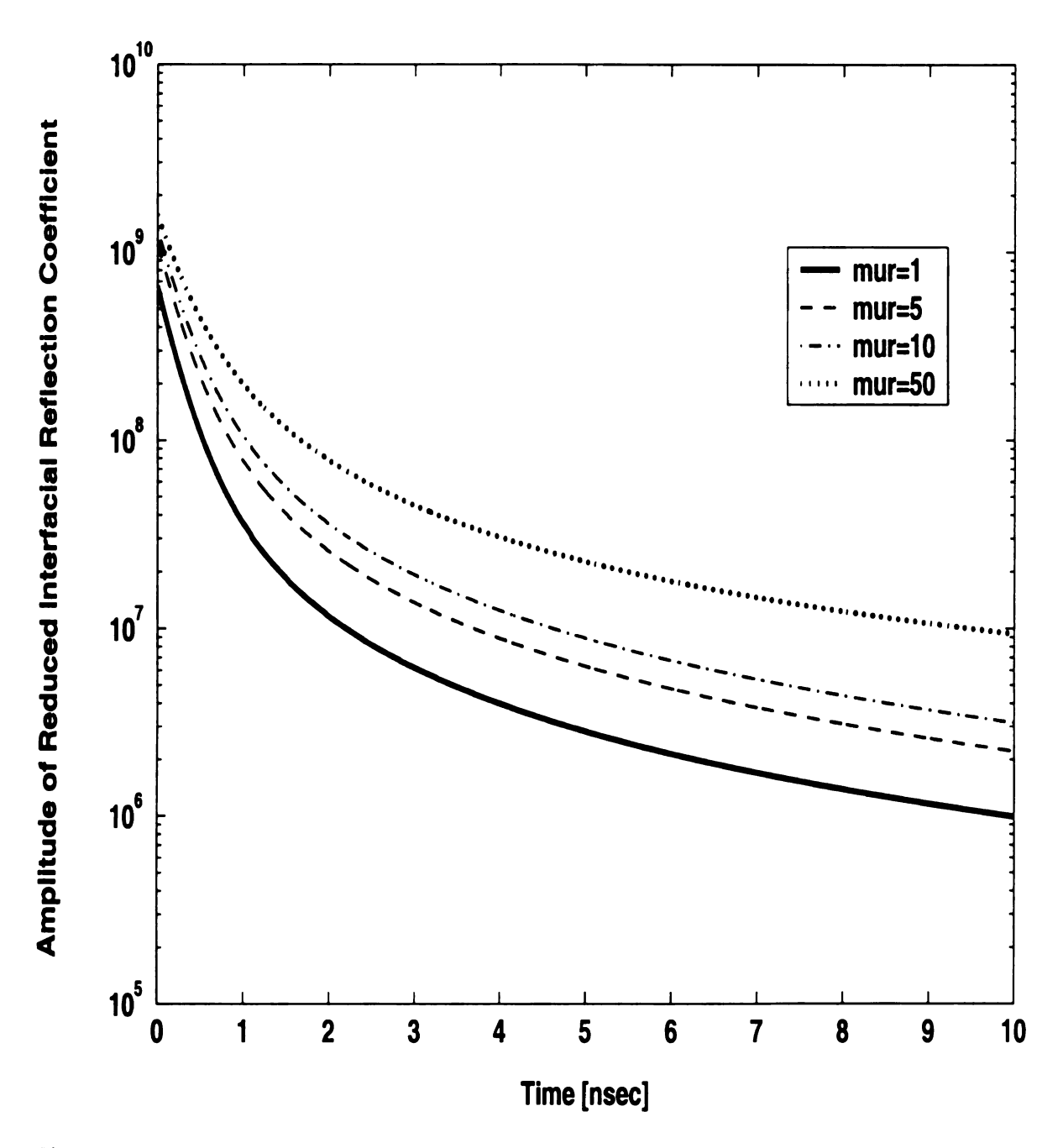


Figure 3.5. Time domain reduced interfacial reflection coefficients for various values of permittivity (TM polarization):  $\epsilon_n = \epsilon_0$ ,  $\mu_n = \mu_{n+1} = \mu_0$ ,  $\sigma_n = 0$ ,  $\sigma_{n+1} = 4[\mho/m]$ ,  $\theta_{i1} = 30^\circ$ .



**Figure 3.6.** Time domain reduced interfacial reflection coefficients for various values of permeability (TM polarization):  $\epsilon_n = \epsilon_0$ ,  $\epsilon_{n+1} = 72\epsilon_0$ ,  $\mu_n = \mu_0$ ,  $\sigma_n = 0$ ,  $\sigma_{n+1} = 4[\mho/m]$ ,  $\theta_{i1} = 30^\circ$ .

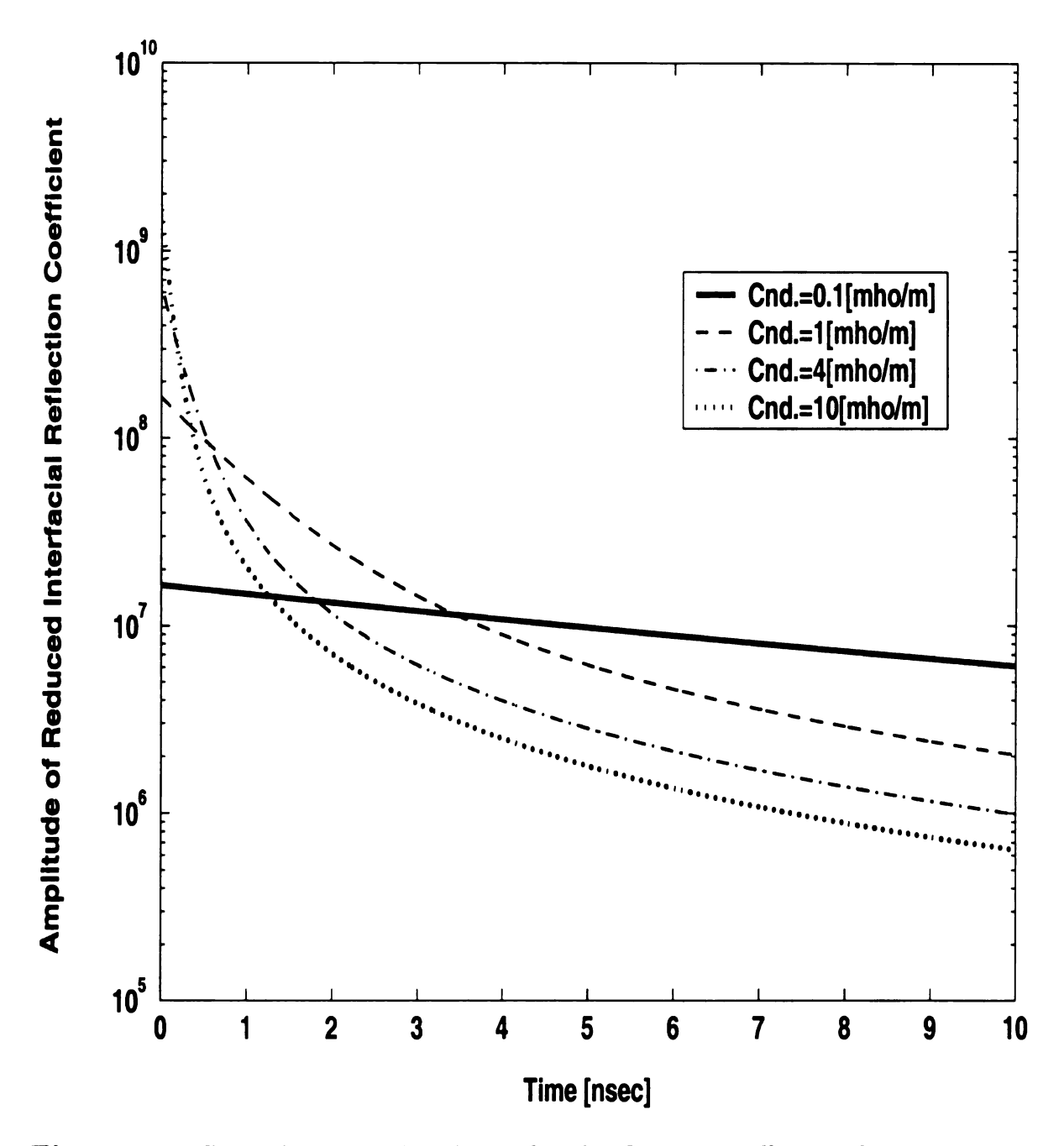
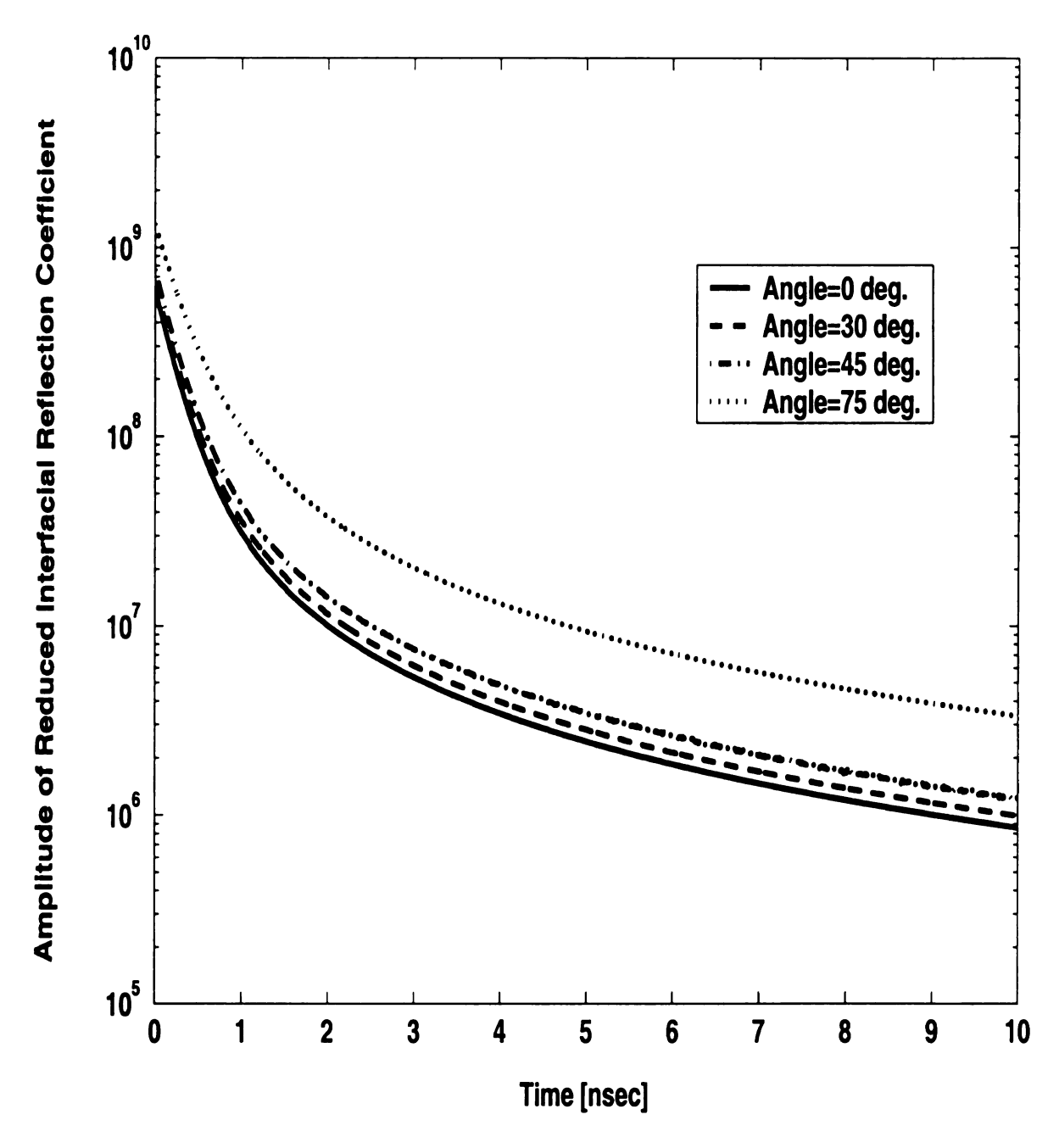


Figure 3.7. Time domain reduced interfacial reflection coefficients for various values of conductivity (TM polarization):  $\epsilon_n = \epsilon_0$ ,  $\epsilon_{n+1} = 72\epsilon_0$ ,  $\mu_n = \mu_{n+1} = \mu_0$ ,  $\sigma_n = 0[\mho/m]$ ,  $\theta_{i1} = 30^\circ$ .



**Figure 3.8.** Time domain reduced interfacial reflection coefficients for various values of incident angle (TM polarization):  $\epsilon_n = \epsilon_0$ ,  $\epsilon_{n+1} = 72\epsilon_0$ ,  $\mu_n = \mu_{n+1} = \mu_0$ ,  $\sigma_n = 0$ ,  $\sigma_{n+1} = 4[\mho/m]$ .

#### CHAPTER 4

#### SCATTERING FROM A MULTI-LAYERED MEDIUM

#### 4.1 Introduction

The overall reflection coefficient is defined as the ratio of the reflected wave amplitude to the incident wave amplitude at the first interface of a muti-layered medium, for which the effect of scattering from the other layers must be considered. In this study, the overall transient scattering from a multi-layered medium is derived from a combination of propagation terms for the layers and the individual interfacial coefficients for which closed forms have been derived in the chapters 2 and 3 for each polarization. To obtain the transient formulation for the overall reflection coefficient, its frequency domain formula is derived first using the wave matrix method, and then time domain expressions are found using a series expansion and the convolution theorem. For this derivation, the analytical form of the transient propagation term is found. Finally, the obtained transient expression is verified by numerical computation examples, and various aspects of the formula are discussed.

#### 4.2 Formulation of Transient Overall Reflection Coefficient

The overall reflection coefficient for a multi-layered medium (assumed to have N layers) can be computed in the frequency domain using wave matrices [22]. Several other techniques can also be used, but this is the most common technique. Figure 4.1 shows the geometry of the  $n^{th}$  layer of a multi-layered configuration. The incident and reflected waves immediately to the left of the  $(n-1 \mid n)$  interface are  $c_n$  and  $b_n$  respectively. Similarly, the waves immediately to the left and right of the  $(n \mid n+1)$  interface are  $c_{n+1}$ ,  $b_{n+1}$  and  $c_{n+2}$ . The overall reflection coefficients immediately to the left of the  $(n-1 \mid n)$  and  $(n \mid n+1)$  interfaces are  $\Gamma_n = b_n/c_n$  and  $\Gamma_{n+1} = b_{n+1}/c_{n+1}$ ,

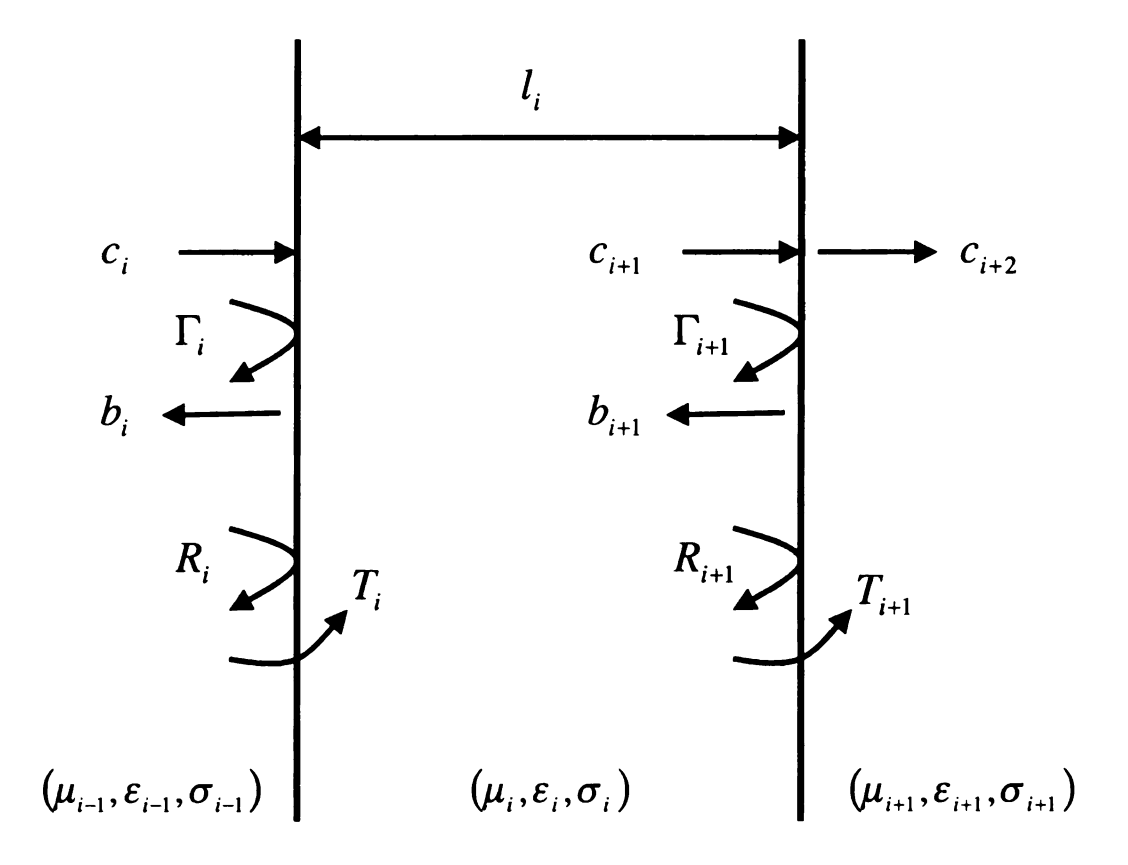


Figure 4.1. The  $n^{th}$  layer of a multi-layered environment.

respectively. The interfacial reflection and transmission coefficients are  $R_n$ ,  $T_n$  and  $R_{n+1}$ ,  $T_{n+1}$ . Wave matrices are used here to relate  $\Gamma_n$  to  $\Gamma_{n+1}$ . By doing so, we can develop a recursive relation that will ultimately relate the reflection coefficient at the front of the interface (i.e. the first layer) to the reflection coefficients of the underlying layers.

Using Collin's wave matrix result [22],  $c_n$  and  $b_n$  are related to  $c_{n+1}$  and  $b_{n+1}$  by the following relation

$$\begin{bmatrix} c_n \\ b_n \end{bmatrix} = \frac{1}{T_n} \begin{bmatrix} P_n^{-1}(\omega) & R_n P_n(\omega) \\ R_n P_n^{-1}(\omega) & P_n(\omega) \end{bmatrix} \begin{bmatrix} c_{n+1} \\ b_{n+1} \end{bmatrix}$$
(4.1)

where  $P_n(\omega) = e^{\gamma_{nx}l_n}$  is the frequency domain propagation term, and  $l_n$  is the length of layer n. Then, the recursive formula for  $\Gamma_n$  in terms of  $\Gamma_{n+1}$  can be computed using Collin's wave matrix result as follows

$$\Gamma_n(\omega) = \frac{b_n}{c_n} = \frac{\frac{1}{T_n} \left\{ R_n P_n^{-1}(\omega) c_{n+1} + P_n(\omega) b_{n+1} \right\}}{\frac{1}{T_n} \left\{ P_n^{-1}(\omega) c_{n+1} + R_n P_n(\omega) b_{n+1} \right\}}$$
(4.2)

Factoring out  $P_n^{-1}(\omega)c_{n+1}$  from the numerator and denominator and using  $\Gamma_{n+1} = b_{n+1}/c_{n+1}$  produces the desired frequency domain result

$$\Gamma_n(\omega) = \frac{R_n(\omega) + P_n^2(\omega)\Gamma_{n+1}(\omega)}{1 + R_n(\omega)P_n^2(\omega)\Gamma_{n+1}(\omega)}.$$
(4.3)

To obtain the transient form of overall reflection coefficient, (4.3) is expanded as a series summation, because it is difficult to find directly the inverse Fourier transform of the formula. For example, assume the three layer case. Then  $\Gamma_2 = R_2$  and

$$\Gamma_1(\omega) = \frac{R_1(\omega) + P_1^2(\omega)R_2(\omega)}{1 + R_1(\omega)P_1^2(\omega)R_2(\omega)}$$

$$= \{R_{1}(\omega) + P_{1}^{2}(\omega)R_{2}(\omega)\} \left[1 - P_{1}^{2}(\omega)R_{1}(\omega)R_{2}(\omega) + \{P_{1}^{2}(\omega)R_{1}(\omega)R_{2}(\omega)\}^{2} - \{P_{1}^{2}(\omega)R_{1}(\omega)R_{2}(\omega)\}^{3} + \cdots \right]$$

$$= R_{1}(\omega) + P_{1}^{2}(\omega)R_{2}(\omega)\{1 - R_{1}^{2}(\omega)\} - P_{1}^{4}(\omega)R_{1}(\omega)R_{2}^{2}(\omega)\{1 - R_{1}^{2}(\omega)\} + P_{1}^{6}(\omega)R_{1}^{2}(\omega)R_{2}^{3}(\omega)\{1 - R_{1}^{2}(\omega)\} - P_{1}^{8}(\omega)R_{1}^{3}(\omega)R_{2}^{4}(\omega)\{1 - R_{1}^{2}(\omega)\} + \cdots$$

$$(4.4)$$

This series expansion is possible because of radiation condition referred in section 2.2.2. To be able to expand by a series summation, the amplitude of  $R_n(\omega)$  and  $P_n(\omega)$  must be equal to or less than unity. This is satisfied due to radiation condition (leading to the branch cut definition), which requires a non-positive real part of the propagation constant. That is,

$$|P(\omega)| = |e^{\gamma_{nx}l_n}| = e^{Re\{\gamma_{nx}\}l_n} \le 1 \tag{4.5}$$

and

$$R^{TE}(s) = \frac{\sqrt{s + B_n} - \sqrt{D_n}\sqrt{s + B_{n+1}}}{\sqrt{s + B_n} + \sqrt{D_n}\sqrt{s + B_{n+1}}}$$

$$= \frac{\{-a(\omega) \pm jb(\omega)\} - \{-c(\omega) \pm jd(\omega)\}}{\{-a(\omega) \pm jb(\omega)\} + \{-c(\omega) \pm jd(\omega)\}}$$

$$= \frac{-\{a(\omega) - c(\omega)\} \pm j\{b(\omega) - d(\omega)\}}{-\{a(\omega) + c(\omega)\} \pm j\{b(\omega) + d(\omega)\}}$$

$$(4.6)$$

where  $a(\omega)$ ,  $b(\omega)$ ,  $c(\omega)$  and  $d(\omega)$  are arbitrary positive functions of frequency. Thus,

$$|R^{TE}(s)| = \frac{\sqrt{\{a(\omega) - c(\omega)\}^2 + \{b(\omega) - d(\omega)\}^2}}{\sqrt{\{a(\omega) + c(\omega)\}^2 + \{b(\omega) + d(\omega)\}^2}} \le 1.$$
(4.7)

The overall reflection coefficient for a medium having more layers can be found replacing  $R_2(\omega)$  with  $\Gamma_2(\omega)$  in (4.4) and using recursive relation given by (4.3). To obtain the transient overall reflection coefficient, the convolution theorem is used, which says that the multiplication in frequency domain is equivalent to convolution in time domain. Therefore, the transient form of (4.4) is given by

$$\Gamma_{1}(t) = R_{1}(t) + P_{1}(t) * P_{1}(t) * R_{2}(t) * \{\delta(t) - R_{1}(t) * R_{1}(t)\} -$$

$$P_{1}(t) * P_{1}(t) * P_{1}(t) * P_{1}(t) * R_{1}(t) * R_{2}(t) * R_{2}(t) * \{\delta(t) - R_{1}(t) * R_{1}(t)\}$$

$$+ \cdot \cdot \cdot . \qquad (4.8)$$

And finally, the reflection S(t) from the first interface of a multi-layered medium due to an input waveform X(t) can be obtained as

$$S(t) = X(t) * \Gamma_1(t). \tag{4.9}$$

# 4.3 Transient Propagation

To compute the transient overall reflection given by (4.9), the transient propagation terms must be found. By letting

$$d_n = \mu_n \epsilon_n - \mu_1 \epsilon_1 \sin^2 \theta_{i1}$$

$$b_n = \mu_n \sigma_n, \qquad (4.10)$$

the definition of the propagation constant in (2.38) is rewritten as

$$\gamma_{nx} = \sqrt{d_n s^2 + b_n s} = -\sqrt{d_n} \sqrt{s^2 + \frac{l_n}{d_n} s}$$
 (4.11)

for  $d_n > 0$ , and

$$\gamma_{nx} = \sqrt{d_n s^2 + b_n s} = \pm j \sqrt{|d_n|} \sqrt{s^2 - \frac{l_n}{|d_n|} s}$$
 (4.12)

for  $d_n < 0$ , and where the upper sign is used for  $\omega > 0$  and the lower sign for  $\omega < 0$ . Only the  $d_n > 0$  case will be considered due to the causality difficulties mentioned in

## Chapter 2.

Now the frequency domain propagation term is written as

$$P_n(\omega) = e^{\gamma_x l_n}$$

$$= e^{-l_n \sqrt{d_n} \sqrt{s^2 + \frac{l_n}{d_n} s}}.$$
(4.13)

To obtain the inverse Fourier transform of (4.13), the transform pair in [23],

$$e^{-\frac{x}{v}\sqrt{(s+\rho)^2-\sigma^2}} \Leftrightarrow e^{-\frac{\rho x}{v}}\delta\left(t-\frac{x}{v}\right) + \frac{\sigma x}{v\sqrt{t^2-\left(\frac{x}{v}\right)^2}}e^{-\rho t}I_1\left(\sigma\sqrt{t^2-\left(\frac{x}{v}\right)^2}\right)u\left(t-\frac{x}{v}\right) \quad (4.14)$$

where  $Re\{\rho,\sigma\} \ge 0$ , is used. When (4.13) and (4.14) are compared, it can be realized that  $\frac{b_n}{2d_n} > 0$  corresponds to  $\rho$ , and  $\sigma = \rho > 0$ . Then,

$$e^{-\frac{\rho l_n}{v}}\delta\left(t - \frac{l_n}{v}\right) \rightarrow e^{-\frac{b_n}{2d_n}l_n\sqrt{d_n}}\delta(t - l_n\sqrt{d_n})$$

$$\frac{\sigma l_n}{v\sqrt{t^2 - \left(\frac{l_n}{v}\right)^2}} \rightarrow \frac{\frac{b_n}{2d_n}l_n\sqrt{d_n}}{\sqrt{t^2 - l_n^2d_n}}$$

$$e^{-\rho t}I_1\left(\sigma\sqrt{t^2 - \left(\frac{l_n}{v}\right)^2}\right)u\left(t - \frac{l_n}{v}\right) \rightarrow e^{-\frac{b_n}{2d_n}t}I_1\left(\frac{b_n}{2d_n}\sqrt{t^2 - l_n^2d_n}\right)u(t - l_n\sqrt{d_n}).$$

$$(4.15)$$

As a result, the transient propagation term is given by

$$P_{n}(t) = e^{-\frac{b_{n}}{2\sqrt{d_{n}}}l_{n}}\delta(t - l_{n}\sqrt{d_{n}}) + \frac{(b_{n}l_{n}/2\sqrt{d_{n}})}{\sqrt{t^{2} - l_{n}^{2}d_{n}}}I_{1}\left(\frac{b_{n}}{2d_{n}}\sqrt{t^{2} - l_{n}^{2}d_{n}}\right)u(t - l_{n}\sqrt{d_{n}}).$$
(4.16)

Also, it can be easily shown that

$$\{P_{n}(s)\}^{k} \Leftrightarrow e^{-\frac{b_{n}}{2\sqrt{d_{n}(kl_{n})}}} \delta(t - kl_{n}\sqrt{d_{n}}) \\
+ \frac{(kl_{n}b_{n}/2\sqrt{d_{n}})}{\sqrt{t^{2} - l_{n}^{2}d_{n}}} I_{1}\left(\frac{b_{n}}{2d_{n}}\sqrt{t^{2} - (kl_{n})^{2}d_{n}}\right) u(t - kl_{n}\sqrt{d_{n}}). (4.17)$$

The transient form (4.17) should be verified by numerical inverse Fourier transform, but it is difficult to compute directly the transient form because it includes the  $\delta$ -function. Therefore, a modified form obtained by removing the  $\delta$ -function term is compared with its corresponding frequency domain form. That is, by being modified as

$$\tilde{P}_n(t) = P_n(t) - e^{-\frac{b_n}{2\sqrt{d_n}}l_n}\delta(t - l_n\sqrt{d_n}),$$
(4.18)

the corresponding frequency domain transform becomes

$$\tilde{P}_{n}(s) = P_{n}(s) - F\left\{e^{-\frac{b_{n}}{2\sqrt{d_{n}}}l_{n}}\delta(t - l_{n}\sqrt{d_{n}})\right\} 
= e^{-\sqrt{d_{n}}\sqrt{s^{2} + \frac{b_{n}}{d_{n}}}sl_{n}} - e^{-\frac{b_{n}}{2\sqrt{d_{n}}}l_{n}}e^{-(l_{n}\sqrt{d_{n}})s} 
= e^{-\sqrt{d_{n}}\sqrt{s^{2} + \frac{b_{n}}{d_{n}}}sl_{n}} - e^{-(\frac{b_{n}}{2\sqrt{d_{n}}} + \sqrt{d_{n}}s)l_{n}},$$
(4.19)

and the transform pair of (4.18) and (4.19) may be compared using numerical inverse Fourier transform. The plot in Figure 4.2 shows an example of such a comparison obtained using a 2048 point IFFT with a 20 nano second interval. The transient form and the IFFT result are well matched, and therefore the correctness of the transient propagation term has been verified.

# 4.4 Numerical Examples of Overall Reflection

The previously derived transient overall reflection form may be verified using numerical computation to ensure its correctness. Considering there are  $\delta$ -function terms included in both the transient propagation and interfacial reflection terms,

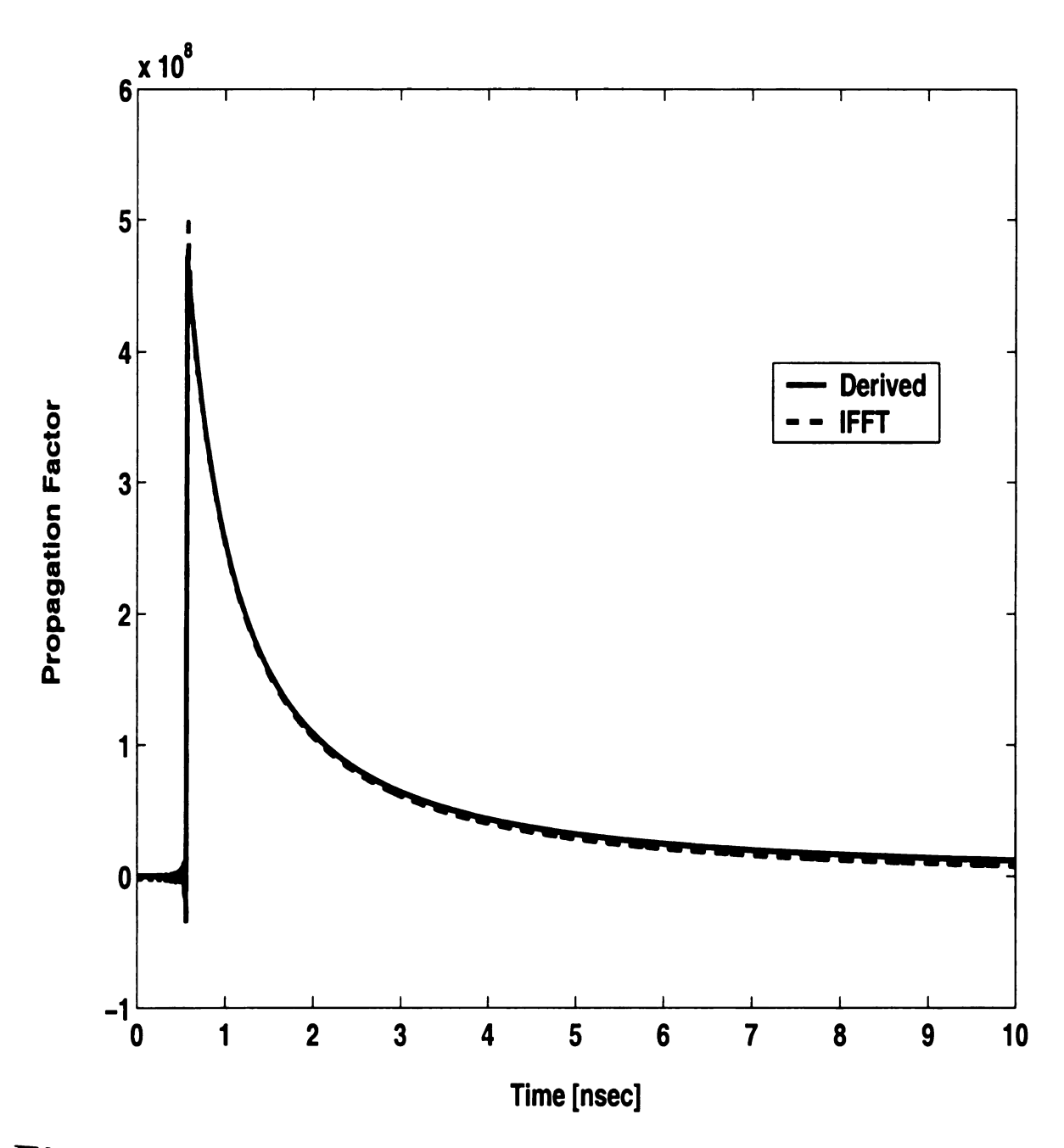


**Figure 4.2.** Numerical comparison of the derived transient propagation term with that from the IFFT:  $\mu_n = \mu_0$ ,  $\epsilon_n = 72\epsilon_0$ ,  $\sigma_n = 4[\mho/m]$ ,  $l_n = 0.01[m]$ ,  $\theta_{i1} = 30^\circ$ .

direct numerical computation of (4.8) may not produce an accetable result. Therefore, the following numerical implementation is used in this study. When assuming  $P(t) = A\delta(t - t_d) + \tilde{P}(t - t_d)$  and  $R(t) = R_{\infty}\delta(t) + \tilde{R}(t)$  for example, the convolution becomes

$$P(t) * R(t) = \{A\delta(t - t_d) + \tilde{P}(t - t_d)\} * \{R_{\infty}\delta(t) + \tilde{R}(t)\}$$

$$= AR_{\infty}\delta(t) * \delta(t - t_d) + A\delta(t - t_d) * \tilde{R}(t)$$

$$+ R_{\infty}\delta(t) * \tilde{P}(t - t_d) + \tilde{P}(t - t_d) * \tilde{R}(t)$$

$$= AR_{\infty}\delta(t - t_d) + A\tilde{R}(t - t_d) + R_{\infty}\tilde{P}(t - t_d) + \tilde{P}(t - t_d) * \tilde{R}(t).$$
(4.20)

The amplitude and position of the  $\delta$ -function in (4.20) are stored separately for use in subsequent computations. To compute  $\tilde{P}(t-t_d)*\tilde{R}(t)$ , several different numerical algorithms are available [24], but the simple discrete convolution algorithm is used in this study, and it turns out that the method provides sufficient accuracy when compared with IFFT results. Detailed programming source codes for numerical implementation can be found in Appendix C.

Numerical examples of scattering excited by the input waveform shown in Figure 4.3 from the simplest 3 lossless layer (free space, 10cm thick-plexiglass and free space) cases for both polarizations are shown in Figure 4.4 and Figure 4.5. The double exponential input waveform shown in Figure 4.3 is produced as

$$X(t) = 10.24 \times \left( e^{-8 \times 10^9 t} - e^{-16 \times 10^9 t} \right). \tag{4.21}$$

The permittivity value at 10GHz for the plexiglass layer,  $2.59\epsilon_0$ , is found in [21]. The results from the transient formulas are compared with those obtained from a 2048 Point IFFT with a 20 nano second range, although only the first 10 nano seconds

are shown. The comparison shows good agreement in both polarizations. The phase reversed reflected waveforms at each edge are seen in the both plots.

To see explicitly mutiple reflections due to time-delaying propagation terms, the scattering from a 5-layered lossless medium (free space, 10cm plexiglass, 10cm free space, 10cm plexiglass and free space) is computed, and shown in Figure 4.6. Because this medium consists of lossless layers, the reflected waveforms are controlled only by the asymptotic reflection coefficients, and there is no attenuation suffered by the reflected waves. Instead, the amplitudes of reflected waves decrease after each reflection because the amplitude of each asymptotic reflection coefficient must be less than unity.

The overall reflections from a lossy layered medium are plotted Figure 4.7 and Figure 4.8 for both polarizations respectively. The 5 layered medium is identical to the previous case except that the third layer is distilled water with parameter values taken at 10 GHz, and the equivalent conductivity used to represent the dielectric loss of water at that frequency. As expected, the mutiple reflections suffer severe attenuation, and the reflections after a short period peter out.

It may be interesting and practical to identify each reflected waveform in the mutiple reflections shown in Figure 4.6 - Figure 4.8, by associating them with each term in (4.8). The time domain waveform identification makes it possible to remove unwanted signals, for an example, multi-path echos. Figure 4.9 shows the individual reflections in Figure 4.7 due to the first through the fourth term in (4.8). The first peak obviously is the reflection from the first interface of air to plaxiglass, and depends on the asymptotic reflection coefficient only. Also, notice that the sign of the amplitude is inverted since the wave is reflected from a electrically denser layer. The second Peak comes from the reflection at the plexiglass-water interface. Similary, the sign of amplitude is reversed, but the large reflection occurs because the permittivity profile difference between the two layers is larger than for the previous interface. Now the

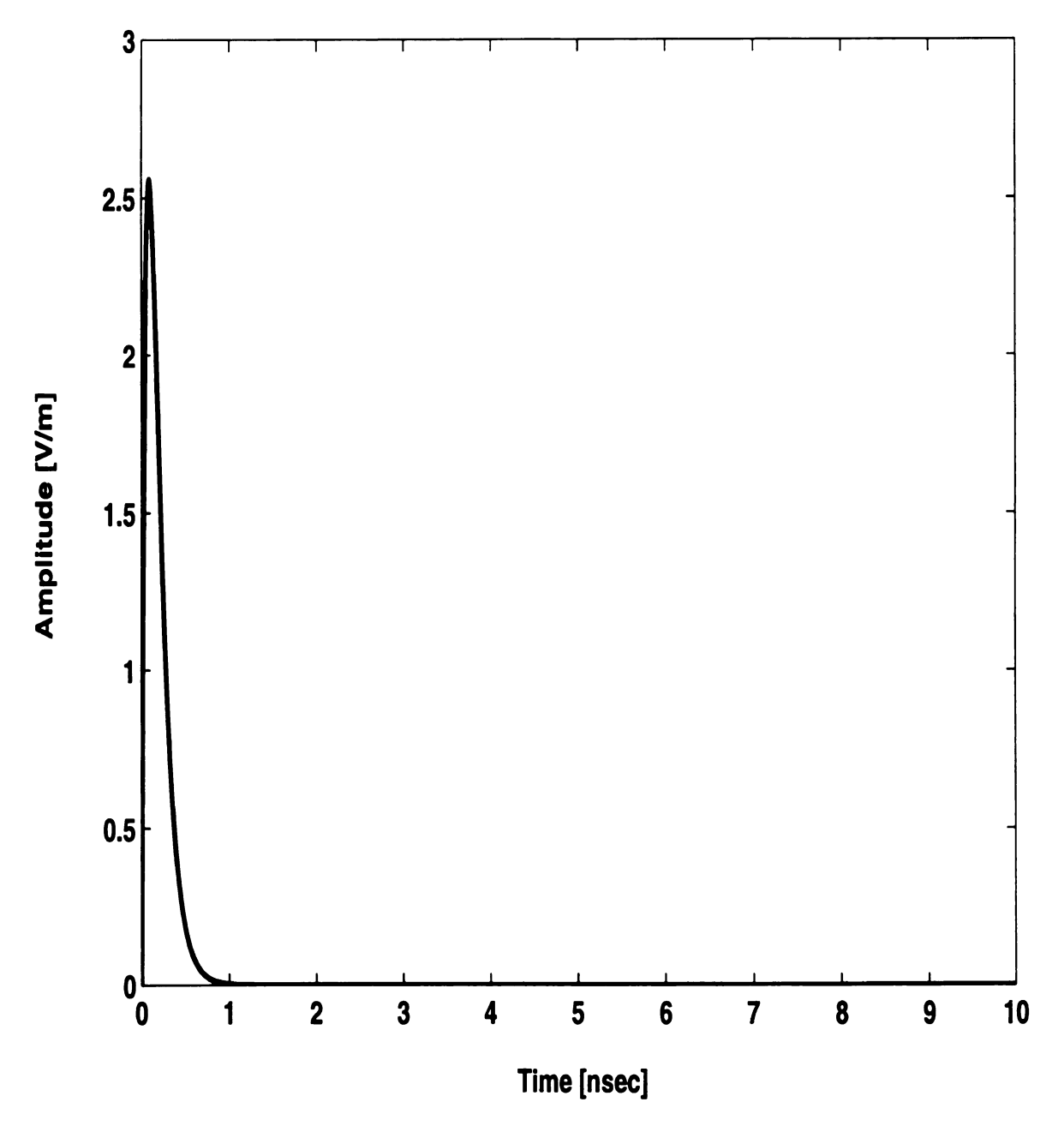


Figure 4.3. A double exponential input waveform

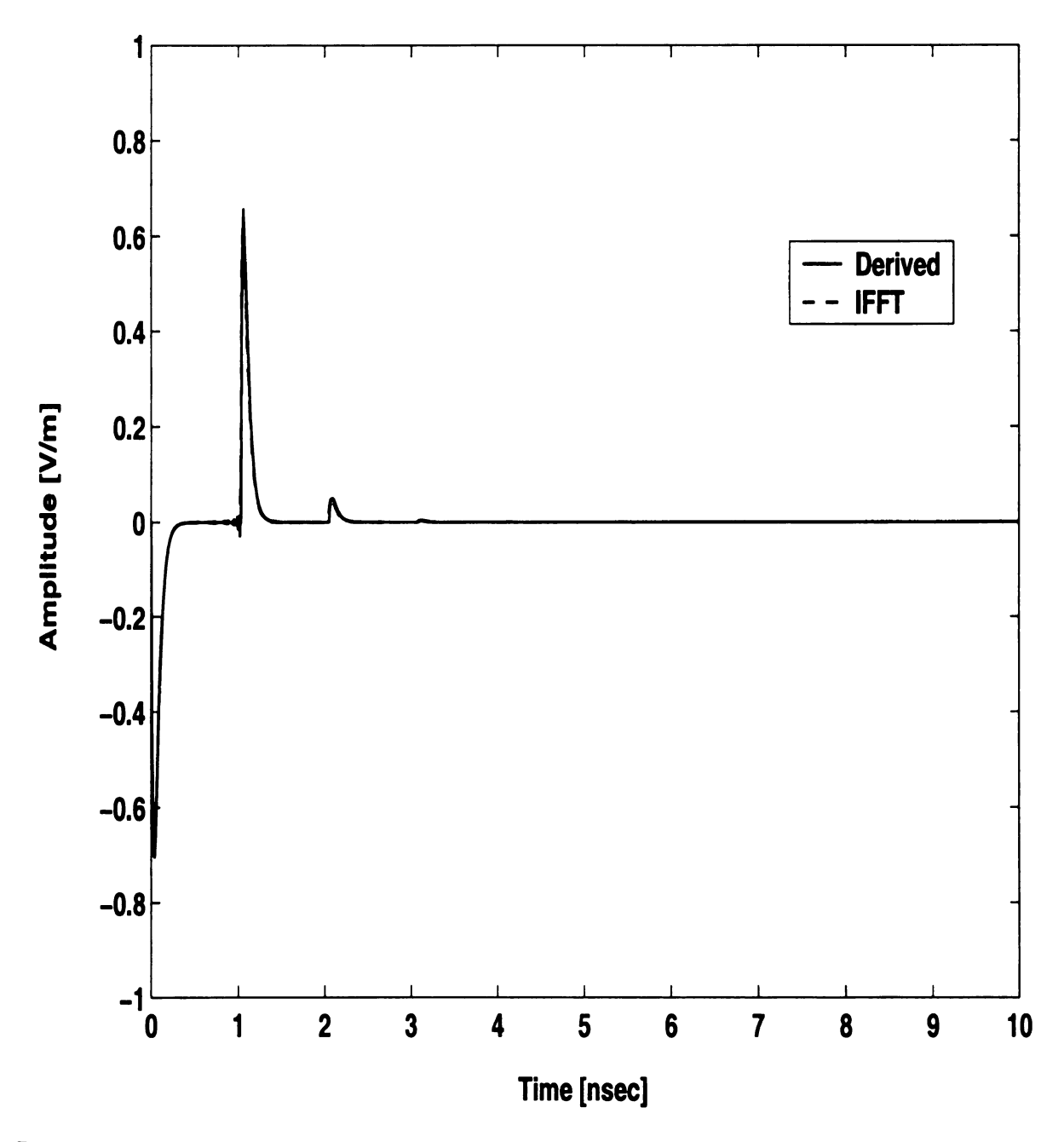
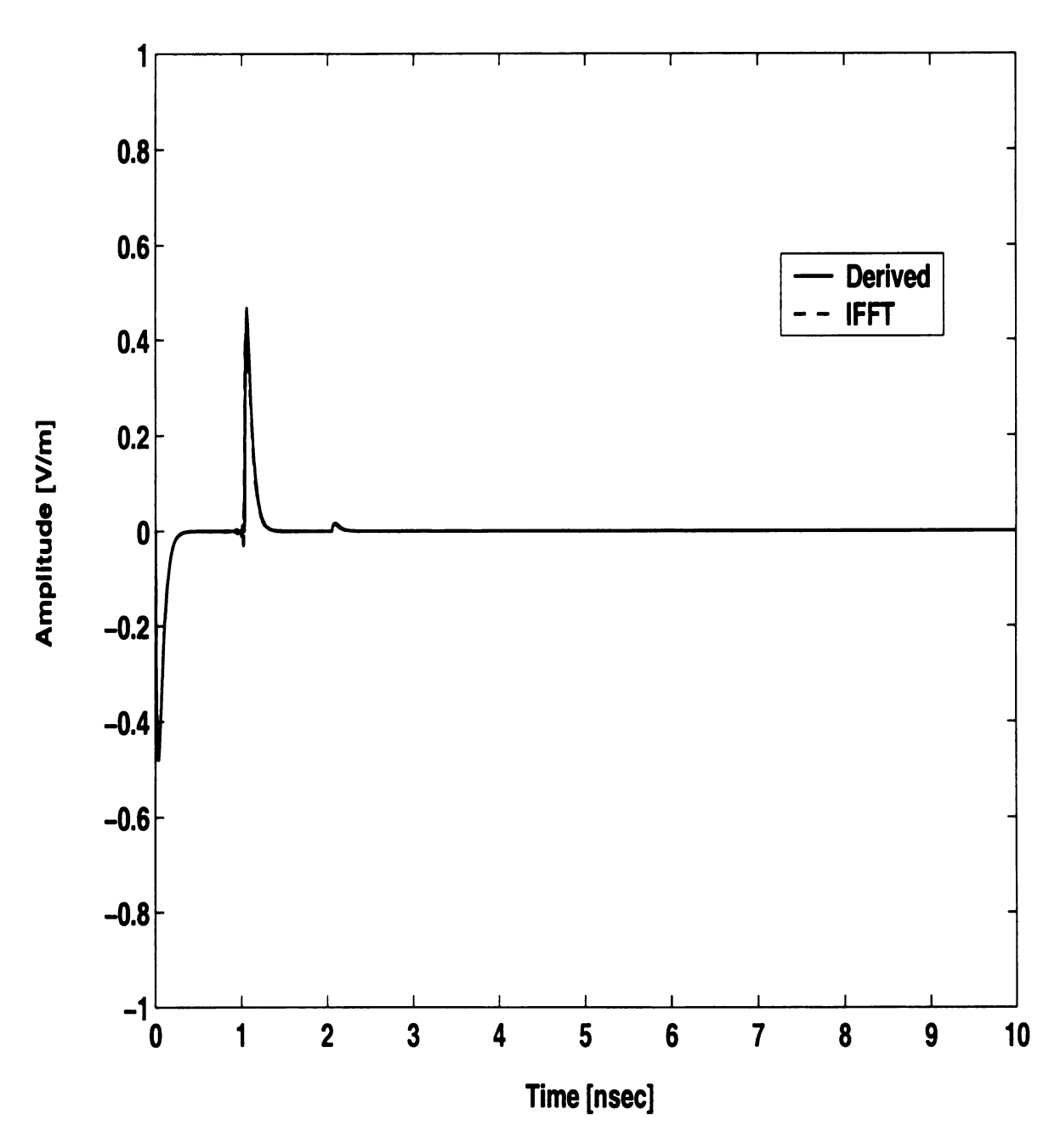
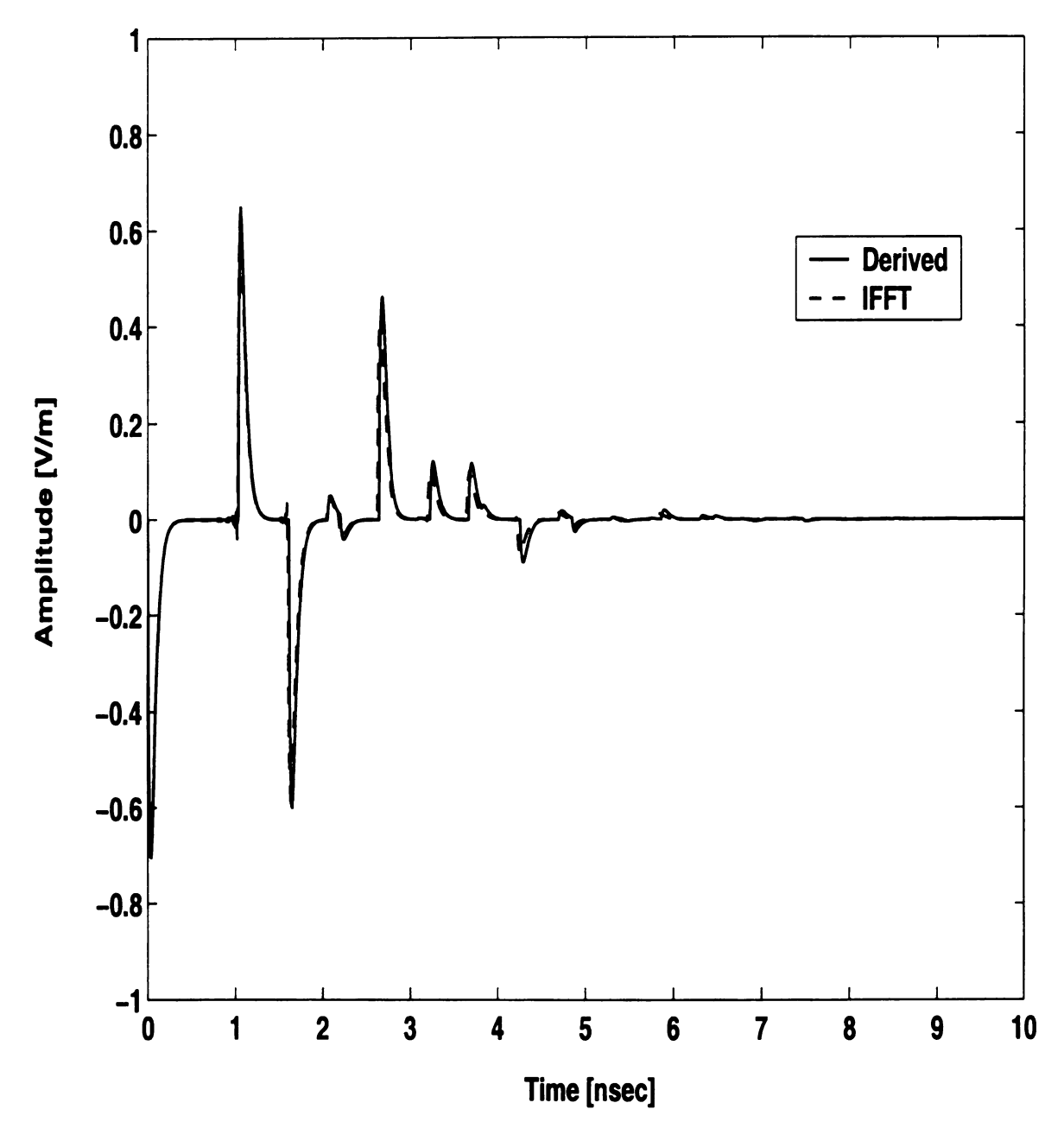


Figure 4.4. Numerical comparison of the derived overall reflection from a 3 layered medium with that from the IFFT (TE polarization):  $\mu_2 = \mu_0$ ,  $\epsilon_2 = 2.59\epsilon_0$ ,  $\sigma_2 = 0[\mho/m]$ ,  $l_2 = 0.1[m]$ ,  $\theta_{i1} = 30^\circ$ .



**Figure 4.5.** Numerical comparison of the derived overall reflection from a 3 layered medium with that from the IFFT (TM polarization):  $\mu_2 = \mu_0$ ,  $\epsilon_2 = 2.59\epsilon_0$ ,  $\sigma_2 = 0[\mho/m]$ ,  $l_2 = 0.1[m]$ ,  $\theta_{i1} = 30^\circ$ .



**Figure 4.6.** Mutiple reflection from a lossless 5 layered medium (TE polarization) :  $\mu_2 = \mu_0$ ,  $\epsilon_2 = 2.59\epsilon_0$ ,  $\sigma_2 = 0[\mho/m]$ ,  $l_2 = 0.1[m]$ ,  $\mu_3 = \mu_0$ ,  $\epsilon_3 = \epsilon_0$ ,  $\sigma_3 = 0[\mho/m]$ ,  $l_3 = 0.1[m]$ ,  $\mu_4 = \mu_0$ ,  $\epsilon_4 = 2.59\epsilon_0$ ,  $\sigma_4 = 0[\mho/m]$ ,  $l_4 = 0.1[m]$ ,  $\theta_{i1} = 30^\circ$ .

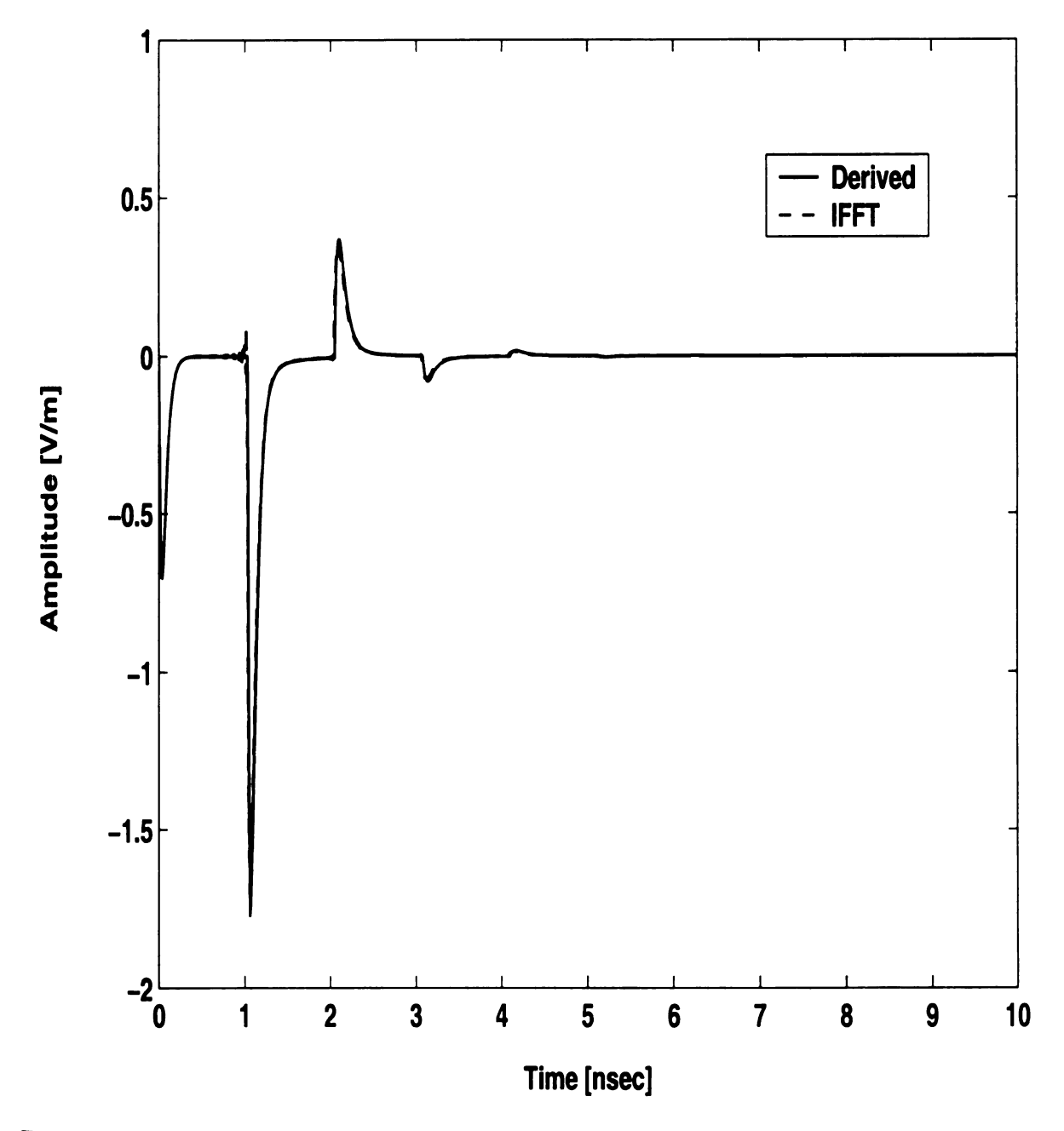


**Figure 4.7.** Mutiple reflection from a lossy 5 layered medium (TE polarization):  $\mu_2 = \mu_0$ ,  $\epsilon_2 = 2.59\epsilon_0$ ,  $\sigma_2 = 0[\mho/m]$ ,  $l_2 = 0.1[m]$ ,  $\mu_3 = \mu_0$ ,  $\epsilon_3 = 55\epsilon_0$ ,  $\sigma_3 = 16.7[\mho/m]$ ,  $l_3 = 0.1[m]$ ,  $\mu_4 = \mu_0$ ,  $\epsilon_4 = 2.59\epsilon_0$ ,  $\sigma_4 = 0[\mho/m]$ ,  $l_4 = 0.1[m]$ ,  $\theta_{i1} = 30^\circ$ .

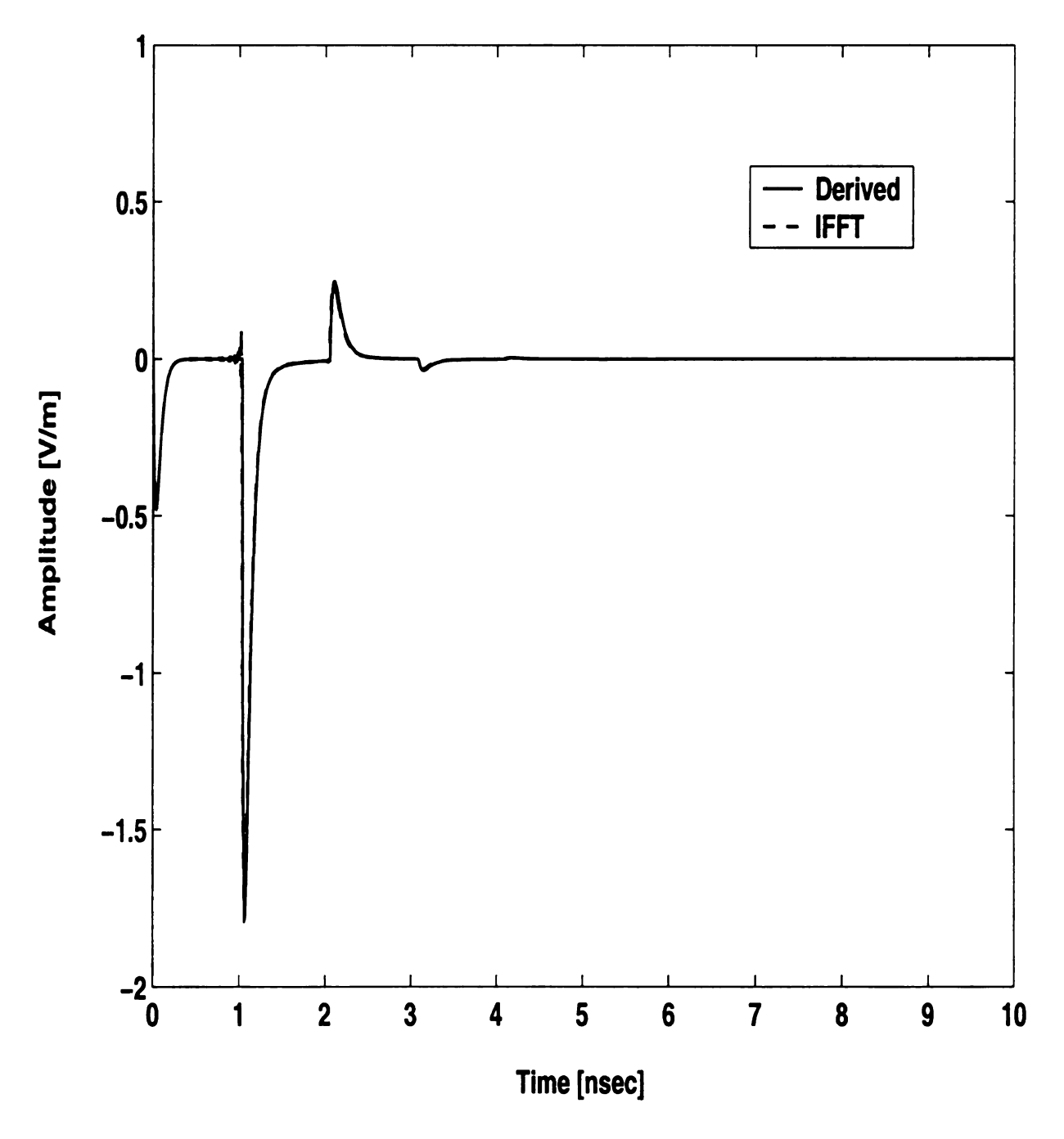


**Figure 4.8.** Mutiple reflection from a lossy 5 layered medium (TM polarization):  $\mu_2 = \mu_0$ ,  $\epsilon_2 = 2.59\epsilon_0$ ,  $\sigma_2 = 0[\mho/m]$ ,  $l_2 = 0.1[m]$ ,  $\mu_3 = \mu_0$ ,  $\epsilon_3 = 55\epsilon_0$ ,  $\sigma_3 = 16.7[\mho/m]$ ,  $l_3 = 0.1[m]$ ,  $\mu_4 = \mu_0$ ,  $\epsilon_4 = 2.59\epsilon_0$ ,  $\sigma_4 = 0[\mho/m]$ ,  $l_4 = 0.1[m]$ ,  $\theta_{i1} = 30^\circ$ .

reflected waveform is contributed by the reduced reflection coefficient as well as the asymptotic component. The polarity of the third peak is the same as that of the input waveform. Therefore, there is a possibility that it comes from the reflection at the water-plexiglass interface. However, considering the relatively high permittivity profile of water which makes the waveform propagation much slower than in plexiglass, as well as the heavy attenuation that the wave suffers due to the dielectric loss of water, this possibility must be discarded. Therefore, the third peak originates from three reflections at the interfaces of plexiglass-water, air-plexiglass, plexiglass-water and transmission through the air plexiglass interface. The fourth peak comes from an additional two reflections at the air-plexiglass and plexiglass-water interfaces. Of course, this rigorous geometical ray optics approach is possible because of the exact timing analysis.

The incident angle dependence of the overall reflection is shown in Figure 4.10 for the same 5 layered lossy medium used in Figure 4.9. In the first reflected waveform set, the largest angle produces the largest peak waveform because the asymptotic reflection coefficient is proportional to angle as described in section 2.4.2. In the second reflected waveform set, the smallest angle produces the largest peak, due to its large reduced reflection coefficient components (see Figure 2.12). The same explanation can be applied to the other reflected waveform sets. Note that the multiple reflections with the largest incidence angle occur earliest. Although this phenomenon may be intuitively confusing since a longer travel path for a ray inside of a layer is expected for a larger incidence angle, it can be justified by considering the time delay in (4.16), or by the rigorous geometrical ray optics research found in [25].

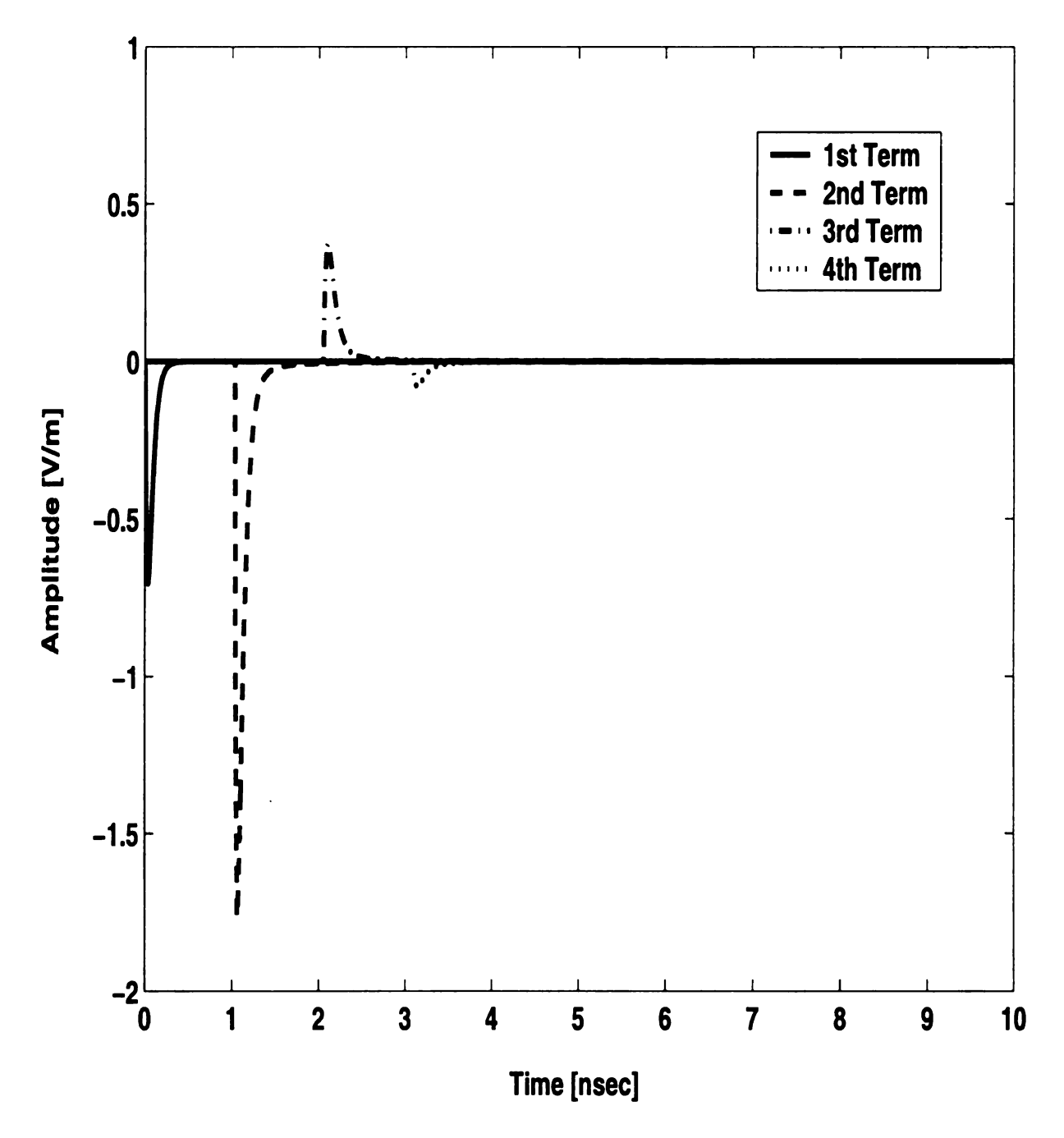
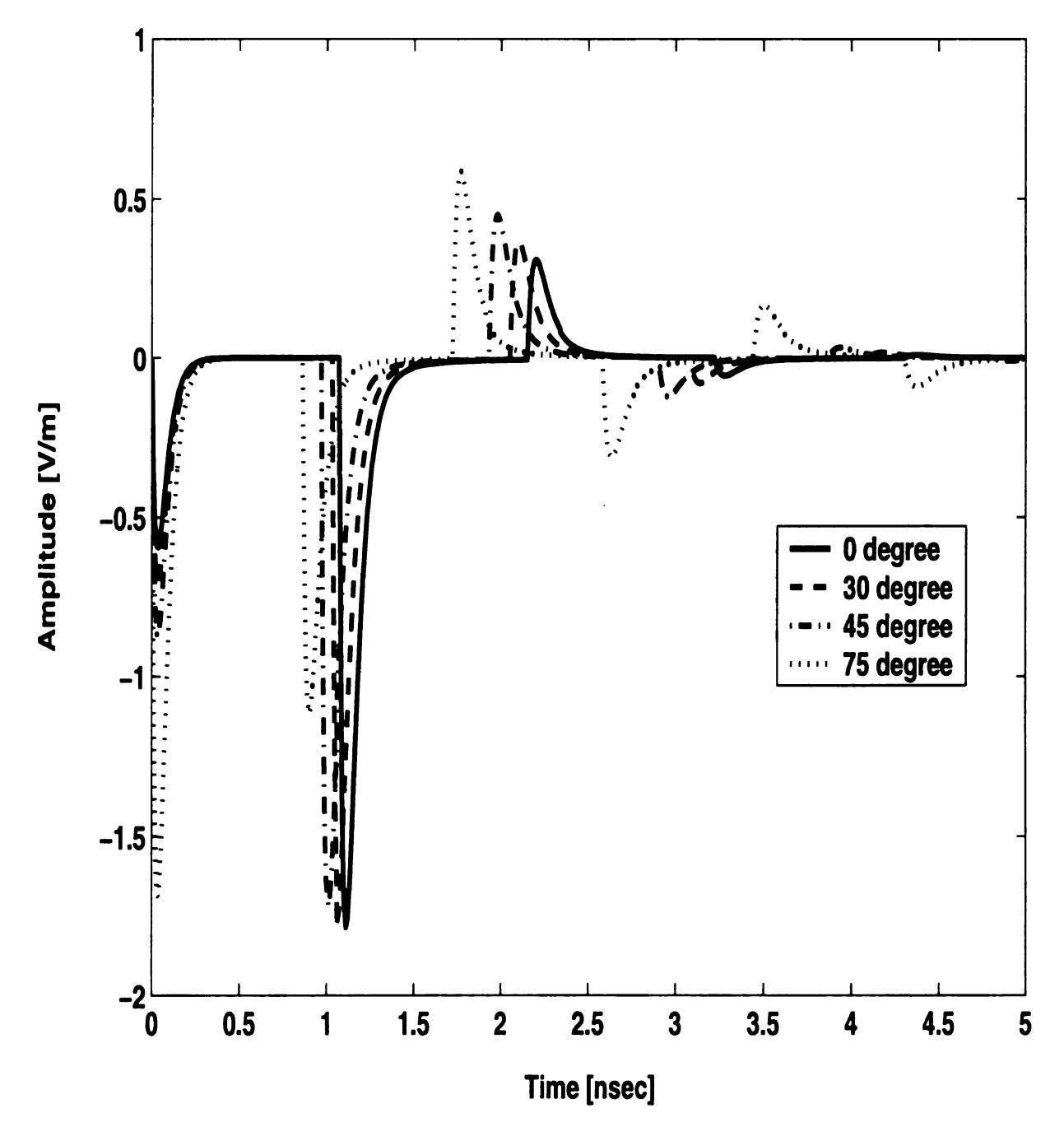


Figure 4.9. Indentification of indivisual reflection in overall scattering from a 5 layered medium (TE polarization):  $\mu_2 = \mu_0$ ,  $\epsilon_2 = 2.59\epsilon_0$ ,  $\sigma_2 = 0[\mho/m]$ ,  $l_2 = 0.1[m]$ ,  $\mu_3 = \mu_0$ ,  $\epsilon_3 = 55\epsilon_0$ ,  $\sigma_3 = 16.7[\mho/m]$ ,  $l_3 = 0.1[m]$ ,  $\mu_4 = \mu_0$ ,  $\epsilon_4 = 2.59\epsilon_0$ ,  $\sigma_4 = 0[\mho/m]$ ,  $l_4 = 0.1[m]$ ,  $\theta_{i1} = 30^\circ$ .



**Figure 4.10.** Time domain overall reflection for various values of incident angle (TE polarization):  $\mu_2 = \mu_0$ ,  $\epsilon_2 = 2.59\epsilon_0$ ,  $\sigma_2 = 0[\mho/m]$ ,  $l_2 = 0.1[m]$ ,  $\mu_3 = \mu_0$ ,  $\epsilon_3 = 55\epsilon_0$ ,  $\sigma_3 = 16.7[\mho/m]$ ,  $l_3 = 0.1[m]$ ,  $\mu_4 = \mu_0$ ,  $\epsilon_4 = 2.59\epsilon_0$ ,  $\sigma_4 = 0[\mho/m]$ ,  $l_4 = 0.1[m]$ .

# **CHAPTER 5**

#### **EXPERIMENTS**

#### 5.1 Introduction

The derived formulas in the previous chapters have so far been verified only by numerical computation. However, verification by actual experiments may provide additional valuable knowledge such as practical limits in real world applications. In this chapter, the description and results of the measurement processes which have been used to verify previously derived expressions are provided. Also, various aspects of the information obtained from the experiments are discussed. The descriptions of the experimental set up and the equipment are given first, and the calibration procedure which is needed to obtain 'refined' results from the raw measurement data in order to compare with theory are described. Finally, the experiment results from acutal measurements are provided and discussed.

# 5.2 Experimental Set Up

For experiments, the set up depicted in Figure 5.1 is used. The arch range at Michigan State University consists of two 90° steel rail arcs on to which are attached movable transmitting and receiving antenna mounts. The radius of the rail is 120" (3.05m), and the height of the rail is 47" (1.19m), while the center axes of the antennas are placed at 59" (1.50m) height. Note that although several EM wave absorbers are used to reduce reflection from surrounding environments (e.g. wall, door, or metal rails), this arch range is fundamentally NOT an 'anechoic' chamber like those used in frequency domain radiation measurements. A target object (material plates fixed on a metal mounter in this study) is placed at the center of the range. More detailed descriptions on the arch range facility in Michigan State University can be found in

[26].

For time domain measurements, Hewelett Packard's digital sampling oscilloscope HP54750A and its HP54753A time domain transmission/reflectometery (TDT/TDR) plug-in module, providing 20GHz and 18GHz channels, are used. The TDR unit has a built-in step waveform generator that creats pulse trains with 5msec pulse width, 20msec period, and 190mV amplitude. The rising edge of each pulse is used to trigger a Picosecond Pulse Labs (PSPL) 4015B pulse generator. This instrument creates another step using a remote pulse head, which is connected to the input of PSPL 5208 Impulse Forming Network (IFN). The secondary step waveform has a leading edge fall time less than about 15psec, and an amplitude of -9V. An impulse forming network generates the impulse shaped waveform shown in Figure 5.2, using the step as an input. The impulse waveform is fed through connecting cables to a transmitting horn antenna mounted on the arch rail through connecting cables. The plots for the intermidiate waveforms can be found in [27]. The equipment is prone to time-axis drifting, which causes degrading of the measurements. Therefore, pre-measurement warm-up of equipment is required several hours prior to the measurements.

Both the transmitting and receiving horn antennas used for these experiments have a 2 - 18GHz bandwidth, and the polarization of transmitted wave may be changed by rotating the antennas. Dielectric lenses are used to collimate the transmitted spherical wavefront to create an incident plane wave, and also to ensure that a major amount of the transmitted energy is projected on the target. There is a considerable amount of coupling between the two antennas observed in the measured waveform, but most of the coupling can be removed by the calibration process which will be explained later.

Several different target objects have been used for the experiments. Polystyrene  $(\mu = \mu_0, \epsilon_r = 2.55, \text{ and } \sigma = 0 \text{ at 10GHz})$  and plexiglass  $(\mu = \mu_0, \epsilon_r = 2.59, \text{ and } \sigma = 0 \text{ at 10GHz})$  are used for 3 lossless layer (free space, the material and free space)

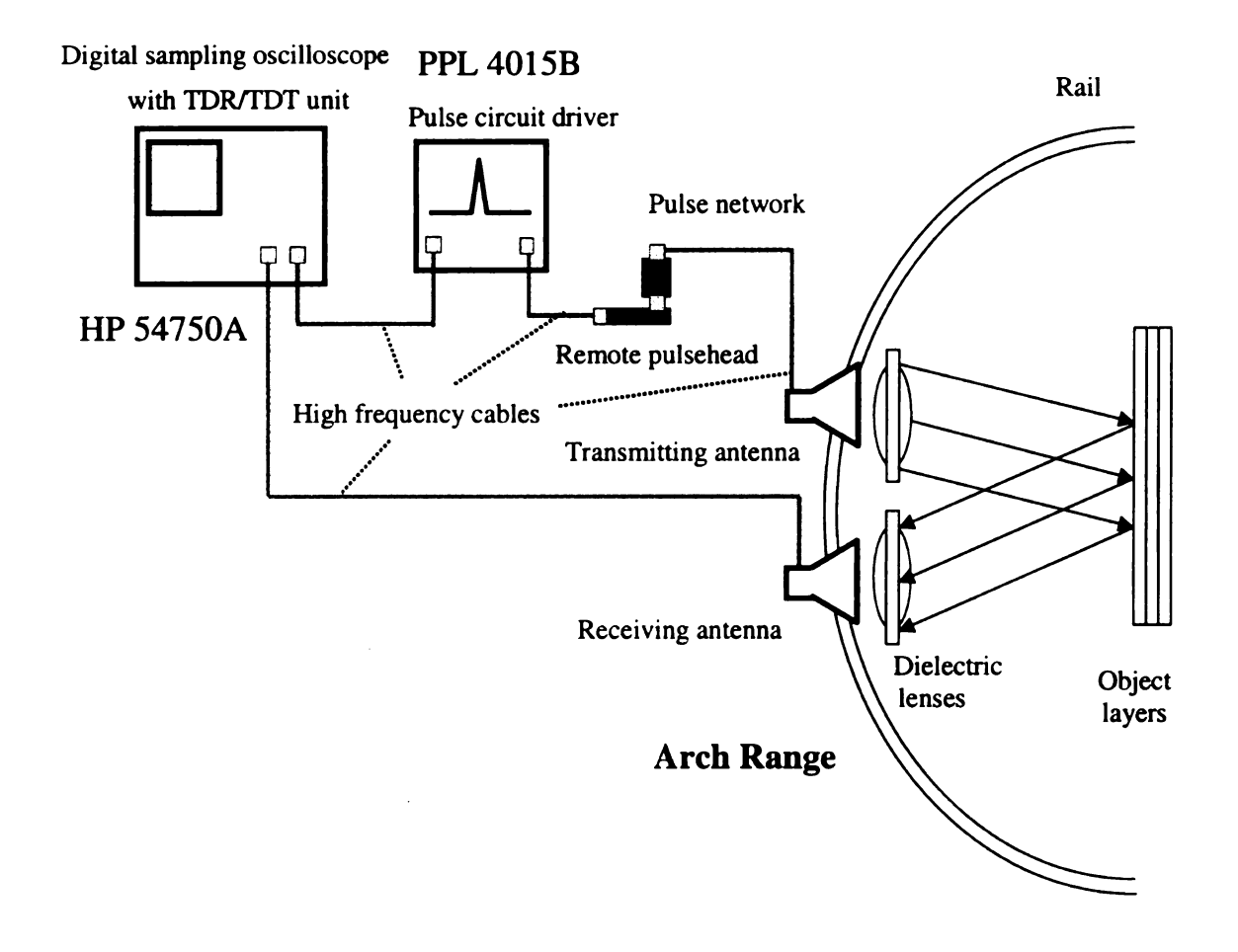


Figure 5.1. Experimental set up.

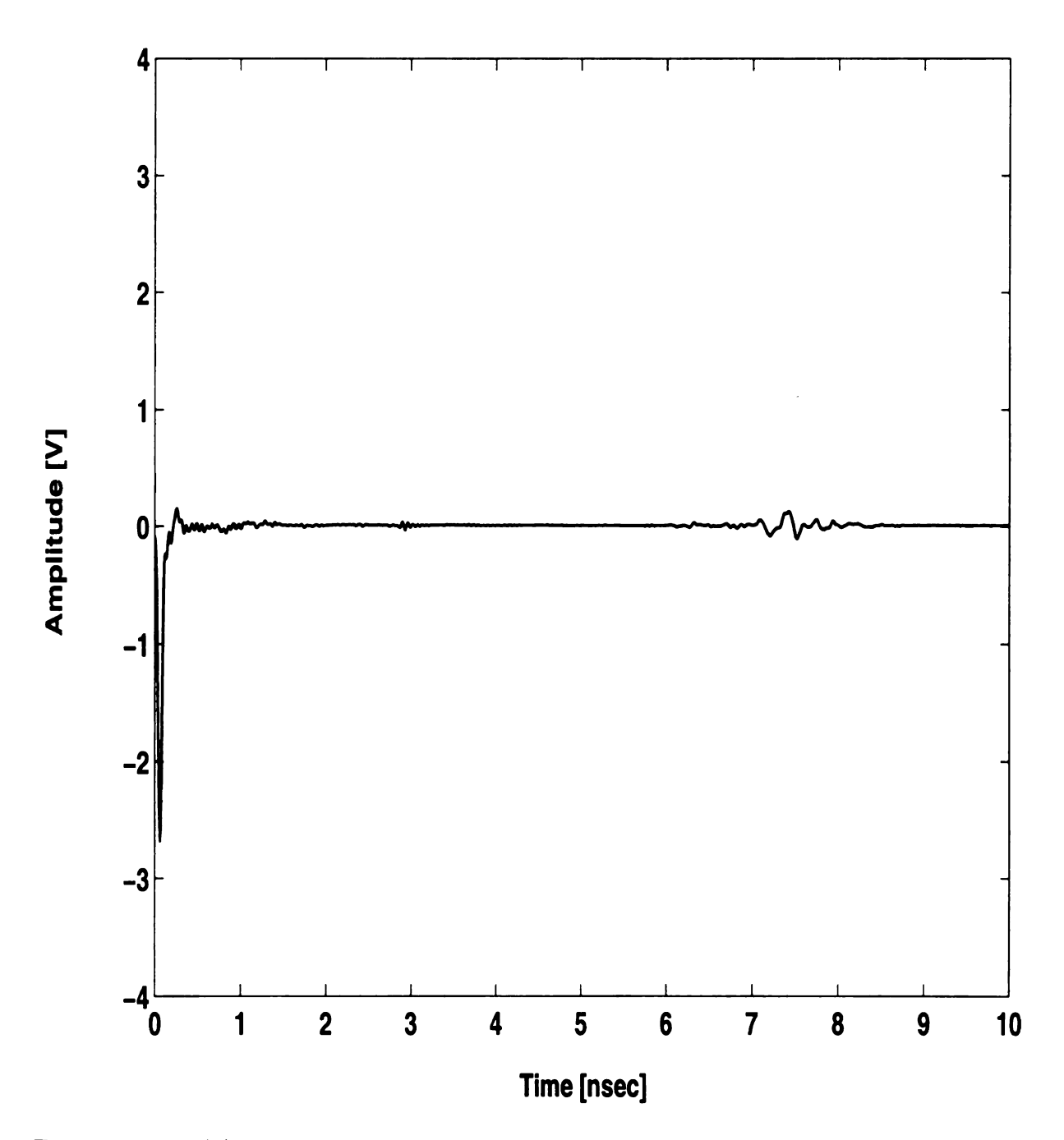
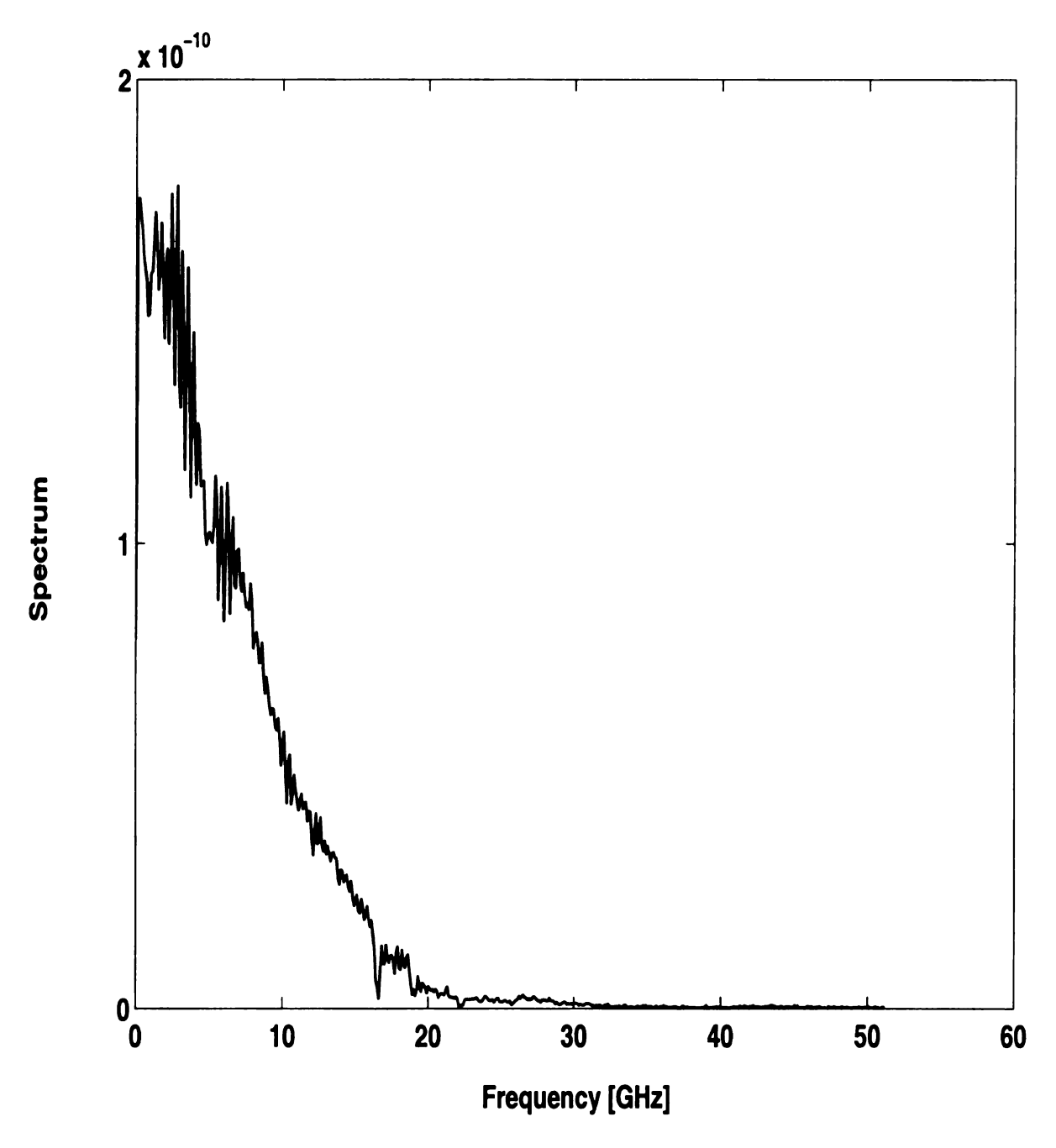


Figure 5.2. (a) Impulse shaped waveform transmitted from pulse forming network.



 ${\bf Figure~5.2.}$  (b) Spectrum of impulse shaped waveform transmitted from pulse forming network.

measurements, while a water container made of plexiglass plates is used for 5 lossless or lossy (by filling it with distilled water) measurements. All the plates are 2 feet by 2 feet square in size, and have an approximate thickness of 4.7mm for polystyrene and 5.3mm for plexiglass. Also, an aluminum plate is used as a perfect conductor (PEC) for calibration measurements.

### 5.3 Calibration

Each intermediate component (e.g. cables, antennas) of the experimental set up shown in Figure 5.1 has its own system function due to dispersion, propagation time delay, amplitude attenuation, etc., and each of these changes the original shape of transmitted waveform. Therefore, a calibration procedure is required to isolate and eliminate the effects of the intermediate system functions from the measured waveform.

Let's denote the original transmitted input waveform by x(t), the impulse response of target object by r(t), the intermediate system impulse response including component effects and time delays in both transmitting and receiving paths by  $h_{sys}(t)$ , and the received waveform at the scope by s(t), and denote their Fourier transforms as  $X(\omega)$ ,  $R(\omega)$ ,  $H_{sys}(\omega)$ ,  $S(\omega)$  respectively. Then, in a measurement, it is expected that

$$S(\omega) = X(\omega)H_{sys}(\omega)R(\omega), \tag{5.1}$$

and equivalently in the time domain

$$s(t) = x(t) * h_{sys}(t) * r(t).$$
 (5.2)

To isolate the unwanted system response  $H_{sys}(\omega)$ , a measurement is performed using an object with a known response. One of the appropriate choices for the object would be a PEC plate, for which the theoretical frequency domain reflection coefficient is

-1. Let's denote the scattering measurement from a PEC plate as  $C(\omega)$ . Then

$$C(\omega) = -X(\omega)H_{sys}(\omega). \tag{5.3}$$

Therefore the intermediate system function is simply given by  $H_{sys}(\omega) = -C(\omega)/X(\omega)$  and the calibrated scattering from a target object is

$$S_{cal}(\omega) = S(\omega)/H_{sys}(\omega)$$
  
=  $X(\omega)R(\omega)$  (5.4)

and 
$$s_{cal}(t) = F^{-1}\{S_{cal}(\omega)\}.$$

There is another factor to be considered in actual calibration procedure. Because of the bandwidth limit of the transmitting and receiving antennas, the measurement data outside of the bandwidth range are unreliable and should be discarded by truncating the frequency domain data in outside of the 2-18GHz band and restoring the reduced data size by interpolation. All the data manipulation for the calibration process is executed by using the software WAVECACULATOR, written by Dr. J. E. Ross.

#### 5.4 Measurements

# 5.4.1 Three lossless layer measurements

Using the previously described experimental set up and calibration procedure, actual measurements for several different object layers are performed. For each measurement, scattering from an object is measured first, and then the noise signal from the background environment is measured and subtracted from the target signal. A test measurement of the background noise is plotted in Figure 5.3. Due to absorbers used at several critical spots in these experiments, there are no large undesired reflections

and the remaining background noise level is usually much smaller than that of the target signal. Also, appropriate time windowing helps remove unwanted strong reflections from in background objects or mutipath signals. Next, the reflection from PEC plate is measured for calibration purposes and the background noise signal is measured and subtracted again. Ideally, once the system response has been obtained, the calibration measurement does not have to be repeated. But, in practice, it is necessary to repeat it for each measurement, so as to minimize the noise effect from time drifting of the equipment. For the same reason, the time consumed by each measurement must be minimized. Therefore, as a trade off between these considerations, 1024 points of data are taken within 10 nano second time range with 256 time averages for each data point.

A square polystyrene plate is selected as the first object layer to be measured, because its permittivity ( $\epsilon = 2.55\epsilon_0$ ) has been already verified by a frequency domain measurement at Michigan State University. Figure 5.4 (a) and Figure 5.4 (b) show the time domain object measurement data and its frequency spectrum obtained using a 1024 point fast Fourier transform (FFT), while Figure 5.5 (a) and Figure 5.5 (b) show those of PEC plate measurement data for calibration. These measurements were performed at a 6° aspect angle, which is the closest to normal that is allowed by the experiment system. Note that the amplitude of the reflected wave from the object is quite a bit smaller than that of the transmitted impulse shown in Figure 5.2, so it is plotted on a different scale. Also, it can be recognized that the reflection from the conductor plate is changed significantly from its original transmitted impulse waveform due to the effect of intermediate system function. The system function  $H_{sys}(\omega)$  is obtained by the method described in previous section 5.2, and shown in Figure 5.6 (a) and (b). The big peaks in the high frequency region ( > 20GHz) come from division errors due to lack of signal content in this band. This fact shows the necessity of truncation of the data spectrum. Finally, the calibrated target responses

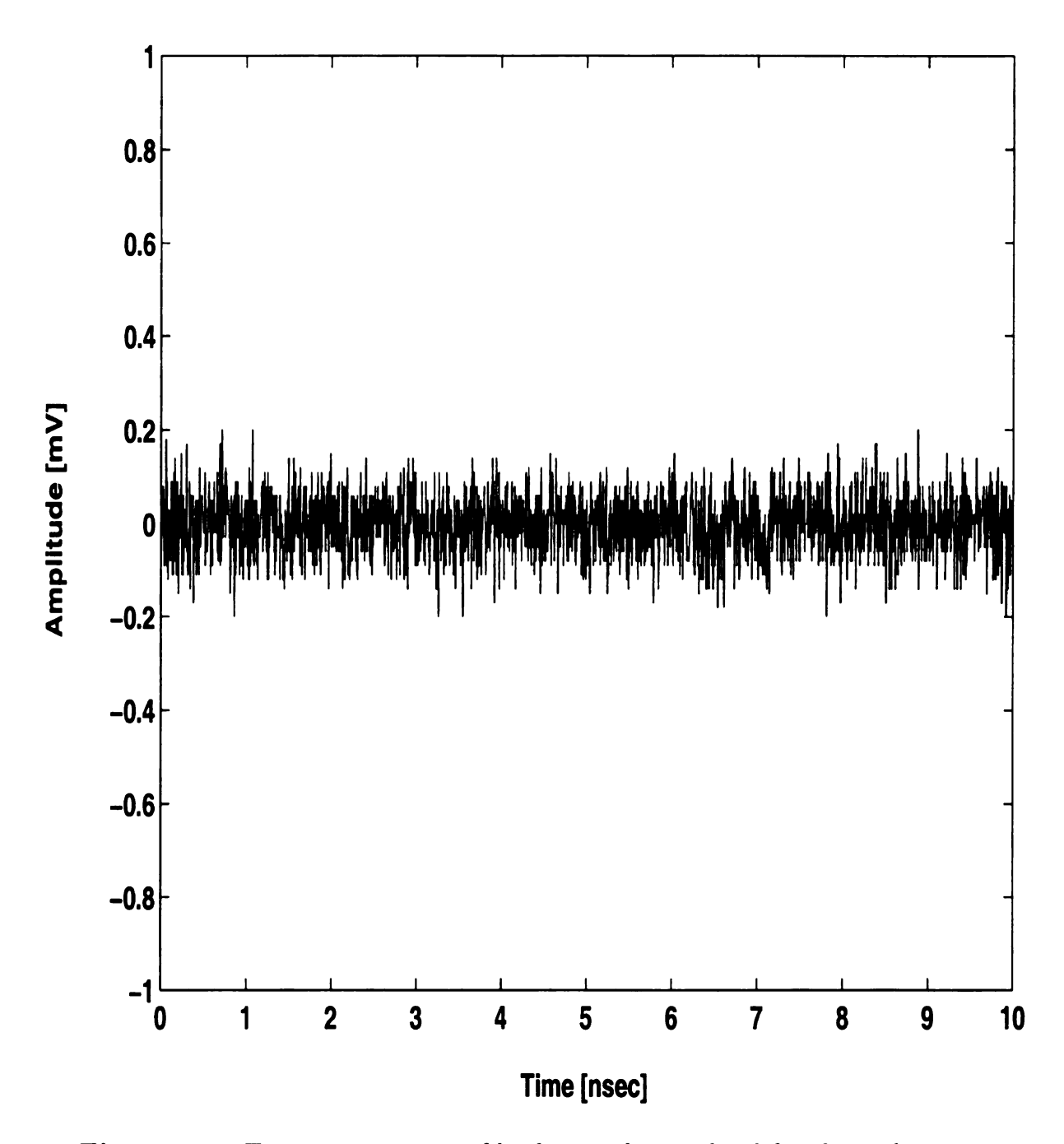


Figure 5.3. Test measurement of background noise level for the arch range.

using the system fucntion are shown in Figure 5.7 (a) and (b) for the results without and with the spectrum truncation, respectively. It is obvious that the out-band noise enlarged by division errors produces significant ringing in the calibrated waveform. The calibrated waveform after truncation processing matches well with that from theoretical computation. The slight mismatchs occuring at the third and fourth peaks are mainly due to tilt angle error of the mounted target. The electromagnetic wave propagation velocity inside of polystyrene is  $\frac{1}{\sqrt{2.55\mu_0\epsilon_0}} = 1.88 \times 10^8$  m/s. Thus, the distance between the third peaks of the measured and theoretical results of about 10 pico seconds corresponds to a two way propagation distance of 1.88mm. Therefore, a slight tilt error or warping of the surface of less than 1mm can make that difference.

Similar measurements are performed using a plexiglass (thickness=5.3mm,  $\epsilon = 2.59\epsilon_0$ ) layer for both polarizations and three different incidence angles of 6°, 15° and 30°. The reults are compared with the corresponding theoretical computations and shown in Figure 5.8, Figure 5.9, and Figure 5.10, respectively. Again, all the results show good agreement with the theoretical curves.

# 5.4.2 Five lossless layer measurements

An empty plexiglass container was built to be used as a three lossless layered medium, consisting of three even thickness (5.3mm) layers (plexiglass, free space and plexiglass). Then, scattering from the five layered object (free space, plexiglass, free space, plexiglass and free space) can be measured. The calibrated results for both polarizations and three different incidence angles are shown in Figure 5.11, Figure 5.12 and Figure 5.13 respectively. All the measurements are well matched with the theoretical results, although they are slightly worse than those from the three layer measurements. This is probably because of the crude construction of the container, with layer thicknesses different from the designed values. But, still mutiple reflections at the layer interfaces can be clearly identified.

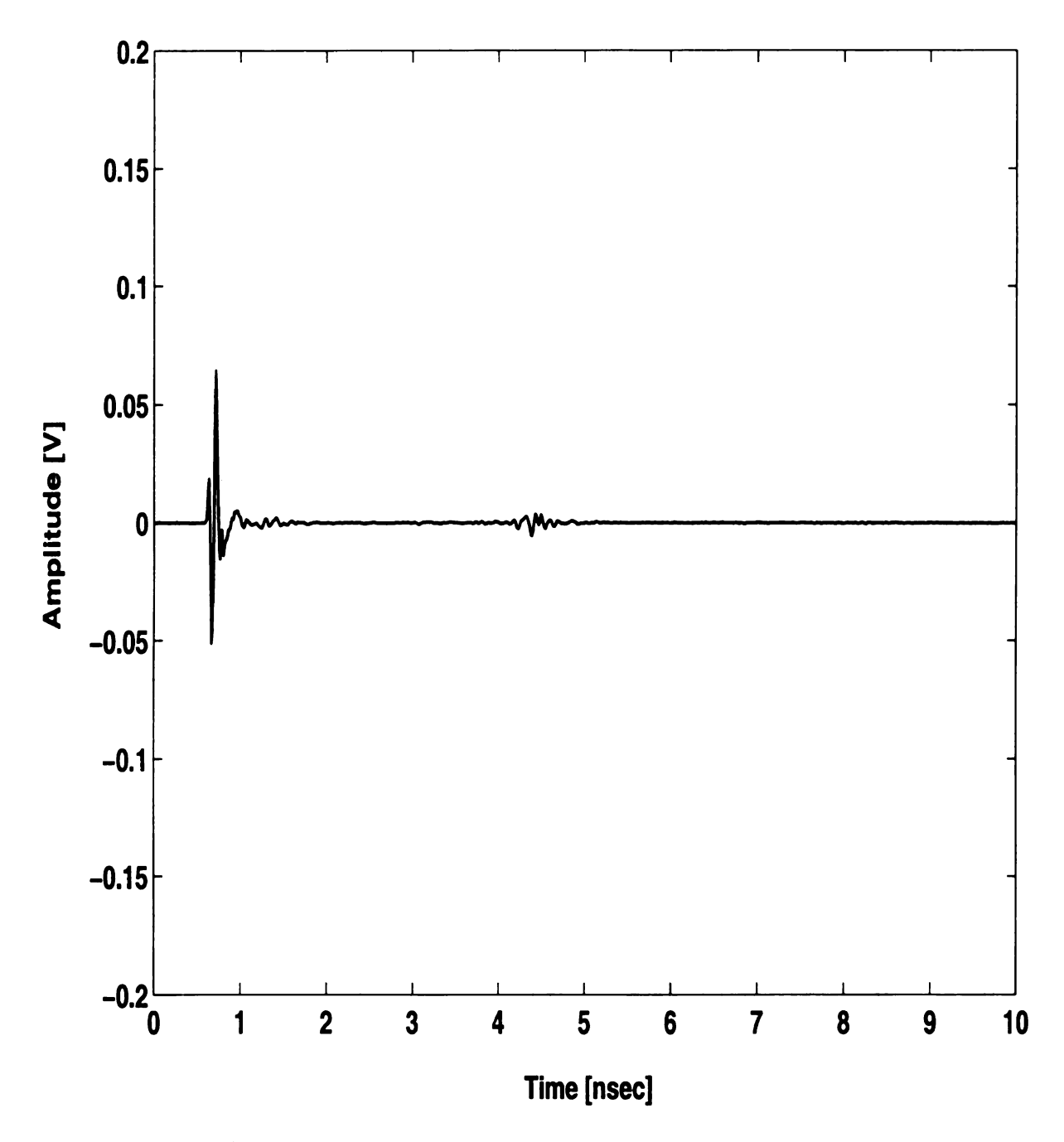


**Figure 5.4.** (a) Time domain raw measurement data of a polystyrene plate with  $\theta_{i1} = 6^{\circ}$  (TE polarization).

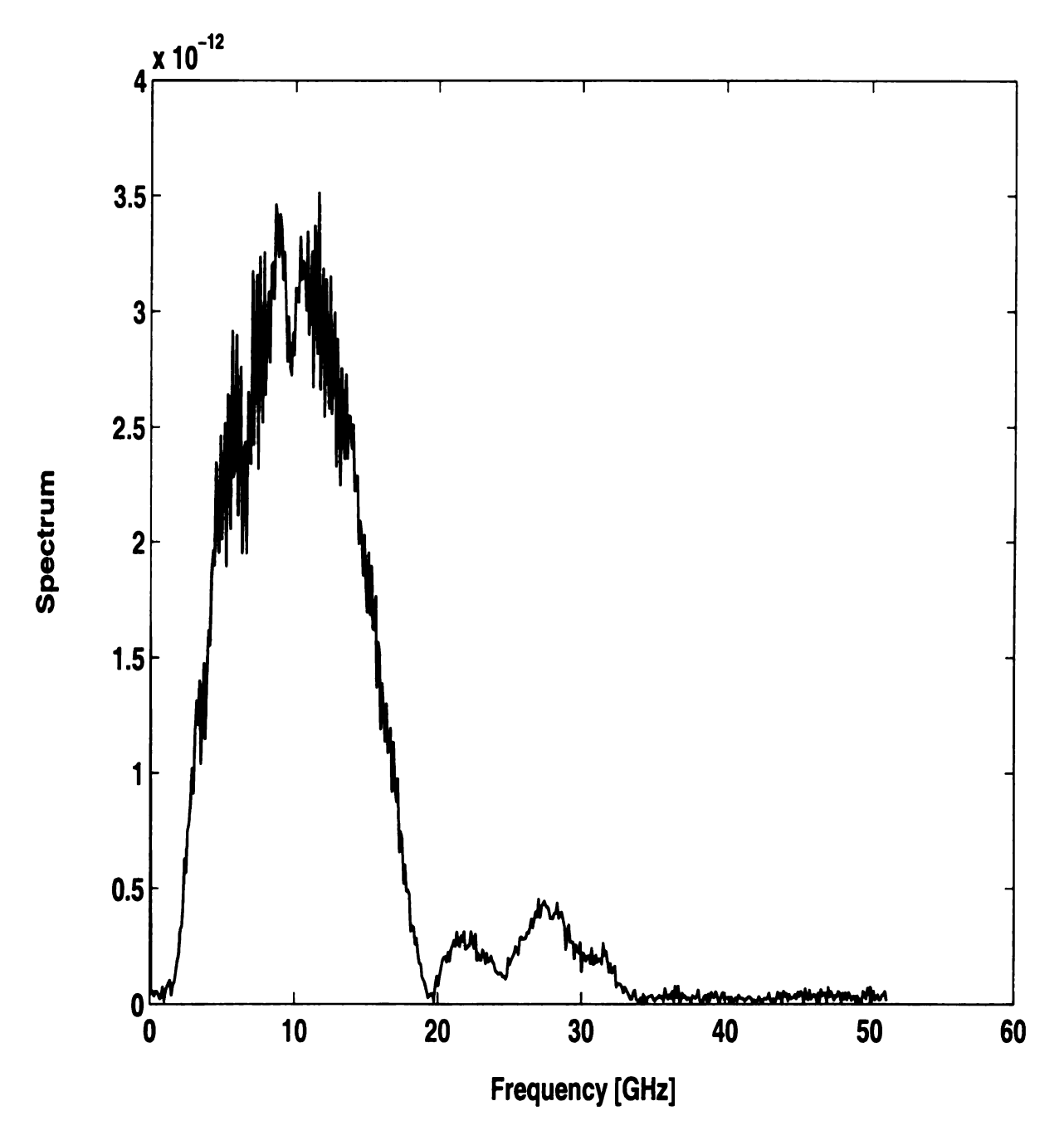


**Figure 5.4.** (b) Frequency domain spectrum of raw measurement data of a polystyrene plate with  $\theta_{i1}=6^{\circ}$  (TE polarization).

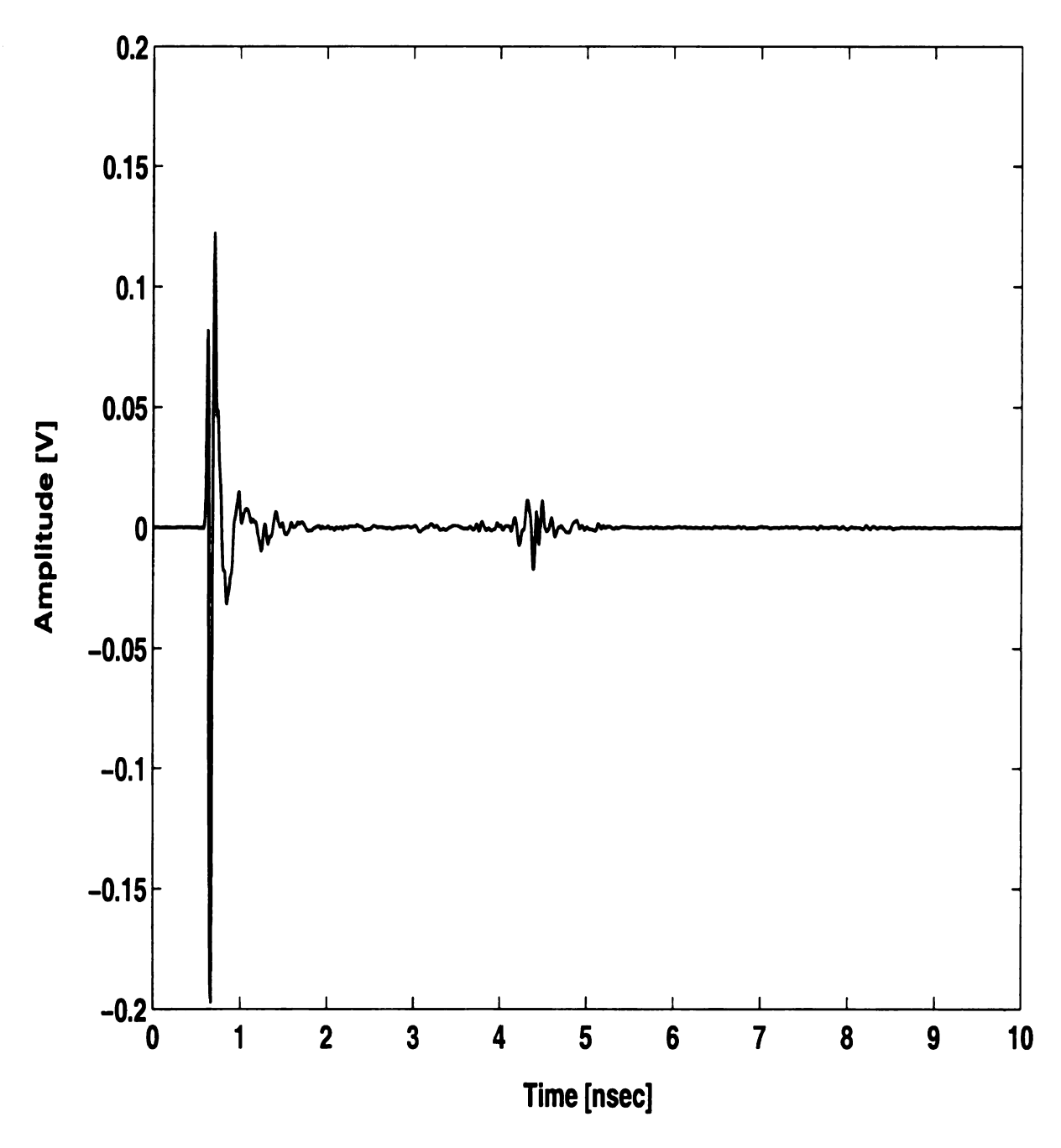


**Figure 5.5.** (a) Time domain raw measurement data of a PEC plate with  $\theta_{i1} = 6^{\circ}$  (TE polarization).

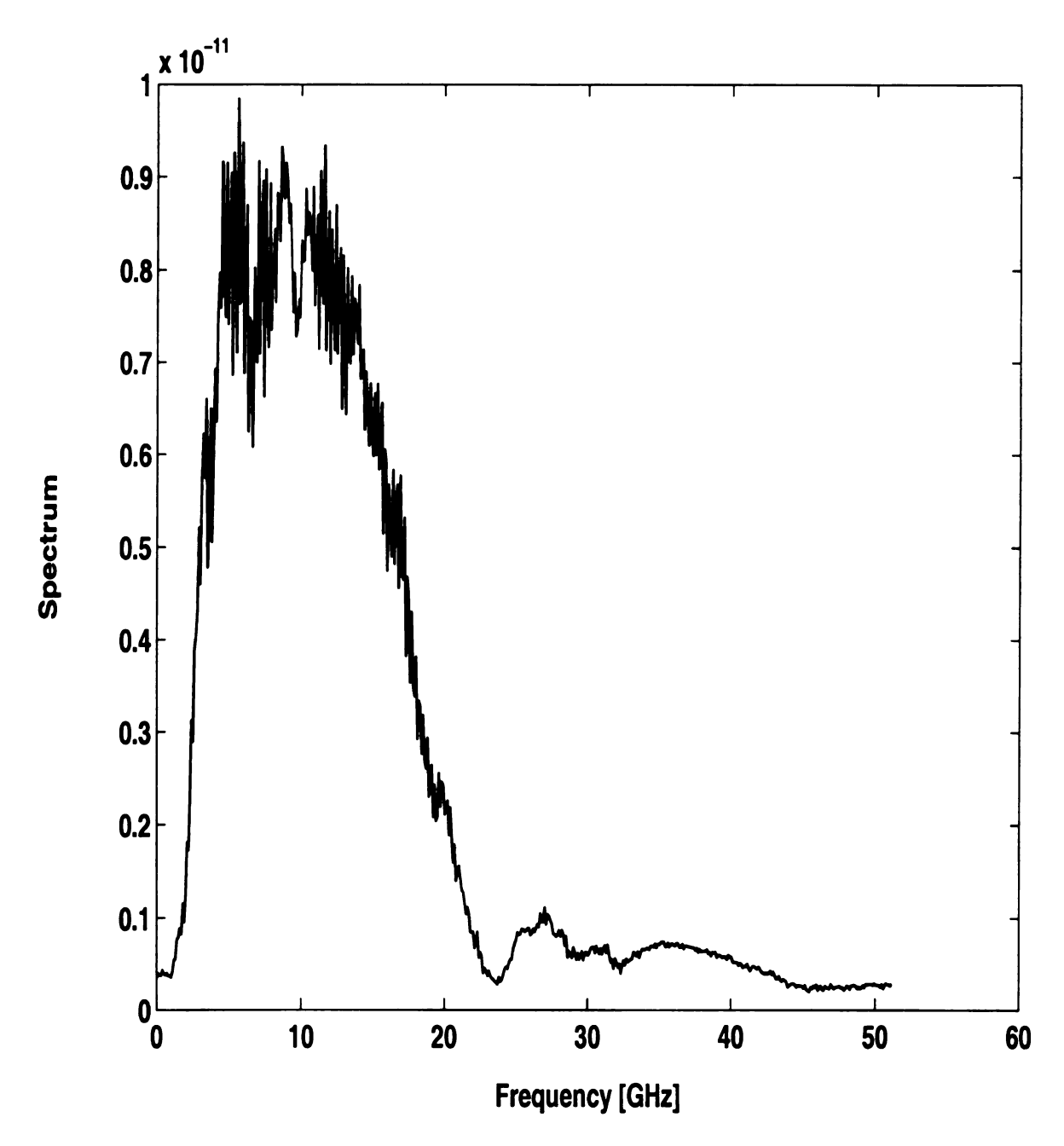


**Figure 5.5.** (b) Frequency domain spectrum of raw measurement data of a PEC plate with  $\theta_{i1} = 6^{\circ}$  (TE polarization).

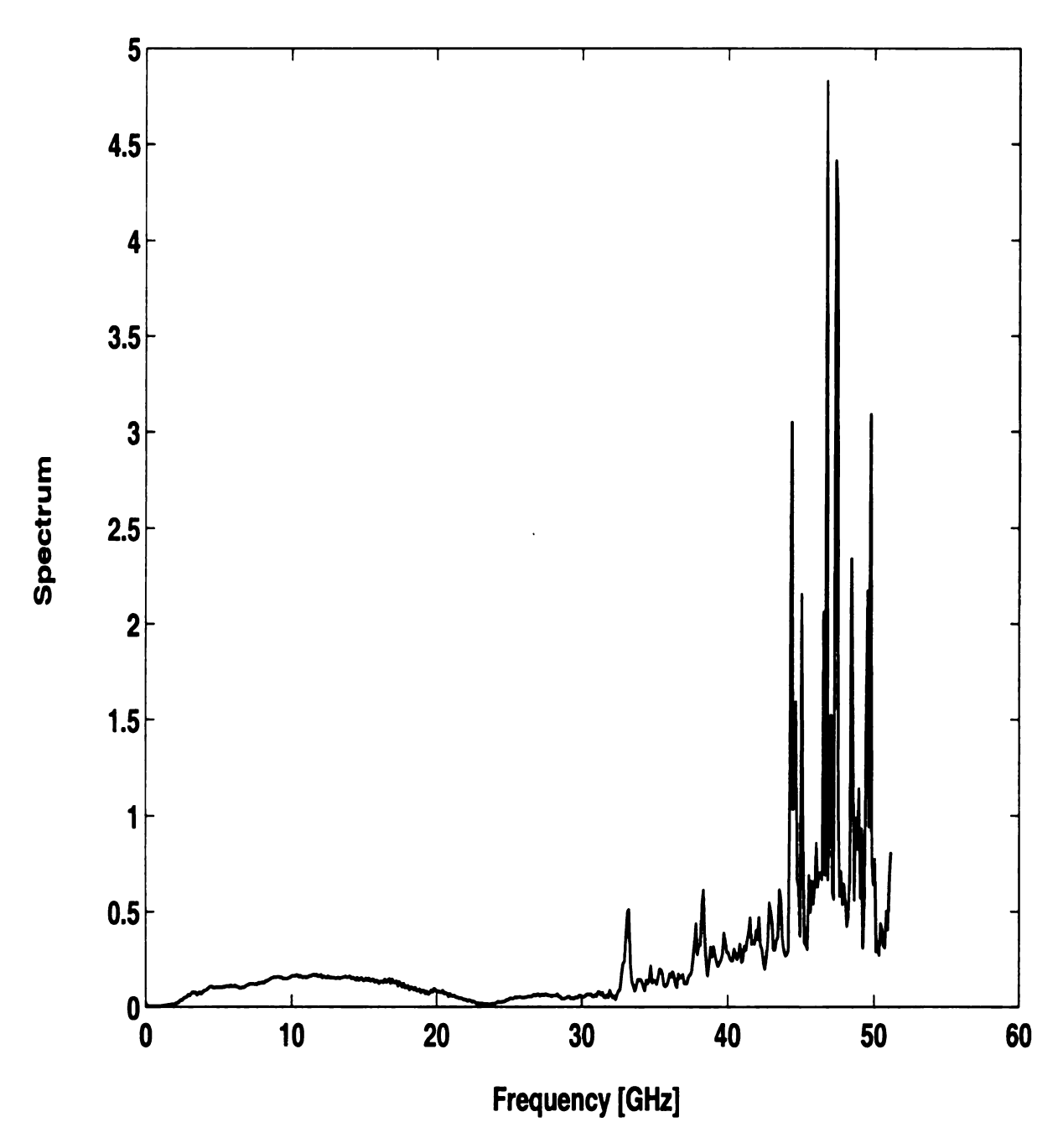


Figure 5.6. (a) Spectrum of intermediate system function.

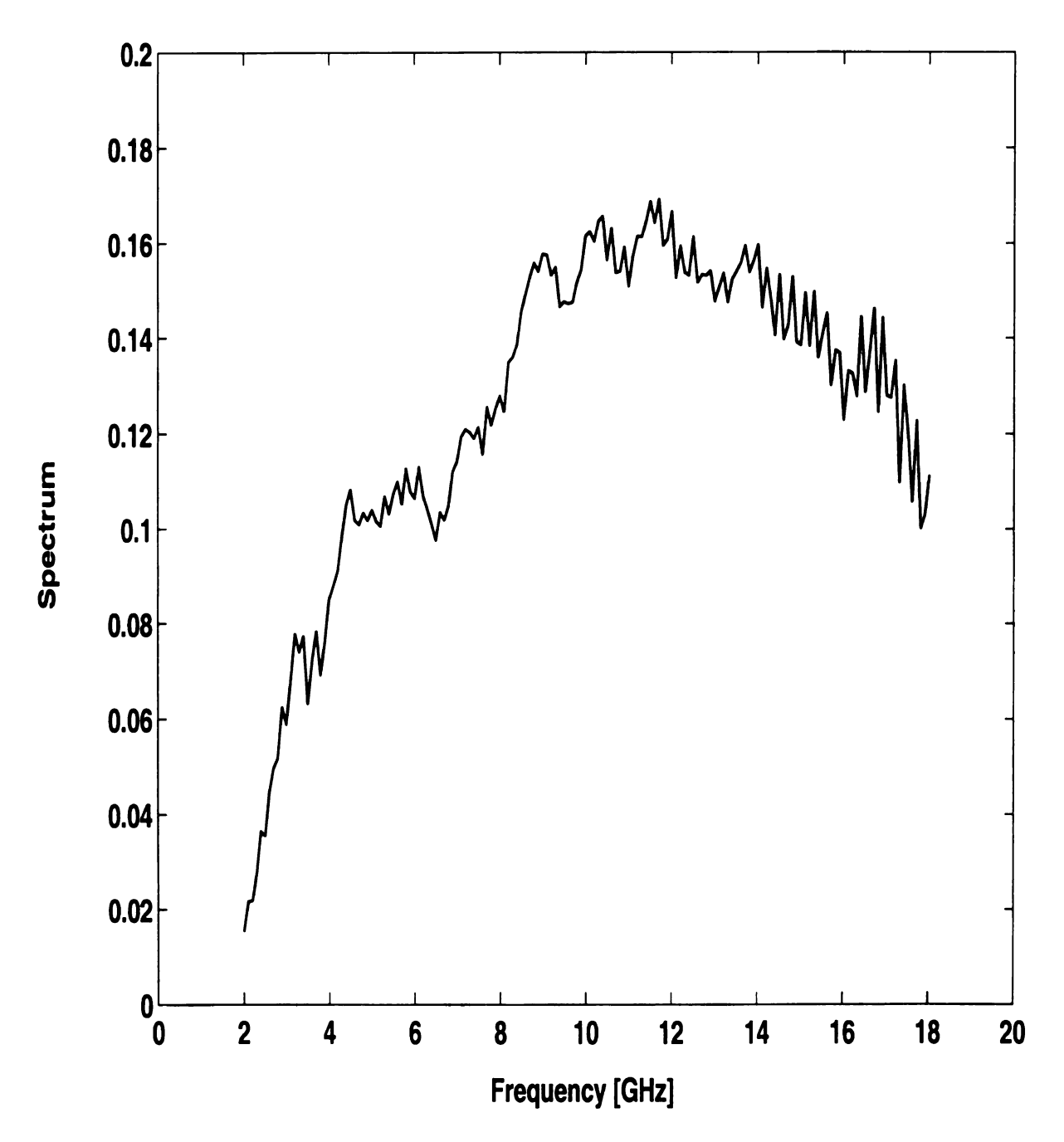


Figure 5.6. (b) Spectrum of intermediate system function after truncation.

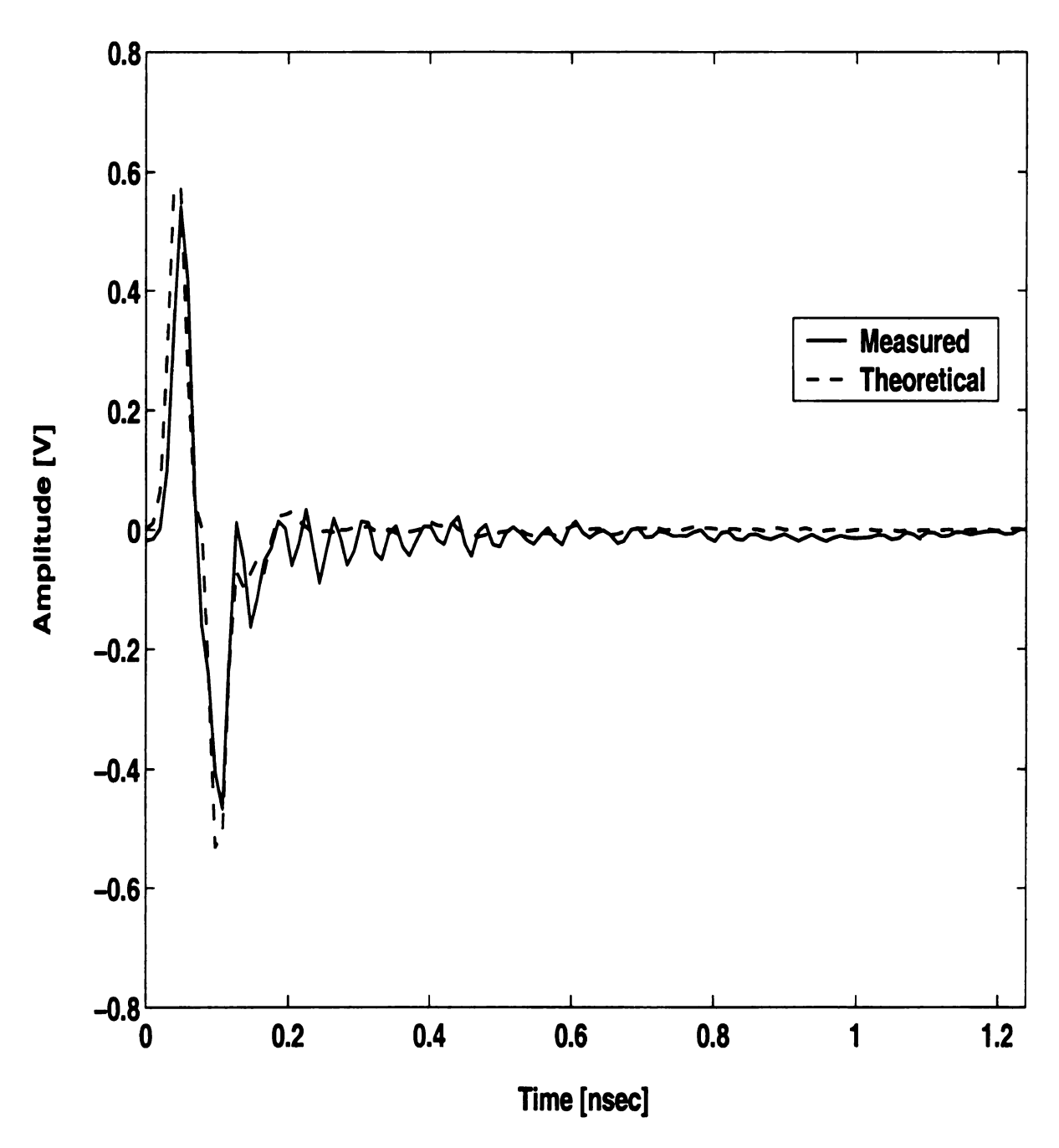
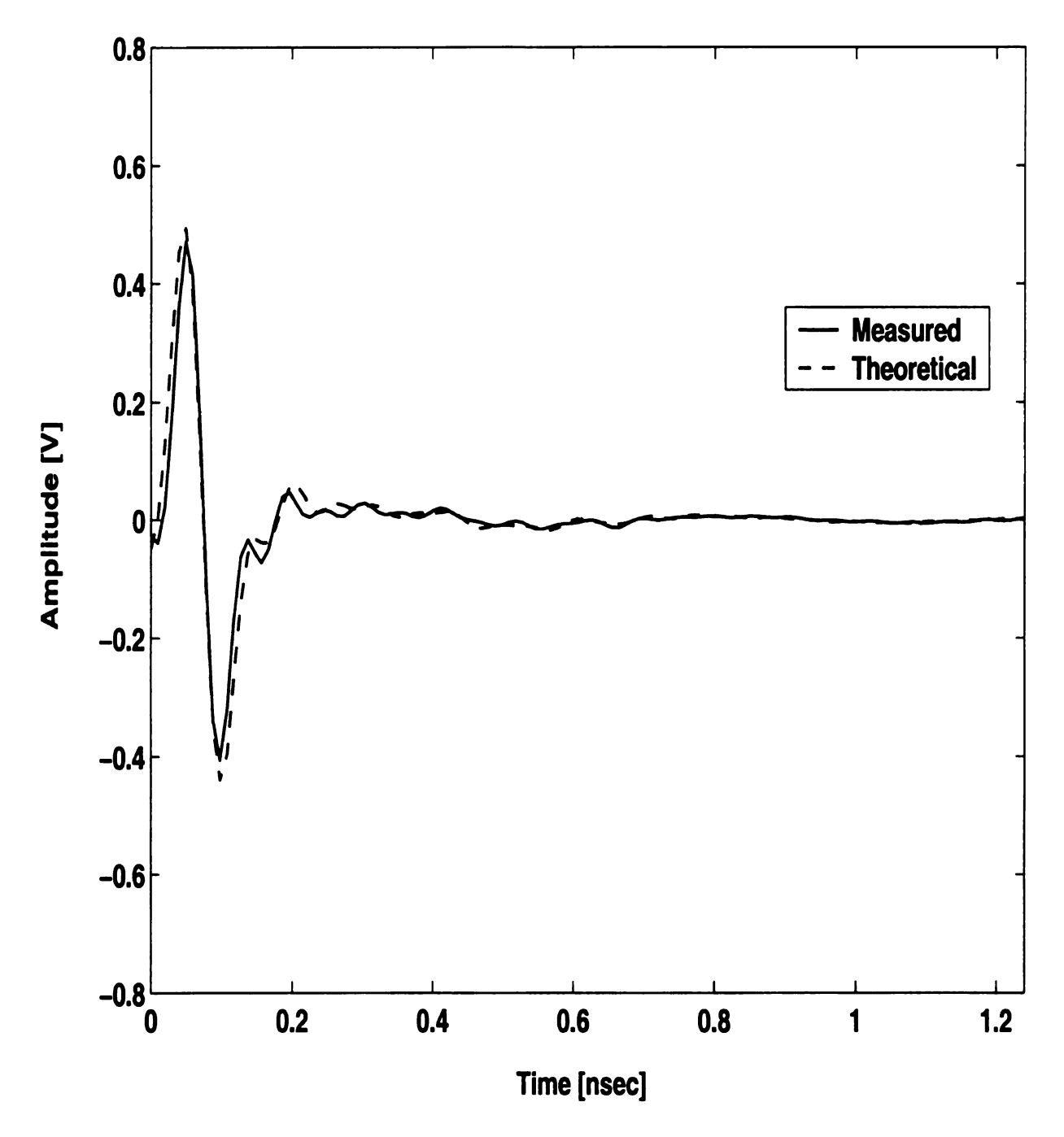


Figure 5.7. (a) Calibrated trasient scattering from a polystyrene layer without spectrum truncation (TE polarization).



**Figure 5.7.** (b) Calibrated trasient scattering from a polystyrene layer with spectrum truncation (TE polarization).

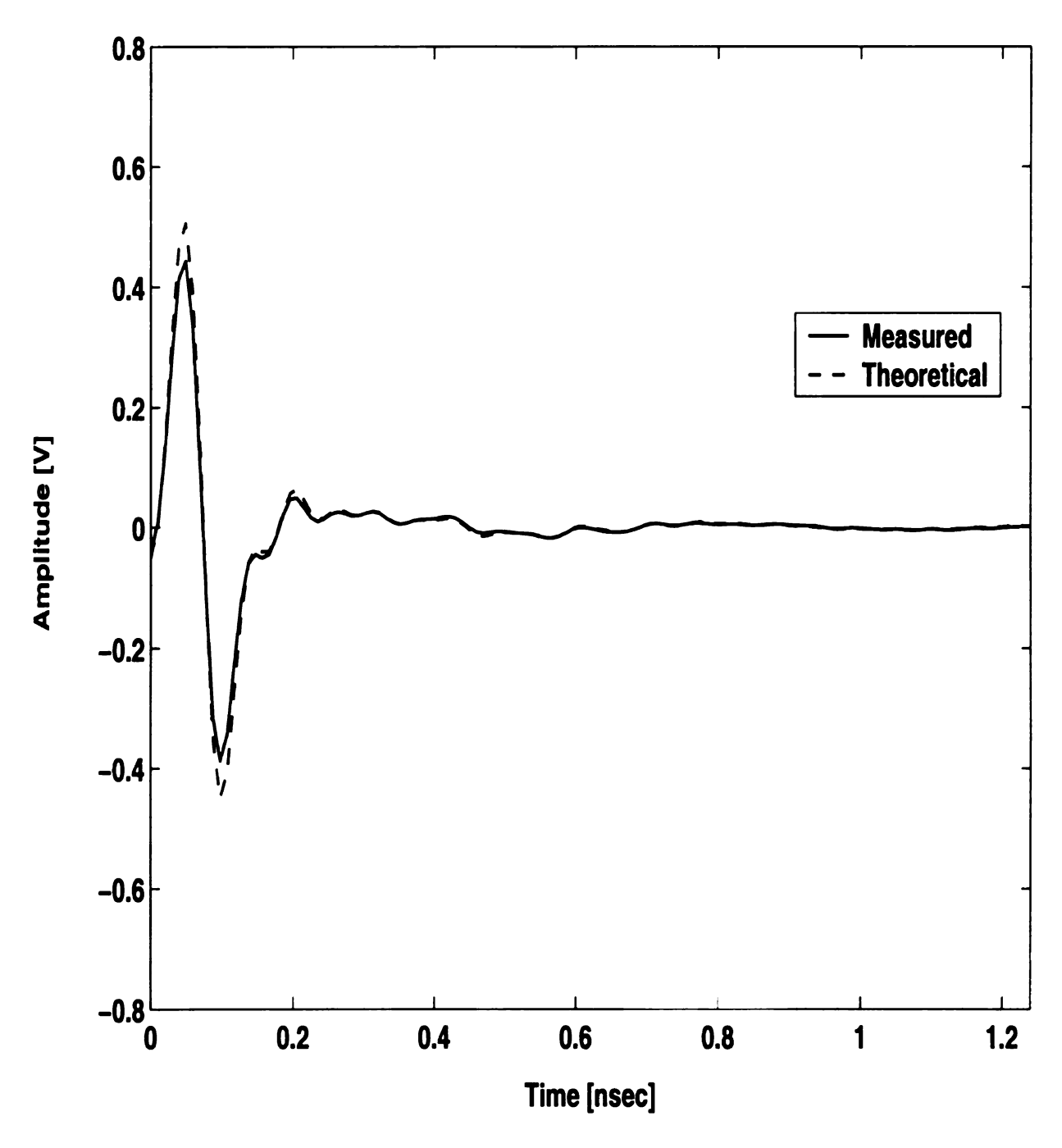
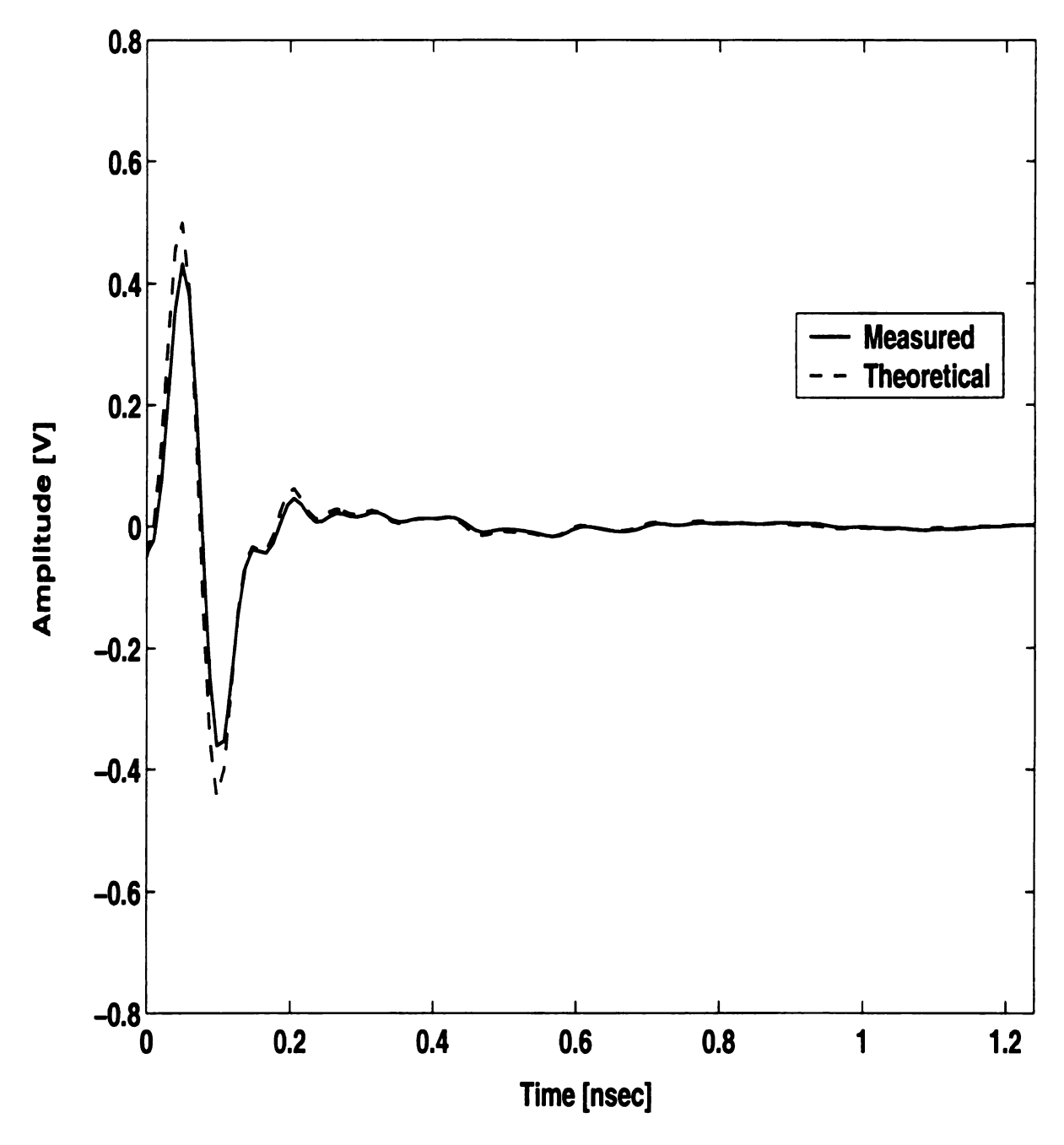
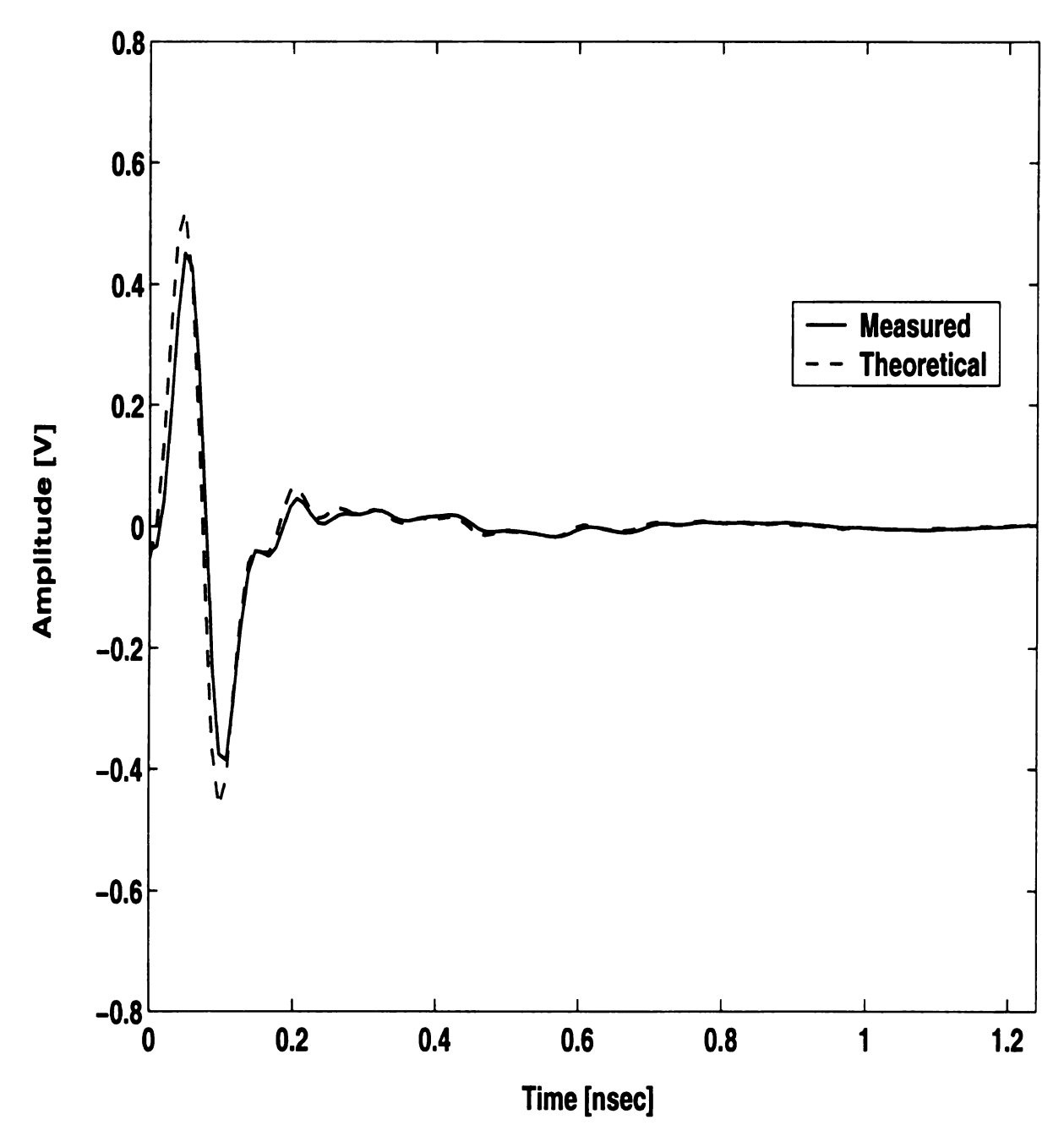


Figure 5.8. (a) Transient scattered field from a plexiglass layer with incidence angle 6° (TE polarization).



**Figure 5.8.** (b) Transient scattered field from a plexiglass layer with incidence angle 6° (TM polarization).



**Figure 5.9.** (a) Transient scattered field from a plexiglass layer with incidence angle 15° (TE polarization).

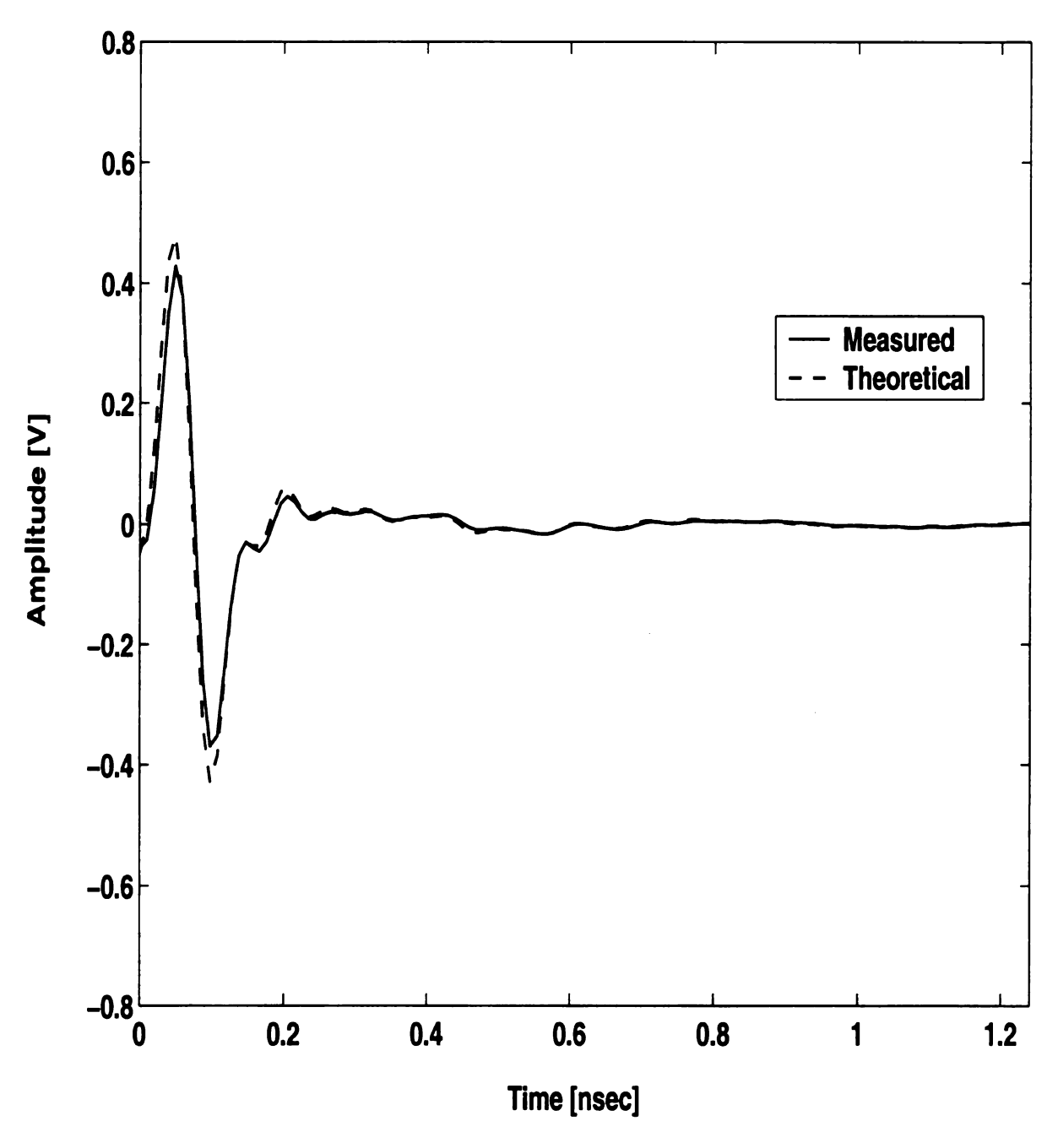


Figure 5.9. (b) Transient scattered field from a plexiglass layer with incidence angle 15° (TM polarization).

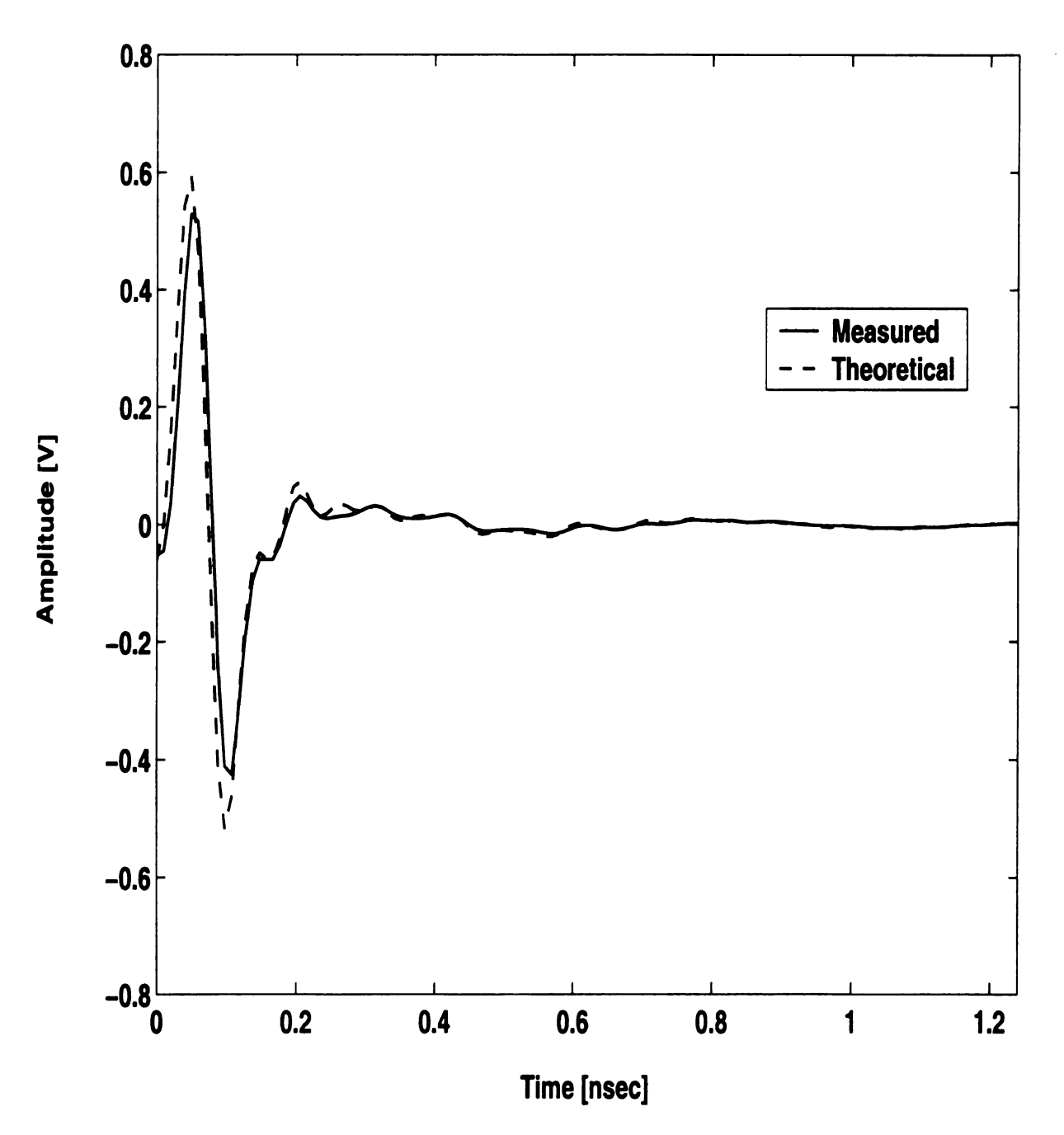


Figure 5.10. (a) Transient scattered field from a plexiglass layer with incidence angle 30° (TE polarization).

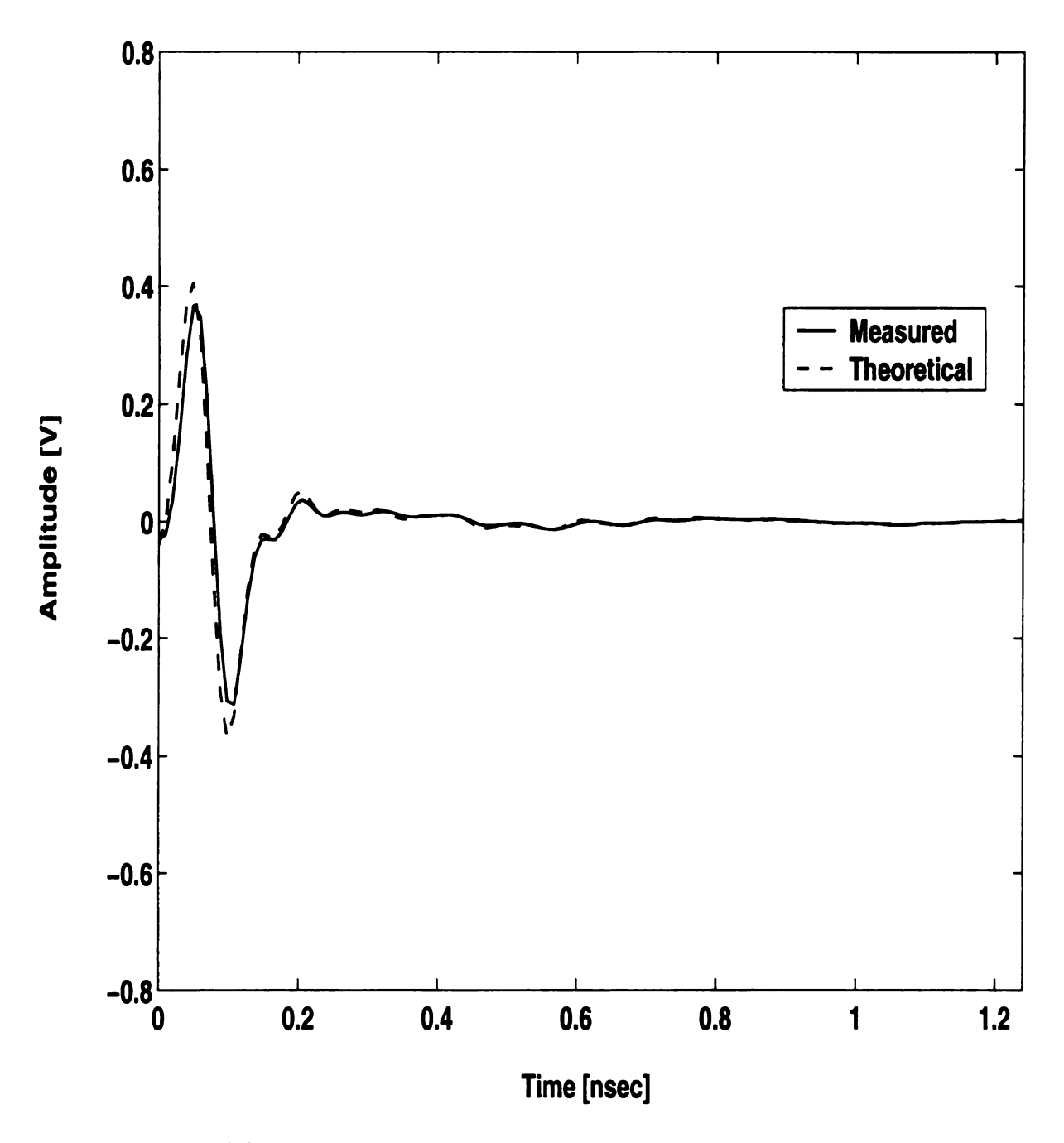


Figure 5.10. (b) Transient scattered field from a plexiglass layer with incidence angle 30° (TM polarization).

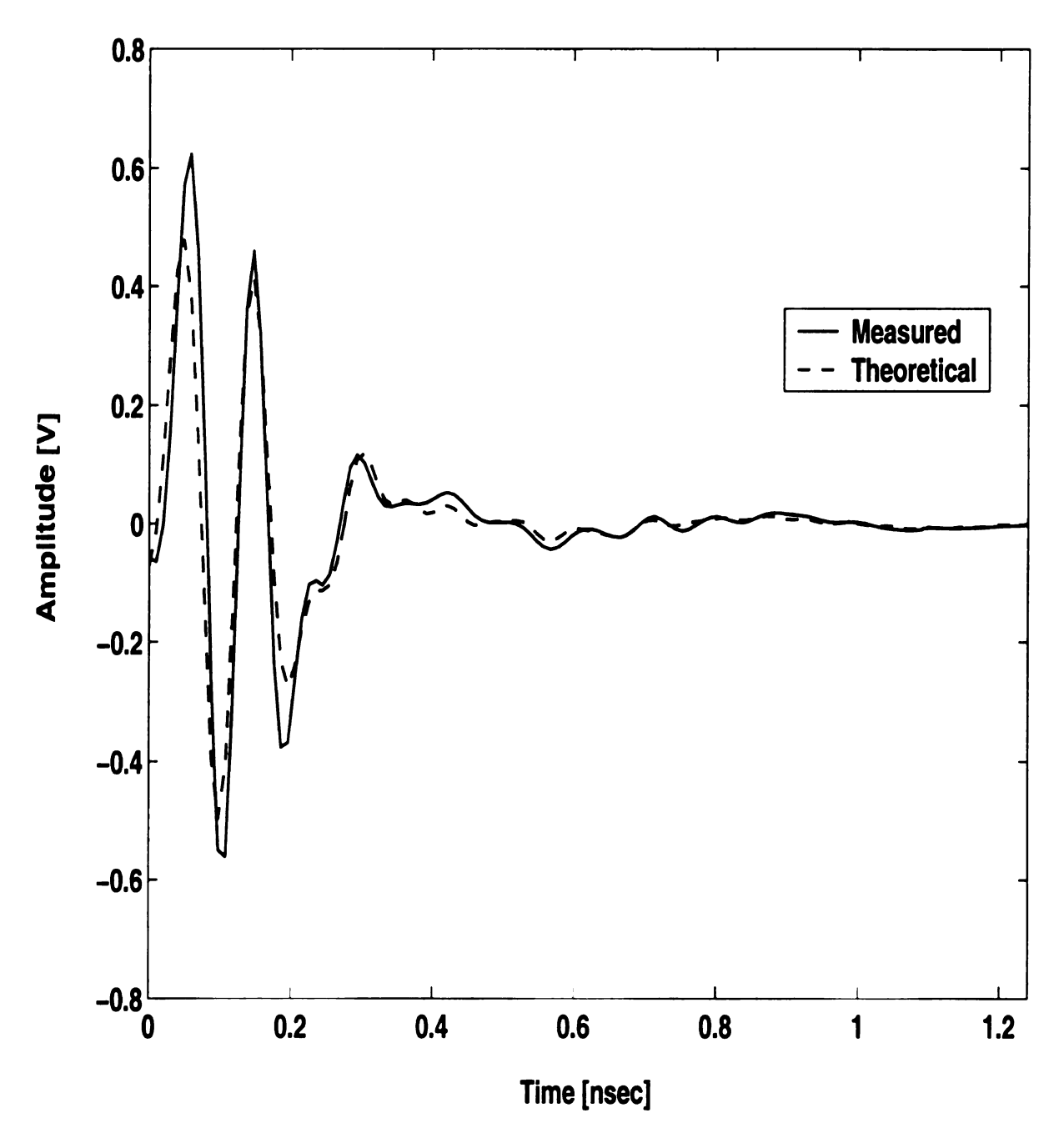


Figure 5.11. (a) Transient scattered field from a plexiglass container with incidence angle 6° (TE polarization).

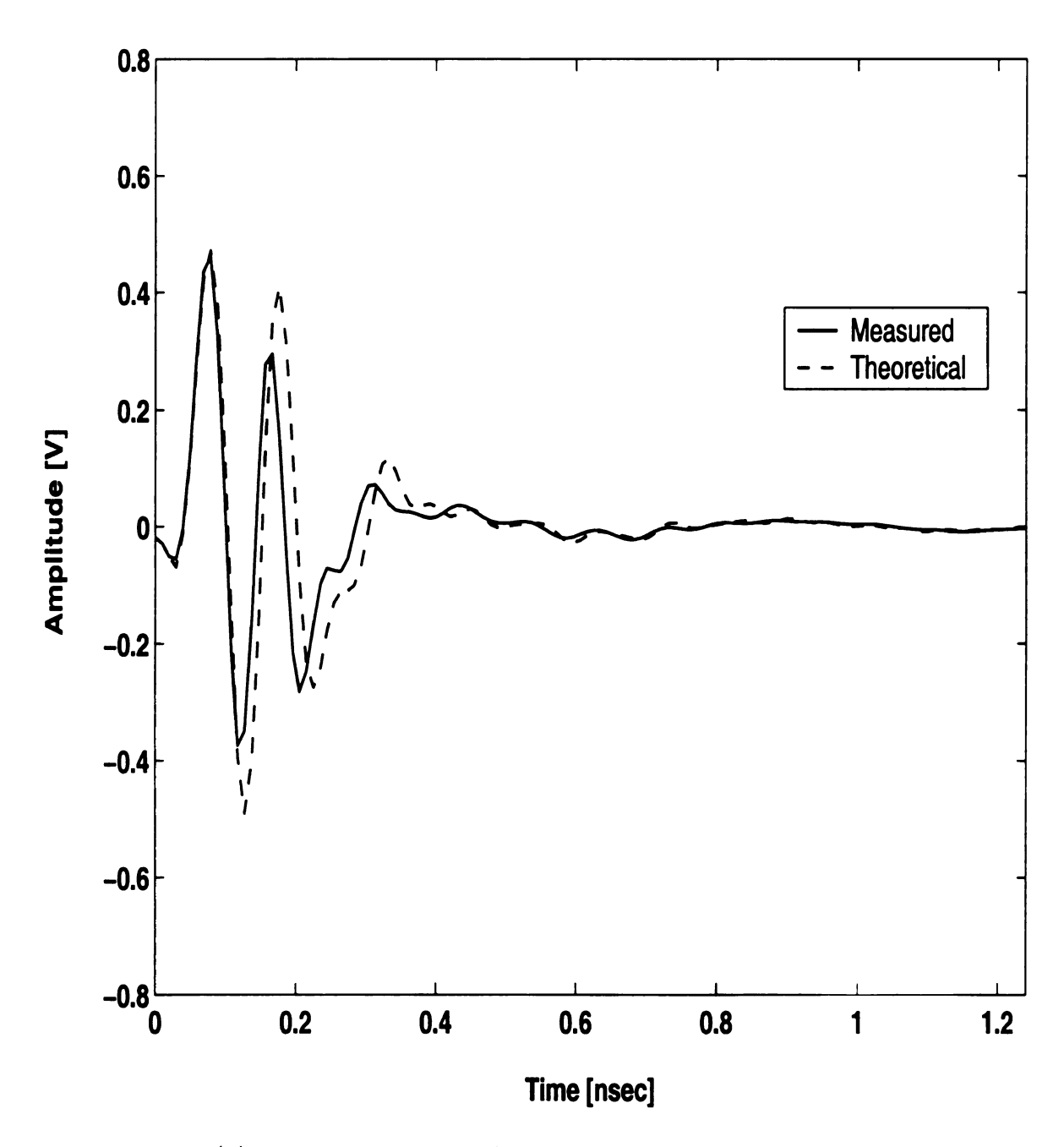


Figure 5.11. (b) Transient scattered field from a plexiglass container with incidence angle 6° (TM polarization).

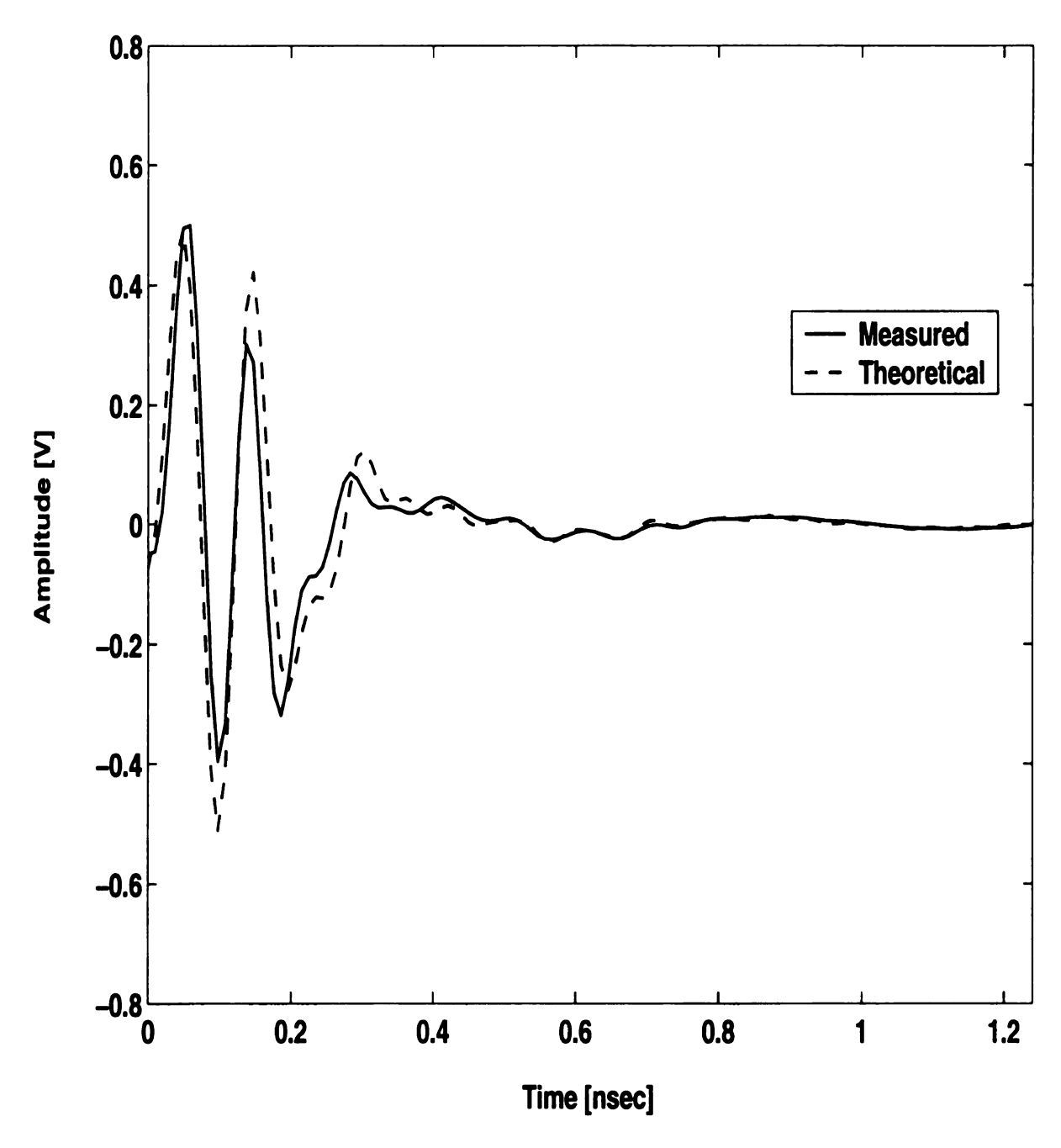


Figure 5.12. (a) Transient scattered field from a plexiglass container with incidence angle 15° (TE polarization).

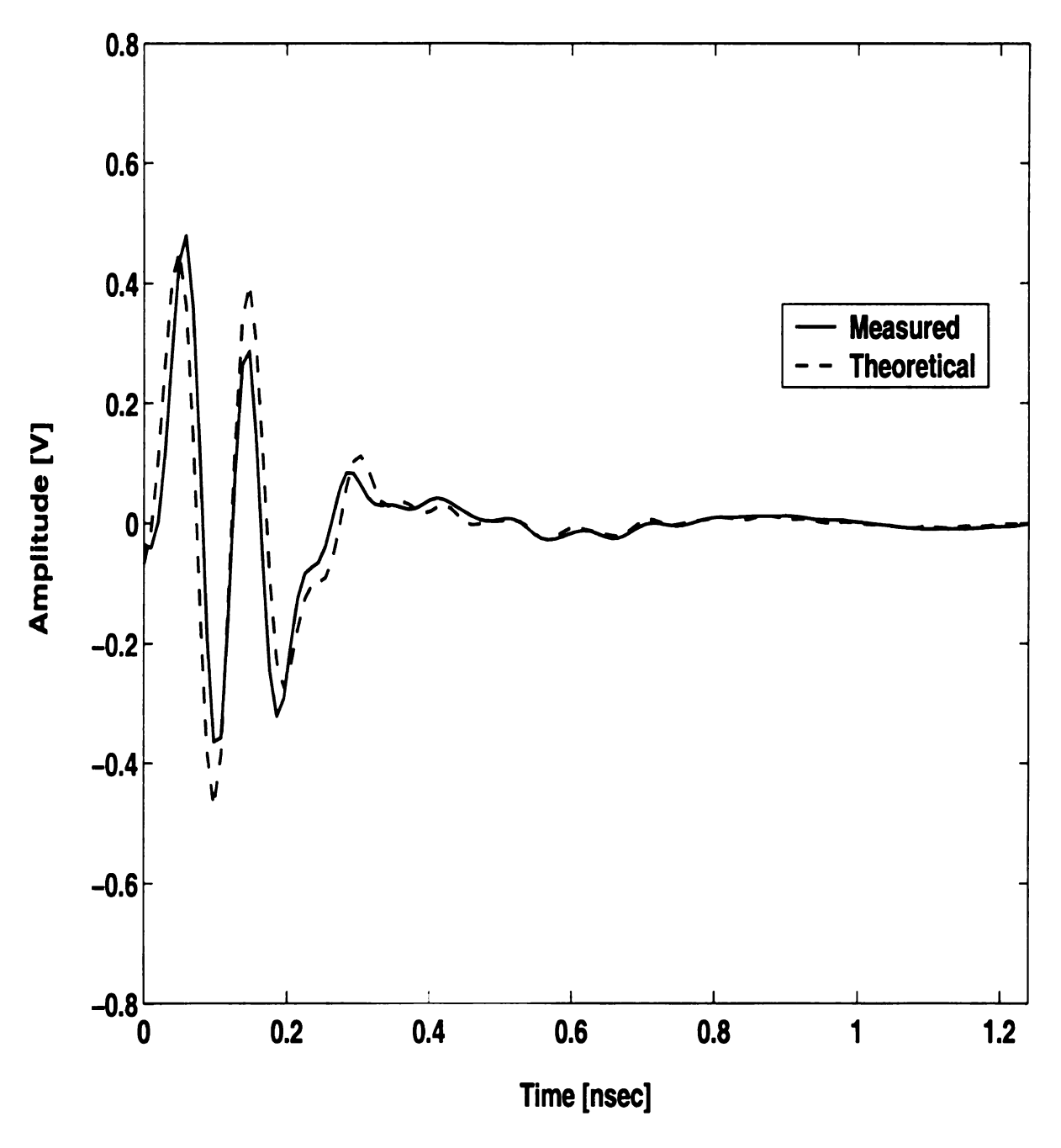


Figure 5.12. (b) Transient scattered field from a plexiglass container with incidence angle 15° (TM polarization).

Another measurement that may have practical interest is performed. Two plates of plexiglass are 'mechanically' adhered with some pressure, and the total thickness is 9.8mm. Then, the scattering from the object is measured and plotted in Figure 5.14 (a). What is expected is a reflection from a 'single' plate of thickness 9.8mm, and is a waveform consisting of two isolated peaks. But the actual measurement is shows quite a different waveform. Therefore, the theoretical reflection from a three layered object (the five layered medium case) is computed under the assumption that there is a small 'invisible' air gap of 0.05mm thickness between the two plexiglass plates, and compared with the measured data. As shown in Figure 5.14, the modified model gives a good match with the measured data. This is a good example of 'non destructive' TDR inspection which is being widely used in industry, and suggests the possibility that more accurate information (size and kind) of mechanical defects smaller than the transmitted pulse width can be obtained, since the exact theoretical response can be found for even lossy materials from the theory derived in this study.

# 5.4.3 Lossy layered medium measurements

The plexiglass container used in the previous measurement is filled with distilled water for the measurement of scattering from a lossy five layered object. Note that water is a strong polar material, and therefore has significant dielectric loss at high frequency. The theoretical response is computed by converting this dielectric loss to an equivalent conductivity  $\sigma_{eq}$ . Unfortunately, the dielectric loss is a function of frequency, while frequency independent parameters are assumed in this study. The frequency dependence of permittivity which is usually denoted using complex permittivity  $\epsilon = \epsilon' - j\epsilon''$  where  $\epsilon'' = \frac{\sigma_{eq}}{\omega}$ , can be modelled by various functions, including Debye equation [28] as shown in Figure 5.15 for distilled water at 20°C. Considering the available distilled water parameters at several frequency points found in [21], the bandwidth range of 2-18GHz, and the maximum dielectric loss frequency in the Debye model, the equivalent constant conductivity is chosen to be 16.7 $\sigma$ /m, the

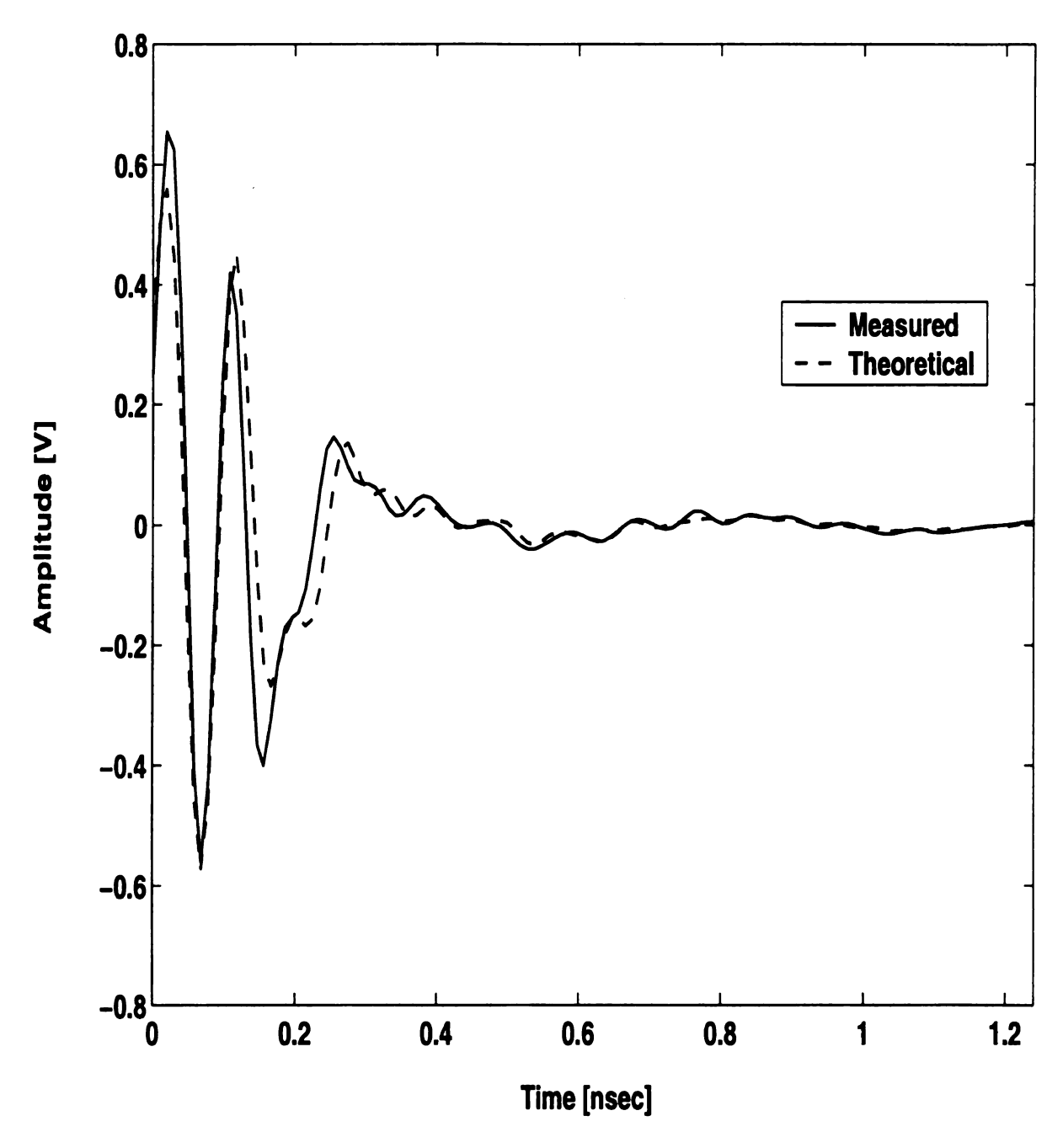


Figure 5.13. (a) Transient scattered field from a plexiglass container with incidence angle 30° (TE polarization).

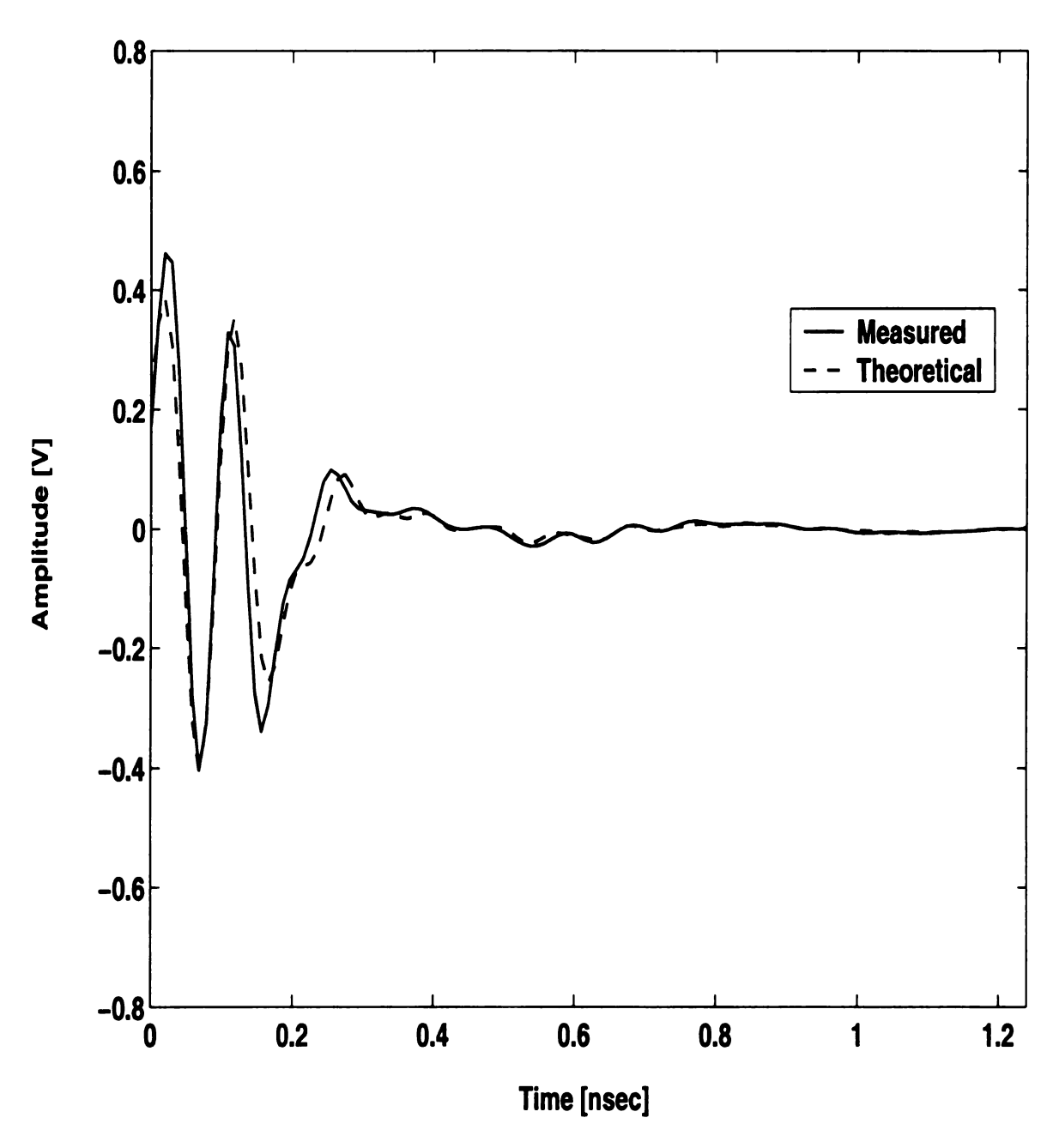


Figure 5.13. (b) Transient scattered field from a plexiglass container with incidence angle 30° (TM polarization).

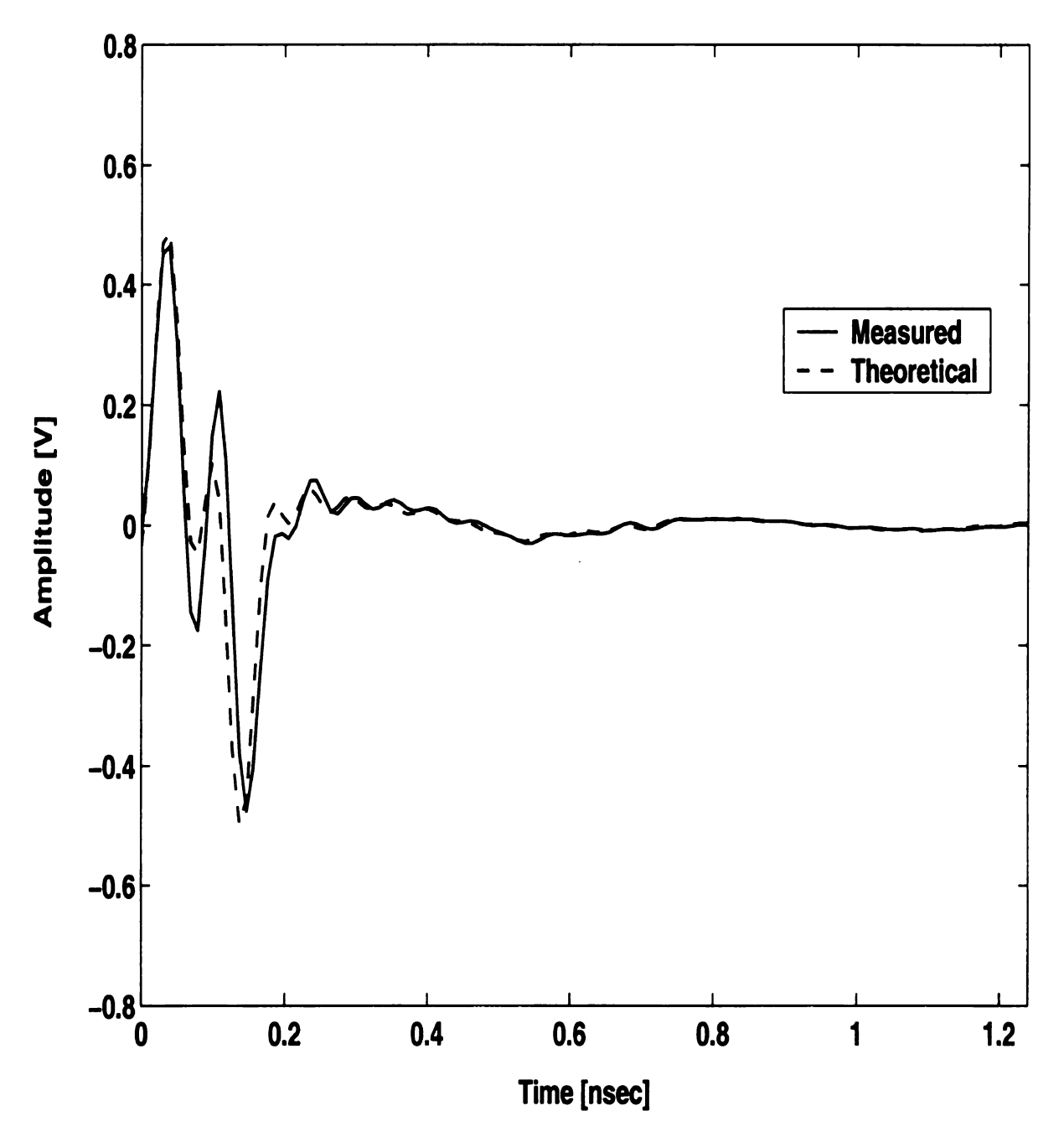
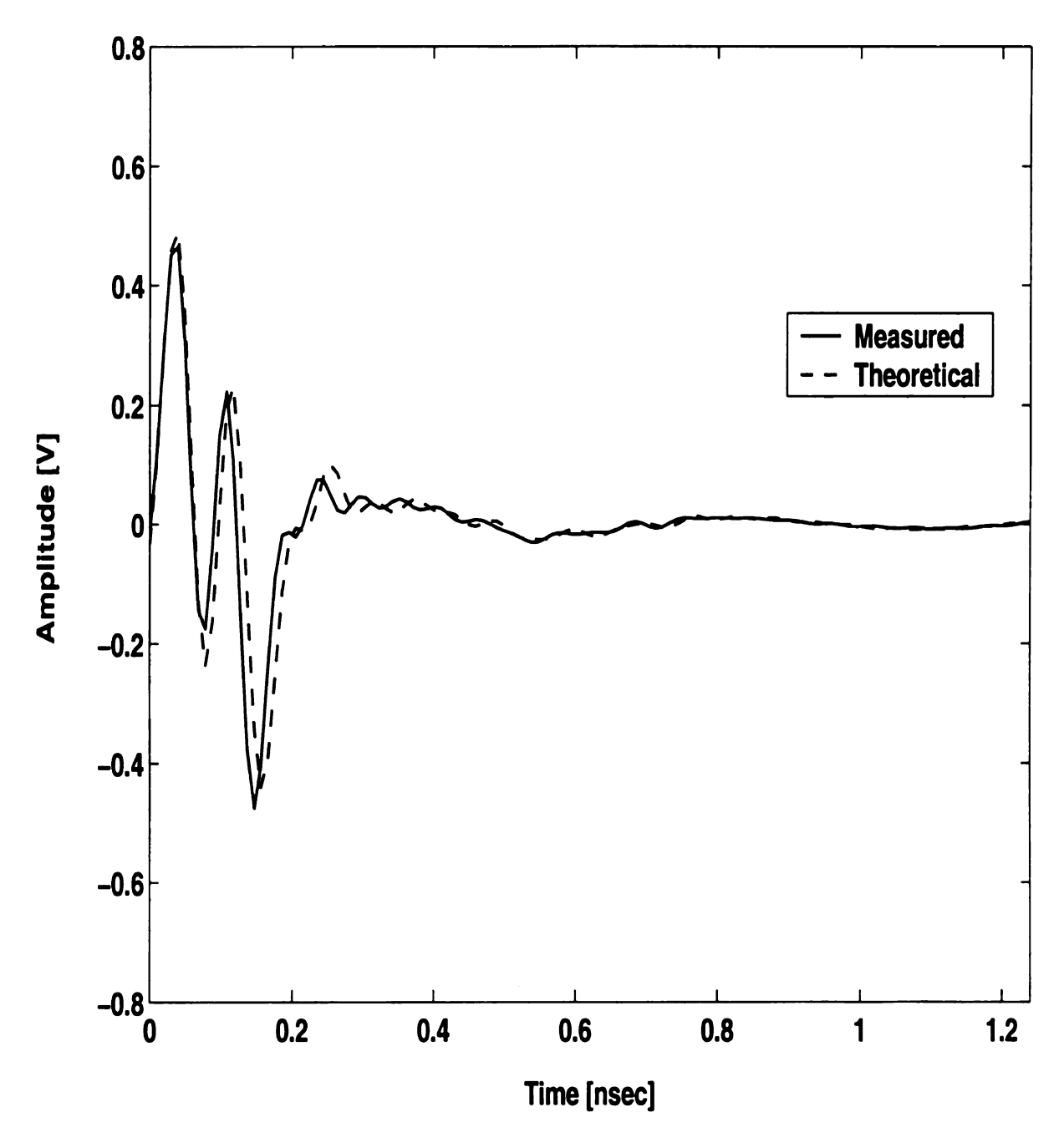
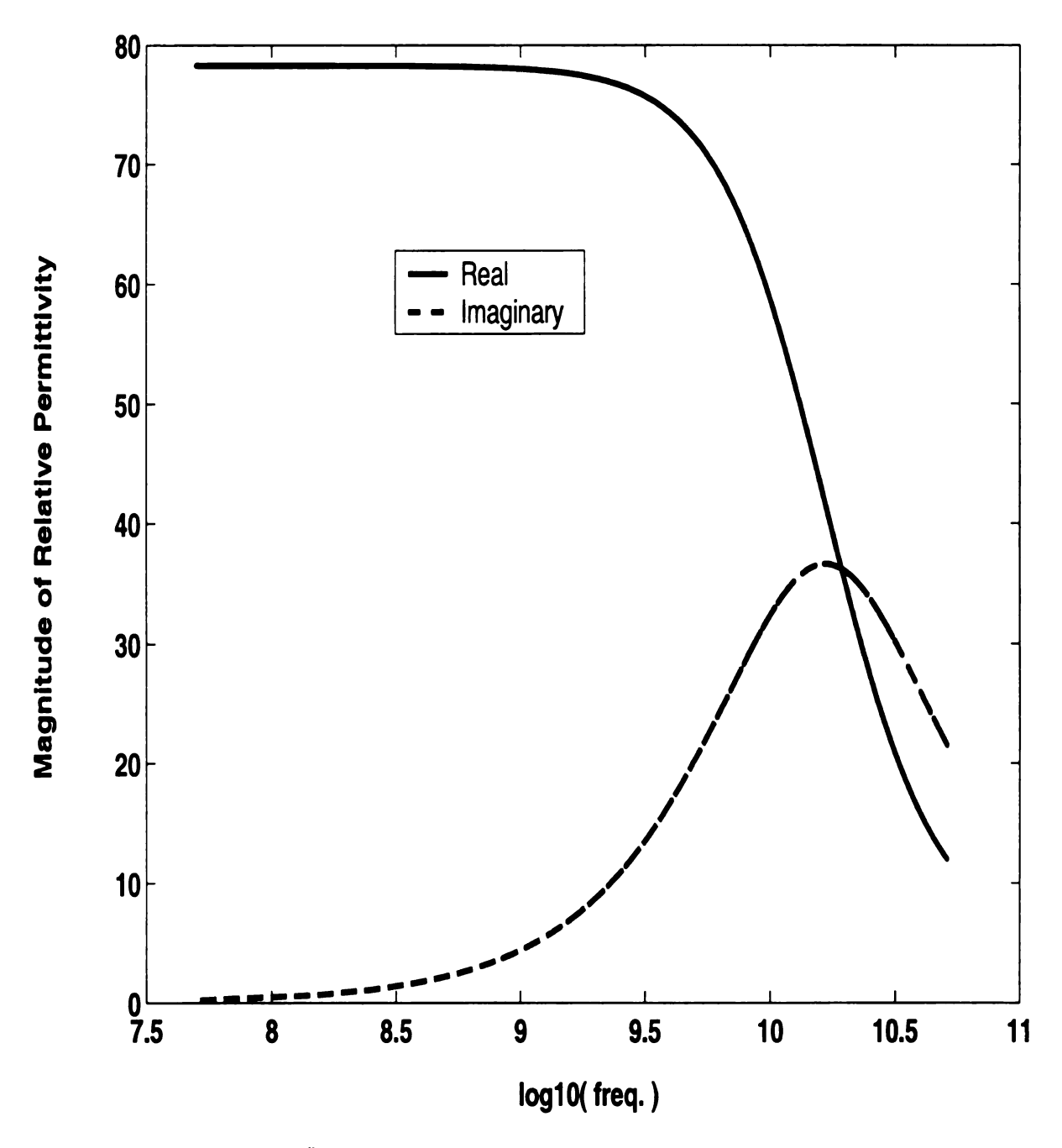


Figure 5.14. (a) Comparison of trasient reflection from a mechanically adhered plexiglass plates with that for a single material ( $\theta_{i1} = 6^{\circ}$ , TE polarization).



**Figure 5.14.** (b) Comparison of trasient reflection from a mechanically adhered plexiglass plates with that for an air gap inserted model ( $\theta_{i1} = 6^{\circ}$ , TE polarization).



**Figure 5.15.**  $-\epsilon$ "  $/\epsilon_0$  curve for water at 20°C given by the Debye model.

value at 10GHz. Therefore the resulting material parameters for the layers are given by  $\mu_2 = \mu_0$ ,  $\epsilon_2 = 2.59\epsilon_0$ ,  $\sigma_2 = 0\mho/m$ ,  $l_2 = 5.3$ mm,  $\mu_3 = \mu_0$ ,  $\epsilon_3 = 55\epsilon_0$ ,  $\sigma_3 = 16.7 \mho/m$ ,  $l_3 = 5.3$ mm,  $\mu_4 = \mu_0$ ,  $\epsilon_4 = 2.59\epsilon_0$ ,  $\sigma_4 = 0\mho/m$ ,  $l_4 = 5.3$ mm.

A measurement result for  $\theta_{i1}=6^{\circ}$  incidence angle is shown in Figure 5.16. As seen in the figure, there is considerable mismatch in the theoretical and measured data. However, by careful observation, it can be realized that there is a constant scaling relationship between the two curves. It turns out that the cause of this mismatch is 'mechanical' rather than 'electrical'. That is, the shape of the water filled container has been changed by water pressure and gravity, and it causes a tilt angle which result in a reduction of the received wave amplitude. This explanation can be justified from the observation that the first reflection peak from air and plexiglass interface, which can not be effected by the third layer material, has been reduced. By considering this phenomenon, all the measurements for the distilled water container are scaled by the ratio of the first peak amplitudes of the measured data to that of the theoretical result. The scaled measurements are shown in Figure 5.17-Figure 5.19, and all of them show a good match between measurements and theoretical expectations.

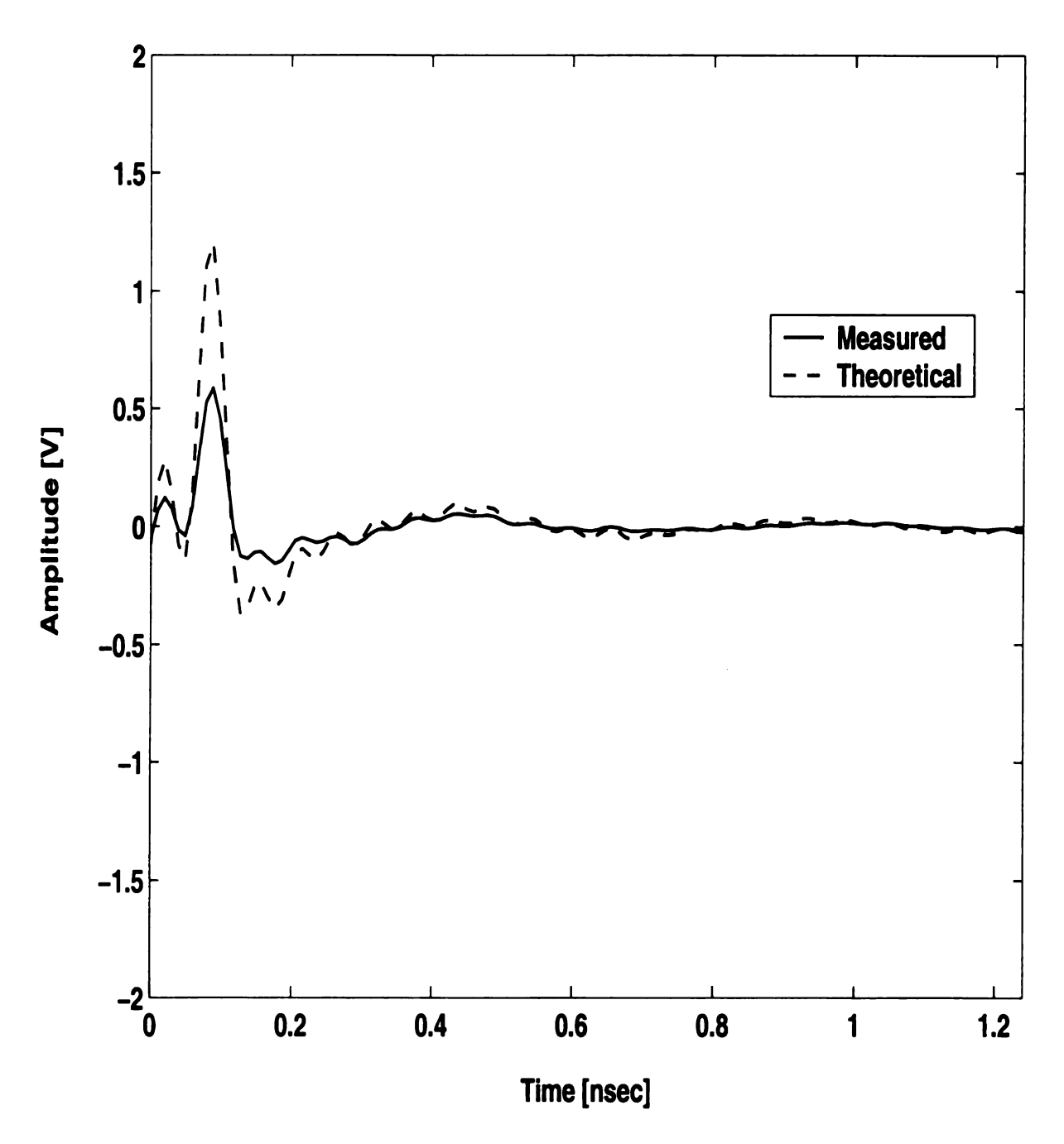


Figure 5.16. Trial measurements for trasient scattered field from a 5 lossy layered medium with incidence angle 6° (TE polarization).

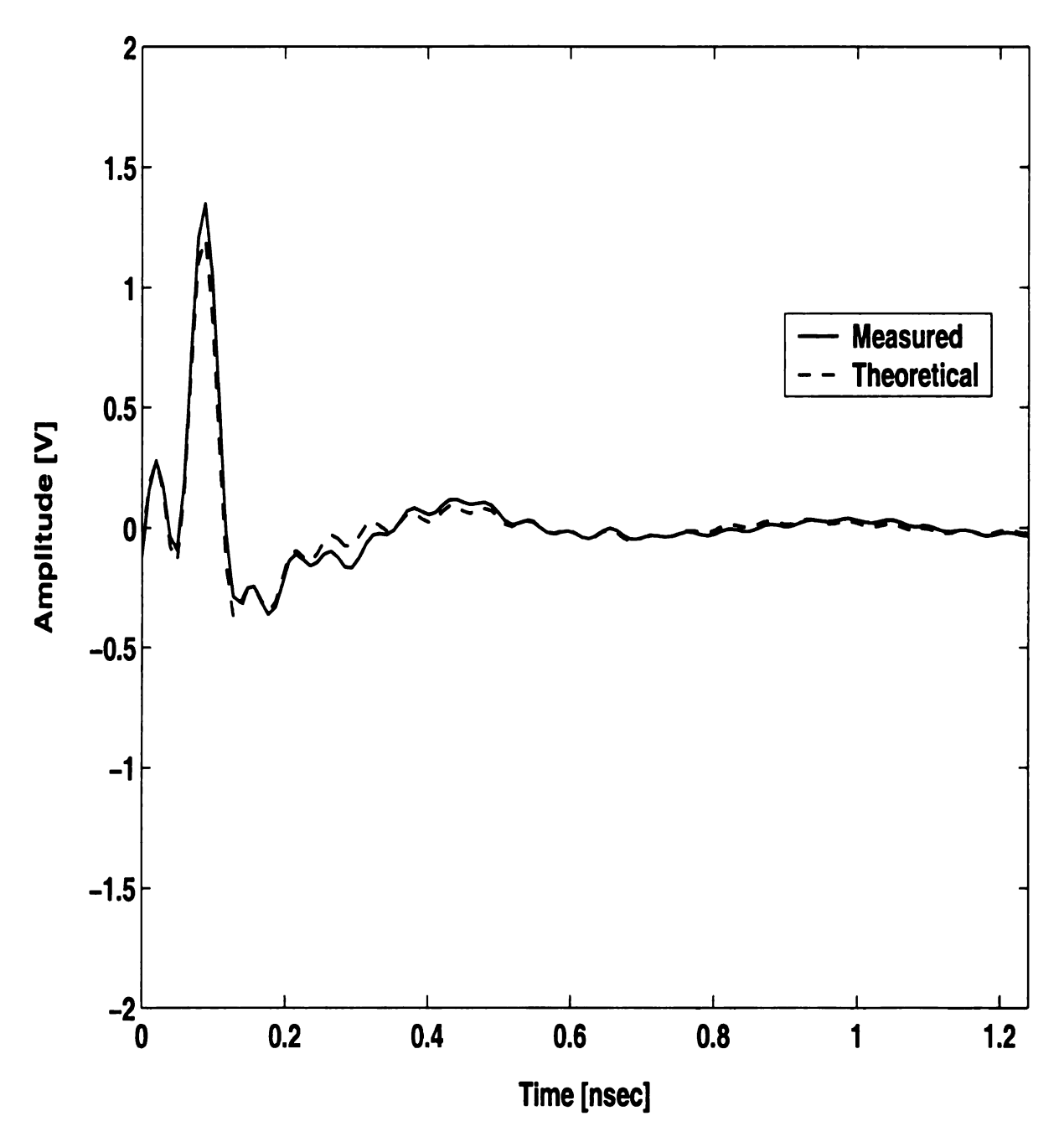


Figure 5.17. (a) Transient scattered field from a 5 lossy layered medium with incidence angle 6° (TE polarization).

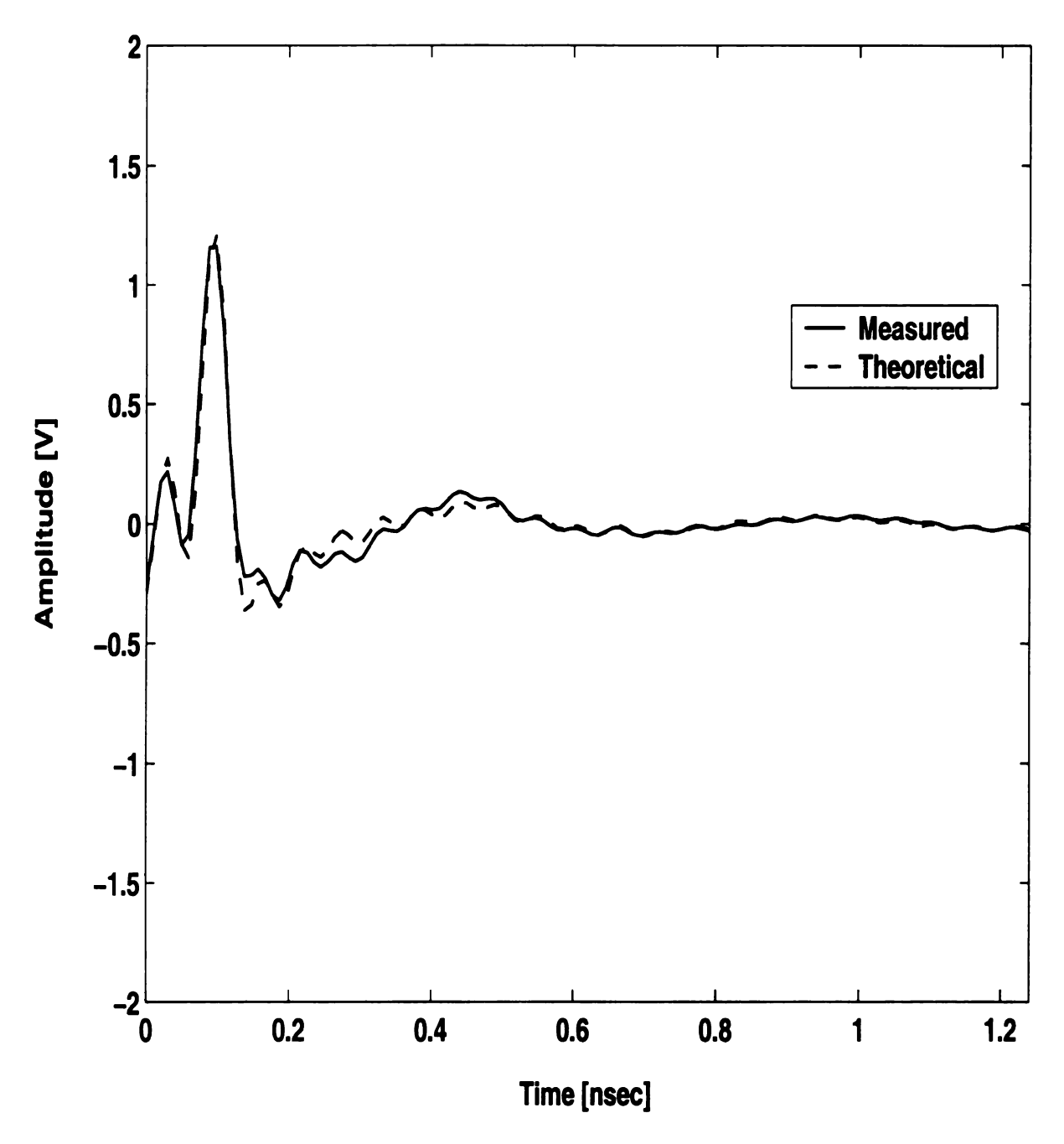


Figure 5.17. (b) Transient scattered field from a 5 lossy layered medium with incidence angle 6° (TM polarization).

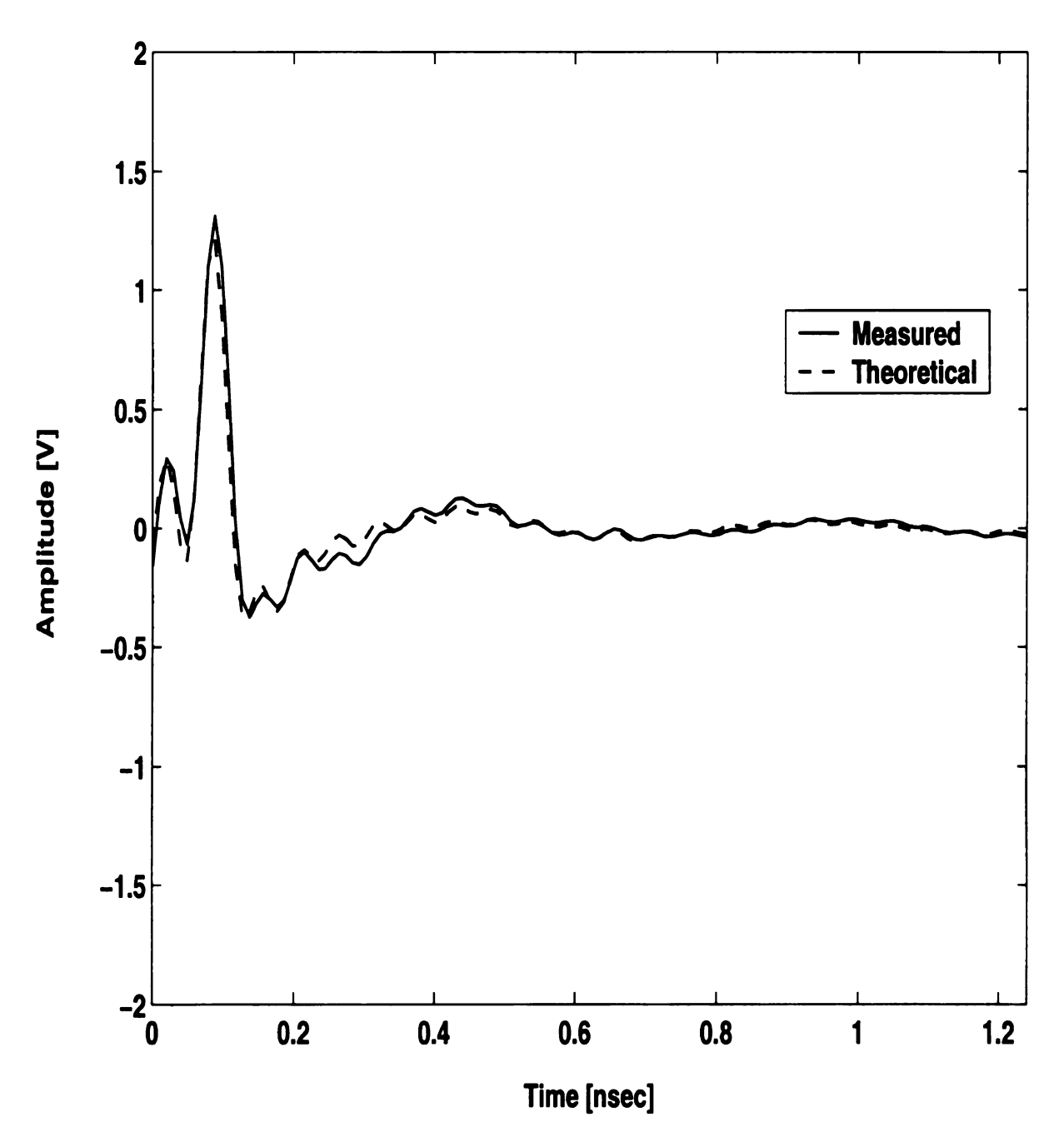


Figure 5.18. (a) Transient scattered field from a 5 lossy layered medium with incidence angle 15° (TE polarization).

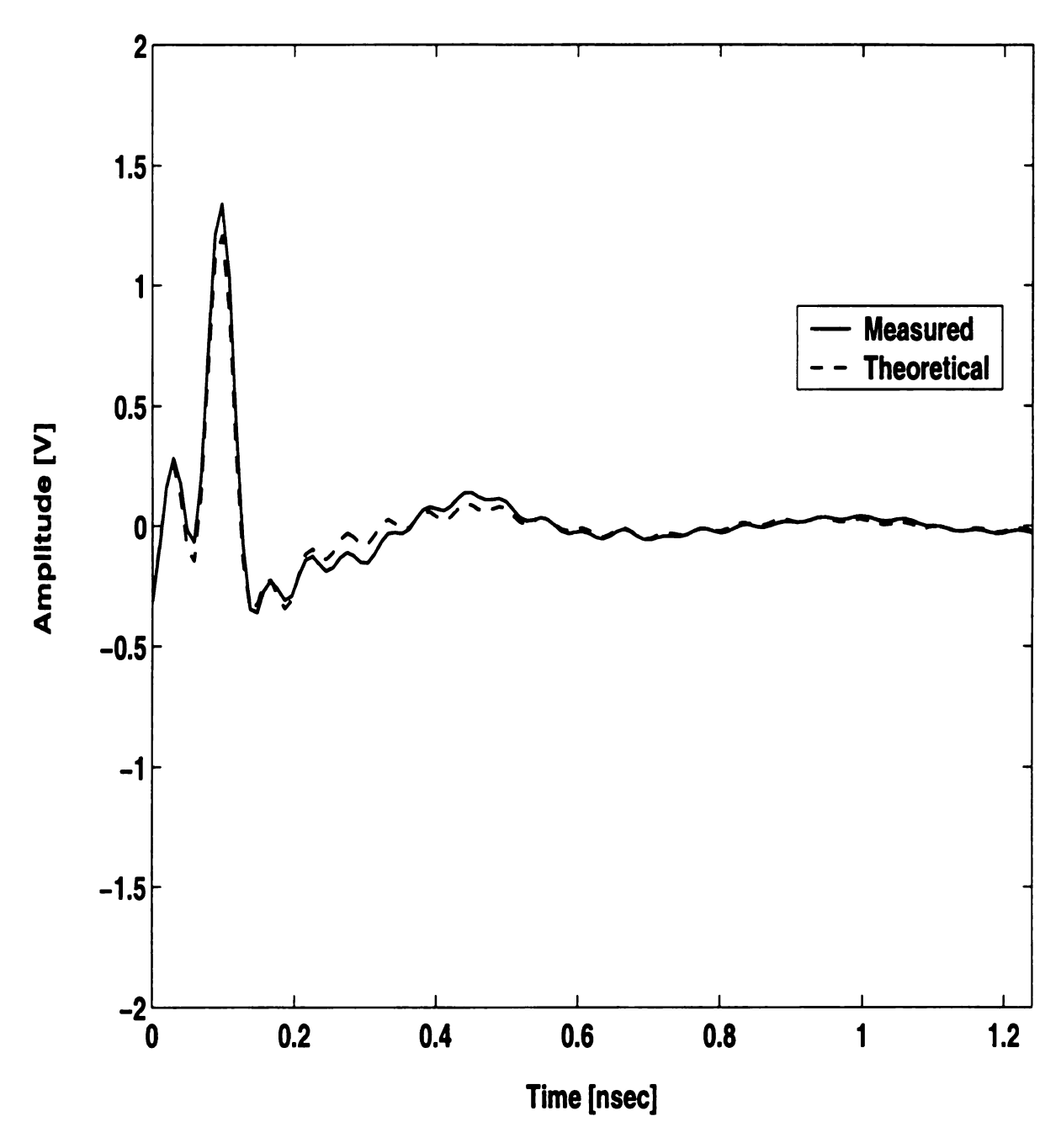


Figure 5.18. (b) Transient scattered field from a 5 lossy layered medium with incidence angle 15° (TM polarization).

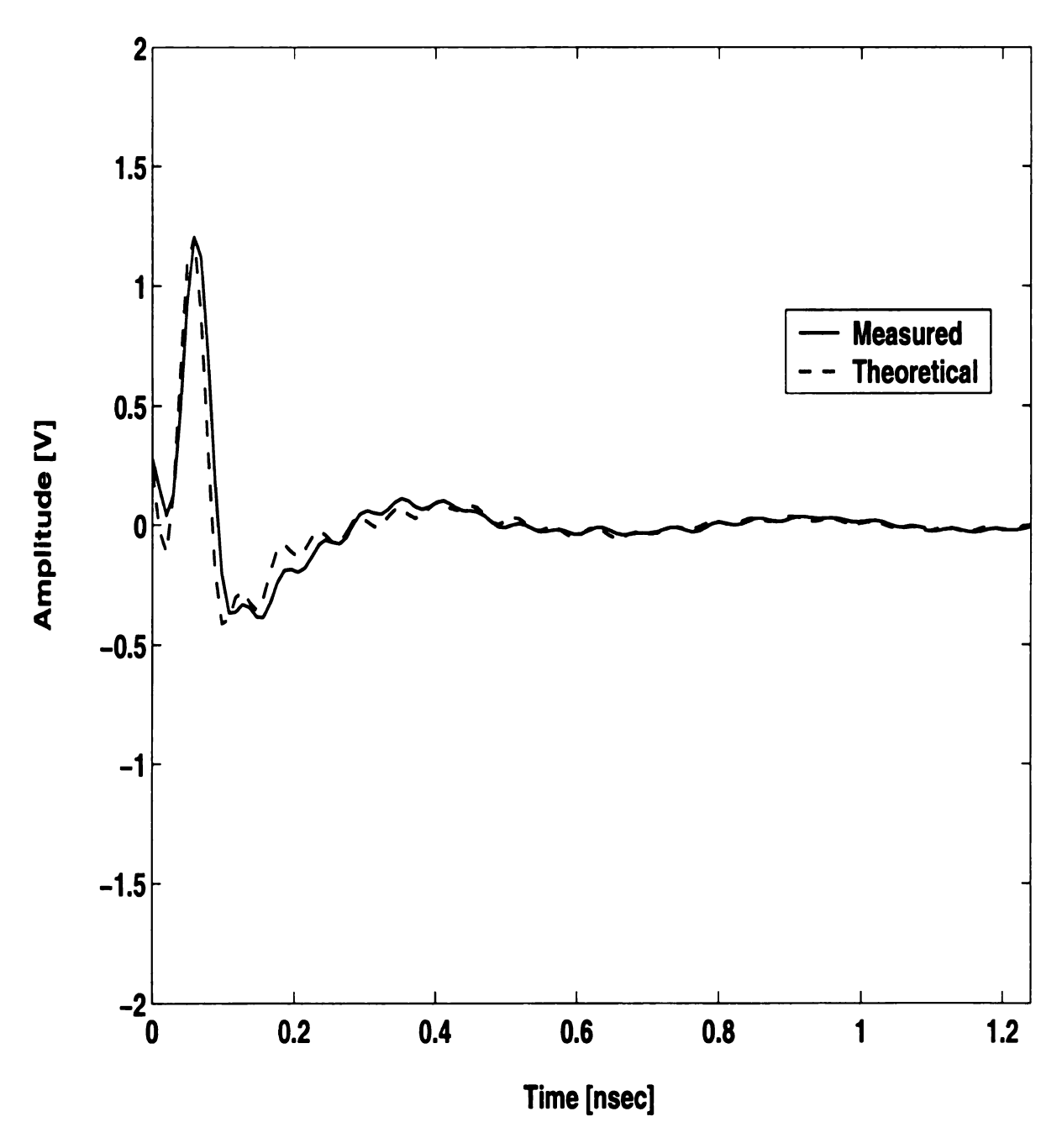


Figure 5.19. (a) Transient scattered field from a 5 lossy layered medium with incidence angle 30° (TE polarization).

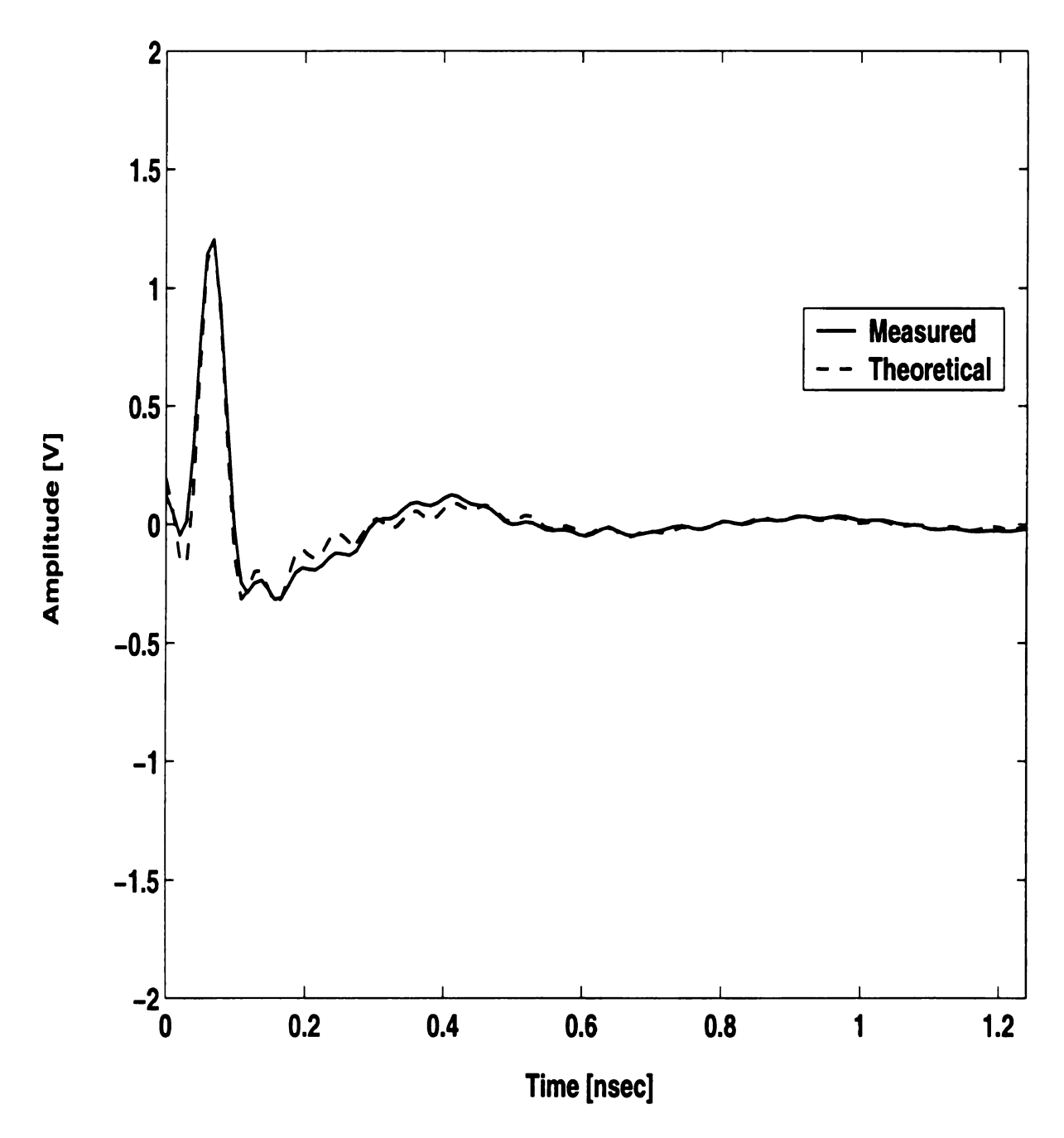


Figure 5.19. (b) Transient scattered field from a 5 lossy layered medium with incidence angle 30° (TM polarization).

## CHAPTER 6

#### CONCLUSIONS

Transient scattering from a multi-layered medium by an oblique uniform plane wave has been studied in this thesis. The frequency domain reflection coefficients were classified according to their different corresponding inverse Fourier transform pairs through careful algebraic manipulation and by using appropriate branch cuts. The exact analytical transient reflection coefficients of a single interface for TE and TM polarizations have been developed from inverse Fourier transforms of the frequency domain reflection coefficients. Also, approximate forms of the reflection coefficients were suggested for the TE polarization case as an example. It was found that all coefficients are causal for certain case. A reasonable explanation for the non causality of other cases could not be found. However, several reports about the occurrence of non causality in theoretical or experimental developments observed by other researchers were introduced. The expressions for the overall transient reflection coefficients were derived using a series expansion and the convolution theorem. The derived interfacial and overall reflection coefficients were verified by numerical computation using the IFFT. Also, actual time domain reflection measurements were performed to compare with the theoretically derived results, using lossless and lossy layers as the objects. All the measured and calibrated results have matched well with computed results based on the derived theory, and therefore verified the correctness of the derived transient expressions.

As discussed in Chapter 1, the purpose of this study is to provide fundamental background for parameter estimation of a multi-layered object using the transient scattered field. Except for the unexplained non causal cases, which should be studied separately in the future, the exact theoretical solutions for the transient scattered

field have been made available by the results of this study. Because each reflection from each layer has the information about the constitutive parameters, and because their functional relationship with the input waveform has been determined by this study, the next step is to find reliable methods to extract the information from the measured transient waveform.

**APPENDICES** 

# APPENDIX A

# OPERATIONS OF COMPLEX VALUED SQUARE ROOT FUNCTIONS USING THE BRANCH CUTS

The derivation processes of frequency domain expressions explained in Chapter 2 and Chapter 3 require algebraic manipulations of square roots of which arguments are complex numbers. Sometimes, the results of algebraic manipulations using conventional negative real axis branch cut are different from those using the branch cuts derived section 2.2.2 from radiation condition. Because the branch cuts from radiation condition are consistantly used in this thesis, it is helpful to introduce selected algebraic manipulations for derivation of frequency domain expressions using the branch cuts.

When D > 0 and B > 0

$$\sqrt{Ds^2 + Bs} = -\sqrt{D}\sqrt{Ds + B} = -\sqrt{D}\sqrt{s}\sqrt{s + \frac{B}{D}}$$
 (A.1)

while for D < 0 and B > 0

$$\sqrt{Ds^2 + Bs} = \sqrt{s}\sqrt{Ds + B} = \begin{cases} +j\sqrt{|D|}\sqrt{s}\sqrt{s - \frac{B}{|D|}} & : (\omega > 0) \\ -j\sqrt{|D|}\sqrt{s}\sqrt{s - \frac{B}{|D|}} & : (\omega < 0) \end{cases}$$
(A.2)

By denoting a square root from the conventional negative real axis branch cut as  $\sqrt[4]{()}$ ,

$$\frac{\sqrt{s+B_{n+1}}}{\sqrt{s+B_n}} = \pm \sqrt{\frac{s+B_{n+1}}{s+B_n}} = \sqrt[4]{\frac{s+B_{n+1}}{s+B_n}}$$
(A.3)

where the upper sign corresponds to  $B_{n+1} > B_n$  and lower sign does to  $B_{n+1} < B_n$ . The relationship between the two different branch cut square roots is needed because its inverse Fourier transform pair in reference material is given by using the negative real axis branch cut. Similarly,

$$\frac{\sqrt{s - B_{n+1}}}{\sqrt{s - B_n}} = \pm \sqrt{\frac{s - B_{n+1}}{s - B_n}} = \sqrt[4]{\frac{s - B_{n+1}}{s - B_n}}$$
(A.4)

where the upper sign corresponds to  $B_{n+1} < B_n$  and lower sign does to  $B_{n+1} > B_n$ . On the other hand, to find its inverse Fourier transform more easily, each of the other fraction of square root terms can be rewritten as

$$\frac{\sqrt{s+B_{n+1}}}{\sqrt{s-B_n}} = \sqrt{\frac{s+B_{n+1}}{s-B_n}}$$

$$= \sqrt{\frac{s+B_{n+1}}{s}}\sqrt{\frac{s}{s-B_n}}$$

$$= \sqrt[3]{\frac{s+B_{n+1}}{s}}\sqrt{\frac{s}{s-B_n}}$$
(A.5)

and

$$\frac{\sqrt{s - B_{n+1}}}{\sqrt{s + B_n}} = -\sqrt{\frac{s - B_{n+1}}{s + B_n}}$$

$$= -\sqrt{\frac{s - B_{n+1}}{s}} \sqrt{\frac{s}{s + B_n}}$$

$$= -\sqrt[3]{\frac{s - B_{n+1}}{s}} \sqrt[3]{\frac{s}{s + B_n}}.$$
(A.6)

## APPENDIX B

#### INVERSE FOURIER TRANSFORM PAIRS

In this appendix, the inverse Fourier transform pairs which are used to derive transient expressions, are provided. Some of these can be directly found from [23], while the others are derived from the given pairs.

Assume  $R(\omega) = G(\omega)U^*(\omega) + G(-\omega)U(-\omega)$  where  $G^*(\omega)$  is a complex conjugate of  $G(\omega)$ , and  $U(\omega)$  is a frequency domain unit step function. By letting  $g(t) = F^{-1}\{G(\omega)\}, g^*(t) = F^{-1}\{G^*(\omega)\}$  and using the duality theorem for Fourier transform that says,  $F(t) = F^{-1}\{2\pi f(-\omega)\}$  when  $f(t) = F^{-1}\{F(\omega)\}$ ,

$$\pi \delta(t) + \frac{1}{jt} = 2\pi F^{-1} \{ U(-\omega) \}$$

$$\frac{\delta(t)}{2} - \frac{1}{2j\pi t} = 2\pi F^{-1} \{ U(\omega) \}$$
(B.1)

and

$$R(t) = g(t) * \left\{ \frac{\delta(t)}{2} - \frac{1}{2j\pi t} \right\} + g^*(t) * \left\{ \frac{\delta(t)}{2} + \frac{1}{2j\pi t} \right\}$$

$$= \left\{ g(t) + g^*(t) \right\} * \frac{\delta(t)}{2} + \left\{ g(t) - g^*(t) \right\} * \frac{1}{2j\pi t}$$

$$= \frac{1}{2} \left\{ g(t) + g^*(t) \right\} + \frac{j}{2\pi t} * \left\{ g(t) - g^*(t) \right\}. \tag{B.2}$$

From the inverse transform pair of

$$\frac{1}{s+P} \Leftrightarrow e^{-Pt}u(t) \tag{B.3}$$

for P > 0, and  $-e^{-Pt}u(-t)$  for P < 0, its time derivative form is given by

$$\frac{s}{s+P} \Leftrightarrow \frac{d}{dt} \left\{ e^{-Pt} u(t) \right\}$$

$$= -Pe^{-Pt} u(t) + e^{-Pt} \delta(t)$$

$$= e^{-Pt} \left\{ \delta(t) - Pu(t) \right\}$$
(B.4)

for P > 0, and

$$\frac{s}{s+P} \iff \frac{d}{dt} \left\{ -e^{-Pt} u(-t) \right\}$$

$$= Pe^{-Pt} u(-t) + e^{-Pt} \delta(t)$$

$$= e^{-Pt} \left\{ \delta(t) + Pu(t) \right\}$$
(B.5)

for P < 0.

From 561.0 of [23],

$$1 - \sqrt[4]{\frac{s + B_{n+1}}{s + B_n}} \Leftrightarrow -\frac{B_{n+1} - B_n}{2} e^{-\frac{(B_{n+1} + B_n)}{2}t} \left\{ I_1 \left( \frac{B_{n+1} - B_n}{2} t \right) + I_0 \left( \frac{B_{n+1} - B_n}{2} t \right) \right\} u(t),$$
(B.6)

and it can be derived that

$$1 - \sqrt[4]{\frac{s - B_{n+1}}{s - B_n}} \Leftrightarrow \frac{B_{n+1} - B_n}{2} e^{\frac{(B_{n+1} + B_n)}{2}t} \left\{ I_1 \left( \frac{B_{n+1} - B_n}{2} t \right) - I_0 \left( \frac{B_{n+1} - B_n}{2} t \right) \right\} u(-t).$$
(B.7)

Also, from (A.5),

$$\sqrt[4]{\frac{s+B_{n+1}}{s}} \Leftrightarrow \delta(t) + \frac{B_{n+1}}{2}e^{-\frac{B_{n+1}}{2}t} \left\{ I_1\left(\frac{B_{n+1}}{2}t\right) + I_0\left(\frac{B_{n+1}}{2}t\right) \right\} u(t) \tag{B.8}$$

and

$$\sqrt[4]{\frac{s}{s-B_n}} \Leftrightarrow \delta(t) - \frac{B_n}{2} e^{-\frac{B_n}{2}t} \left\{ I_1\left(\frac{B_n}{2}t\right) + I_0\left(\frac{B_n}{2}t\right) \right\} u(-t), \tag{B.9}$$

the inverse Fourier transform of  $1 - \sqrt{\frac{s + B_{n+1}}{s - B_n}}$  is given by

$$\delta(t) - \left[\delta(t) + \frac{B_{n+1}}{2}e^{-\frac{B_{n+1}}{2}t} \left\{ I_1 \left( \frac{B_{n+1}}{2}t \right) + I_0 \left( \frac{B_{n+1}}{2}t \right) \right\} u(t) \right] 
* 
$$\left[ \delta(t) - \frac{B_n}{2}e^{\frac{B_n}{2}t} \left\{ I_1 \left( \frac{B_n}{2}t \right) + I_0 \left( \frac{B_n}{2}t \right) \right\} u(-t) \right] 
= \frac{B_n}{2}e^{\frac{B_n}{2}t} \left\{ I_1 \left( \frac{B_n}{2}t \right) + I_0 \left( \frac{B_n}{2}t \right) \right\} u(-t) 
- \frac{B_{n+1}}{2}e^{-\frac{B_{n+1}}{2}t} \left\{ I_1 \left( \frac{B_{n+1}}{2}t \right) + I_0 \left( \frac{B_{n+1}}{2}t \right) \right\} u(t) 
+ \frac{B_{n+1}B_n}{4}e^{\frac{B_n}{2}t} \int_{\max(t,0)}^{\infty} e^{-\frac{(B_{n+1}+B_n)}{2}x} \left\{ I_1 \left[ \frac{B_n}{2}(t-x) \right] + I_0 \left[ \frac{B_n}{2}(t-x) \right] \right\} 
\times \left\{ I_1 \left( \frac{B_{n+1}}{2}x \right) + I_0 \left( \frac{B_{n+1}}{2}x \right) \right\} dx.$$
(B.10)$$

By similar approach, the inverse Fourier transform of  $1+\sqrt{\frac{s-B_{n+1}}{s+B_n}}$  can be found as

$$\frac{B_{n+1}}{2}e^{\frac{B_{n+1}}{2}t}\left\{I_{1}(\frac{B_{n+1}}{2}t)-I_{0}(\frac{B_{n+1}}{2}t)\right\}u(-t) \\
-\frac{B_{n}}{2}e^{-\frac{B_{n}}{2}t}\left\{I_{1}(\frac{B_{n}}{2}t)-I_{0}(\frac{B_{n}}{2}t)\right\}u(t) \\
+\frac{(B_{n+1}B_{n})}{4}e^{\frac{B_{n+1}}{2}t}\int_{\max(t,0)}^{\infty}e^{-\frac{(B_{n+1}+B_{n})}{2}x}\left\{I_{1}\left[\frac{B_{n+1}}{2}(t-x)\right]-I_{0}\left[\frac{B_{n+1}}{2}(t-x)\right]\right\} \\
\times\left\{I_{1}(\frac{B_{n}}{2}x)-I_{0}(\frac{B_{n}}{2}x)\right\}dx. \tag{B.11}$$

#### APPENDIX C

#### PROGRAM SOURCE CODES IN FORTRAN 77

A computer program to compute theoretical TE polarization overall reflection from a multi-layered medium is provided. This program is written in standard Fortran 77 programming language, except a subroutine called Q2AGI from MICROSOFT IMSL package, which is used to compute infinite integral term in interfacial reflection coefficient when  $P_2 < 0$  (see 2.83).

This program reads an input waveform data from a text file 'inwave.dat', the material parameters of each layer (thickness, permeability, permittivity, conductivity) and initial incident angle from a text file 'layers.dat', and computes the layer parameter sets defined in this thesis, and writes them in a text file 'param.buf' for verification purpose. Also, the information about time range, number of data points and number of convolution terms are read from command line inputs. After the input stage, program computes the interfacial reflection coefficients for each interface, overall reflection and finally writes the outputs in a text output file 'gammax.out'. The structure of the programe to compute TM polarization is basically same. The differences are subroutines to compute interfactial reflection coefficients, and layer parameter definitions.

# (1) An example of input data file 'layers.dat'

The value of incident angle is computed using the value in the data file as a denominator of a fraction, of which numerator is fixed by  $\pi$  radian. That is, for an example, when given "thetai 30.0" in the data file, the incident angle will be  $\frac{\pi}{30}$  radian = 6°. Metric unit is used for thickness input. The first and the last layer have infinite thicknesses, therefore their values are meaningless.

thetai 30.0

mur1 1.0

er1 1.0

sigmal 0.0

thick1 0.0

mur2 1.0

er2 2.59

sigma2 0.0

thick2 0.0053

mur3 1.0

er3 55.0

sigma3 16.7

thick3 0.0053

mur4 1.0

er4 2.59

sigma4 0.0

thick4 0.0053

mur5 1.0

er5 1.0

sigma5 0.0

thick5 0.0

# (2) Main program

Because the products of a exponential function and a modified Bessel function appear frequently, the product is computed altogether using a subroutine. The expressions for numerical computation of the modified Bessel functions can be found in [29].

```
PROGRAM GAMXTE
     USE MSIMSL
C *******************
C
     This program computes transient overall reflection
\mathbf{C}
     using iterative convolutions, about the case for
C
     DN1>0 .AND. DN>0.
C
C
     An input waveform is obtained from a text data file which
C
     contains actual measurement data of transmitting impulse,
С
     called "inwave.dat"
С
С
     Text data file "layers.dat" is required as an input
C
     parameter description for each layer.
\mathbf{C}
C
     Text data file "gammax.out" will be output.
CHARACTER*8 TMPS
      INTEGER ITCONV
      INTEGER NT, SMAX, LMAX, I, K, NL
     PARAMETER (SMAX=10250)
     PARAMETER (LMAX=10)
     REAL MU(LMAX), EN(LMAX), SIG(LMAX), THCK(LMAX), B(LMAX), DN(LMAX)
     REAL C1(LMAX-1), C2(LMAX-1), C3(LMAX-1), P1(LMAX-1), P2(LMAX-1)
     REAL BTA (LMAX-1), D(LMAX-1), CD(LMAX-1)
     REAL T(SMAX), X(SMAX)
     REAL R(LMAX-1, SMAX), P(LMAX-1, SMAX), GAM(LMAX-1, SMAX)
     REAL THETAI, G, H, TMAX, DT
     REAL TMP, PSZERO
     REAL PI, E0, MU0
     COMMON /PWRS/C1, C2, C3, P1, P2, BTA, CD
     COMMON /ARRS/R, P, GAM
     COMMON /TARRS/T
     COMMON /INDX/I
     COMMON /TINDX/K,NT
     COMMON /LINDX/ITCONV, NL
     PI=4.*ATAN(1.)
     E0=1.0E-9/(36.0*PI)
     MU0=4.0*PI*1.0E-7
     PSZERO=1.0E-25
     OPEN(5, FILE='layers.dat', STATUS='unknown')
     OPEN(6,FILE='gammax.out',STATUS='unknown')
     OPEN(7,FILE='param.buf',STATUS='unknown')
     OPEN(8, FILE='inwave.dat', STATUS='unknown')
```

```
C **********
C READ AND COMPUTE CONSTANTS OF EACH LAYER
      WRITE(*,*) 'Enter the number of layers in <<layers.dat>> :'
      READ(*,*) NL
      ******
С
C
     READ INCIDNET ANGLE
     *******
С
11
     FORMAT (A8, F12.4)
12
     FORMAT (3x, F12.4, 2x, A8, '= ', E12.4)
20
      FORMAT(/)
      READ(5,11) TMPS, TMP
      THETAI = PI/TMP
      WRITE(*,12) TMP, TMPS, THETAI
      WRITE (7,12) TMP, TMPS, THETAI
      ********
C
С
      READ MATERIAL PARAMETERS
      *******
      DO 21 I=1,NL
        READ(5,11) TMPS, TMP
        MU(I) = TMP * MU0
        WRITE(*,12)TMP,TMPS,MU(I)
        WRITE(7,12)TMP,TMPS,MU(I)
        READ(5,11) TMPS,TMP
        EN(I) = TMP * E0
        WRITE(*,12)TMP,TMPS,EN(I)
        WRITE(7,12)TMP,TMPS,EN(I)
        READ(5,11) TMPS, SIG(I)
        WRITE(*,12)SIG(I),TMPS,SIG(I)
        WRITE(7,12)SIG(I),TMPS,SIG(I)
        READ(5,11) TMPS, THCK(I)
        WRITE(*,12) THCK(I), TMPS, THCK(I)
        WRITE(7,12) THCK(I), TMPS, THCK(I)
        TMP=MU(1) *EN(1) * ((SIN(THETAI)) **2)
        DN(I) = MU(I) *EN(I) - TMP
        B(I) = MU(I) * SIG(I) / ABS(DN(I))
        WRITE(*,13) DN(I),B(I)
        WRITE(7,13) DN(I),B(I)
13
        FORMAT(5X, 'Dn=', E10.3, 2X, 'Bn=', E10.3, /)
21
     CONTINUE
```

```
C ************
C COMPUTE LAYER PARAMETERS FOR EACH INTERFACE
     DO 22 I=1, NL-1
       WRITE(*,14) I
       WRITE(7,14) I
14
       FORMAT(/,3X,'Interface Index =',I3)
       D(I) = ((MU(I) **2) *DN(I+1)) / ((MU(I+1) **2) *DN(I))
       CD(I) = (1.0 - SQRT(D(I))) / (1.0 + SQRT(D(I)))
       WRITE(*,15) D(I),CD(I)
       WRITE(7,15) D(I),CD(I)
15
       FORMAT(3X, 'D=', E10.3, 3X, 'CD=', E10.3)
       BTA(I) = (B(I+1)-B(I))/2.0
       P1(I) = (B(I+1)+B(I))/2.0
       P2(I) = (B(I) - D(I) * B(I+1)) / (1.0 - D(I))
       WRITE(*,16) P1(I), P2(I), BTA(I)
       WRITE(7,16) P1(I), P2(I), BTA(I)
16
       FORMAT(3X,'P1=',E10.3,2X,'P2=',E10.3,2X,'BETA=',E10.3)
       C1(I) = (B(I) - B(I+1)) * SQRT(D(I)) / (1.0-D(I))
       C2(I) = ((B(I)-B(I+1))**2)*D(I)*SQRT(D(I))/((1.0-D(I))**2)
       C3(I) = 2.0*D(I)*(B(I+1)-B(I))/((1.0-D(I))*(1.0+SQRT(D(I))))
       WRITE(*,17) C1(I),C2(I),C3(I)
       WRITE(7,17) C1(I), C2(I), C3(I)
17
       FORMAT (3X, 'C1=', E10.3, 2X, 'C2=', E10.3, 2X, 'C3=', E10.3)
22
     CONTINUE
C READ TIME RANGE, NUMBER OF PARAMETERS AND CONVOLUTIONS
WRITE(*,*) 'Enter the Time range in seconds :'
     READ(*,*) TMAX
     WRITE(*,*) 'Enter the Number of Points (SMAX<=10250)'
     WRITE(*,*) 'EVEN number recommended to avoid zero freq. :'
     READ(*,*) NT
     WRITE(*,*) 'Enter the Number of Convolution Sum : '
     READ(*,*) ITCONV
C **********
C DEFINE TIME INTERVAL OF EVALUATION
     NT=NT-1
     DT=TMAX/REAL(NT)
     DO 31 K=1,NT+1
       T(K) = DT*(K-1)
31
     CONTINUE
```

```
DO 32 I=1, NL-1
      DO 33 K=1,NT+3
        R(I,K) = 0.0
        P(I,K) = 0.0
        GAM(I,K)=0.0
        X(K) = 0.0
33
      CONTINUE
32
     CONTINUE
     WRITE(7,18) TMAX, (NT+1), DT, (1.0/DT)
18
     FORMAT(/,3X,'TMAX=',E10.3,' [sec]',2X, I7,' Pts.',2X,/,
            3X 'DT=',E10.3,' [sec]',2X, '1/DT=',E10.3)
C *************
C READ INPUT WAVEFORM FROM DATA FILE
C **************
     DO 61 K=1,NT+1
      READ(8, *) X(K)
     CONTINUE
61
C COMPUTE INTERFACIAL REFL. COEFF.'S AND PROPAGATION TERMS
DO 89 I=1,NL-1
      CALL REFLCOEFF (R(I,:),DT)
      G=DN(I)
      H=MU(I)*SIG(I)
      CALL PROPA (P(I,:), THCK(I), G, H, 2, DT)
89
     CONTINUE
C *************
C COMPUTE THE FINAL IMPULSE RESPONSE OF LAYERS
C *************
     DO 87 K=1,NT+3
      GAM(NL-1,K) = R(NL-1,K)
87
     CONTINUE
     CALL GAMX(1, X, DT)
     *********
С
     WRITE TIME, INPUT AND OUTPUT WAVEFORM DATA
     ***********
C
     DO 50 K=1,NT+3
      IF (ABS(GAM(1,K)).LT.PSZERO) GAM(1,K)=0.0
      WRITE (6,99) T(K), X(K), GAM (1,K)
99
      FORMAT(1X, E10.3,1X, E13.5,1X, E13.5)
50
     CONTINUE
     ENDFILE 5
     ENDFILE 6
     ENDFILE 7
     ENDFILE 8
```

```
END
C SUBROUTINE TO COMPUTE OVERALL REFLECTION OF EACH LAYER
RECURSIVE SUBROUTINE GAMX(I,XIN,DT)
      INTEGER NT, I, SMAX, LMAX, NL, ITCONV, K, N
      REAL DT
      PARAMETER (SMAX=10250)
      PARAMETER (LMAX=10)
      REAL XIN(SMAX), BUF(LMAX-2, SMAX), GBUF(SMAX)
      REAL R(LMAX-1, SMAX), P(LMAX-1, SMAX), GAM(LMAX-1, SMAX)
      COMMON /ARRS/R, P, GAM
      COMMON /TINDX/K,NT
      COMMON /LINDX/ITCONV, NL
      IF (I.EQ.(NL-2)) THEN
        CALL CONVOL(R(I,:), XIN, GAM(I,:), DT)
        CALL CONVOL(R(I,:),R(I,:),GBUF,DT)
        GBUF(NT+2) = 1.0/DT-GBUF(NT+2)
        DO 41 K=1,NT+1
          GBUF(K) = -GBUF(K)
41
        CONTINUE
        CALL CONVOL(GBUF, P(I+1,:), GBUF, DT)
        CALL CONVOL (GBUF, GAM(I+1,:), GBUF, DT)
        CALL CONVOL (GBUF, XIN, GBUF, DT)
        DO 42 K=1,NT+1
          GAM(I,K) = GAM(I,K) + GBUF(K)
42
        CONTINUE
        DO 43 N=1, ITCONV
          CALL CONVOL(GBUF, R(I,:), GBUF, DT)
          CALL CONVOL (GBUF, GAM (I+1,:), GBUF, DT)
          CALL CONVOL (GBUF, P(I+1,:), GBUF, DT)
          DO 61 K=1,NT+2
            GBUF(K) = -GBUF(K)
61
          CONTINUE
          DO 44 K=1,NT+1
            GAM(I,K) = GAM(I,K) + GBUF(K)
44
          CONTINUE
43
        CONTINUE
        WRITE(*,19) I
19
        FORMAT(3X, 'IN=', I3)
      ELSE
        CALL CONVOL(R(I,:), XIN, GAM(I,:), DT)
        CALL GAMX(I+1,XIN,DT)
        CALL CONVOL(R(I,:), R(I,:), BUF(I,:), DT)
        BUF(I,NT+2)=1.0/DT-BUF(I,NT+2)
        DO 55 K=1,NT+1
          BUF(I,K) = -BUF(I,K)
```

```
55
        CONTINUE
        DO 65 K=1,NT+3
          GBUF(K)=BUF(I,K)
65
        CONTINUE
        CALL CONVOL (GBUF, GAM (I+1,:), GBUF, DT)
        CALL CONVOL (GBUF, P(I+1,:), GBUF, DT)
        DO 56 K=1,NT+1
          GAM(I,K) = GAM(I,K) + GBUF(K)
56
        CONTINUE
        DO 57 N=1, ITCONV
          CALL CONVOL(GBUF, R(I,:), GBUF, DT)
          CALL CONVOL(GBUF, P(I+1,:), GBUF, DT)
          DO 62 K=1, NT+2
            BUF(I,K) = -GBUF(K)
62
          CONTINUE
          BUF(I,NT+3) = -GBUF(NT+3)
          CALL GAMX(I+1,BUF(I,:),DT)
          DO 58 K=1,NT+1
            GAM(I,K) = GAM(I,K) + GAM(I+1,K)
58
          CONTINUE
          DO 63 K=1, NT+3
            GBUF(K) = GAM(I+1,K)
63
          CONTINUE
57
        CONTINUE
        WRITE(*,59) I
59
        FORMAT(3X, 'IN=', I3)
      ENDIF
      RETURN
      END
C ****************
C SUBROUTINE TO COMPUTE INDIVIDUAL TIME DOMAIN REFLECTION
      SUBROUTINE REFLCOEFF (R, DT)
      EXTERNAL FUNCP, FUNCN
      REAL SIO, SI1
      INTEGER K, NT, I, L, SMAX, LMAX
      PARAMETER (SMAX=10250)
      PARAMETER (LMAX=10)
      REAL C1(LMAX-1), C2(LMAX-1), C3(LMAX-1), P1(LMAX-1), P2(LMAX-1)
      REAL BTA (LMAX-1), CD (LMAX-1)
      REAL TMP, S, Q1, Q2, Q3, DT
      REAL T(SMAX), R(SMAX)
      COMMON /PWRS/C1, C2, C3, P1, P2, BTA, CD
      COMMON /TARRS/T
      COMMON /INDX/I
      COMMON /TINDX/K,NT
```

```
REAL ERRREL, RESULT, ERREST
      INTEGER MAXSUB, NEVAL, NSUBIN
      PARAMETER (MAXSUB=2000)
      REAL ALIST (MAXSUB), BLIST (MAXSUB), RLIST (MAXSUB), ELIST (MAXSUB)
      INTEGER IORD (MAXSUB)
      ERRREL=1.0E-03
      IF (P2(I).GE.O.) THEN
        DO 31 K=1, NT+1
          TMP = -P1(I) *T(K)
          Q1=C1(I)*(SI1(BTA(I)*T(K),TMP)+SI0(BTA(I)*T(K),TMP))
          S=0.0
          IF (K.GT.1) THEN
            02 = 0.0
            DO 32 L=2, K
              CALL OTRAP(FUNCP, T(L-1), T(L), S)
              Q2 = Q2 + S
32
            CONTINUE
            Q2=C2(I)*Q2
          ELSE
            Q2=0.0
          ENDIF
          Q3=C3(I)*EXP(-P2(I)*T(K))
          R(K) = Q1 - Q2 + Q3
          WRITE(*,34) I,K
34
          FORMAT (3X, 'I=', I3, 2X, 'K=', I5)
31
        CONTINUE
      ELSE
        DO 51 K=1,NT+1
          TMP = -P1(I) *T(K)
          Q1=SIO(BTA(I)*T(K),TMP)
          Q1=Q1+SI1(BTA(I)*T(K),TMP)
          Q1=C1(I)*Q1
          CALL Q2AGI(FUNCN, 0., 1, 0., ERRREL, RESULT, ERREST, MAXSUB,
                      NEVAL, NSUBIN, ALIST, BLIST, RLIST, ELIST, IORD )
          Q2=C2(I)*RESULT/P2(I)
          R(K) = Q1 - Q2
          WRITE(*,54) I,K
54
          FORMAT (3X, 'I=', I3, 2X, 'K=', I5)
51
        CONTINUE
      ENDIF
С
С
      ADD AMPLITUDE AND POSITION OF DELTA FUNCTION
      **********
      R(NT+2)=CD(I)/DT
      R(NT+3)=1.0
      RETURN
      END
```

```
C SUBROUTINE TO COMPUTE TIME DOMAIN PROPAGATION TERM
SUBROUTINE PROPA (P, THCK, G, H, N, DT)
     REAL SI1
     INTEGER K, NT, SMAX, N, M
     PARAMETER (SMAX=10250)
     REAL Z, W1, W2, TRIG, THCK, G, H, DT
     REAL T(SMAX), P(SMAX)
     COMMON /TARRS/T
     COMMON /TINDX/K,NT
     THCK=N*THCK
     TRIG=THCK*SQRT(G)
     W1=0.5*H/SQRT(G)
     W2=0.5*H/G
     DO 71 M=1,NT+1
       IF (T(M).GT.TRIG) THEN
        Z=SQRT(T(M)**2-G*(THCK**2))
        P(M) = W1 * THCK * SI1 (W2 * Z, -W2 * T(M)) / Z
       ENDIF
71
     CONTINUE
     **********
С
     ADD AMPLITUDE AND POSITION OF DELTA FUNCTION
     DO 72 M=1,NT+1
       IF (T(M).GT.TRIG) THEN
        P(NT+2) = EXP(-W1*THCK)/DT
        P(NT+3) = REAL(M)
        GO TO 73
       ENDIF
72
     CONTINUE
73
     RETURN
     END
C **************
C SUBROUTINE TO COMPUTE TIME DOMAIN CONVOLUTION
C **************
     SUBROUTINE CONVOL(IN1, IN2, OUT, DT)
     REAL DT, S, A, B, PSZERO
     INTEGER K, NT, SMAX, N, M, L
     PARAMETER (SMAX=10250)
     REAL IN1 (SMAX), IN2 (SMAX), OUT (SMAX), LOBUF (SMAX)
     COMMON /TINDX/K,NT
     PSZERO=1.0E-25
     DO 80 M=1, NT+3
       LOBUF (M) = 0.0
```

```
80
      CONTINUE
      LOBUF (NT+2) = IN1 (NT+2) * IN2 (NT+2) * DT
      LOBUF (NT+3) = (IN1(NT+3)-1.0) + (IN2(NT+3)-1.0) + 1.0
      L=INT(IN1(NT+3))
      IF (L.LE.(NT+1)) THEN
        DO 81 M=1, (NT+2-L)
          LOBUF (M+L-1) = LOBUF (M+L-1) + IN1 (NT+2) * IN2 (M) *DT
81
        CONTINUE
      ENDIF
      L=INT(IN2(NT+3))
      IF (L.LE.(NT+1)) THEN
        DO 82 M=1, (NT+2-L)
          LOBUF (M+L-1) =LOBUF (M+L-1) +IN2 (NT+2) *IN1 (M) *DT
82
        CONTINUE
      ENDIF
      DO 83 M=2,NT+1
        S = 0.0
        DO 84 N=2, M
          A=IN1 (M-N+1) *IN2 (N)
          B=IN1(M-N+2)*IN2(N-1)
          IF (ABS(A*B).GT.PSZERO) S=S+0.5*DT*(A+B)
84
        CONTINUE
        LOBUF(M) = LOBUF(M) + S
83
      CONTINUE
      DO 85 M=1,NT+3
        OUT (M) = LOBUF (M)
85
      CONTINUE
      RETURN
      END
C INNER INTEGRATION ROUTINE USING SIMPSON'S RULE
SUBROUTINE qtrap(FUNC,a,b,s)
      EXTERNAL FUNC
      INTEGER JMAX
      REAL a, b, EPS
      REAL olds, s, FUNC
      PARAMETER (EPS=1.e-3, JMAX=20)
C
      USES trapzd
      INTEGER j
      olds=0.0
      do 41 j=1,JMAX
        call trapzd(FUNC,a,b,s,j)
        if (abs(s-olds).lt.EPS*abs(olds)) return
        if (s.eq.0..and.olds.eq.0..and.j.gt.6) return
        olds=s
41
      continue
      WRITE(*, 43)
```

```
43
     FORMAT('Too many steps in gtrap. Press any number to
continue...')
     READ(*,*) TI
     END
C ***************
C TRAPEZOIDAL RULE AS A SUBROUTINE FOR INTEGRATION
C ***************
     SUBROUTINE trapzd(FUNC,a,b,s,n)
     EXTERNAL FUNC
     INTEGER n
     REAL a,b,x
     REAL del, sum, tnm, s
     REAL FUNC
     INTEGER it, j
     if (n.eq.1) then
       s=0.5*(b-a)*(FUNC(a)+FUNC(b))
     else
       it=2**(n-2)
       tnm=it
       del=(b-a)/tnm
       x=a+0.5*del
       sum=0.
       do 41 j=1, it
         sum=sum+FUNC(x)
         x=x+del
41
       continue
       s=0.5*(s+(b-a)*sum/tnm)
     endif
     return
C ***********
C INTEGRAND FUNCTION DEFINITION FOR P2 >= 0
C *******************************
     REAL FUNCTION FUNCP(U)
     INTEGER NT, I, K, SMAX, LMAX
     PARAMETER (SMAX=10250)
     PARAMETER (LMAX=10)
     REAL U, DTMP
     REAL SIO, SI1
     REAL T(SMAX)
     REAL C1(LMAX-1), C2(LMAX-1), C3(LMAX-1), P1(LMAX-1), P2(LMAX-1)
     REAL BTA (LMAX-1), CD (LMAX-1)
     COMMON /PWRS/C1, C2, C3, P1, P2, BTA, CD
     COMMON /TARRS/T
     COMMON /INDX/I
     COMMON /TINDX/K,NT
     DTMP = -(P2(I) *T(K) + (P1(I) - P2(I)) *U)
```

```
FUNCP=SI1(BTA(I)*U,DTMP)+SI0(BTA(I)*U,DTMP)
     RETURN
     END
C *************
C INTEGRAND FUNCTION DEFINITION FOR P2 < 0
C *************
     REAL FUNCTION FUNCN(U)
     INTEGER NT, I, K, SMAX, LMAX
     PARAMETER (SMAX=10250)
     PARAMETER (LMAX=10)
     REAL U.DTMP
     REAL SIO, SI1
     REAL T(SMAX)
     REAL C1(LMAX-1), C2(LMAX-1), C3(LMAX-1), P1(LMAX-1), P2(LMAX-1)
     REAL BTA (LMAX-1), CD (LMAX-1)
     COMMON /PWRS/C1, C2, C3, P1, P2, BTA, CD
     COMMON /TARRS/T
     COMMON /INDX/I
     COMMON /TINDX/K,NT
     DTMP = -P1(I) *T(K) + (P1(I)/P2(I)-1.0) *U
     FUNCN=SIO(BTA(I)*(T(K)-U/P2(I)),DTMP)+
           SI1(BTA(I)*(T(K)-U/P2(I)),DTMP)
     RETURN
     END
C ***********
C PRODUCT OF EXPONENTIAL AND MODIFIED BESSEL
C FUNCTION OF ZEROTH ORDER
C *************
     REAL FUNCTION SIO(X,OFST)
     REAL X, T, Y, OFST
     T = ABS(X)/3.75
     IF (ABS(X).LT.3.75) THEN
       Y=EXP(OFST)
       SI0=1.0*Y
       Y=Y*(T**2)
       SI0=SI0+3.5156229*Y
       Y=Y*(T**2)
       SI0=SI0+3.0899424*Y
       Y=Y*(T**2)
       SI0=SI0+1.2067492*Y
       Y=Y*(T**2)
       SI0=SI0+0.2659732*Y
       Y=Y*(T**2)
       SI0=SI0+0.0360768*Y
       Y=Y*(T**2)
```

```
SI0=SI0+0.0045813*Y
     ELSE
       Y=EXP(ABS(X)+OFST)/SQRT(ABS(X))
       SI0=0.39894228*Y
       Y=Y/T
       SI0=SI0+0.01328592*Y
       Y=Y/T
       SI0=SI0+0.00225319*Y
       Y=Y/T
       SI0=SI0-0.00157565*Y
       Y=Y/T
       SI0=SI0+0.00916281*Y
       Y=Y/T
       SI0=SI0-0.02057706*Y
       Y=Y/T
       SI0=SI0+0.02635537*Y
       Y=Y/T
       SI0=SI0-0.01647633*Y
       Y=Y/T
       SI0=SI0+0.00392377*Y
     ENDIF
     RETURN
     END
C ***********
C PRODUCT OF EXPONENTIAL AND MODIFIED BESSEL
C FUNCTION OF FIRST ORDER
C ***********
     REAL FUNCTION SI1(X,OFST)
     REAL X, T, Y, OFST
     T = ABS(X)/3.75
     IF (ABS(X).LT.3.75) THEN
       Y=X*EXP(OFST)
       SI1=0.5*Y
       Y=Y*(T**2)
       SI1=SI1+0.87890594*Y
       Y=Y*(T**2)
       SI1=SI1+0.51498869*Y
       Y=Y*(T**2)
       SI1=SI1+0.15084934*Y
       Y=Y*(T**2)
       SI1=SI1+0.02658733*Y
       Y=Y*(T**2)
       SI1=SI1+0.00301532*Y
       Y=Y*(T**2)
       SI1=SI1+0.00032411*Y
     ELSE
```

```
Y=EXP(ABS(X)+OFST)/SQRT(ABS(X))
 SI1=0.39894228*Y
 Y=Y/T
 SI1=SI1-0.03988024*Y
 Y=Y/T
 SI1=SI1-0.00362018*Y
 Y=Y/T
 SI1=SI1+0.00163801*Y
 Y=Y/T
 SI1=SI1-0.01031555*Y
 Y=Y/T
 SI1=SI1+0.02282967*Y
 SI1=SI1-0.02895312*Y
 Y=Y/T
 SI1=SI1+0.01787654*Y
 Y=Y/T
 SI1=SI1-0.00420059*Y
 IF (X.LT.0.0) SI1=-SI1
ENDIF
RETURN
```

END

**BIBLIOGRAPHY** 

#### **BIBLIOGRAPHY**

- [1] J. A. Stratton, Electromagnetic Theory. McGraw-Hill, New York, 1941.
- [2] J. R. Wait, "Electromagnetic fields of sources in lossy media," in *Antenna Theory* (R. E. Collin and F. J. Zucker, eds.), vol. 2, ch. 24, pp. 503–505, McGraw-Hill, New York, 1969.
- [3] P. R. Barnes and F. M. Tesche, "On the direct calculation of a transient plane wave reflected from a finitely conducting half space," *IEEE Trans. Electromagn. Compat.*, vol. 33, pp. 90-96, May 1991.
- [4] S. He and S. Ström, "Time-domain propagating modes in a finitely conducting half-space and caculation of the transient reflection," *IEEE Trans. Electromagn. Compat.*, vol. 37, pp. 277–282, May 1995.
- [5] M. Weber and K. Reiß, "Time domain analysis of electromagnetic pulse propagation in stratified conducting media: a riemann's function approach," in *International Conference on Electromagnetics in Advanced Applications*, (Torino Italy), pp. 647-650, Sept. 1999.
- [6] S. L. D. H.-Y. Pao and D. G. Dudley, "An accurate and efficient analysis for transient plane waves obliquely incident on a conductive half space (TE case)," *IEEE Trans. Antennas Propagat.*, vol. 44, pp. 918-924, July 1996.
- [7] S. L. D. H.-Y. Pao and D. G. Dudley, "An accurate and efficient analysis for transient plane waves obliquely incident on a conductive half space (TM case)," *IEEE Trans. Antennas Propagat.*, vol. 44, pp. 925-932, July 1996.
- [8] E. J. Rothwell and M. J. Cloud, "On the natural frequencies of an annular ring above a conducting half space," *J. Electromag. Waves and Appl.*, vol. 10, no. 2, pp. 155-179, 1996.
- [9] L. B. Felsen and N. Marcuvitz, Radiation and Scattering of Waves. Prentice Hall, Englewood Cliffs, NJ, 1991.
- [10] I. S. Gradshteyn and I. M. Ryzhik, *Tables of Integrals, Series, and Products*. Academic Press, London, UK, 1994.
- [11] H.-Y. Pao, "Interaction between a transient plane wave and a conductive half-space," Ph. D. Thesis, Univ. Arizona, Tucson, AZ, 1995.

- [12] E. H. Hauge and J. A. Stoveng, "Tunneling times: A critical review," Rev. Mod. Phys., vol. 61, 1989.
- [13] V. S. Olkhovsky and E. Recami, "Recent developments in the time analysis of tunneling processes," *Phys. Rep.*, vol. 214, 1992.
- [14] J. D. Jackson, Classical Electrodynamics. Wiley, New York, 1974.
- [15] C. Spielmann, R. Szippocs, A. Stingl, and F. Krausz, "Tunneling of optical pulses through photonic band gaps," *Physical. Review Letters*, vol. 73, no. 17, 1994.
- [16] A. M. Steinberg, P. G. Kwiat, and R. Y. Chiao, "Measurement of the single photon tunneling time," *Physical. Review Letters*, vol. 71, no. 5, 1993.
- [17] A. Enders and G. Nimitz, "Evanescent-mode propagation and quantum tunneling," *Phys. Rev. E*, vol. 48, no. 1, 1993.
- [18] T. E. Hartman, "Tunneling of a wave packet," J. Appl. Phys., vol. 33, 1962.
- [19] M. Xiao, "Time diffraction of evanescent wave," Phys. Rev. E, vol. 60, no. 5, 1999.
- [20] David K. Cheng, "Appendix B-3," in *Field and Wave Electromagnetics*, Addison-Wesley Publishing Company, 1986.
- [21] Rodger F. Harrington, "Appendix B," in *Time-Harmonic Electromagnetic Fields*, Mc-Graw Hill, New York, 1961.
- [22] Robert E. Collin, "Field theory of guided waves 2nd ed.," IEEE Press, New York, 1991.
- [23] George. A. Campbell and Ronald M. Foster, "Fourier integrals for practical applications 2nd ed.," p. 160, D. Van Nostrand Company, New York, 1951.
- [24] William H. Press, Saul A. Teukolsky, William T. Vetterling and Brian P. Flannery, "Numerical recipes in fortran 77, 2nd ed.," Cambridge University Press, Cambridge, UK, 1997.
- [25] Edward J. Rothwell and Michael J. Cloud, "Electromagnetics," CRC Press, Boca Raton, FL, 2001.
- [26] S. M. Ottens, "Development of measurement techiniques for michigan state university's free field radar scattering range," Diplomingenieur Thesis, Michigan State Univ. East Lansing, MI, 1995.

- [27] M. Schacht, "Radar target identification of hidden objects using indirect time domain measurements," Master's Thesis, Michigan State Univ., East Lansing, MI, 1999.
- [28] V. Daniel, "Dielectric relaxation," Academic Press, London, UK, 1967.
- [29] M. Abramowitz and I. A. Stegun, *Handbook of Mathematical Functions with Formulas, Graphs, and Mathematical Tables.* U.S. Government Printing Office, Washington, 1964.